Dynamic Modelling and Real-time Monitoring of Intelligent Wells

Ehsan Nikjoo

Submitted for the degree of Doctor of Philosophy

Heriot-Watt University

School of Energy, Geoscience, Infrastructure and Society

October 2018

Abstract

Intelligent Wells (I-Wells) are the wells equipped with in-well Flow Control Devices (FCDs) and sensors. I-Wells offer a wide range of flow control and monitoring options, with the latter often being subject to how well the information is derived from the measured, raw data. Pressure or temperature are the measurements most commonly taken and requiring interpretation in I-Wells.

This work develops innovative methods for modelling and monitoring of dynamic, transient flow in I-Wells. The topics cover:

i. *I-well clean-up modelling and analysis;*
ii. *Integrated Pressure and Temperature Transient Analysis (PTTA) in wells; and*
iii. *Pressure Transient Analysis (PTA) in I-Wells.*

This study starts with addressing the challenging clean-up process in I-Wells. A dynamic, coupled wellbore-reservoir modeling workflow is developed that simulates the whole process from fluid invasion to the flow back period. This is followed by investigating the role of different types of FCDs, e.g. autonomous and passive FCDs, well geometries etc. on the clean-up efficiency. General recommendations to facilitate the clean-up in I-Wells are further provided.

This study continues with a novel methodology integrating mature PTA solutions with the relatively new Temperature Transient Analysis (TTA) ones for various applications such as reservoir characterization, flow rate allocation and completion monitoring. Several available TTA solutions are extended to describe the multiphase flow in the reservoir. The required modifications and workflow are developed and verified using synthetic case studies. The value of the integrated analysis is then demonstrated by presenting a new method applicable for multi-phase production rate allocation in multi-zone, vertical I-Wells. The variable rate problem in the TTA context is later studied where the distorted signal is reconstructed by proposing normalization methods and developing a data-driven deconvolution algorithm.

Finally, the effect of non-linear pressure drop across FCDs in I-Wells on applicability of the classical PTA solutions is investigated. The corrections to incorporate this effect into the classical PTA solutions is implemented as well as a workflow to decompose the total skin is presented. The value and applicability of the proposed workflow are later illustrated using real field case studies.

This thesis is an important contribution into the understanding, modelling, monitoring and analysis of dynamic flow process in advanced wells.

Dedication

I dedicate this thesis to my beloved wife, Mina Jowkar, for her endless support, love and sacrifices

Acknowledgements

I would like to take this opportunity to express my appreciation to all the people who have helped me during my PhD journey.

First of all, I wish to express my gratitude to my supervisors Dr. Khafiz Muradov and Prof. David Davies for their supports and reviewing my thesis and publications.

I also wish to thank the examiners of my PhD thesis, Prof. Britt Halvorsen and Prof. Mahmoud Jamiolahmady, for reviewing my thesis and their valuable comments.

Special thanks to my colleagues and friends for their helps, contributions and invaluable discussions; Dr. Mahmoud Ahmadi, Piyang Liu, Dr. Akindolu Dada, Dr. Reza Malakooti, Dr. Morteza Haghighat Sefat, Saleh Goodarzian, Dr. Amir Jahanbakhsh, Dr. Eltazy Khalid, Dr. Pezhman Ahmadi, Khosro Jarahian, Dr. Mojtaba Moradi, Dr. Bona Prakasa, Dr. Misfer Al Marri…. thank you all.

I would like to thank all the sponsors of VAWE JIP project for the financial support, providing field data, useful discussion and suggestions during the JIP meetings. I would also appreciate the support that I have received from the wonderful staff of Heriot-Watt University.

To my parents and sisters for their prayers, continuous and unparalleled love and encouragement throughout my life.

Last but not least, I must express my very profound gratitude to my wife, Mina Jowkar, for providing me with unfailing support and love. This accomplishment would not have been possible without her. Thank you Mina.

ACADEMIC REGISTRY
Research Thesis Submission

Name*:*	Ehsan Nikjoo		
School:	Energy Geoscience Infrastructure and Society		
Version: (*i.e. First, Resubmission, Final)*	Final	Degree Sought:	PhD in Petroleum Engineering

Declaration

In accordance with the appropriate regulations, I hereby submit my thesis and I declare that:

1) the thesis embodies the results of my own work and has been composed by myself
2) Where appropriate, I have made acknowledgement of the work of others and have made reference to work carried out in collaboration with other persons
3) the thesis is the correct version of the thesis for submission and is the same version as any electronic versions submitted*.
4) my thesis for the award referred to, deposited in the Heriot-Watt University Library, should be made available for loan or photocopying and be available via the Institutional Repository, subject to such conditions as the Librarian may require
5) I understand that as a student of the University I am required to abide by the Regulations of the University and to conform to its discipline.
6) I confirm that the thesis has been verified against plagiarism via an approved plagiarism detection application e.g. Turnitin.

* *Please note that it is the responsibility of the candidate to ensure that the correct version of the thesis is submitted.*

Signature of Candidate*:*		Date:	**15.10.2018**

Submission

Submitted By *(name in capitals):*	
Signature of Individual Submitting:	
Date Submitted:	

For Completion in the Student Service Centre (SSC)

Received in the SSC by *(name in capitals):*			
Method of Submission *(Handed in to SSC; posted through internal/external mail):*			
E-thesis Submitted (mandatory for final theses)			
Signature:		Date:	

Table of Contents

List of Figures

List of Tables

Nomenclature

A	Opening area
B_o	Oil formation volume factor
C	Compressibility
C_v	Discharge Coefficient
C_u	Conversion factor
C_P	Heat capacity
C_{PR}	Ratio of volumetric heat capacity of oil to fluid saturated rock
H	Thickness
H	Enthalpy (chapter 4)
K	Absolute Permeability
M	Pressure and temperature semi-log slope
m(p)	Pseudo pressure
P	Pressure
Q, q	Flow Rate
R	Radius
R_s	Solution gas oil ratio
S	Saturation (chapter 5)
S	Skin factor
T	Temperature
T	Time
ε_{JT}	Joule-Thompson coefficient
φ_t	Thermal expansion factor
$\emptyset$	Porosity
α	FCD's Strength
μ	Viscosity
ω	Acentric factor
λ	Mobility
β	Thermal expansion factor

ρ	Density
η	Diffusivity constant for Pressure equation
η	Adiabatic Coefficient for Temperature Equation
η^*	Formation averaged adiabatic coefficient Temperature Equation

Subscript

Cal	Calibration fluid calculated (chapter 6)
D	Damage
D	Dimensionless
G	Gas
I	Initial, segment
J	Zones
L	Liquid
Mix	Mixture
O	Oil
Obs	Observation
P	Pressure
Pr	Pseudo
R	Radial
S	Skin
Sc	Standard condition
T	Total
T	Temperature
TeDD	Early time
TLDD	Late times
V	Vertical
Wf	Flowing
W	Wellbore
Ws	Static
W	Water
X	Volume flow rate exponent
Y	Viscosity function exponent

Abbreviation

AICD	Autonomous Inflow Control Devices
AICV	Autonomous Interval Control Devices
AFCD	Autonomous Flow Control Devices
AFI	Annular Flow Isolation
BHP	Bottom hole Pressure
DTS	Distributed Temperature Sensing
DAS	Distributed Acoustic Sensing
DSS	Distributed Stain Sensing
DPS	Distributed Pressure Sensing
DD	Draw down
DC	Deformed Configuration
DDA	Dynamic data Analysis
ESP	Electrical submersible pumps
ERWs	Extended reach wells
EOS	Equation of State
EnKF	Ensembled Kalman Filter
FCD	Flow Control Devices
FD-AICD	Fluidic Diode-AICD
FBG	Fiber Bragg Granting
ICD	Inflow Control Devices
ICV	Interval Control Valves
I-Wells	Intelligent Wells
IWC	Intelligent Well Completion
GAED	Golden Eagle Area Development
GNA	Gauss –Newton algorithm
GRG	generalised reduced gradient
GOR	Gas -oil ratio
JT	Joule-Thompson
JIP	Joint Industry Project
L-M	Levenberg-Marquadt

OBM	Oil Based Mud
OTDR	Optical Time Domain Reflectometry
PTA	Pressure Transient Analysis
PBU	Pressure Build-up
PLT	production logging tool
PI	Productivity Index
PDGs	Permanent Downhole Gauges
PTTA	Integrated Pressure and Temperature Transient Analysis
PTD	Pressure Temperature Deconvolution
PNT	Pressure-normalised Temperature
PSS	Pseudo Steady Stare
P-M Method	Perrine-Martin
P-P Method	Pseudo Pressure
PDE	Partial Differential Equation
P-S Method	Pressure square
RTA	Rate Transient Analysis
RCP	Rate Controlled Production
RFT	Repeat Formation Test
RNP	Rate-normalised Pressure
ROI	Radius of Investigation
RNT	Rate-normalised Temperature
RPD	Rate-Pressure Deconvolution
RTD	Rate Temperature Deconvolution
STD	Standard Deviation
SAGD	Steam-assisted gravity drainage
SCOV	Sandface control valve
SS	Steady state
SAS	Stand-alone-screen
sFCC	Sandface Flow Control Devices
TTA	Temperature Transient Analysis
THP	Tubing Head Pressure

THE	Heel-Toe effect
VAWE	Value from Advanced Wells
WCT, WC	Water Cut
WBM	Water Based Mud

Publications by the Candidate

1. A.Dada, K.Muradov , H.Wand, **E.Nikjoo** "Mitigation of the Remote Gauges Problem in Temperature Transient Analysis" *SPE 190863*,presnsted at SPE Europec featured at 80th EAGE Anuual Conference & Exhibition 2018 , Copehnagen 2018 Copenhagen
2. **E.Nikjoo**, K.Muradov, D. Davies." Dynamic Wellbore and Near-wellbore Clean-up in wells with a sandface flow control completion" *SPE 188751*, presented at SPE ADIPEC , 2017,Abu Dhabi, UAE
3. **E.Nikjoo**, K.Muradov, D. Davies." Pressure Transient Analysis in Advanced wells completed with flow control devices " *SPE 185861*, presented at SPE Europec,2017, Paris, France
4. **E.Nikjoo,** M. Haghighat Sefat." Value from Advanced Wells Completed with Inflow Control Devices (ICDs) in Water Flooding" *ID 42195, presented at EAGE,* 2017, Paris, France

Chapter 1 Introduction and Motivation

1.1 Thesis Motivation

Intelligent Wells(I-Wells) add monitoring and zonal control capabilities to conventional wells. Their permanent downhole gauges (PDGs) and sensors measure physical properties such as pressure, temperature, acoustics etc. at a high frequency, resolution and accuracy. The huge collected raw data need to be converted to useful information in order to take advantage of this in-well monitoring capability. Numerical and analytical solutions to quantify the measured data have been developed along with interpretation workflows and analysis methods. Each interpretation method reveals specific information about part of the reservoir and/or the near-wellbore. For example, mature Pressure Transient Analysis (PTA) is a proven tool for characterizing reservoir (middle-time flow regime) and boundaries (late-time flow regime) while the recently developed Temperature Transient Analysis (TTA) methods show a great potential for near-wellbore characterization (early-time flow regime).

Current industry practice is to use these analysis methods separately, i.e. mainly stand-alone PTA, to estimate reservoir and wellbore parameters, therefore, the obtained information is limited to the radius of investigation and accuracy of the method. Installing multiple type of gauges in I-wells provides the opportunity of integrating all the measured data and thereby characterizing reservoir from near wellbore to boundary as well as the performance of the well itself. Multiple data sources also improve the confidence interval for the similar estimated parameters. For example, using integrated Pressure and Temperature Transient Analysis (PTTA) allows TTA and PTA to obtain the same information about the reservoir while TTA can add also near-wellbore characteristics and PTA reveals late-time boundary information.

The value of integration in I-wells can be also shown during well performance modeling. Additionally, the long and short-term performance prediction of an advanced well equipped with different Flow Control Devices (FCDs), Annular Flow Isolation (AFI) etc. depends on the accuracy of model. Stand-alone reservoir and wellbore modeling approaches are unable to fully capture the required physics particularly for highly dynamic and transient processes such as clean up, liquid loading, start-up etc. A dynamic coupled reservoir-wellbore modeling workflow is required to study the performance of these advanced wells and their component.

The main motivation for this thesis is to promote the analysis of I-wells using an integrated approach to both their monitoring and modeling. This work aims to provide further insight into the potentials and added-value offered by this new technology.

1.2 Thesis Scope

This thesis aims to explore some opportunities and challenges in modeling and monitoring aspects of I-wells using synthetic and real case studies. The relatively new TTA method is a promising approach that complements the mature PTA. However, the available TTA solutions have been developed under simplified assumptions such as an infinite acting homogenous reservoir, single-phase flow and constant rate production. This thesis aims to take ideal TTA into the practical world application. The violation of several idealistic TTA assumptions is first investigated and then the required modifications are proposed. This is followed by highlighting the opportunities provided by integrating PTA with TTA in the areas of reservoir characterization, flow rate allocation and completion monitoring.The impact of the three types of FCD completion (passive, active and autonomous) on dynamic transient processes such as clean-up and well test analysis are investigated with a coupled reservoir-wellbore modeling approach.

1.3 Thesis Outline

The thesis is organied as follows;

Chapter 2 reviews the control and monitoring aspects of I-Wells and discusses the available types of FCDs and gauges and sensors. The value of I-Wells is highlighted for a range of applications.

Chapter 3 addresses the clean-up process in I-wells**.** Clean up can be regarded as a preparation stage (well conditioning) in a well's life. The success of this process, which ensures removal of the completion and drilling fluids as well as the external and internal mud cakes, considerably affects both the short- and long-term well performance. This chapter starts with a brief introduction on why clean-up of formation damage in Extended-Reach Wells (ERW) is more complex than for conventional wells. A dynamic integrated wellbore-reservoir model, using OLGA-ROCX^{TM} software, has been developed that enables modelling of the entire process from invasion of drilling fluid to flow back during the initial production phase. The role of passive, active and autonomous FCDs on clean-up have been investigated and

contrasted. This chapter focuses on the clean-up of autonomous FCD completion, a challenging process due to the sensitivity of devices to water-based fluids. Mitigation strategies and recommendations to facilitate and accelerate clean up in I-Wells completed with different FCDs have been prepared.

Chapter 4 presents the concept of PTTA and Dynamic Data Analysis (DDA). The evolution of three analysis methods, Rate Transient Analysis (RTA), PTA and TTA, are presented and their advantages and limitations are compared. This helps to understand how, when and where it is advantageous to integrate rate, pressure and temperature data. Thermal modeling using the STARS^{TM} and GEM^{TM} software packages generated temperature and pressure data for use within this thesis. Finally, a workflow for TTA is demonstrated. The knowledge developed in this chapter is a building block for the next three chapters focusing on PTTA.

Chapter 5 extends the current knowledge of TTA to multiphase flow, bounded and heterogeneous reservoirs because the underlying assumptions for the TTA single-phase flow in a homogenous and infinite-acting reservoir is highly unlikely to occur in practice. The applicability of current TTA methods will therefore be open to question if one or more of these assumptions are not met. The application of TTA in three different multiphase scenarios is tested and the necessary modifications and workflow are presented. The effect of a closed and constant pressure boundary on temperature data is identified and PTTA workflow is then amended to be used for bounded reservoirs. The effect of some types of reservoir heterogeneity on TTA results is also examined and it is shown how TTA and PTA results differ in heterogeneous reservoirs. Finally, the value of PTTA in limited-entry wells is illustrated.

Chapter 6 investigates the application of PTTA for flow rate allocation in multi-zone multi-phase I-wells. A new passive soft-sensing method is presented where the chapter 5 modified version of TTA for the oil-water system is integrated with the available multi-phase PTA for use in the inverse problem. The new soft-sensing algorithm is verified by applying it to several cases studied**.** The algorithm is later modified to be used for monitoring I-wells completed with AFCDs. It is shown how the multi-phase AFCD performance can be generated using this algorithm. Finally, the effect of different measurement uncertainties including noise, bias and faulty gauges on the robustness of the algorithm is discussed.

Chapter 7 addresses the problem of the use of variable rate flow data for TTA and PTA. Variable flow rate distorts the early-time signal so that it cannot be used for the analysis. Different solutions are investigated: Normalisation of the temperature response with respect to

rate and pressure changes is investigated and also a data-driven deconvolution algorithm is developed, verified and tested in multiple case studies. The application of the methods is further examined using a real data set obtained during Interval Control Valve (ICV) cycling in an I-well.

Chapter 8 examines the effect of non-linear pressure drop due to FCD completion on classical PTA. The necessary corrections to incorporate the FCD term in the current PTA solution are implemented and a workflow to decompose the total skin into a formation damage skin and ICD skin, is presented. The value and applicability of the proposed workflow are later verified using real field case studies.

Chapter 9 concludes the thesis with a summary of findings and recommendations for future studies.

Intelligent Well Background

2.1 Introduction

Well technology advanced significantly in the 1970s with the introduction of deviated wells. Later, in 80s and 90s, the horizontal and multi-lateral wells, Extended-Reach Wells (ERWs) and Maximum Reservoir Contact Wells (MRC wells) were introduced aiming to further enhance oil recovery. These wells improved productivity by increasing the contact area between the reservoir and wellbore and/or reducing the pressure drop required for a given production rate. However, this came at the cost of greater exposure to the reservoir heterogeneity, e.g. by crossing multiple reservoirs and layers or faults. Also, the increased effect of frictional pressure drop along the completion zone became high enough to significantly impact the well's performance. As a result, the uneven inflow distribution along the well and early water and gas breakthrough can considerably reduce the well efficiency. I-Wells have been introduced to the oil industry (*Figure 2-1*)in order to mitigate the mentioned production-related problems.

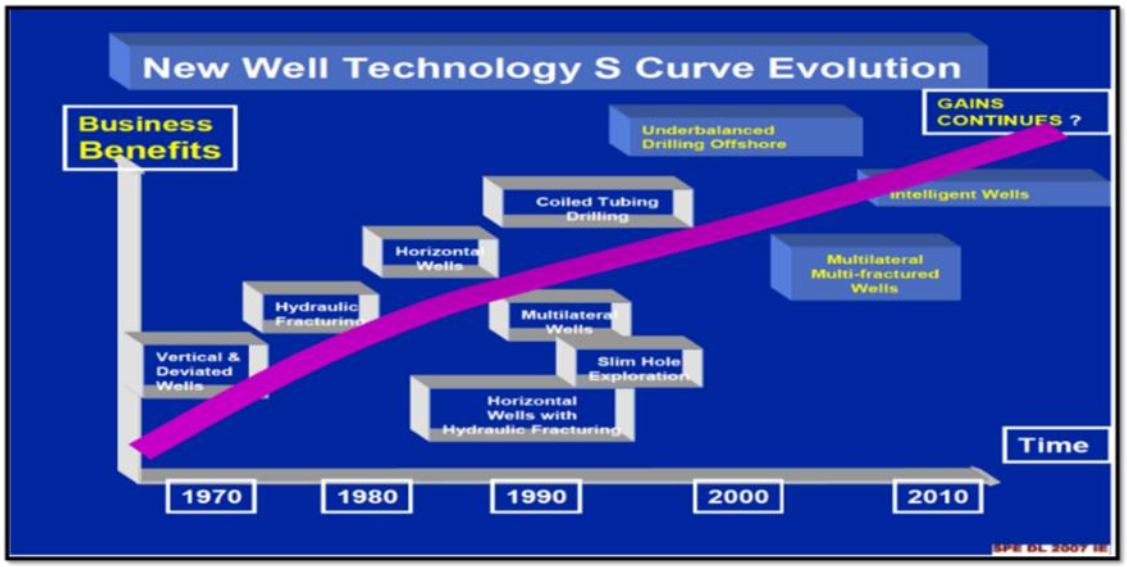

Figure 2-1 Well technology evolution (courtesy of SPE)

I-Wells are equipped with the state-of-art control and monitoring technologies (*Figure 2-2*). The main components of I-wells can be categorized as follows;

1. Flow Control Devices (FCDs)
2. Annular Flow Isolation (AFI)
3. Monitoring Sensors

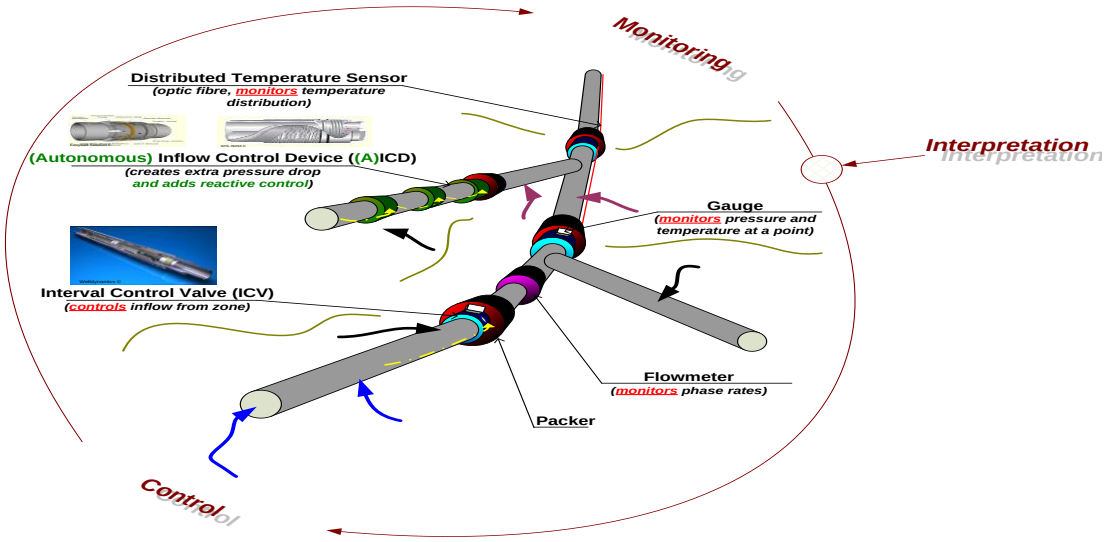

Figure 2-2 Advanced well with control and monitoring devices (courtesy of Khafiz Muradov)

2.2 Intelligent Well Control System

Non-uniform inflow from different parts of a conventional well without flow control results in poor sweep efficiency and premature breakthrough of unwanted fluid. This reduces the well's production life and productivity. For example, due to the frictional pressure drop in long horizontal wells, in a homogenous reservoir, the heel part produces more than the toe; leaving some parts of the reservoir upswept and also increasing the chance of premature gas or water breakthrough at the heel section (*Figure 2-3*).

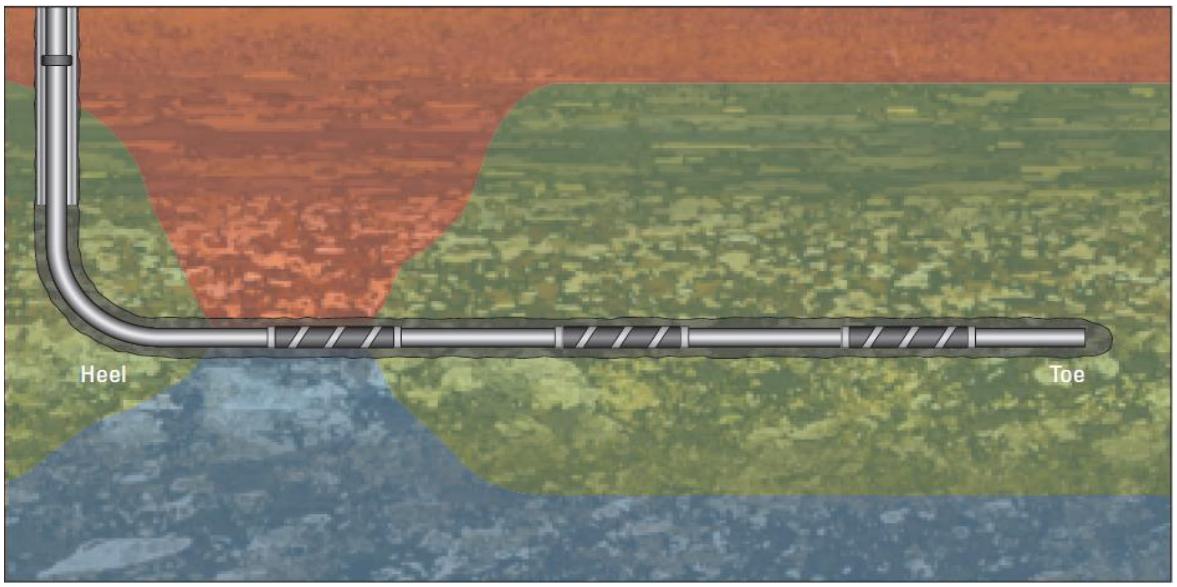

Figure 2-3 Heel-toe effect - oil (green) from sections near toe arrives at the wellbore while gas(red) and water (blue) ware inflowing at the heel(Ellis et al 2009) [1]

By contrast, I-wells employ FCDs to equalise flow along the completion. FCDs impose extra pressure drop, generally proportional to the inflow rate squared, that restricting inflow from high productivity sections of the well, thereby making the inflow more uniform along the length of the completion *(Figure 2-4).*

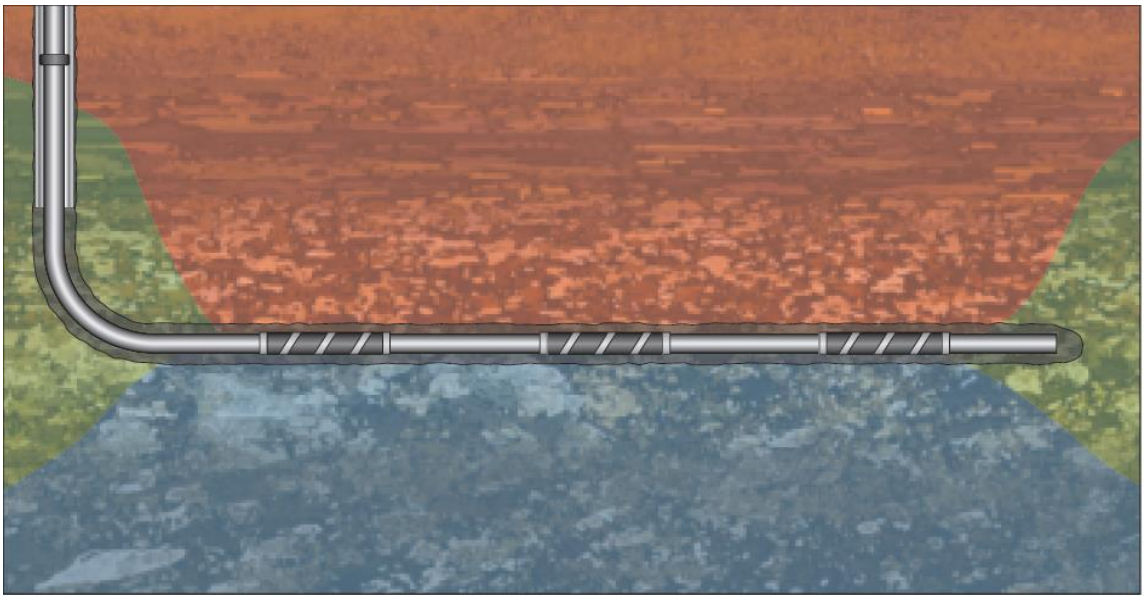

Figure 2-4 Flow control devices equalises flow along the completion (Ellis et al 2009) [1]

The FCDs can be categorised as being either passive, active or autonomous (*Figure 2-5*). The following presents a brief description of the devices and their technologies.

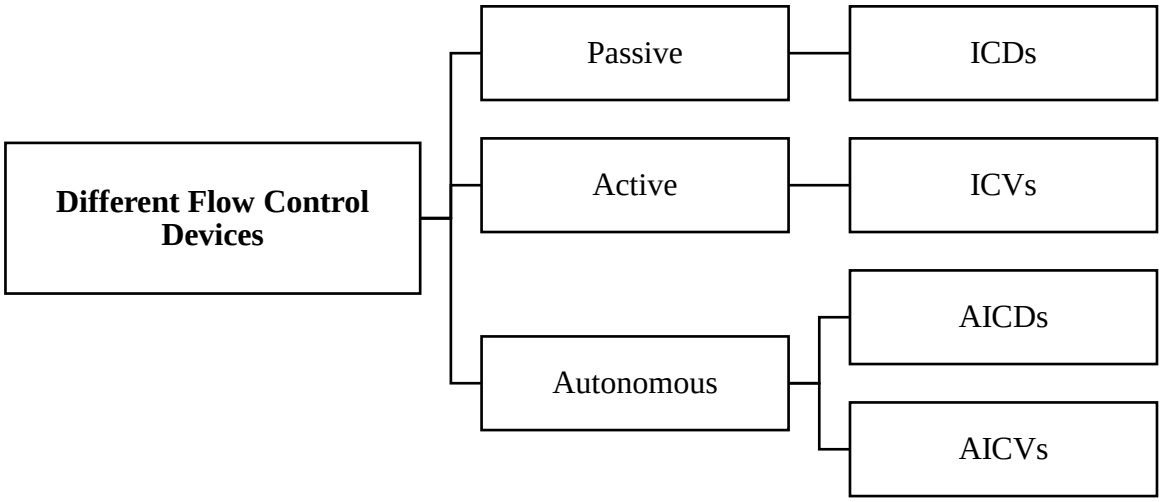

Figure 2-5 Different types of flow control devices

2.2.1 Inflow Control Devices (ICDs)

Norsk Hydro introduced ICD technology in the early 1990s as a means to enhance the performance of horizontal wells in the Troll Field. This field has a thin oil column (4-27 meters) overlain by a large gas cap and underlain by an aquifer, making it subject to early gas and water breakthrough [2]. The ICD is the passive type of FCDs, meaning that once installed it is not adjustable. Therefore, ICD can delay early water and gas breakthrough, but cannot stop the breakthrough once it has occurred. The passive nature of ICDs highlights the need for attention to be paid to their design and optimisation. For example, proactive optimisation[3] with long-term objective is a proper way (though rarely followed due to mathematical complexity) to optimise the I-Wells completed with ICDs. *Figure 2-7* summarises the technology behind the commercially available ICDs introduced by different suppliers (*Figure 2-6* also illustrates two types of ICD with their designed flow path)

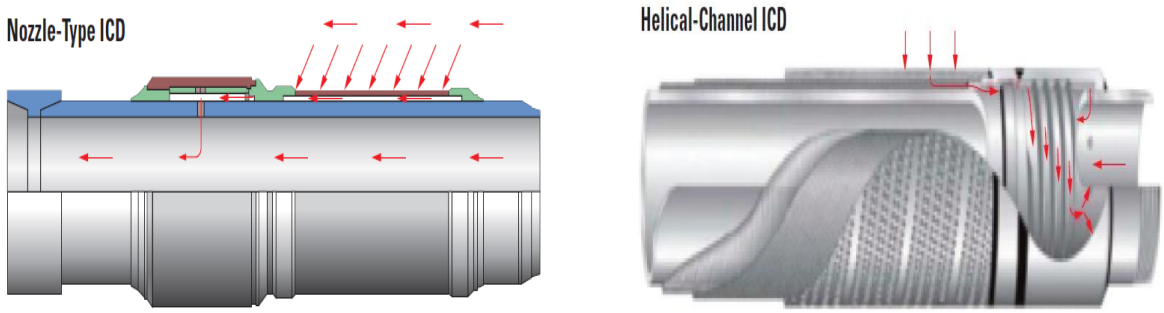

Figure 2-6 Nozzle type (left) and channel type (right)ICDs (Al-Khelaiwi 2013) [2]

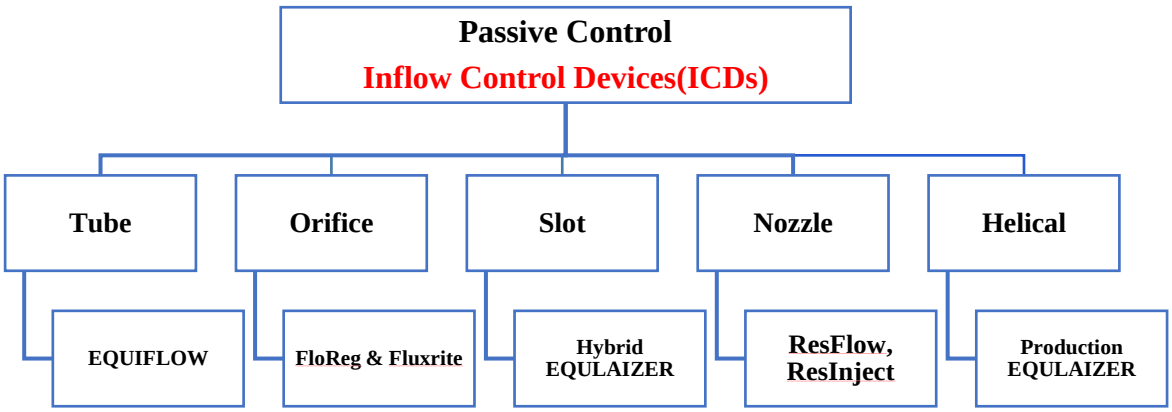

Figure 2-7 Different types of Commercially Available ICDs

2.2.1.1 Flow Performance of ICDs

As discussed before, ICDs are normally installed to improve the non-uniform inflow profile caused by the reservoir heterogeneity and/or HTE. An ICD restricts flow from the more productive zones (compared to the lower production zones in the same well) by imposing an extra pressure drop that is non-linearly proportional to the flow rate (*Figure 2-8*). The drawback is that the reduced reservoir draw down and thus production rate due to ICD restriction will lead to higher completion pressure drop. The reduced flowing bottom hole pressure may require artificial lift or other methods to achieve the target production rate. The extent of the completion's restriction is generally referred to as the "ICD strength. The magnitude of pressure drop induced by ICDs depends on (1) the dimensions of the restriction (i.e. orifice/nozzles or channels) and (2) the number of restrictions installed along the completion.

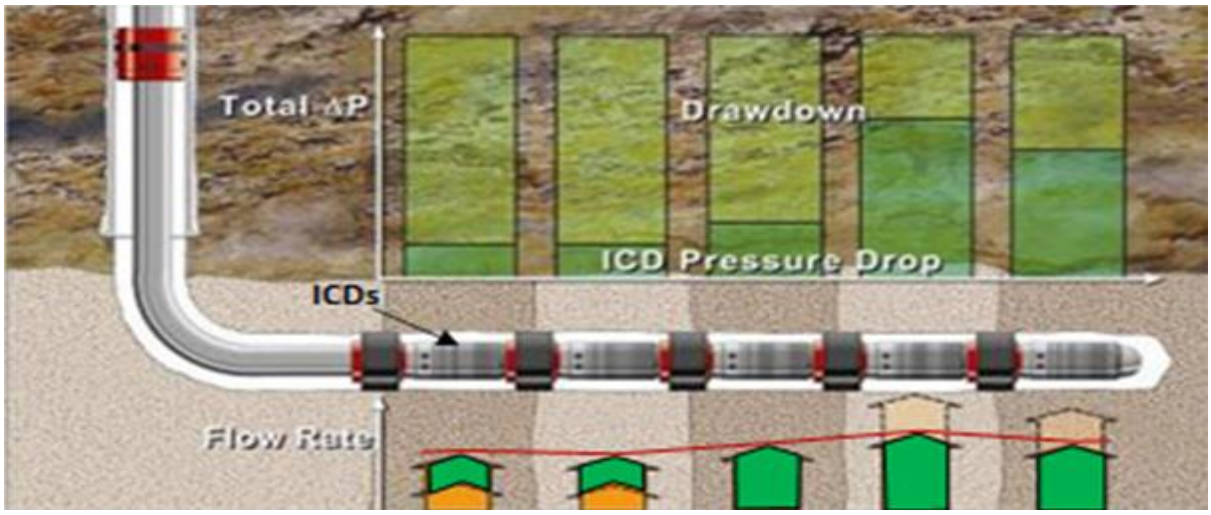

Figure 2-8 Share of ICD and reservoir pressure drop along the completion in heterogenous reservoir (Courtesy of Halliburton)

ICD Pressure drop element	Channel	Slot	Tube	Nozzle	Orifice
Friction	H	L	H	N	N
Acceleration	L	H	L	H	H
L = Low; H=High; N=Negligible					

Table 2-1 Pressure drop in different types of ICD

Pressure drop across an ICD can be due to friction and/or acceleration effects. *Table 2-1* presents the source of the pressure drop in different ICD types (Hybrid (e.g. labyrinth) types rely on both mechanisms of pressure loss). The general equation for modeling ICD pressure drop is as follows,

$$\Delta P_{ICD} = \alpha q^2 \qquad (2\text{-}1)$$

Where,

$$\alpha = \begin{cases} \left(\frac{\rho_{cal}\mu}{\rho\mu_{cal}}\right)^{1/4} \frac{\rho}{\rho_{cal}} l_{ICD}^2 B^2 \alpha_{ICD} & for\ a\ channel\ ICD \\ a_n = \frac{c_u \rho l_{ICD}^2 B^2}{c_d^2 d^4} & for\ a\ nozzle\ or\ orrifice\ ICD \end{cases}$$

These equations imply that the ICD pressure drop is proportional to the flow rate squared. *Figure 2-9* shows the example relationship of the orifice-type ICD pressure drop with respect to flow rate for different number of open orifice (out of total 10 orifices).

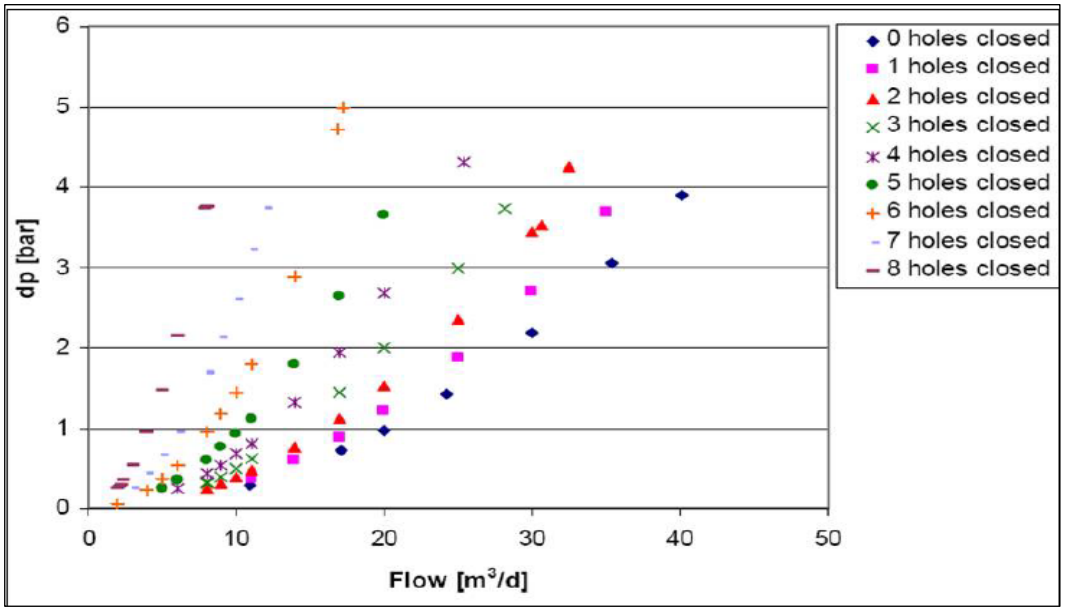

Figure 2-9 Flow test data for an orifice ICD with maximum of 10 open orifices (Al-Khelaiwi 2013) [2]

Note that most PTA pressure measurements are made downstream of ICDs and will therefore be affected by non-linear pressure drop caused by the ICD's restriction; making the conventional PTA methods inapplicable. PTA in ICD-completed wells will be discussed in chapter 8 where real data sets will be used to validate a new modification to conventional PTA for use in such advanced completions.

2.2.2 Interval Control Valves (ICVs)

Active ICVs are controlled remotely from the surface using a hydraulic, or electric or electrohydraulic actuation system. Such completions offer greater flexibility, compared with ICDs, for modifying the inflow from different section of well throughout the production phase. ICVs can be employed for both proactive and reactive strategies where the device can be

adjusted to either react to unwanted fluid once breakthrough has occurred and/or delay early premature water/gas production.

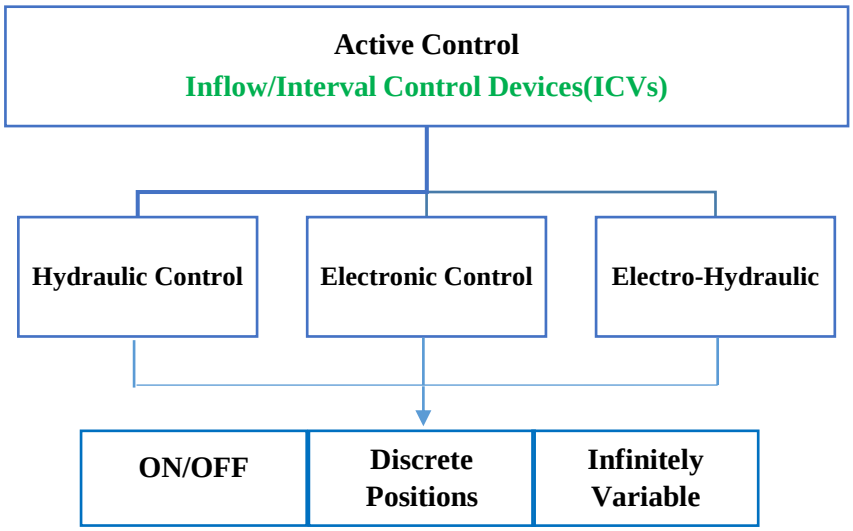

Figure 2-10 ICV Types

As depicted in *Figure 2-10* , ICVs can be grouped into three types;

1. On/off valves with two positions; either fully open or fully closed.
2. Discrete valves between 3 and 10 fixed, positions.
3. Infinitely variable valves which have any position between fully open to fully closed.

2.2.2.1 Flow Performance of ICVs

The flow performance of ICVs can be described using the following equation,

$$\delta P_v = \frac{8 C_u \rho_{mix} q_v^2}{\pi^2 C_d^2 d_v^4} \quad (2\text{-}2)$$

Where ρ_{mix} is the mixture density, A_c is the ICD opening area, C_v is the discharge coefficient, q is the flow rate and $C_u$is a conversion constant.

This equation assumes that frictional pressure drops are negligible and only acceleration effects, caused by the restriction of the fluid flow area, contribute to the pressure drop. The model is normally calibrated to the ICV's actual performance in a flow test using the discharge

coefficient (C_d). *Figure 2-11* illustrates the results of such a flow test. It plots the ICV pressure drop of a 10 different position versus the corresponding flow rate.

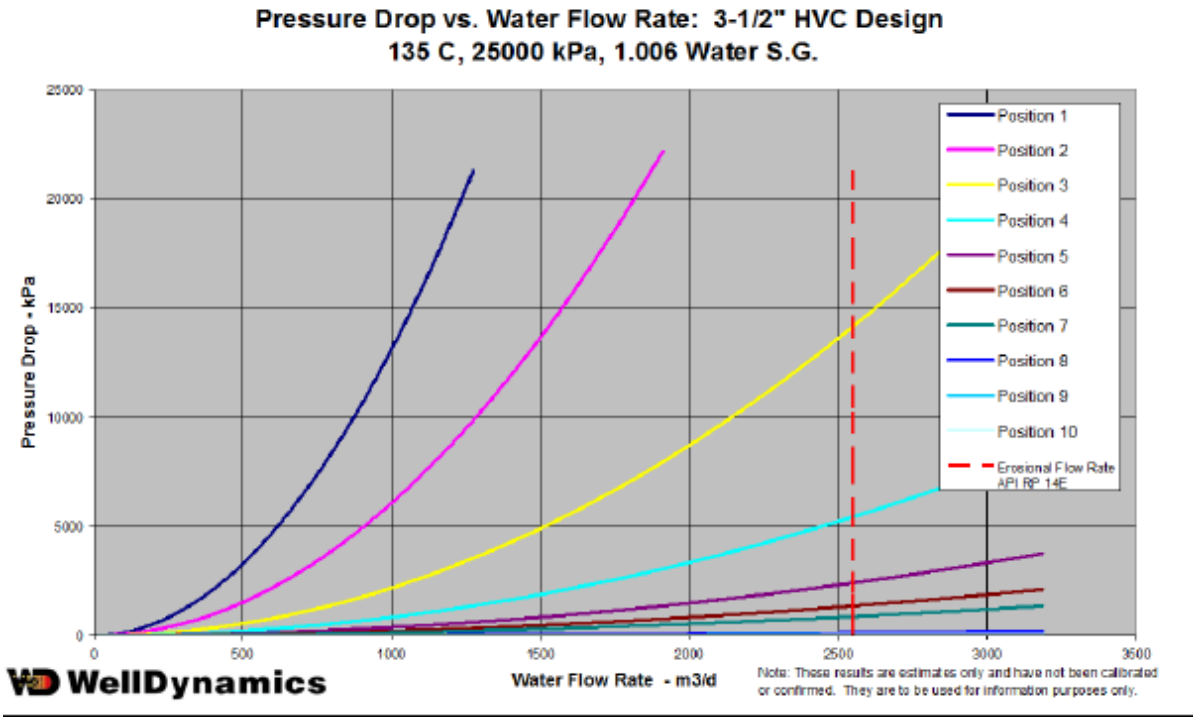

Figure 2-11 Flow performance curve for a discrete position ICV (Courtesy of Well Dynamics) [2]

2.2.3 Autonomous Flow Control Devices (AFCDs)

The AFCD is the latest development in FCDs. The advantage of this device over a passive FCD is its autonomous reaction to the unwanted fluid while being much simpler and cheaper to install than an active FCD. The AFCD autonomously imposes a greater restriction when the type of the fluid changes, e.g. to unwanted water or gas. Therefore, an AFCD completion does not require cables and control lines. AFCDs are also reversible, meaning that the performance of the device autonomously reverts to the minimum restriction if the local flow condition changes e.g. due to water inflow disappearing [5].

Field application of AFCD technology started in 2008 with the deployment of a Rate Controlled Production (RCP) AICD-completion in the Troll Field with the objective of controlling gas production (Halvorsen et al 2012)[6]. A multilateral well, P-13 BYH, with two "horizontal" laterals, BY1H and BY2H, was completed with two different FCD technologies. BY1H was completed with ICDs and BY2H with RCP-AICDs. The two laterals spaced 191 m apart drained formations of similar permeability. As shown in *Figure 2-12*, the two laterals gas

production performance differs considerably. Examination of the cumulative oil production showed that, the lateral BY2H (with RCP completion) produced approximately 20% more oil than lateral BY1H. This is attributed to the additional downhole control applied by the RCP-AICDs' resistance to gas flow compared with the passive control of the ICDs. This downhole control reduced the need for surface control of gas production from this well in order to meet the surface facility's gas handling constraint which limits the field's oil production.

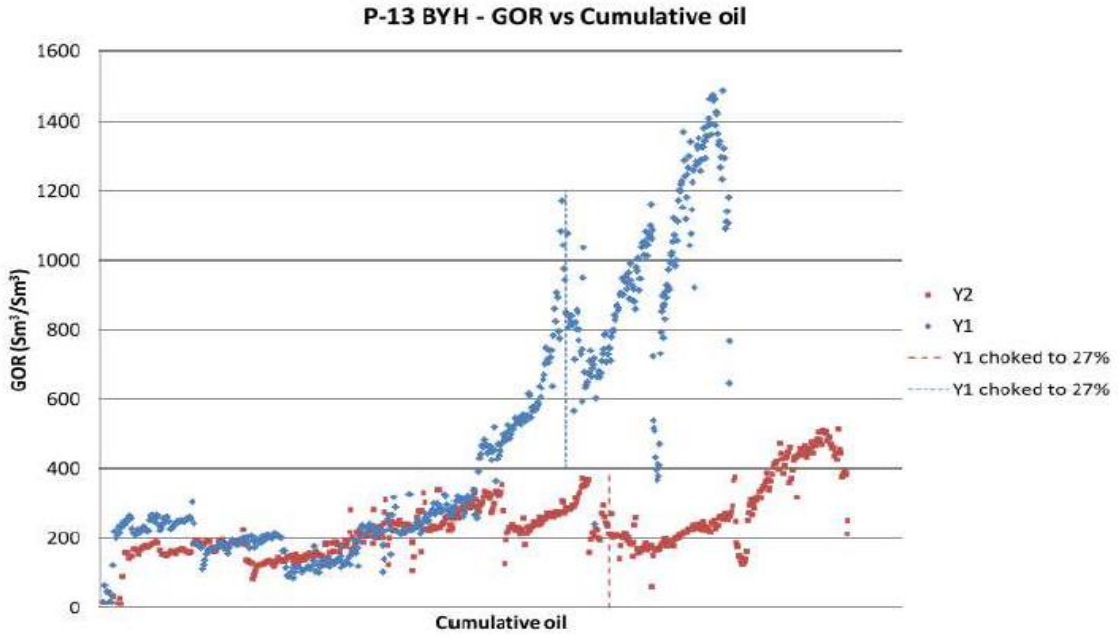

Figure 2-12 P-13 BYH GOR vs. Cumulative oil production performance (Halvorsen, M., et al., 2012) [6]

The aggressiveness of the device's reaction to the unwanted fluid distinguishes AICD from AICVs *(Figure 2-13)*;

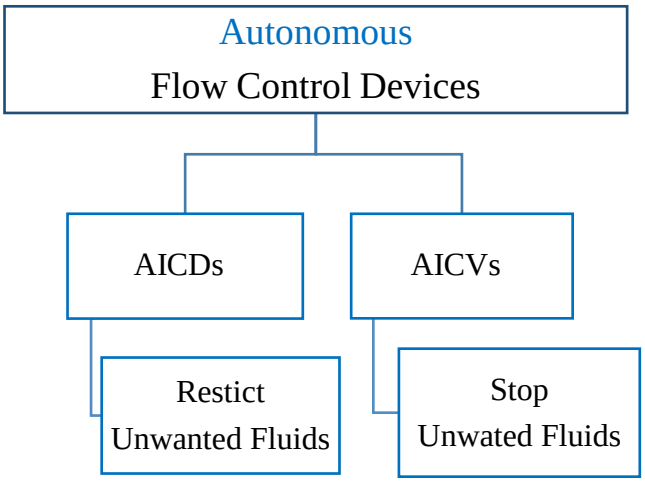

Figure 2-13 Different type of AFCD

2.2.3.1 Autonomous Inflow Control Devices (AICDs)

AICDs combine the passive inflow control with an active flow control element. The active element ensures that the differential pressure across the AICD is dependent on the composition and properties of the flowing fluid and the flow rate. The device reacts autonomously to the changes in the fluid properties however cannot completely stop production of unwanted fluids. AICDs are being installed by many different suppliers, but the two commercially available AICDs are the Rate Controlled Production (RCP-AICD) and the Fluidic Diode (FD-AICD).

- **RCP-AICD Technology**

The RCP device uses a floating disc to alter the geometry of the flow path when the properties of the flowing fluid change (*Figure 2-14*). The RCP-AICD that was first installed in Troll field was developed by Statoil. The working principle is described by Mathiesen, V., et al., (2011) [7] and Halvorsen, M., et al., (2012) [6]. The RCP-AICD is designed to restrict the inflow of low viscosity fluids, e.g. water, and works based on Bernoulli equation as follows;

$$P_1 + \frac{1}{2}\rho v_1^2 = P_2 + \frac{1}{2}\rho v_2^2 + \Delta P_{frictionloss}$$

Where P_1 is the static pressure, $\frac{1}{2}\rho v_1^2$ dynamic pressure and $\Delta P_{frictionloss}$ is the firction pressure loss.

The pressure at the top side of the disk would be lower for lower (than oil) fluid viscosity and thus higher fluid velocity. The total force acting on the disk would then move the disc towards the inlet reducing the flow area. In contrast, for a more viscous fluid, the relative pressure on the bottom side of the disk decreases resulting in a lower force acting on the disc from the bottom and the disk moves away from the inlet allowing the fluid to flow with the maximum area designed (*Figure 2-14*)

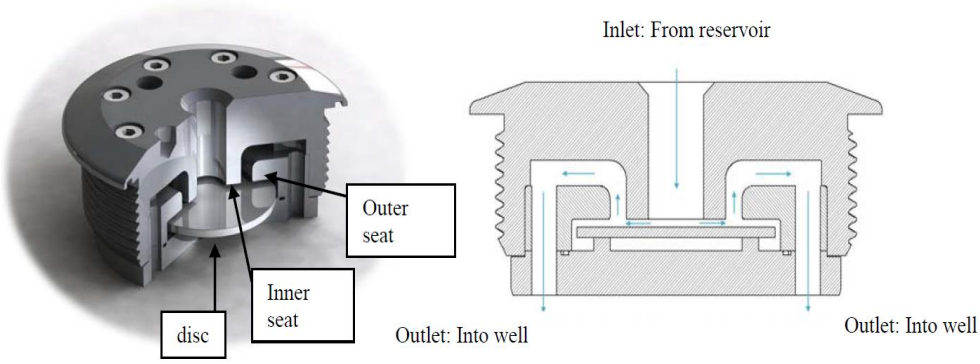

Figure 2-14 RCP AICD [5]

- **Flow Performance of AICDs**

Figure 2-15 shows single flow performance curve for RCP AICD. Such multiphase performance data requires access to the laboratory measurements.
Mathiesen et. al., (2011) [7] and Halvorsen et. al., (2012) [6] provided the following expression to model the performance of RCP-AICDs.

$$\delta P = \left[\frac{\rho_{mix}^2}{\rho_{cal}}\right] . \left[\frac{\mu_{cal}}{\mu_{mix}}\right]^{y} . a_{AICD} . q^{x} \qquad 2\text{-}3$$

Where a_{AICD} is a constant called “strength" of the AICD, x is the volume flow rate exponent with different values reported in the literature between 2 to 4, y is the viscosity function exponent and ρ_{cal} and μ_{cal} are the calibration fluid’s density and viscosity respectively. ρ_{mix} and μ_{mix} are the volumetric averages of the fluid density and viscosity respectively defined as:

$$\rho_{mix} = (\alpha_{oil})^{a} * \rho_{oil} + (\alpha_{water})^{b} * \rho_{water} + (\alpha_{gas})^{c} * \rho_{gas} \qquad 2\text{-}4$$

$$\mu_{mix} = (\alpha_{oil})^{a} * \mu_{oil} + (\mu_{water})^{b} * \mu_{water} + (\mu_{gas})^{c} * \mu_{gas} \qquad 2\text{-}5$$

Alternative workflows to model AICD using commercial software have been developed by e.g. Eltaher *(2017) [8]*.

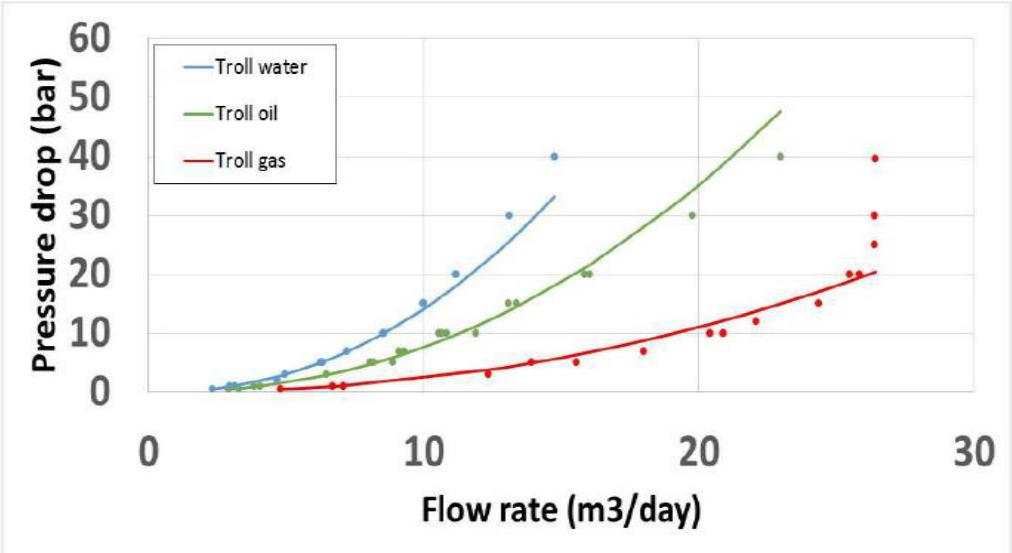

Figure 2-15 Single phase RCP-AICD flow performance curve (Halvorsen et. al., (2012))[6]

- **FD-AICD Technology**

Fluidic Diode (FD) Autonomous Inflow Control Device, also known as Equiflow utilizes the difference in inertia between oil and water to change the flow path of the two phases. The device works based on the vortex principle by which the less viscous water is forced to take a longer path from the devices inlet to nozzle. The water phase thus experiences a higher pressure drop than that for the more viscous oil that travels directly to the nozzle *(Figure 2-16)*. The fluidic diode AICD has no moving parts, unlike the other AICDs.

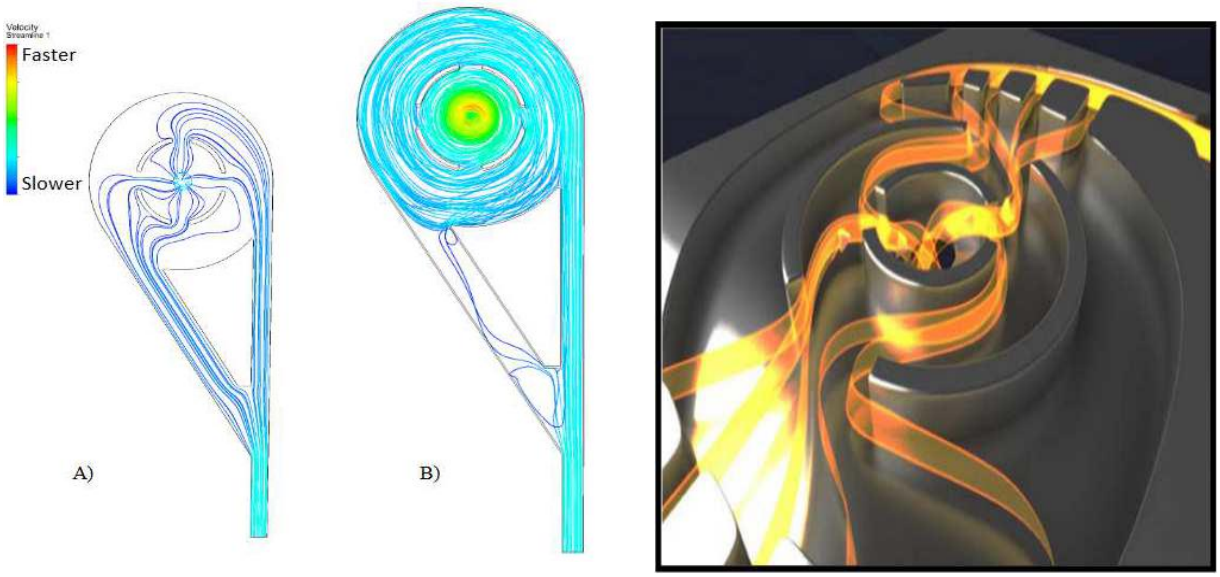

Figure 2-16 CFD simulation results on a simplified AICD showing the fluid flow pathways dependence on the fluid properties (mainly viscosity). (A) Streamline for oil flow and (b) stream lines for water flow and (c) actual valve design (Fripp et al 2013) [9]

The same approach as that described above for the RCP-AICD is used to model the FD-AICD's performance. Halliburton models the performance of the FD-AICD with the formula:

$$\delta P = K.\left[\frac{8\rho_{mix}}{3.14n^2 D_h^4}\right].q^x \quad (2\text{-}5)$$

Where $K = f(Re)$ found by fitting the experimental data and $Re = \left[\frac{4Q\rho_{mix}}{3.14D_h\mu_{mix}}\right]$

Concerns have been expressed on the model's accuracy for polynomial curve fitting of the experimental data and the generality of the obtained solution (Eltaher 2017) [8].

The design of the FD-AICDs depends on the viscosity of the flowing fluids. *Figure 2-17* shows performance curves for the FD-AICD range 3B (light to heavy oil (3 – 200 CP)). The higher flow resistance for water is clearly shown in this graph.

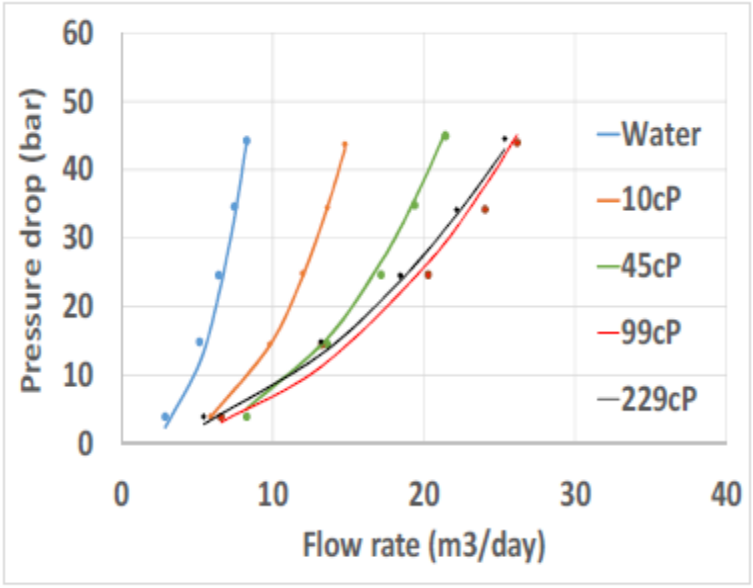

Figure 2-17 FD-AICD flow performance curve (Zhao et al 2014) [10]

2.2.3.2 Autonomous Inflow Control Valves (AICVs)

While ICDs and AICDs have been successfully employed to improve oil recovery and reduce unwanted fluid production, neither of them can almost completely stop the water/gas production once high phase fractions of the unwanted fluid are being produced. AICVs are designed to autonomously (nearly-)stop the unwanted fluids (water/gas) production. Only a few % of the main flow continues to be produced once the AICV action has occurred at the critical phase cut value. Aakre and Halvorsen (2013) [11] presented the physics behind the AICV technology which consists of two main flow paths;

1) Passive part: The main flow area connecting the annulus with the production tubing
2) Active type: A bypass flow consisting of a moveable element (piston) together with laminar and turbulent flow elements (pilot flow)

Figure 2-18 shows the AICV in the open and closed position. The arrows depicted describe the flow paths where the thin blue lines show the pilot flow path and the thick blue arrow show the main flow from the annulus through the valve and into the base pipe (the horizontal arrows).

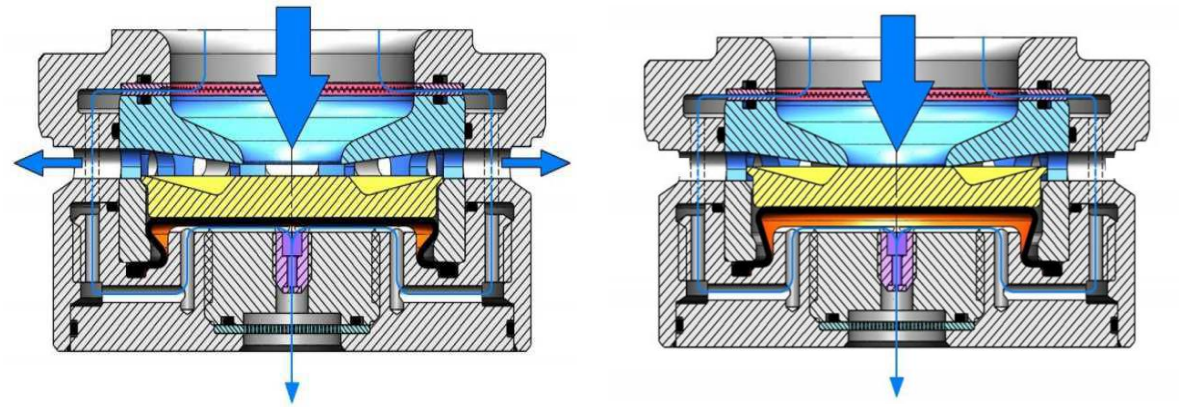

Figure 2-18 AICV in the open (for oil flow) and closed (for water or gas flow) position [5]

The AICV's bypass flow path in a laminar flow element, or pipe, where its pressure drop can be expressed as:

$$\Delta p = \frac{32\mu v L}{D^2} \qquad (2\text{-}6)$$

Where μ is the fluid viscosity, v is the fluid velocity, L and D is the length and diameter of the pipe respectively. The fluid will undergo a pressure drop that is proportional to the fluid viscosity, the fluid velocity and geometrical dimensions in the laminar flow element. The

AICV's pilot flow(passive part) is a turbulent (Inertia causes turbulence, the higher the inertia force, the bigger the Reynolds number leading to turbulent flow regime) flow element, an orifice, where the pressure drop can be expressed as:

$$\Delta p = C\frac{1}{2}\rho v^2 \qquad (2\text{-}7)$$

where C is a geometrical constant. The turbulent flow element's pressure drop is independent of viscosity, but proportional to the density, the fluid velocity squared and a geometrical constant. Different flow elements will have different flow characteristic for the gas water and oil due to different fluid properties.

Figure 2-19 the performance curves for oil, water and gas of the AICV compared to a nozzle ICD is shown, The performance of oil through AICV is identical to the nozzle ICD as long as the same strength is selected, When the AICV closes for low viscous fluids as water and gas, the only flow across the AICV is through the pilot flow, which has a minor flow rate, The flow rates of these fluids are therefore considerable lower for the AICV compared to the flow rate of the ICD, The black arrows illustrate the enhancement in the flow performance curves for water and gas.

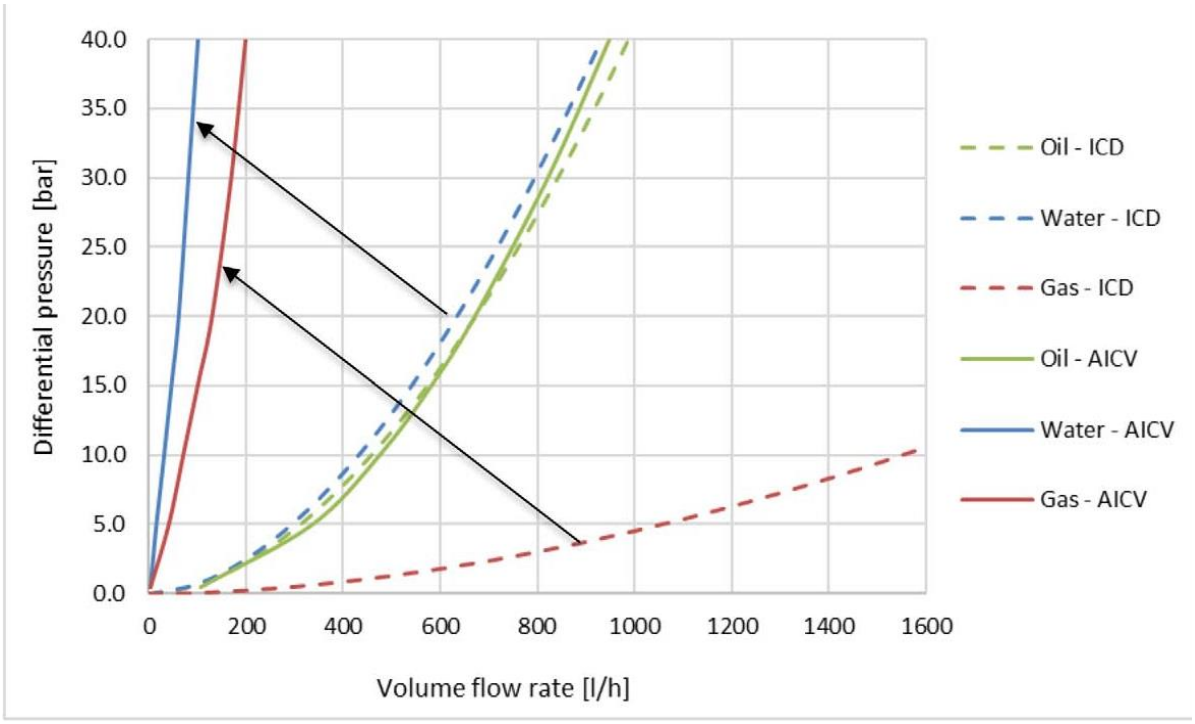

Figure 2-19 Performance curve of the ICD and the AICV for oil, water and gas [12]

The AFCD is a new technology, two aspects of which are addressed in this thesis for the first time:

- Chapter 3: Investigates the challenges faced by an AFCD completion during the wellbore clean-up process where both the near-wellbore and wellbore may be filled with the fluids that will be restricted by the AFCDs.

- Chapter 6: Presents a novel method to produce multiphase flow performance curve for AFCDs to meet the challenge of appropriate experimental data for the AFCD not being available.

2.2.4 Annular Flow Isolation (AFI)

Significant annular flow occurs due to the large permeability contrasts, commingled production from zones with different pressure, large annular space, etc. Annular flow or fluid flow in the annular space between the completion tubular and the sand face or the cemented and perforated casing is one of the major challenges encountered by both production and injection wells. Different technologies for AFI have been developed in recent years to eliminate annular flow and minimise its impact. The negative effect of annular flow, in addition to the loss of flow control between zones, can be the sand production and transport along the length of the completion resulting in erosion, plugging of the sand face, completion or even total loss of the well. There are many types of packers in the market. They are normally categorised by their setting mechanism: mechanical, hydraulic, inflatable, expandable, swell and chemical packers More information about packers can be found in Al-Khelaiwi 2013 [2].

2.3 Intelligent Well Monitoring System

High precision sensors in I-Wells are installed to measure various physical properties including pressure, temperature, acoustic etc. *(Figure 2-20).* The data collected by these monitoring devices can potentially be used for a wide range of applications from reservoir characterisation to completion monitoring. The information obtained from continuous monitoring is also essential for optimising the performance of I-wells completed with different FCDs. For example, the zone/well production strategy can be updated continuously based on the new measurements. Permanent downhole sensors can be classified based on either the measurement technology, electronic or optical sensors, or the number of monitoring points, single-point, quasi-distributed and distributed [13].

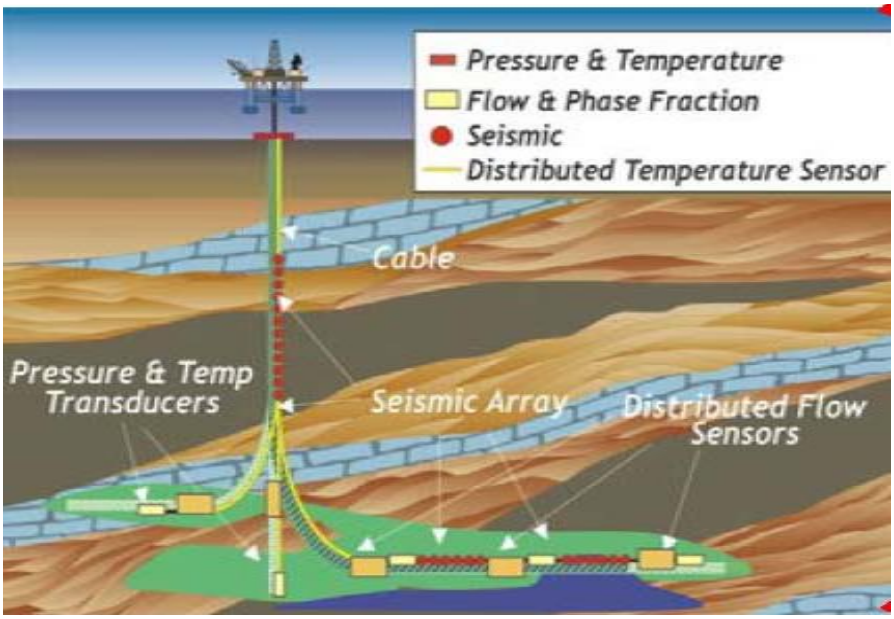

Figure 2-20 An I-well with multiple gauges and sensors [13]

2.3.1 Electronic Sensors

During the past 20 years, the installation of permanently installed gauges has become increasingly common. As of 2006, the number of PDG installations claimed to be in excess of 10,000 worldwide [14] .With Chorneyko et al (2006)[15] referring to more than 1,000 measuring points installed by one major oil company. Most early PDG installations were used for operational objectives, such as monitoring pumps and downhole equipment. However, it soon became evident that PDGs also were a good source of information about the reservoir.

Although PDGs were installed as early back as 1963 they only became a standard completion component in the late 1980s [16].

The increasing sophistication and cost of well completions demands that more comprehensive information about the events taking place downhole is routinely measured. Simultaneously, increasing reservoir complexity added new requirements to downhole reservoir data measurements for maximising reserves [14]. Da Silva et al.(2012) [17] classified the sensors commonly employed for permanent near-wellbore and deep reservoir monitoring as follows;

- Single-point pressure and temperature
- Quasi-distributed temperature
- Single phase and two-phase flowmeter
- Streaming potential
- Permanent 3D resistivity
- Permanent downhole seismic

Table 2-2 summarises the typical accuracy and resolution of commercial downhole pressure and temperature sensors being installed to day.

Table 2-2 Electronic Pressure and Temperature gauges resolution and accuracy

	Pressure	Temperature
Maximum Values	15000 psi	150 ℃
Accuracy	+/-3 psi	+/- 0.5 ℃
Resolution	0.01 psi	0.001 ℃
Long-term stability	1 psi/year	0.1 ℃/year

2.3.2 Fibre Optic Sensors

Electronic gauges are limited to making a measurement at a single point. Multiple measurement requires multiple sensors, or the instrumentation has to be moved between the measurement stations. The disadvantage of such an approach is the inability to make simultaneous measurements at these locations. Further permanent gauges in I-wells are anchored to completion and cannot be moved hence making distributed measurements require an intervention by wireline or coiled tubing. Optical fibres make distributed measurements possible since the entire fibre is used as an array of sensors that can be interrogated with an instrument at the surface. This allows large sections of the well to be surveyed both rapidly and

simultaneously; facilitating cost-effective measurements of potentially transient, distributed phenomena. Permanent installation of fibre offers the opportunity of long-term monitoring. Most distributed measurements use the principles of Optical Time Domain Reflectometry (OTDR). A short laser pulse is generated at the surface and sent into one end of the optical fibre. It travels along the fibre, interacting with natural or artificial imperfections in the fibre and so generates backscatter. This is detected by a receiver at the surface, as shown in Figure 2-21.

It is important to note that the backscatter is generated either continuously along the fibre without the addition of reflectors or other modifications, or at fixed points where Bragg gratings are imprinted. The backscattered light spectrum includes different spectral components such as Rayleigh, Brillouin and Raman bands;

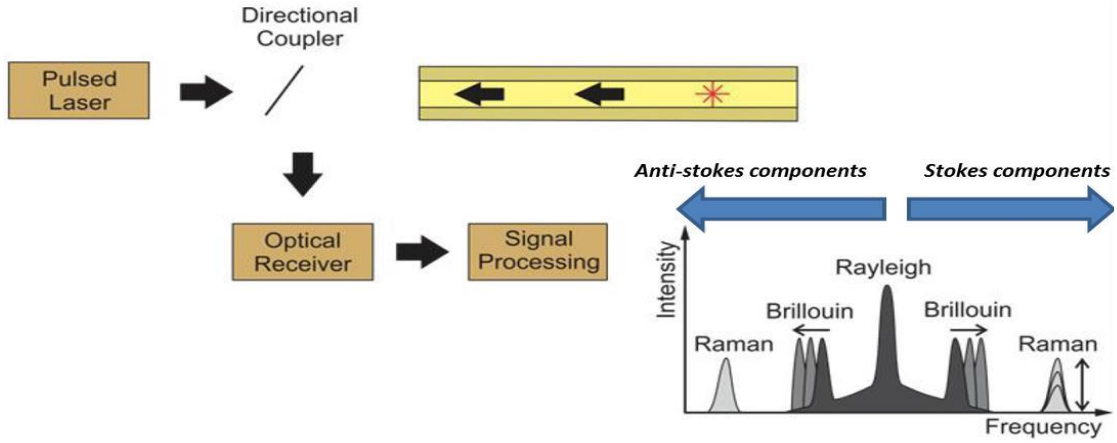

Figure 2-21 Backscattered light spectrum [13]

Rayleigh scattering: Produces the largest magnitude of backscatter at the same frequency as the incident light. It is widely used for evaluating the level of signal attenuation and losses in the optical fibre.

Brillouin scattering: Produces backscatter of lower intensity than Rayleigh with a frequency shift of around 10 GHz (0.1 nm at 1.5-micron wavelength) due to thermally excited acoustic waves (acoustic phonons). This frequency, or Brillouin, shift is directly related to both the local temperature and the strain at a given location along the length of the fibre.

Raman scattering: Produces a low intensity backscatter due to the thermally excited molecular vibrations (optical phonons) and exhibits a frequency shift of up to 13 THz (100 nm at 1.5micron wavelength). The intensity of the Raman backscattered light depends on the local temperature of the fibre. *Figure 2-21* summarises the measurement pieces and the three modes of backscattering.

Fiber optic sensors create a great opportunity for reservoir and well surveillance; however, the massive data recorded by these sensors is a concern. *Figure 2-22* shows the increasing intensity of data generation as downhole surveillance progressed from PDGs to fibre-optic Distributed Temperature Sensing (DTS) and now Distributed Acoustic Sensing(DAS) which may be combined with other types of sensors(DxS). Per-well data rates has increased from a few bytes per day (B/d) to nearly a terabyte per day (TB/d).

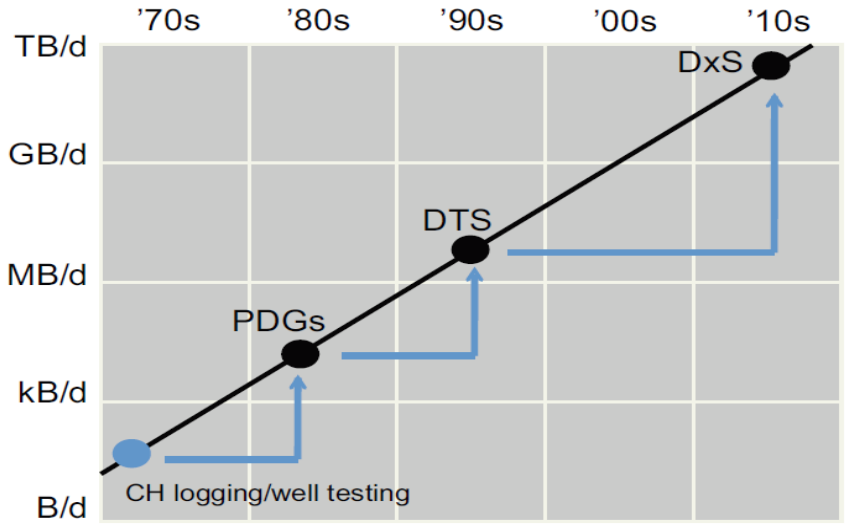

Figure 2-22 Trend line showing the downhole sensing history with daily data rates per well[18]

Many fibre optic sensors have been installed in oil and gas:

- Fibre Bragg Grating fibre-optic sensors (high-precision P and T measurements at several fixed points)
- Distributed Temperature Sensing (DTS)
- Distributed Acoustic Sensing (DAS)
- Distributed Pressure sensing (DPS)
- Distributed Strain sensing (DSS)
- Distributed Chemical sensing (DCS)

The following is a brief description of DTS, DAS and DPS. More information about DSS and DCS can be found in Da Silva et al.(2012) [17]. FBGs with a precision similar to that of the electronic PDGs and are being widely installed and have replaced PDGs as the backbone of transient pressure and temperature transient measurement in modern I-wells.

2.3.2.1 Distributed Temperature Sensors (DTS)

Fibre-optic temperature monitoring of steam flood wells became available in the early 1990s. The Raman spectral band can be used to obtain information about the distribution of temperature along the fibre. The Raman backscattered light has two components, Stokes and Anti- Stokes *(Figure 2-21)*, one being only weakly dependent on temperature and the other being greatly influenced by temperature. The relative intensities between the Stokes and Anti-Stokes light amplitudes is a function of temperature at which the backscattering occurred. Therefore, temperature can be determined at a remote point in the optical fibre by analysing the light in these wavelength bands. *Table 2-3* compares the accuracy and resolution of temperature measurement using DTS and PDGs/FBGs. PDG/FBG offer a higher accuracy and resolution for temperature measurements but of course are not distributed.

Table 2-3 Comparison between DTS and PDG gauges

	DTS	PDGs
Resolution	0.2 ℃	0.001 ℃
Accuracy	1 ℃	0.5 ℃

DTS probably is the most popular fibre optic sensor at the moment with its data being used in many applications either qualitatively or quantitatively. *Table 2-4* lists some published application of DTS in various areas.

Table 2-4 Example of DTS application

Subject	Example of References
Stimulation and Fracturing	Tabatabaei et al (2011)[19] , Sierra et al (2008) [20], Huckabee et al (2009) [21]
Flow Rate Profiling	Kabir et al (2008) [22] , Muradov et al (2009) [23]
Flow assurance (detection of Scale and wax)	Almutairi et al (2008) [24] ,Wilson et al (2013) [25]
Well integrity (Cross flow and leak detection)	Mishra et al (2017) [26] , Oftedal et al (2013) [27]
Reservoir Characterisation	Xu et al (2017) [28] , Tabatabaei et al (2012)[29]

2.3.2.2 Distributed Acoustic Sensors (DAS)

DAS was first employed in a field trial of DAS by Shell during the completion of a tight gas well in February 2009. The sensing principle of DAS relies on Rayleigh scattering of light within the optical fibre. A laser interrogator generates sequences of light pulses, detects the back-scattered light and translates it into individual strain measurement values at sensing points with whatever sampling interval is desired (*Figure 2-23*).

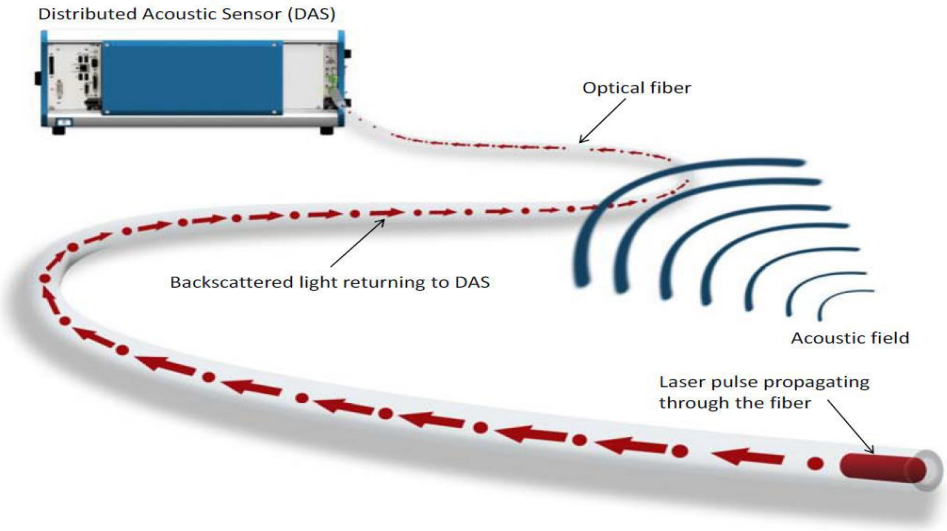

Figure 2-23 Principle operation of DAS [30]

Table 2-5 lists some example applications of DAS:

Table 2-5 Published DAS application

Application	Example Publications
Fracturing and Stimulation	Molenaar et al (2011) [31]
Flow Rate Profiling	In 't Panhuis et al (2014) [32]
Flow Assurance (detection of Scale and wax)	In 't Panhuis et al (2014) [32]
Well integrity (leak detection)	Hull et al (2010) [33]
Geophysical monitoring	Molenaar et al (2011) [31]

2.3.2.3 Distributed Pressure Sensors (DPS)

A DPS to measures the pressure profile along a specified interval of interest. This technology has long existed but the business case for the development a commercial device for downhole installation in an oil or gas well has not been made.

There are several principles that can be used for a DPS system such as Brillouin scattering, in which the frequency of shift of backscattered light is dependent on the local strain and consequently on local pressure. However, regardless of the type of sensors, the sensor system provides pressure measurement along the deployed cable and conveys the signal to a data acquisition system.

DPS like DTS has a significantly poorer pressure resolution and accuracy compared to the current generation of quartz electrical gauges *Table 2-6.*

Table 2-6 Performance Comparison of current electrical and DPS (@ 150 C and 68.9 Mpa)

	DPS	PDGs
Pressure Resolution	1.38 Kpa	0.07 Kpa
Accuracy	13.79 Kpa	8.27 Kpa

DPS systems are a novel concept and many aspects are currently subject to investigation, ranging from installation, testing and maintenance to interpretation and value estimation. Farshbaf Zinati et al (2012) [34]used DPS data for estimating the productivity index in horizontal wells where they used adjoint-based minimisation algorithm for the study. Yoshioka et al. (2009) [35] also proposed an inversion algorithm to invert DPS and DTS measurements to inflow profiles.

2.4 Dynamic Simulation

The numerical simulation of reservoir flow is typically based on a modified set of conservation equations. In particular the classic conservation-of-momentum equation is replaced by a semi-empirical quasi-steady-state relationship known as Darcy's law justified by the very slow movement of fluids through the pores. Typical state variables are pressure, enthalpy (in case of thermal simulation), and either the (pseudo-) component accumulations, or the phase saturations (the dimensionless fractions of the pore space filled with oil, gas or water). The hydrocarbons are described with black or volatile oil models or, occasionally, fully compositional. The essential nonlinearity in reservoir simulation stems from the fact that the presence of a phase influences the flow of the other phases in a non-trivial manner.

The underlying mechanisms involve (fluid-fluid) interfacial tensions and (solid-fluid) capillary effects which are taken care of by macroscopic semi-empirical relationships. The resulting systems of PDEs typically contain a parabolic (near-elliptic) pressure equation and one or more

parabolic (near-hyperbolic) saturation equations. The equations are usually semi-discretised in space with the aid of the finite volume and finite difference methods, although sometimes (mixed) finite element discretization are used. The number of grid cells is usually in the order of 10^4 to 10^6, and the resulting systems of ODE's are therefore typically very large.

The temporal discretization is usually performed either fully implicitly, with a simple backward Euler scheme and full Newton-Raphson iteration at each time step, or sequentially, with an implicit treatment of the pressure equation and an explicit treatment of the saturations (IMPES). Most simulators use an adaptive time stepping scheme that reduces the step size if the Newton-Raphson procedure does not converge within a predefined number of iterations and increases the step size when the procedure converges quickly. The values of permeability (inverse resistance to flow) in the grid cells may vary with several orders of magnitude from cell to cell, which results in numerically poorly conditioned systems of equations requiring specialized linear solvers. Moreover, the poorly known reservoir geology often results in the need to work with ensembles of reservoir models to span the underlying uncertainty.

Moreover, most reservoir simulators consider isothermal conditions, in which case the conservation-of-energy equation becomes superiors. In this thesis different types of reservoir simulator have been used for different studies. For example, in chapters 4 to 7 non-isothermal STARS and compositional GEM was used to generate both single-phase and multi-phase transient pressure and temperature data for PTA, TTA and PTTA applications. In chapter 3 and 8, a near wellbore simulator, ROCX, was used to be integrated with a wellbore simulator, OLGA, for clean-up and well test studies in advanced well completions.

Regarding the wellbore simulation, the numerical simulation of well bore flow is based on the classic set of conservation equations in fluid dynamics: i.e. those for mass, momentum and energy, leading to a system of coupled nonlinear partial differential equations (PDEs). Nearly always the simulations are one-dimensional, using averaged properties over the pipe area, and typical state variables are pressure, enthalpy, and mass flow rates for water and two hydrocarbon pseudo components. The pseudo components are usually taken as the oil and gas phases at standard conditions, and represent lumped hydrocarbon components (methane, ethane, propane etc.). They form the two constituents of the oil and gas phases which are functions of pressure and temperature. The simplest hydrocarbon model, the black oil model, assumes that gas can dissolve in oil, but not vice versa, i.e. the gas phase contains only the gas pseudo-component, whereas the liquid phase contains both oil and gas pseudo components. The volatile oil model is a slightly more complex model in which both pseudo components can be present in both phases. Finally, a fully compositional model can be used in which the mass

flow rate of each individual hydrocarbon component is tracked. Such a compositional analysis is unusual for wellbore flow simulation, unlike what is customary in chemical engineering. However, currently there are groups in the petroleum community working towards the development of compositional well modelling.

Two-phase flow of gas and liquid (in which the oil-water mixture is effectively treated as a single phase), or three- phase flow of gas, oil and water, can be simulated at various levels of sophistication. More details about different approaches for wellbore modelling is presented in chapter 3. In this thesis a dynamic multi-phase transient wellbore simulator, OLGA, was used in chapters 3 and 8 to study clean-up and well test in advanced wells completed with different flow control devices.

2.5 Summary

This chapter provided an introduction into the advanced well completion technology. Different elements of I-wells including FCD types, in-well gauges and sensors and AFI were described. This knowledge will be used throughout this thesis where some aspects of the modelling and real-time monitoring of I-wells are studied.

The control and monitoring capabilities of an I-well provide an opportunity to optimise zones' and wells' production. However, quantifying and delivering the potential added value from I-wells depends on taking advantage of all the state-of-art technologies installed in them.

I-wells offer the potential for real-time data analysis when their in-well sensors measure different physical properties, such as pressure and temperature. Integrated data analysis combines all these measurements, improves the confidence of the estimated parameters together with the accuracy of the interpretation. This thesis addresses the potential of integrating transient pressure and temperature data for multiple applications, such as reservoir characterisation, completion monitoring and flow rate allocation (Chapters 4 to 8). The performance of I-Wells with different FCD also presents challenges during well clean-up process. This is also investigated by developing an integrated dynamic wellbore-reservoir modelling approach (Chapter 3).

Chapter 3 Dynamic Wellbore and Near-Wellbore Clean-up Modelling in Wells with Flow Control Completion

3.1 Introduction

Clean up is an important stage in well's life, the efficiency of which affects both the short and long-term well performance. This chapter presents a comprehensive analysis of the well performance during clean-up when the well is equipped with different FCDs such as passive ICDs, active ICVs and autonomous AICDs/AICVs. Few studies have investigated this important aspect for I-wells. Clean-up modelling is especially important in wells equipped with the relatively new AFCDs. This device is designed to spontaneously react to the presence of water and/or free gas. The performance of an AFCD completion during the clean-up stage will be restricted when both the wellbore and the near-wellbore zone can be saturated with drilling and/or completion fluids. Accurate analysis is required to sufficiently remove this saturation.

Clean-up is a transient process rather than a steady-state. An integrated, coupled wellbore-reservoir, dynamic simulation is required to capture all the physics involved. This comprehensive modelling workflow cover the entire process from formation damage and mud cake formation by the filtrate invasion to flow back period during which lift-off of the mud-cake occurs. The performance of different FCD completion designs are modelled and verified using published data. This is followed by studying the role of the FCD type in the clean-up process. Finally, a discussion on how to possibly improve the FCD completion clean-up is presented.

3.2 Formation Damage and Clean-up Background

This section aims to provide the background on how formation damage is created during a well intervention and the methods employed to clean-up the wellbore and the near wellbore formation from drilling /completion fluids and different mud cake types.

3.2.1 Formation Damage

Formation damage is defined as impairment of the effective permeability of petroleum bearing formations by various adverse processes associated with the well construction and operation. Any unintended impedance to the flow of fluids into or out of a wellbore is referred to as Formation Damage [37]. This is an undesirable operational and economic problem that can occur during all well operation such as drilling, completion, stimulation, production, injection,

etc. For example, mud, mud filtrate and completion fluids are lost to the formation during the overbalanced drilling and well completion process *(Figure 3-1)*. Such invasion of fluids and solids alters the near-wellbore formation properties resulting in e.g. relative permeability reduction and, consequently, reduction in well productivity.

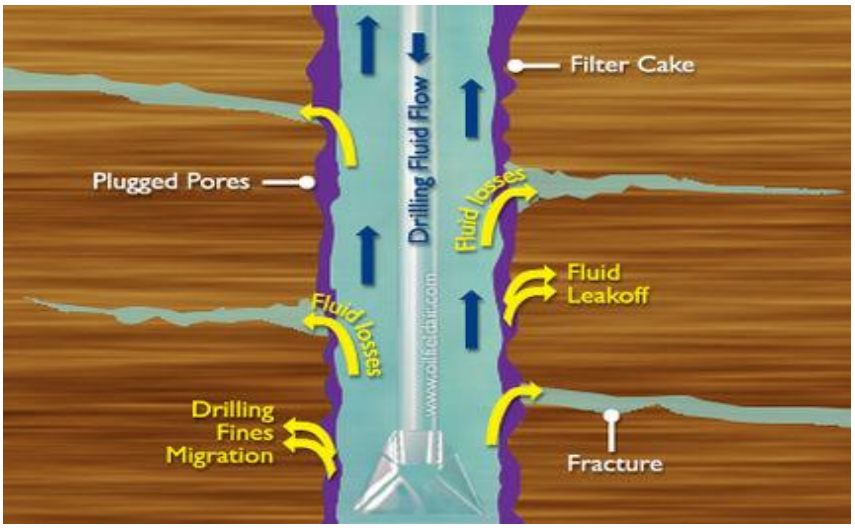

Figure 3-1- Formation damage during overbalanced drilling (www.airdrilling.com)

As shown in *Figure 3-2*,the dynamic process of fluid loss occurs during the following stages *([38]):*

1. *Spurt loss*

   This period happens as soon as the drilling bit comes in contact with the reservoir. There is a nearly instantaneous loss of mud to the formation while the filter cake is being formed.

2. *Dynamic Invasion*

   In this period the mud cake is forming and becoming thicker. The filtrate-loss rate is often decreasing approximately as unity over square root of elapsed time. The filter cake will also be eroded if drilling fluid is being circulated. The process is now called cross-flow filtration.

3. *Static Invasion*

   When the drilling process is finished, filtrate invasion can continue due the over balanced wellbore pressure. The thickness of the external mud cake also keeps increasing during the static invasion due to the absence of shear stresses from wellbore

flow. This static filtrate invasion is normally slower than during the preceding periods since the filter cake is no longer being eroded.

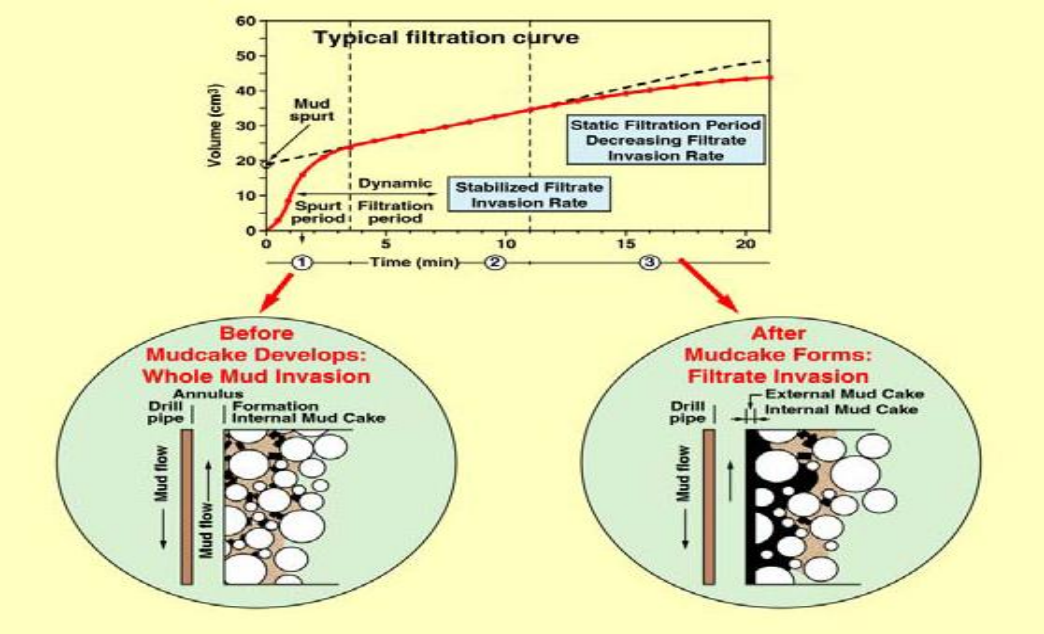

Figure 3-2 Drilling fluid invasion and filter cake formation [36]

The level of formation damage in the reservoir can also be affected by the well completion type and well geometry. For example, formation damage in horizontal wells is more severe than vertical ones. This is due to the fact that the horizontal wells have greater exposure to reservoir, they often cross multiple formations. Also, a higher over balanced pressure and longer time is required to drill them. As for the well completion, the productivity loss in open hole formations is often greater than in the cased hole completion where the damage zone maybe bypassed by the perforations [38].

3.2.2 Well Clean-up

Well clean-up is the process of removing drilling and completion fluids from the wellbore and formation as well as removing the external and internal mud cake. Effective clean up can result in an increase or even complete restoration of the permeability in the damage zone; maximizing the well productivity. On top of this, it is often important to clean up the well fast to save the rig time. As for the wellbore, ineffective clean-up of the drilling and completion fluids can result in stagnant mud or completion fluid in the lower sections of the well which can cause back-pressure and lower inflow rate. Well productivity and subsequently oil sweep efficiency

can both be significantly reduced. From the wellbore flow point of view, the common clean-up methods include:

- ***Natural Clean-up***

This process uses the pressure difference applied between the reservoir and the wellbore during production to remove the filter cake. When this pressure is large enough the external cake can be lifted and flow is initiated to further clean up the wellbore and the damage zone.

- ***Clean-up assisted by Artificial Lift***

This method includes artificial lift (either permanent or temporary, e.g. coiled tubing-conveyed), like Gas lift or ESP, to increase drawdown. This also assists the low productivity zones to start and speed up their clean up. Other well clean-up methods using acids, breakers, chemicals etc are outwit the scope of this thesis and will not be considered further. This study aims to investigate the role of advanced wells completed with different FCDs in the clean-up. As described earlier, the main idea of FCDs is to restrict flow by imposing extra pressure drop and thereby making the production along the completion more uniform; delaying unwanted water and gas breakthrough and improving the sweep efficiency[37]. This restriction imposed by an FCD might have positive or negative effect on well clean-up, hence it is a subject requiring further analysis.

There are few studies in the literature addressing clean up in FCD completion. For example, Al-khelaiwi et al(2009*)* [39] and Olowoleru et al(2009) [40] showed the role of ICDs and ICVs in facilitating and accelerating clean up in different reservoir scenarios. Kerem [41] also reported the advantage of using ICVs in long horizontal wells as compared to conventional wells in a real case study. Gottumukkala (2009) [42] discussed experience of cleaning an ICD-completed well. This work contributes to these previous studies by analysing the well clean-up performance of autonomous, passive as well as active FCDs. It focuses on the impact of fluid flow in complex completion designs and well trajectory. The integrated dynamic reservoir-wellbore modelling will be used to simulate the entire process from filtrate invasion to flow back. It should be noted that this study mainly focuses on clean-up in conventional reservoirs, more information about clean-up in unconventional low permeability reservoirs can be found in Jamiolahmady et al (2014) [43] where the effect of capillary pressure and relative permeability is also investigated.

3.3 Formation Damage and Clean-up Modelling

Well clean-up is a transient process. Hence its simulation requires a suitable tool that can handle the physics of transient reservoir inflow, multiphase wellbore flow, simultaneous flow of hydrocarbons and mud, etc. *Figure 3-3* shows the time scale of the dynamic interaction between the reservoirs and the wellbore during clean-up. An integrated model clearly is essential for this type of study.

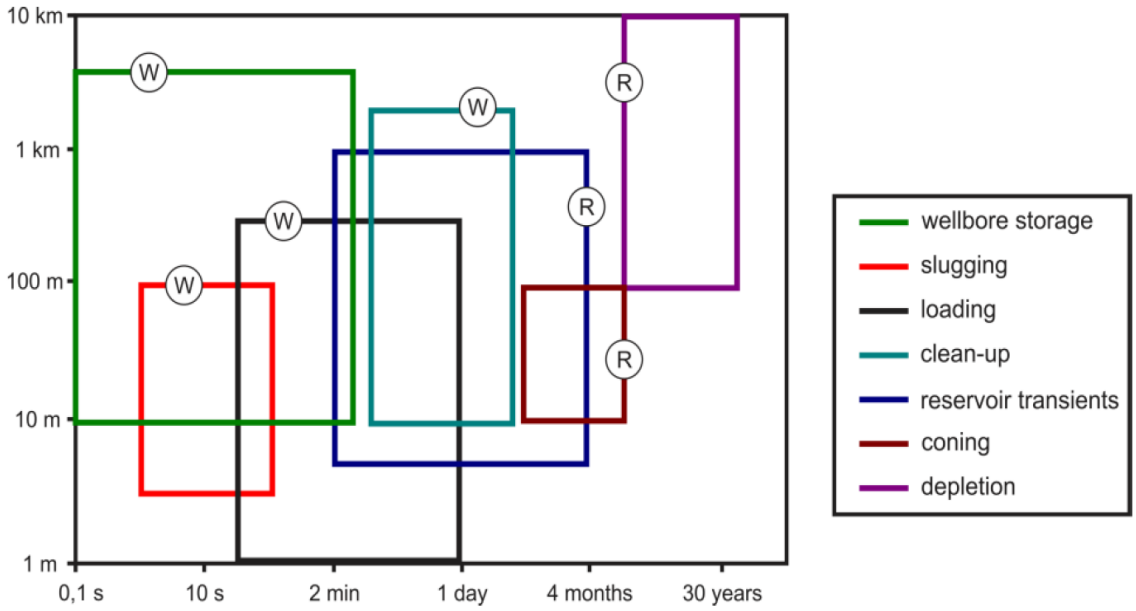

Figure 3-3 Time and Spatial scales for well (W) and Reservoir (R) processes ([44])

Clean-up studies in the literature have been modelled using two approaches *(Table 3-1):*

1. Type 1 studies focused primarily on the near-wellbore clean-up and on the removal of the external and internal mud cake [38] . Wellbore or completion flow modelling was not included in these studies since only a dynamic reservoir simulator was employed.
2. Type 2 studies concentrated on the wellbore clean-up [39, 41]. The main drawback of these studies is that the dynamic reservoir flow model was not coupled to the dynamic well flow model. The dynamic integration between the wellbore and reservoir was ignored (or implicitly included).

Table 3-1 Comparison of FCDs's clean-up study modelling approaches

		Filtrate Invasion Process	**Formation Damage** **Near-wellbore Clean-up**	**Completion Fluid &** **Wellbore Clean-up**	**Example of Previous studies**
1	Dynamic Reservoir + Steady/Semi Steady-state Wellbore (e.g. Eclipse+ Multi segment Well)	✓	✓	×	(Ding, 2002) (Al-khelaiwi, 2009) (Olowoleru, 2009)
2	Semi Transient Inflow + Dynamic Wellbore (e.g. Constant/variable PI+ OLGA)	×	✓ (except autonomous FCDs)	✓	(Al-khelaiwi, 2009) (B Hu ,2009) (Kerem, Proot,2008)
3	Dynamic Reservoir + Dynamic Wellbore (e.g. ROCX+ OLGA)	✓	✓	✓	This study

By contrast, in this chapter an integrated near-wellbore and wellbore clean-up is simulated using a dynamic, coupled wellbore-reservoir modelling approach. A dynamic transient commercial wellbore simulator, *OLGA*^{TM}, is coupled with a reservoir simulator, *ROCX*^{TM} to fully capture the dynamic and transient interaction between reservoir and wellbore during clean-up.

The clean-up modelling approach in this chapter involves two steps: the first step is to model the actual filtrate invasion and mud cake formation process taking place during drilling and completion, followed by modelling of the wellbore/near wellbore clean-up during the flow back period.

3.4 Integrated Wellbore-Reservoir Modelling with OLGA-ROCX

The integrated wellbore-reservoir modelling approach, using *OLGA-ROCX*, has been used for a wide range of transient problems in the literature. This includes flow rate allocation in I-wells [46], well testing[47, 48] , well shut-in/start-up[47, 49] , liquid loading in gas wells[50] , gas-lift and gas coning[47] etc.

In the following first a brief description of each simulator and the integrated approach are presented and then details of each step in the clean-up modelling are described ;

3.4.1 Wellbore Model (OLGA)

In the Petroleum Engineering context, wellbore pressure can be modelled using the following approaches *(Figure 3-4)*;

1. **Empirical correlations:** are based on the curve fitting of experimental and/or field measured data. Their applicability is generally limited to the range of variables explored in the experiments. These correlations can be either specific for each flow pattern or can be flow pattern independent.
2. **Homogenous models:** assumes that the fluid properties can be represented by mixing the single-phase properties and the single-phase flow equations can be applied to this mixture. These models can also allow slip between the phases; requiring the use of several empirical parameters. Homogenous models with slip are called drift-flux models. e.g. the multi-segment well model option used for modelling advanced well completions in Eclipse ^{TM} black oil and compositional reservoir simulator uses the drift-flux approach.
3. **Mechanistic models:** The models based on the physics of multi-phase flow patterns. OLGA uses this approach for wellbore modelling.

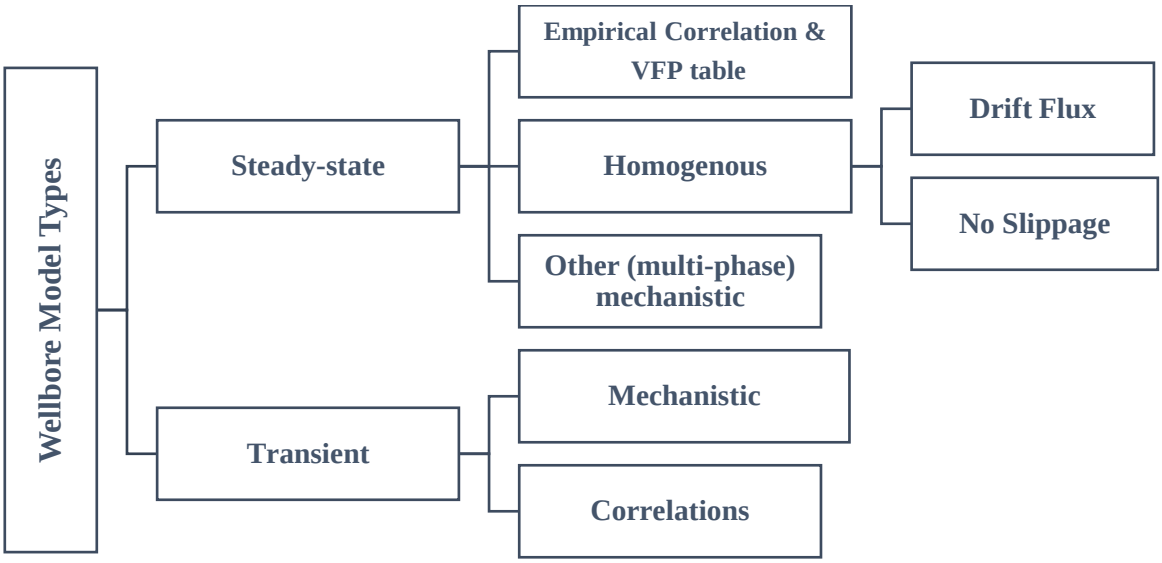

Figure 3-4 Possible wellbore modelling approaches

This wellbore modelling tool (OLGA) first proposed by *Bendiksen et al (1991)* [51] is capable of simulating transient three-phase gas-oil-water flow in pipes . At each time step, a set of five coupled mass conservation equations are solved respectively for gas phase, the water droplets, the oil droplets, the oil film and the water film. Three momentum equations are also solved for (1) the gas/droplet field, (2) the oil bulk and (3) the water bulk and one energy balance equation

are solved for the fluid mixture. The above assumes thermal equilibrium among all the phases at the same location in the wellbore. [52]

Another useful feature of OLGA is its capability to model transient co-flow of the reservoir fluids and the drilling or completion fluids. This feature makes it possible for the well clean-up process to be modelled. Such fluids, including diesel and brine, are assumed to be miscible with the produced oil, water or gas phase. Slip is not allowed between miscible phases, but is allowed with slip to the other, non-miscible phases.[53]

3.4.2 Reservoir model (ROCX)

The model first described by *Sagen et al (2007)* [49] is capable of simulating transient three-phase oil-gas-water Darcy flow in porous media .The flow equations can be solved in 1 , 2 or 3 dimensions, giving as output the of saturations and pressure varying in space and time. The model solves fully implicitly the oil, water and gas mass conversation equations plus the energy balance equation using the Newton-Raphson method at each time step.

3.4.3 Integrated Model (OLGA-ROCX)

The reservoir model (ROCX) is a plug-in to the well model (OLGA), hence the integrated simulation is fully controlled by the well model. The numerical coupling between the two models is implemented in an implicit scheme as outlined below [49] :

Step 1: the wellbore model starts integration to time step n+1 by requesting the reservoir model to calculate the a_i and b_i coefficients defined in equation 3-1:

$$Q_i^{n+1} = a_i P_{bh,i}^{n+1} + b_i \qquad 3\text{-}1$$

Where $P_{bh,i}^{n+1}$ is the pressure in the relevant control volume in the pipeline model and Q_i^{n+1} is the mass flow rate for each phase. The explicit method is a special case of the implicit coupling setting $a_i = 0$ and leaving b_i equal to the flow rate from the reservoir simulator.

Step 2: The wellbore model uses the above equation as a boundary condition and solves the complete flow network. The pipeline model then completes time step n+1 and returns $P_{bh,i}^{n+1}$ and Q_i^{n+1} back to the reservoir simulator.

Step 3: The reservoir model completes the time step by using the computed values from the wellbore model as boundary conditions.

3.5 Formation Damage and Clean-up Modelling

The described integrated modelling approach is used to chronologically model formation damage and subsequent clean-up. The simulation steps include filtrate invasion, external and internal mud cake formation removal and permeability restoration. Moreover, advanced well completions with different well trajectory and FCD types can also be incorporated into the models. Before describing each step, some details on the reservoir model and also main assumptions used in this study is presented below;

As mentioned before the reservoir models in this study were built by a near wellbore simulator, ROCX. The reservoir was discretised into 22 grids in x and y and 9 grids in z direction where Local Grid Refinement (LGR) was also used for better representation of near wellbore changes during both clean-up and flow back periods. Homogeneous reservoir with no flow boundaries considered, some other parameters listed in *Table 3-2.*

Porosity(dimensionless)	0,2
Heat Conductivity (w/m k)	1,59
Heat Capacity (J / Kg K)	1256
K_x(md)	100
K_y(md)	100
K_z(md)	5
S_{or} (dimensionless)	0.1
S_{wi} (dimensionless)	0.1
P_i(bar)	250
T (C)	60

Table 3-2 Reservoir Parameters

In order to simplify the problem and also mainly focus on the objective of this chapter, which is about the performance of different completions during flow back period, the following main assumptions have also been taken into account;

1. Although ROCX simulator was initialised with relative permeability curve shown in *Figure 3-5* and end points of capillary pressure, the effect of hysteresis phenomena during invasion and flow back was not included here. Not using the corresponding relative permeability and capillary pressure information for filtrate invasion and flow back period might affect the depth of invasion and/or recovery of the invaded filtrates during production phase (for more on this refer to Jamiolahmady et al (2014) [43]).

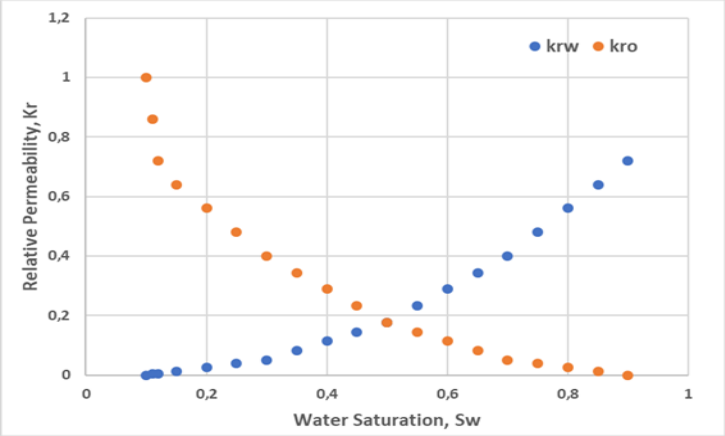

Figure 3-5- Relative Permeability Curve used for Simulation

2. The effect of internal mud cake was implicitly modelled by absolute permeability reduction and it is assumed that the changes uniformly distributed near wellbore. This could be more accurately modelled by limiting permeability reduction to only invaded region in the model.
3. It was assumed that the mud cake debris do not plug FCDs' nozzle during the production

3.5.1 Filtrate Invasion Process

This study models water injection (assuming the mud is water based) into a gradually opening (drilled) wellbore to model the mud filtrate invasion process **(***Figure 3-6***)**. Mud cake formation and filtrate invasion in the near wellbore region can thus be related to the drilling rate of penetration (ROP). In this study ROP is assumed to be 400 ft/day and the overbalance pressure of 400 Psi is also imposed to mimic overbalanced drilling *[51]*.

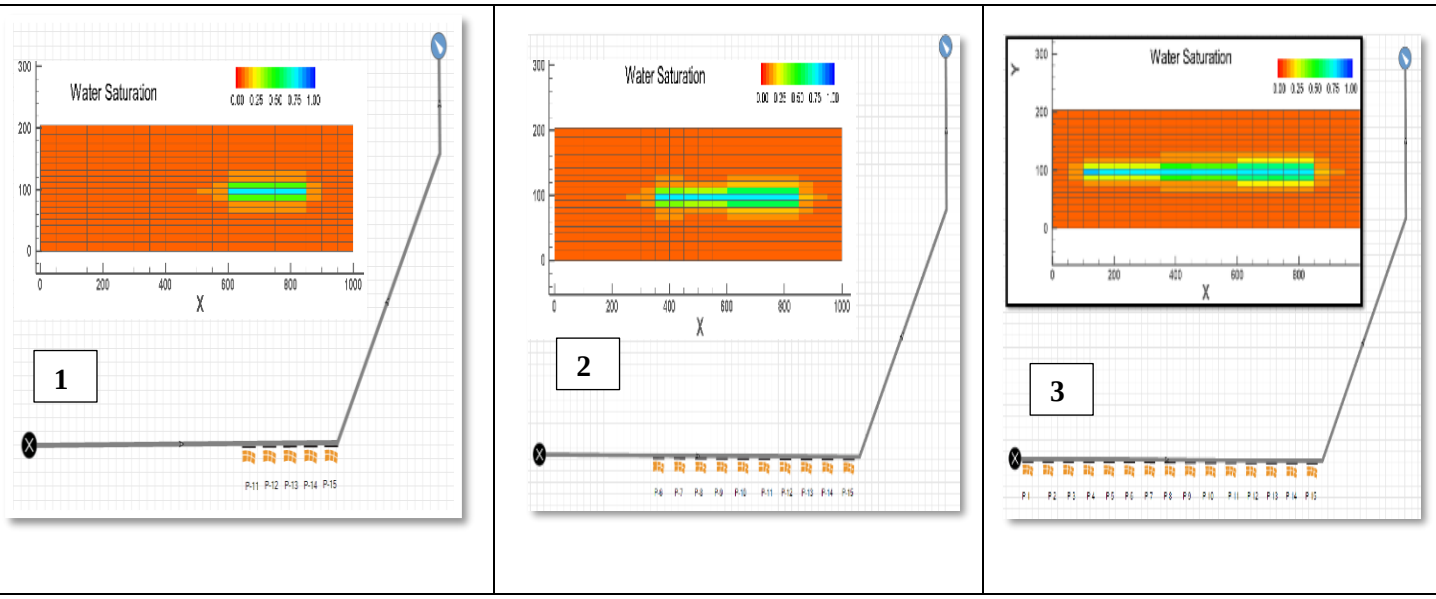

Figure 3-6 Filtrate invasion modelling - Saturation Profile

Figure 3-6 (from right to left) depicts the cone shaped the water invasion profile in the x-y plane. This cone is elliptical in the y-z plane due to the vertical permeability being smaller than the horizontal value. These results are consistent with other studies *[54]*.

It should be noted that after modelling the invasion process of each zone, their restart file was used for next zone's simulation and finally once the entire process of filtrate invasion(drilling) had completed, the flow back simulation has started from the last time step of the invasion model. By doing so the near wellbore changes during the invasion process was considered as an initial condition for flow back simulation. *Figure 3-7 shows how* heterogeneity can affect the pattern of invasion.

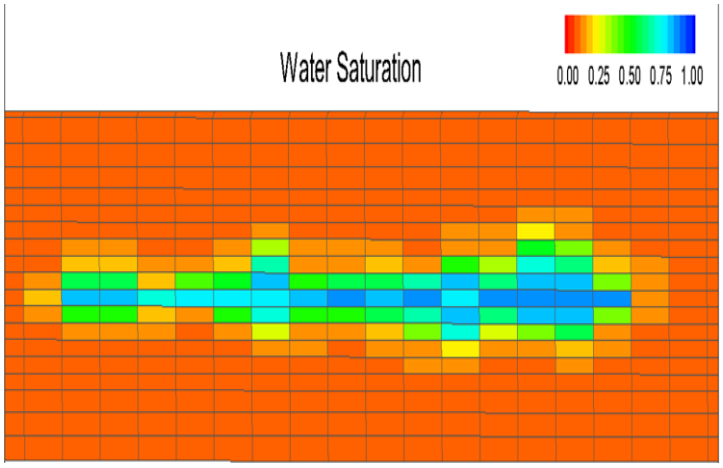

Figure 3-7 Effect of heterogeneity on filtrate invasion

3.5.2 Mud Cake Formation

The second parameter for formation damage simulation is modelling the mud cake formation. External and internal mud cakes in this study were modelled implicitly by introducing a time-dependent reduction of the permeability in a thin layer around the wellbore. We assume the virtual mud cake thickness formation grows at an initial rate of 1mm/hr, decreasing exponentially to a plateau *[55]*. The mud cake thickness controls the fluid loss rate. A thicker mud cake can thus have a positive effect on clean-up by reducing the volume of mud filtrate invades into the reservoir.

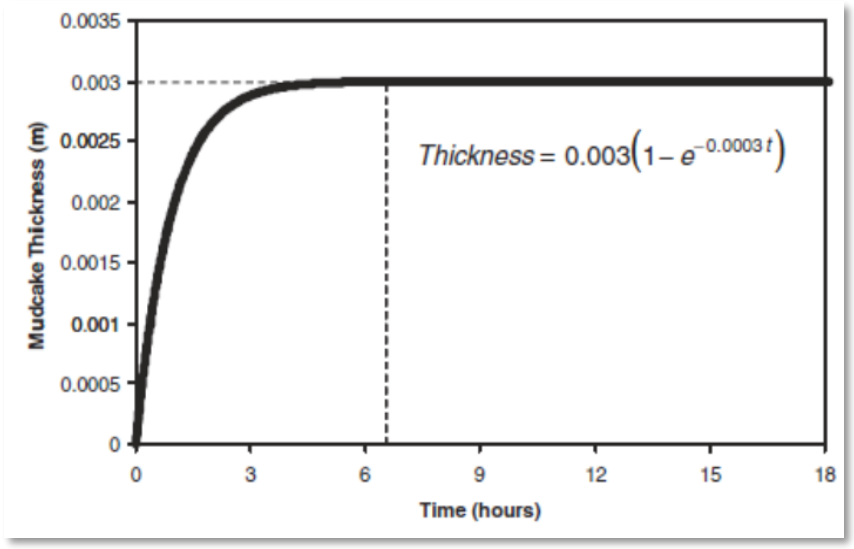

Figure 3-8 Variation of mud cake thickness with time ([55])

3.5.3 Lift-off Pressure

The mud cake lift-off pressure is defined as the pressure differential needed to remove the external mud cake. This parameter can be measured in the laboratory, it depends on the rock properties and the type of mud used *[56]*.

3.5.4 Retained Permeability

The return permeability factor is defined as the ratio of the stabilised, damage zone permeability, k_d measured after the majority of the mobile mud filtrate has flowed back, to the initial formation permeability k. It is, among others, a function of the pore throat size and mud cake particle size but may also be estimated by core tests. This example study assume a return permeability of 80% of the original value to account for the permanent reduction due to the presence of an internal mud cake [39].

3.5.5 Post Drilling Modelling

After the drilling process is finished, the wells, which are mainly horizontal, deviated and undulated wells in this chapter, are completed open hole with FCDs. An open-hole completion is modelled in this study because it is common for advanced well completions and outlines the main challenges of the well clean up discussed in this chapter: mud cake removal, filtrate flow back, etc. The length of the horizontal section for most the cases in this chapter is 750 meter, divided into different zones. *Figure 3-9* shows the lower completion (the FCD completion annulus and tubing) is filled with the completion fluid(brine) while the upper completion (the

tubing) contains diesel (more details on the wells model presented in *Appendix A*). *Table 3-3* lists the properties of these fluids:

Table 3-3 Completion fluid properties

Completion fluids	Density (kg/m^3)	Viscosity (CP)
Brine	1100	1
Diesel	819	10

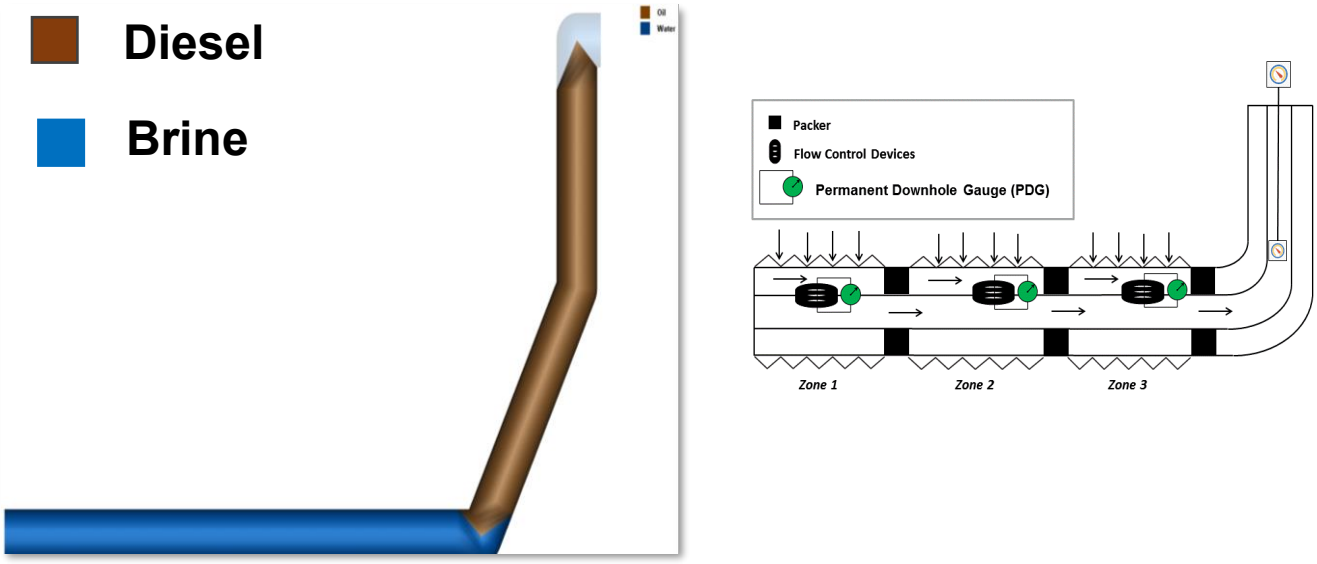

Figure 3-9 Wellbore completion schematic view and the location of completion fluids at the beginning of clean up

3.6 Modelling Flow Control Devices

In the following the modelling approaches are presented that are also employed throughout this thesis, e.g. in chapter 8, to simulate the FCD completion performance.

3.6.1 ICD and ICV Modelling

The ICD-equipped completion is modelled as one equivalent, 'up-scaled ICD' per zone with a diameter equal to the inflow area of all the individual ICDs installed in the zone at every tubing joint [57, 58]. A single ICV per zone is also modelled similarly. The main difference is that the ICVs' opening area can be changed through a controller while the ICD area is fixed throughout the simulation. The pressure drop for ICDs and ICV is calculated using the Bernoulli equation,

$$\Delta P = \frac{C_u \rho_{mix} q_{ICD}^2}{2 C_v^2 A_c^2} \qquad 3\text{-}2$$

where $\rho_{mix} is\ the$ mixture density, A_c is the ICD/ICV opening area, C_v is the discharge coefficient, q is the flow rate and $C_u$is a conversion constant

3.6.2 AICD and AICV Modelling

AICDs and AICVs can be modelled as a valve with the variable opening area based on the current zonal water-cut (or sometimes on hold-up) of the fluid flowing into the valve from the zone's annulus. OLGA does not offer an AFCD modelling option, nor does it provide the necessary flexibility to add an equation describing the devices performance. Therefore, a table, relating the water cut to the area open to flow must be incorporated into the wellbore simulator allowing OLGA to autonomously update the valve performance. There are different ways to generate the tables, including:

1. A formula or a correlation describing the differential pressure across the installed AFCDs.
2. Experimental results.

Both methods have been used, and the results compared, to model the performance of AFCD completion;

- **Method 1 (suitable for AICDs)**

Equation 3-2 is used to relate the pressure drop across an AFCD to the fluid flow rate and properties:

$$\Delta P = \left(\frac{\rho_{mix}}{\rho_{cal}}\right)\left(\frac{\mu_{cal}}{\mu_{mix}}\right)^{y} \alpha_{AICD} q^{x} \quad 3\text{-}2$$

Where α_{AICD} is strength of the AFCDs , x is the volumetric flow rate exponent , y is the viscosity function exponent , ρ_{mix} and μ_{mix} are the volumetric average of fluid density and viscosity respectively and ρ_{cal} and μ_{cal} are the calibration fluid's density and viscosity respectively.

The workflow presented by *Eltaher et al [58]* is adopted to calculate the coefficients of this equation. The AFCD strength, α_{AICD} ,and viscosity component y are calculated for the oil/water system and a table of water cuts versus the AFCD's opening area is generated for each valve:

Table 3-4 AFCD open area versus water cut (Method-1)

Water Cut	0	0.1	0.2	0.3	0.4	0.5	0.6	0.7	0.8	0.9	1
AFCD Opening Area (Fraction)	1	0.90	0.79	0.69	0.59	0.49	0.39	0.29	0.19	0.09	0.02

- **Method 2 (suitable for AICVs)**

In this approach the inflow area of the AFCDs installed in a zone are (nearly) closed sequentially based on the water cut. *Table 3-5* describing the overall zonal performance was generated based on the *Aakre, Halvorsen [59]* workflow for modelling the AICV completion zone's performance. Note that the flow area of a "closed" AICV is 2% of an "open AICV".

Table 3-5 Example performance of a group of 8 AFCDs in a zone versus the zones' water cut (Method-2)

Number of valves fully open	Number of valves closed	Annulus water cut of a zone
8	0	wc<0.12
7	1	0.12<wc<0.14
6	2	0.14<wc<0.16
5	3	0.16<wc<0.2
4	4	0.2<wc<0.25
3	5	0.25<wc<0.33
2	6	0.33<wc<0.5
1	7	0.5<wc<0.98
0	8	wc>0.98

Method 2 is usually used to model AICVs which have an aggressive reaction to unwanted fluids whereas the model 1 is more suited for modelling AICDs.

- **AFCD modelling result comparison**

Figure 3-10 compares the results of AICD and AICV modelling for a single-zone deviated well, with the toe down and 8 AFCDs installed along the completion. AFCD-1 is installed at the toe of the well and AFCD-8 at its heel. The well produces the fixed liquid flow rate with a water cut of 40 percent. The well has already been cleaned up.

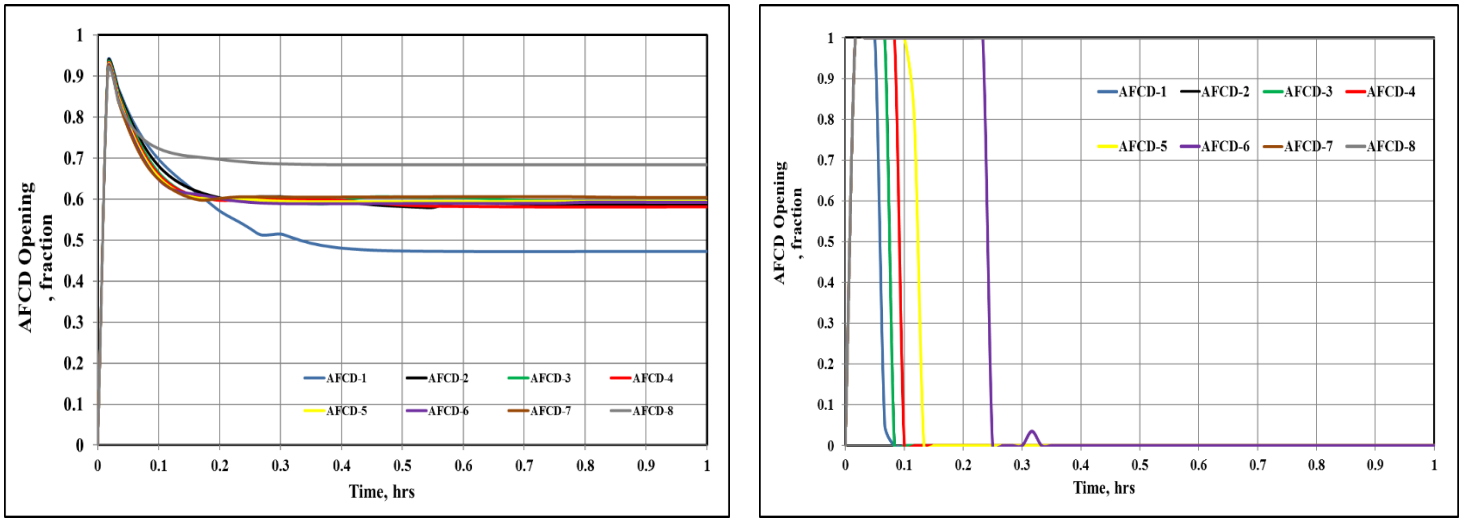

Figure 3-10 Composition between the result of AFCD modelling: Methods-1 (left) and Method-2(right)

The figures show that for AICV modelling, the devices are closed sequentially based on the tabulated input in *Table 3-5*. AFCD-1 will be the first to accumulate water due to the well trajectory (the toe is deeper than the heel). This zone will be first to close. In contrast, an AICD completion is modelled with the devices restricting the water production. The performance of an AFCD completion during the clean-up process will be discussed later in this chapter.

3.7 Clean-up in Conventional Wells

In a homogenous reservoir, the drawdown and flow contribution in the heel section of a horizontal well can be much higher than that in the toe due to the pressure losses experienced along the wellbore from heel to toe (i.e. the heel-to-toe effect HTE). This complicates the efficient wellbore clean-up since a minimum differential pressure required to lift off the mud cake and consequently enable flow back the filtrate from the toe might not be sufficient. The heel section may clean up first and start producing which results in further restricting the toe's clean up. This conclusion can be extended to heterogeneous reservoirs as well where flow from a channel or high permeable layer can be dominated in both clean up and production phases.

Figure 3-11 shows irregular wellbore clean up caused by uneven inflow from different zones along the completion. This results in reducing the clean-up efficiency as well as prolonging the clean-up process; decreasing the well's productivity and potentially longevity. Also, the allowable, maximum drawdown of a horizontal well is often limited by the maximum flow rate, sand production, wellbore stability limits, etc.

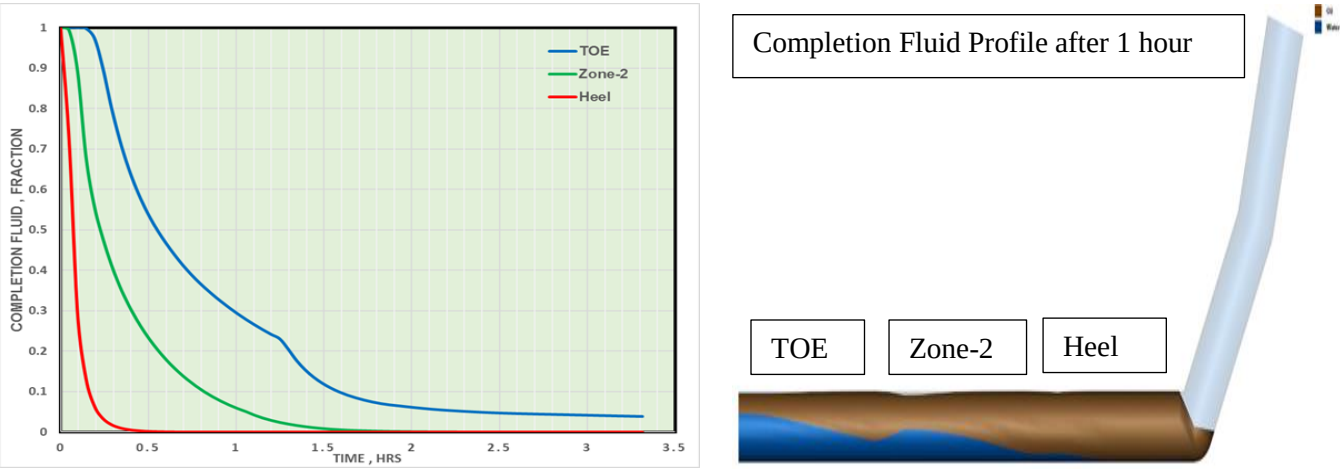

Figure 3-11 Zonal completion fluid fraction (Zero lift-off pressure)

3.8 Clean-up in Advanced Wells

3.8.1 ICD Completed Wells

As mentioned previously, the ICDs impose an extra pressure drop to make the inflow distribution more uniform and therefore mitigate the production-related problems in conventional ERWs. The effect of the ICD completion on clean up can be in two ways:

- The ICD reduces the reservoir pressure draw down at the required for production due to the flow choking effect
- On the other hand, the ICDs make the inflow profile more uniform by restricting the productivity of the heel and higher productivity zones; allowing greater drawdown at the toe and, consequently, an improved clean-up of the production interval.

Therefore, optimum ICD design is a trade-off between the advantage of equalizing the inflow along the completion against the disadvantage of reducing the drawdown pressure available.

Figure 3-12 compares the differential pressure achieved in a three-zone ICD-completed and conventional wells (called 'NO-ICD' case). The mud-cake lift-off pressure value of 75 Psi is assumed. We assume the mud cake debris break-up and flow through the screens without plugging them. The required lift-off pressure at the toe of the conventional well is higher than the achievable reservoir draw-down while for the ICDs-completed well the sandface drawdown is more uniformly distributed. In the ICD case, the returned completion fluid fractions for all three zones are for the ICD completion similar. However, for the openhole case the higher

production from the heel results in earlier removal of its external mud cake; increasing the contribution from this zone. The flow from the toe zone is much smaller; delaying its clean-up also preventing the speedy recovery of the completion fluid that had leaked off into this zone.

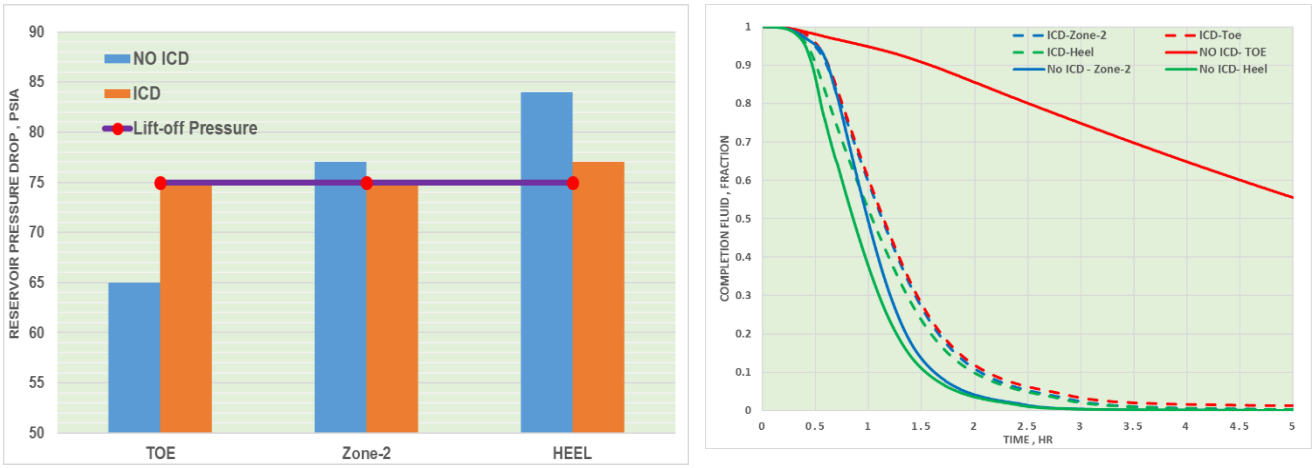

Figure 3-12 Effect of lift-off pressure on the conventional and ICD-equipped completions clean up

3.8.2 ICV Completed Wells

The benefit of clean-up of ICV-completed wells is that they allow sequential control of zonal flow. Limiting the clean-up to a zone rather the whole completion interval ensures a higher differential pressure is available for mud-cake lift-off. This makes it certain that the pressure drop exceeds the lift-off pressure and, consequently, the external mud cake of each zone is removed.

The main challenge, however, in this type of FCD completion is to choose the order in which the ICVs should be opened and how long it is necessary to produce each ICV zone to minimize the clean-up time. This is explained together with a zone performance monitoring method proposed in *Olowoleru, Muradov 2009 [40]* .

3.8.3 AFCD Completed Wells

The performance of the AFCD-completion during the clean-up process can be counterintuitive. During normal production, when the well initially produces oil, the AFCDs are all in the fully open position. Later once the unwanted fluid (water /gas) production increases, the AFCDs begin to restrict/shut the flow. By contrast, at the beginning of the clean-up process the annulus,

tubing and near wellbore formation is saturated with drilling and completion fluids. Production of these low viscosity, e.g. water-based, fluids will immediately reduce the open area of the valves.

Figure 3-13 shows the filtrate invasion profile of a homogenous reservoir with a single-zone well completed with 5 AICD devices, i.e. AICD-1 is placed at the toe and AICD-5 at the heel of the well. The heel section of the well has the highest invaded water volume since it has had longer exposure to the drilling fluid.

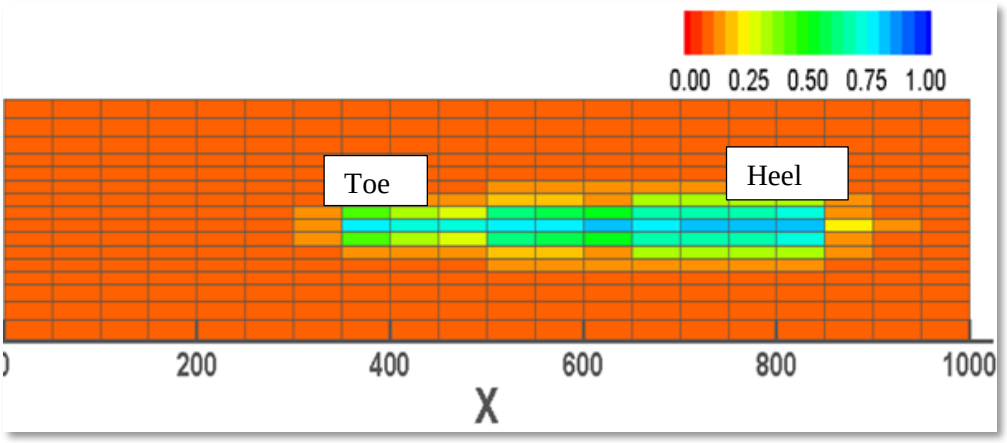

Figure 3-13 Water saturation near the wellbore right after drilling

Figure 3-14 shows the open area of the AICDs versus time. As can be seen the AICD closer to the heel section, AICD-5, opens later compared to the AICD-1 near the toe. This behaviour is due to the greater filtrate invasion at the heel than at the toe. A uniform invasion profile would be expected to have the reverse order due to the greater draw down at the heel. For example, if filtrate invasion profile near the wellbore is not included in the study or an arbitrary pattern for invasion is selected the order of the AICDs clean-up rate would be completely different.

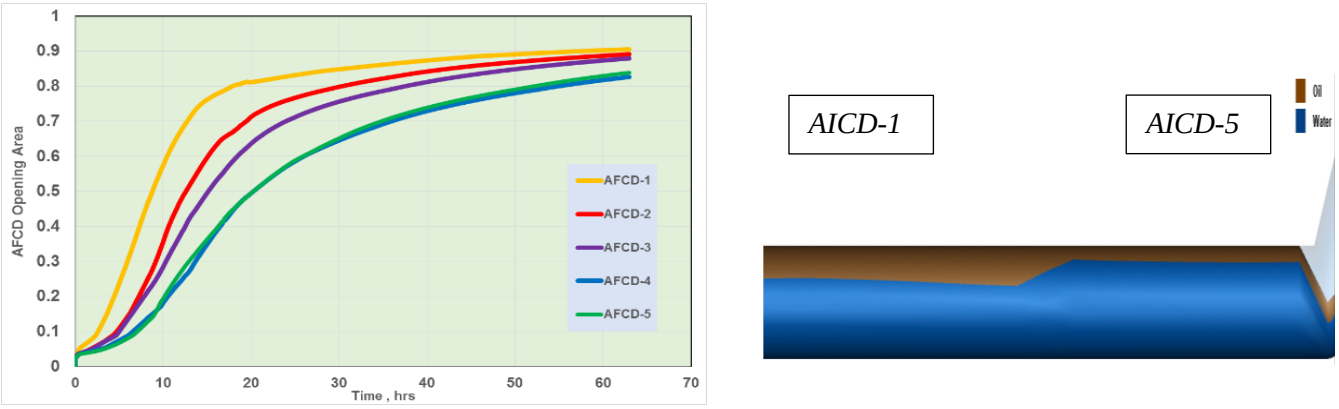

Figure 3-14 AICD equivalent opening area (left), water profile in the well (right)

For instance, if a uniform invasion pattern is assumed the AICD-5 is supposed to open first, as opposed to the current result. However, the opening pattern will be greatly influenced by the well trajectory due to the relatively low rate of clean-up (will be explained in the next section)

3.8.3.1 Effect of Well Trajectory

The well trajectory is also important as no well is perfectly horizontal and some degree of deviation and undulation always exists. The effect of the well deviation is illustrated below in the model consisting of a two-zone well with a packer between them. The wellbore is deviated from 10 degrees from horizontal. Each zone is completed with 4 AICDs and the well is produced at a constant flow rate. Again, the reservoir is first saturated with drilling fluid filtrate. The filtrate invasion profile has been affected by the well geometry with the highest water saturation close to the heel **(***Figure 3-15***)**.

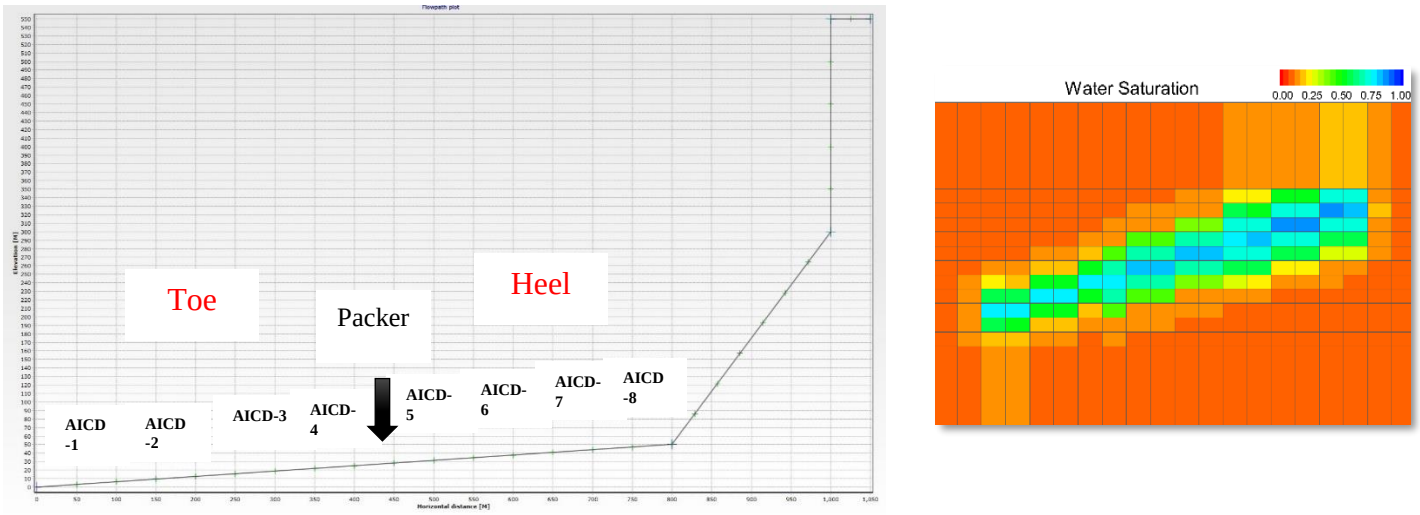

Figure 3-15 Well Schematic (left) and filtrate invasion profile (right)

As shown in *Figure 3-17*, the fastest clean-up happens via AICD-4 located high in the (toe) zone. As a result, this section is cleaned faster, and the valve's flow restriction will be reduced, further promoting flow and clean-up from the toe zone. By contrast, the worst scenario is for the device placed in the heel zone next to the packer where there is a combined effect of higher water saturation as well as water accumulation in the annulus above to packer, which considerably affects the performance of the AICD-completion clean-up.

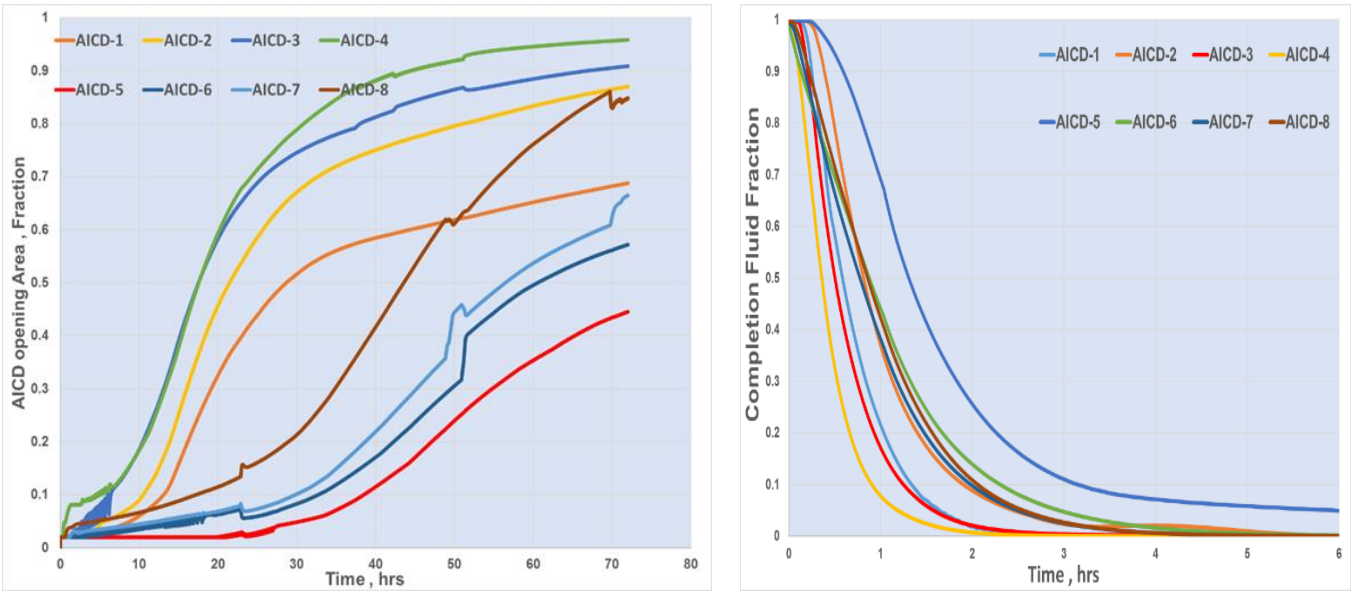

Figure 3-17 Dynamics of the AICDs virtual opening area (left) and the completion fluid fraction in the annulus (right)

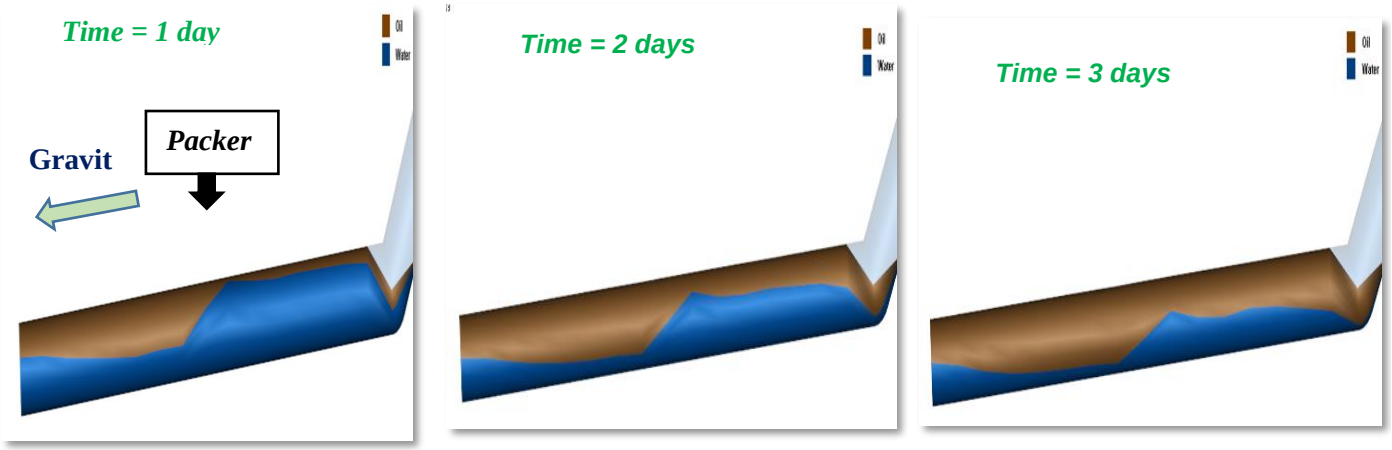

Figure 3-16 Water hold-up in the annulus during clean up

Figure 3-18 compares the clean-up performance of the stand-alone screen (SAS), ICD and AICD completions for the deviated well trajectory (toe-down). As can be seen when the SAS option is used the heel section produces more due to HTE. ICDs being passive are nearly insensitive to the flowing fluid composition, which result in the FCD production, and clean-up in both zones more uniform. By contrast, AICDs are sensitive to water and thus, interestingly, promote the toe zone clean up.

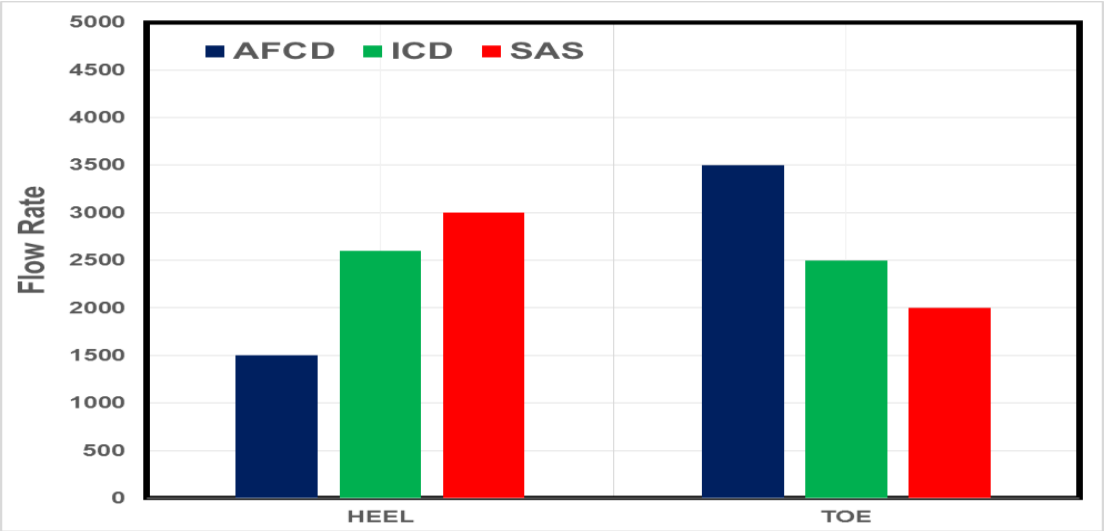

Figure 3-18 Comparison between the upper (heel) and lower (toe) zones' flow rates in FCDs during clean up at the same well production rate

3.9 Clean-up Improvement Strategies

As discussed in the previous section, the clean-up process in AFCD completion is complex and sensitive to a range of conditions. To facilitate and accelerate the clean-up process in these FCDs some mitigation strategies can be proposed.In this section, an undulated well is used to investigate the mitigation strategies in an AFCD completion**.** *Figure 3-19* is the well schematic similar to the real North Sea well trajectory studied by *Kerem, Proot [41]* . They reported that the well toe was not expected to contribute to flow if the well was an open hole completion. Installing three ICVs across zones was expected to solve this problem and bring the complete well into production faster. Our study completed this well with two zones and 4 AICDs per zone **(***Figure 3-19***).**

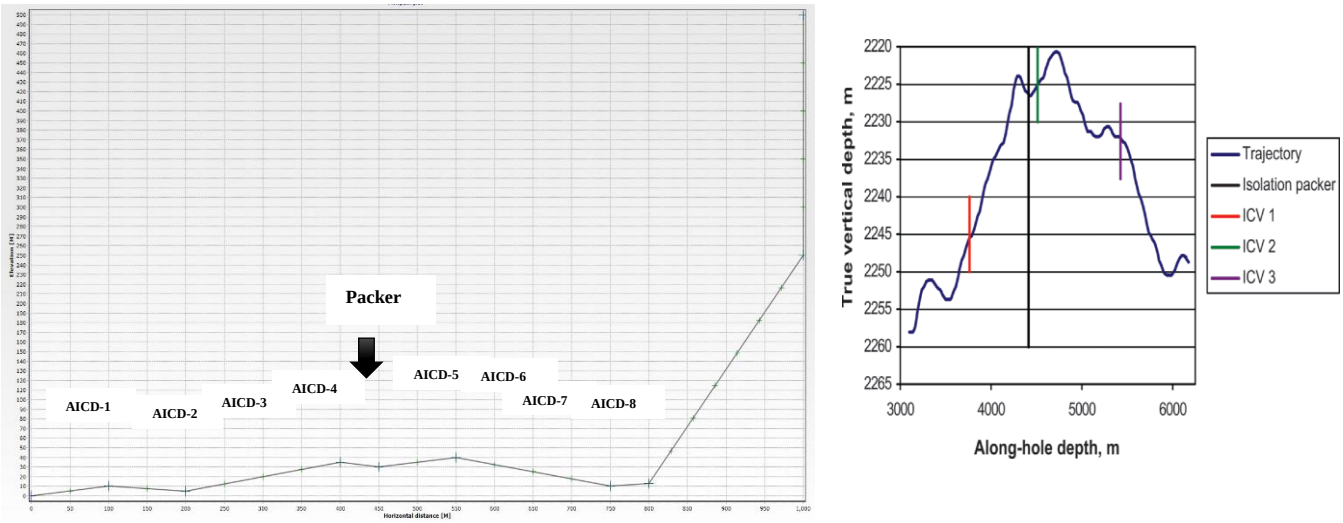

Figure 3-19 Well Schematic view used in this study (left) similar to the real well (right) presented by Kerem, Proot [41]

As can be seen in *Figure 3-20* , there is an interesting dynamic in the virtual opening area of AFCDs along the completion. This is due to the combined effect of the well trajectory of the well segments, with the 'toe up' and 'toe down' effects discussed earlier in this thesis, and the pattern of mud filtrate invasion with the higher volumes of mud and completion fluid filtrate invading at the heel compared to the toe. In addition, oscillation of the AFCD open areas is observed, e.g. in AFCD-5 and AFCD-7, which is due to the interaction between the adjacent valves and changes in the composition of the fluid flowing through the AFCDs.

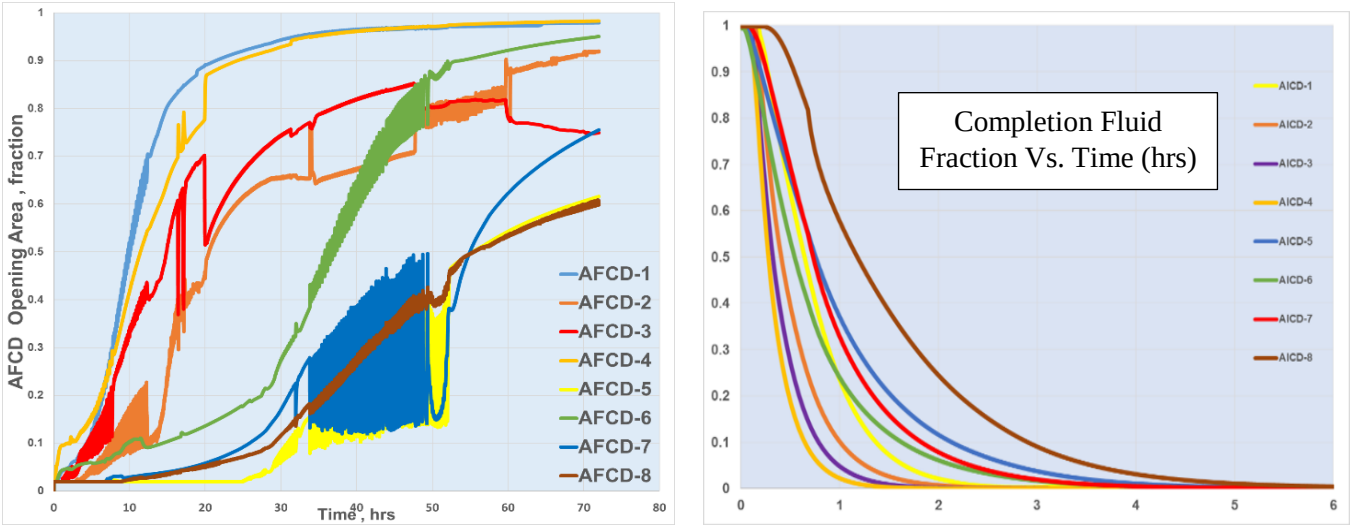

Figure 3-20 AICD opening area (left) and completion fluid fraction in annulus (right)

As a result, the total open area of the AFCDs at the heel is generally smaller than in the toe. Clean-up will be delayed for a well completed with AFCDs. The following section examines mitigation methods to accelerate and facilitate clean-up for this well.

3.9.1 Viscosified Brine or Viscous Mud

AFCDs are designed to operate based on the flowing fluid's property differences. As the viscosity of water or gas is normally less than oil, particularly heavy oil, the valve is designed to restrict the flow of the less viscous fluid. Therefore, one mitigation to improve AFCD-completion clean-up is to replace lower viscosity water-based completion or drilling fluid with viscous or viscosified fluid as discussed in *Nugraha et al, 2016 [60]*.

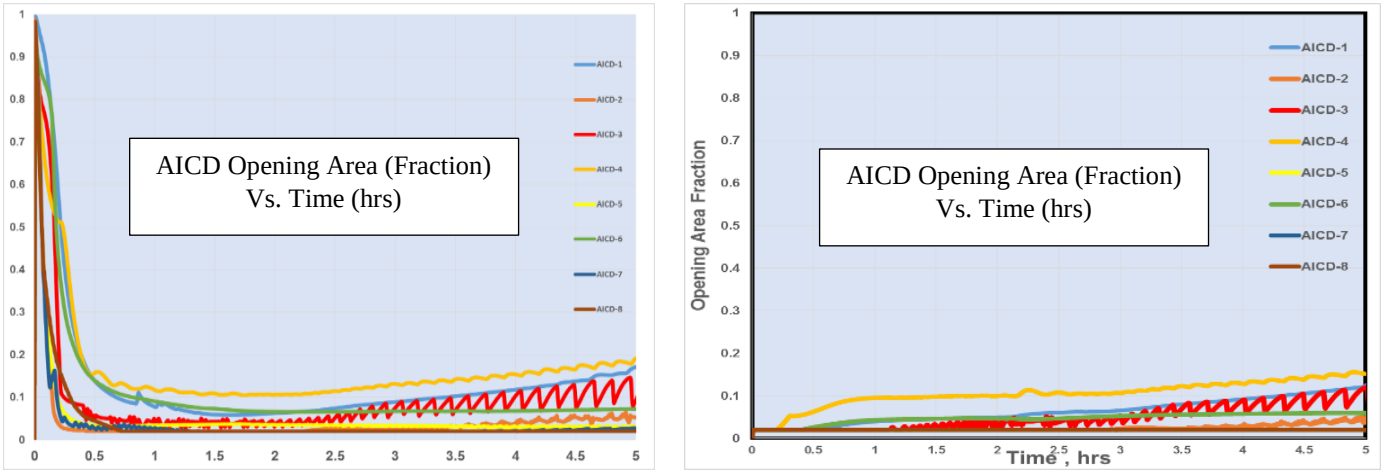

Figure 3-21 AICD opening area for Viscosified brine (left) and Pure brine(right)

Our modelling results show (*Figure 3- 21)* that during the early flow back period all the AFCDs are open when viscosified brine was used as the completion fluid. This accelerates the production and clean-up in the beginning of the process. However, after recovery of the completion fluid - viscosified brine, the mud filtrate brine enters the wellbore from the reservoir. The AICDs react to this fluid by imposing a flow restriction limiting the production and preventing/delaying clean-up from several intervals

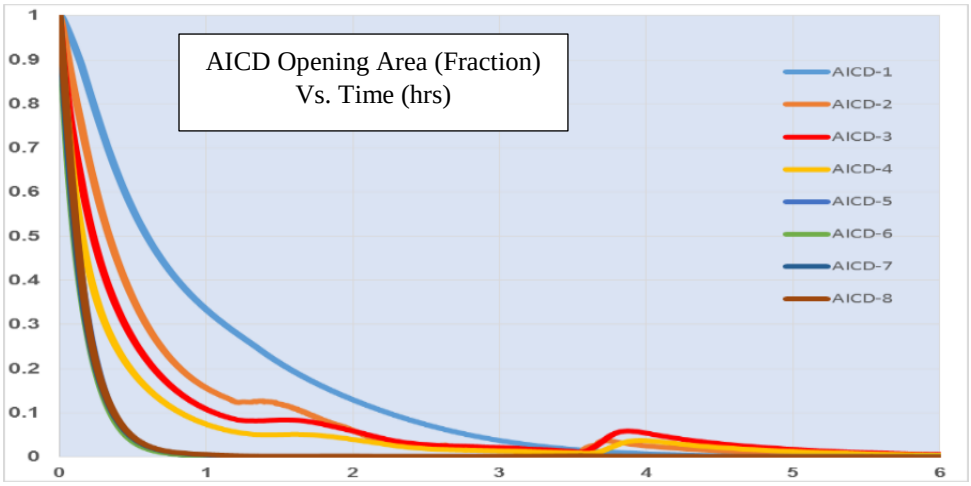

Figure 3-22 Completion fluid in the annulus

3.9.2 AFCD with Sandface Clean-out Valves *(*SCOVs)

Another strategy to facilitate clean-up is to install SCOVs in the completion string that can be programmed, or controlled, to open during well clean-up. In this study there is one SCOVs modelled in each zone and they are open for one day, opening time of devices is an optimisation parameter and can vary depending on depth of invasion, well trajectory and etc. *Figure 3-23*,

the SCOVs assist removal of the completion fluid from the heel zone while delaying the toe zone's clean-up. This is due to the open SCOVs increasing the heel-to-toe effect, i.e. reducing the contribution of the toe.

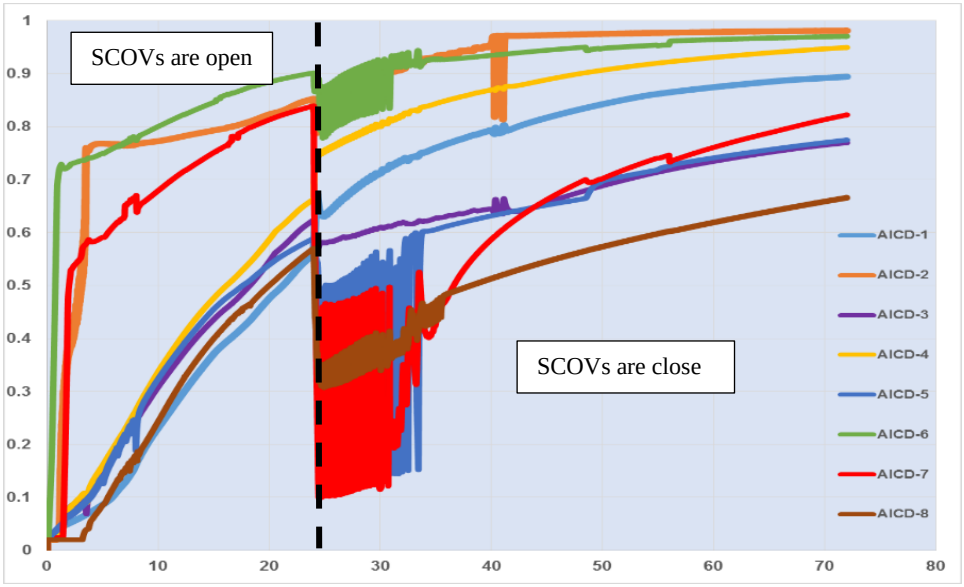

Figure 3-23 AICD virtual open area (fraction) versus time (hr)

In addition, *Figure 3-23,* shows the AICDs' virtual opening area when the SCOVs are used. Clearly, addition of SCOV increases production from the zones helping to remove completion fluids and therefore reduces the unwanted fluid (brine) saturation near wellbore. This results in a less restrictive behaviour and improved well productivity during the well clean-up period.

It should be noted that if the opening time of SCOVs is not long enough, there will still be filtrate being produced from reservoir when the SCOVs close. This can be seen in *Figure 3-23* where, once the SCOVs are closed the flow rate from the heel zone greatly reduce followed by fluctuations in the AICD's virtual open to flow area. A closure strategy for SCOVs is thus essential.

3.9.3 Drilling with Oil Based Mud (OBM)

A final mitigation strategy is to drill the well with an OBM instead of a WBM. In this case, the AFCDs are less sensitive to the flow back of the (viscous) filtrate, and the major problem is presence of the low viscosity (e.g. brine) completion fluid in the well. As a result, after cleaning out this completion fluid, the AICD-completion performs similar to the ICD one. However, the well deviation and packers affect the speed of the clean-up as can be seen in *Figure 3-24*.

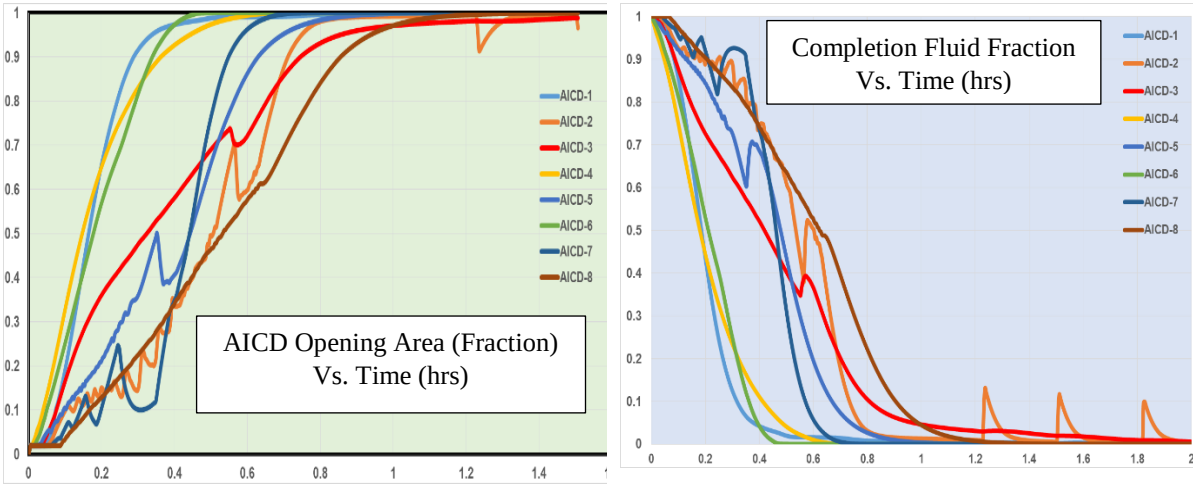

Figure 3-24 AICD opening area (left) and completion fluid in the annulus (right)

Comparison between the clean-up improvement strategies is presented in *Figure 3-25*: the inclusion of SCOVs significantly improves clean-up of the heel zone. However, this can happen at the expense of the toe zone's clean-up efficiency if the SCOVs' operation strategy is not programmed properly. Use of viscosified brine as the completion fluid to facilitate clean-up at the beginning of process but the improvement is limited once mud filtrate production from the formation starts.

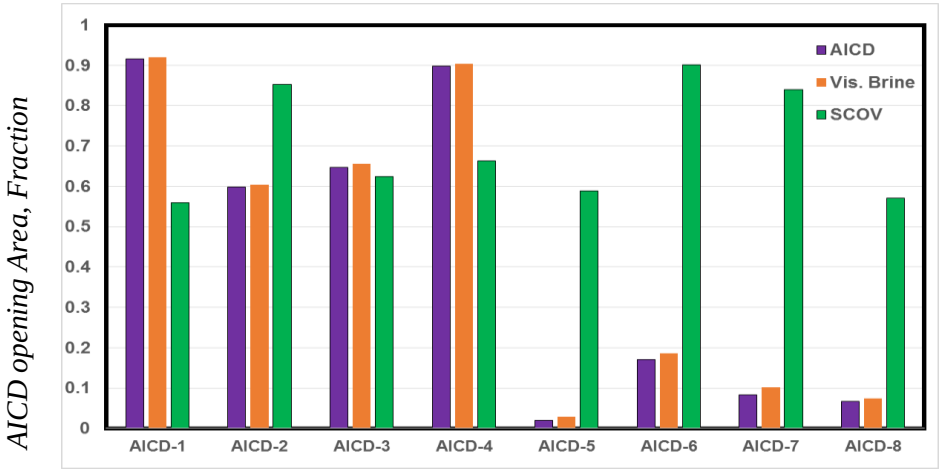

Figure 3-25 Performance of AFCD mitigation strategies compared

3.10. Summary

This chapter developed better understanding of the role of different FCD types in the well clean-up process. This knowledge helps to improve the efficiency and reduce the cost and time of clean-up of advanced wells. The results are summarized below:

ICD-Completion

- The effect of this completion in the clean-up efficiency is a trade-off between the inflow profile equalisation it offers and extra restriction to flow it imposes. It is suggested to investigate clean-up performance of this completion separately from the conventional ICD-completion design studies aimed at sizing it for production conditions.
- The ICD-completion increases the flow contribution from the low permeability and the toe zones increasing their drawdown and consequently achieving the lift-off pressure and better clean-up.

AFCD Completion

- An AFCD completion takes much longer to clean-up than an ICD completion.
- AFCD completion performance in the clean-up process is affected by the drilling and completion fluid composition, the pattern of filtrate invasion and the well trajectory.
- In homogenous reservoirs and horizontal wells, due to the deeper filtrate invasion in the heel, the AFCDs installed in that part of the well are likely to stay restrictive for longer compared to the toe. This increases the flow contribution from the toe and its clean-up. As a result, the risk of not exceeding the lift-off pressure in the heel and hence not cleaning it up increases, which is opposite to what is normally observed in other well completion types.
- Inclusion of SCOVs in the AFCD-completion can improve the clean-up efficiency especially in the heel and lower parts of the well but if their operation strategy is inappropriate this may increase the heel-to-toe effect.
- Filling annulus and tubing with viscous completion fluid can also be a solution to facilitate the AFCD completion's clean-up.

Chapter 4 Integrated Pressure and Temperature Transient Analysis (PTTA) in I-Wells: Background, Modelling and Workflow

4.1 Introduction

This chapter aims to introduce the concept of Dynamic Data Analysis (DDA) and Integrated Pressure and Temperature Transient Analysis (PTTA). The main objective of DDA is to integrate all the data from different measurement sources to fully and continuously characterise reservoir from near wellbore to boundaries. Pressure Transient Analysis (PTA), Rate Trainset Analysis (RTA) and Temperature Transient Analysis (TTA) are the main methods forming the workflow of DDA.

The chapter reviews the background of the three analysis methods, how they have evolved over years as well as their current status. The governing equations, corresponding analytical solutions, weakness, strength and expected results of each method are discussed and compared. The acquired knowledge from this comparison develops a better understating on the possibility and value of integration between the methods. The rest of the chapter focuses on the relatively new TTA method. Non-isothermal numerical modelling approach used in this study is first described and then validated against available analytical solutions. Thermal numerical simulators, i.e. SATRS and GEM[1], are employed to generate the measured data for case studies in the following chapters. Finally, TTA workflow used in this thesis and the methods to estimate thermodynamic properties such as Joule-Thomson (JT) coefficient and adiabatic expansion required for TTA solutions is presented.

4.2 Dynamic Data Analysis (DDA)

Intelligent wells are equipped with down hole permanent gauges and sensors, which can measure different physical properties such as pressure, temperature and flow rate with high resolution, accuracy and frequency. This provides rich source of data to be used for different purposes such as reservoir and completion real-time monitoring and formation characterisation. DDA is a general terminology that refers to the result of different transient data analysis approaches at different scales in time and space, from the shortest formation tests to the full production life of the wells. Current DDA consists of the following main methods;

[1] With thermal option enabled.

PTA, RTA as well as PLT and RFT data analysis. The recently introduced TTA method has also shown great potential to be tailored to the current DDA family *(Figure 4-1)***.** In the following section a brief description, including background, governing equations and available solutions, of PTA, RTA and TTA methods is presented.

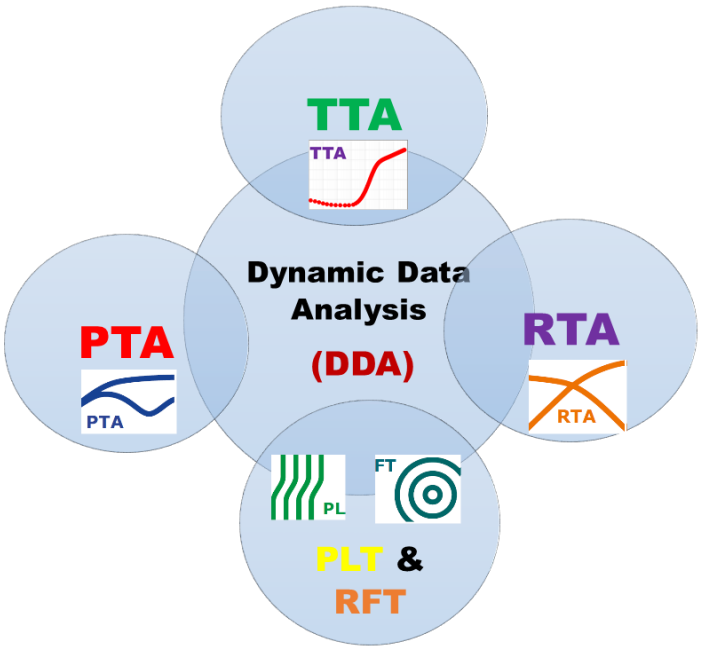

Figure 4-1 New DDA workflow

4.2.1 Pressure Transient Analysis (PTA)

Well test analysis, also called as PTA, has been used for many years to monitor well condition and determine reservoir properties. The advance in PTA analysis techniques are closely tied with improvement in surveillance methods and measurement technologies.

The early PTA methods, illustrated in the works of Miller [61] and Horner [62], focused on straight line analysis and applied to middle-time semi log data. During 1960 and early 1970 most major development originated from Ramey's work [63, 64] focused on early-time data analysis. Type-curve analysis is then introduced in 1970 by Ramey [64] and later developed by Agrawal [65] and Gringarten's [66] works .

PTA became a true reservoir characterisation tool with the introduction of derivatives by Bourdet et al (1983) [67]. Since then the effect of reservoir heterogeneity [68], complex well geometries[69, 70] and boundary effect [71] has been addressed.

Van Schroeter (2001)[72] has further extended the power of well test analysis with the introduction of an effective algorithm for deconvolution.

Evolution of state-of-the-art techniques in PTA has been reviewed and updated by many authors (e.g. Ramey 1980, 1992 [73, 74] , Gringarten's 1986, 2003 and 2008 [75-77] and Ehlig-Economideis et al 1990 [78]). The main PTA achievements in the past decades are listed in *Table 4-1*.

Table 4-1 Evolution of PTA Methods

Time period	Analysis Method	Tools	Relative Accuracy/ Applicability	Emphasis
50s	Straight lines	Laplace Transform	Poor	Homogenous Reservoir
Late 60s 70s	Type-Curve	Green's functions , Integrated methodology Stehfest algorithm	Fair (Limited)	Near-wellbore Effect, Dual Porosity
80s	Pressure Derivative	Computerised analysis	Very Good	Heterogeneous Reservoir
90s and 00s	Deconvolution	Deconvolution, Computer-aided analysis downhole rate measurements integration with interpretation methods from other data	Good	Enhanced radius of investigation boundary, Multi-Layer

The governing equation for PTA is diffusivity equation, which is derived from the combination of mass continuity equation, equation of motion (Darcy's Law) and equation of state (isothermal compressibility for a liquid);

$$\frac{1}{r}\frac{\partial}{\partial r}\left(r\frac{\partial P}{\partial r}\right) = \frac{\emptyset C_t \mu_o}{k}\frac{\partial P}{\partial t} \qquad \textbf{4-1}$$

The simplest form of the well test is a constant flow rate draw down followed by a perfect shut-in test. Based on the analysis of semi-log slope, permeability and skin can be estimated from the equations in *Table 4-2*; based on the identified flow regimes on log-log plot, PTA can be

employed to estimate other parameters such as fractured reservoir and well properties , distance to boundaries/fault and etc.

Table 4-2 Basic pressure build-up and draw down equations

Test Period	Analytical Solution (Radial Flow)	Slope	Skin
draw down(DD)	$P_{wf} = P_i - m_p \left[\log t + \log\left(\frac{\eta}{r_w^2}\right) + 0.351378 + 0.87S\right]$ **(4-2)**	$m_p = 0.183234\frac{qB}{kh/\mu}$ **(4-3)**	$S = 1.15129\left[\frac{P_i - P_{1hr}}{m_p} - \log\left(\frac{k}{\emptyset c_T \mu r_w^2}\right) - 0.351378\right]$ **(4-4)**
Build-up(PBU)	$P_{ws} = P_i - m_p\left[\log\frac{t_p + \Delta t}{\Delta t}\right]$ **(4-5)**	$m_p = 0.183234\frac{qB}{kh/\mu}$ **(4-6)**	$S = 1.15129\left[\frac{P_{1hr} - P_{wfs}}{m_p} + \log\left(\frac{t_p + 1}{t_p}\right) - \log\left(\frac{k}{\emptyset c_T \mu r_w^2}\right) - 0.351378\right]$ **(4-7)**

4.2.2 Rate Transient Analysis (RTA)

RTA and PTA are both about measuring pressure and rate data and almost perform the same analysis. The main conceptual difference between PTA and RTA originated from that fact that pressure transient data is "high frequency/high resolution" data and production data are "low frequency/low resolution" data. In presence of continuous long-term pressure measurement the first idea is to do PTA. However, PTA methodology was not designed for this type of data. Material balance errors and over-simplifications using Perrine's approach for multiphase flow property evaluation were among the most frequent encountered error.

The journey of RTA was started by Arps in 1940 [79] who published a formulation of constant pressure production including exponential, hyperbolic and harmonic decline responses. Fetkovich 1980 [80] later introduced production decline curve analysis (DCA) using a type curve approach. This was a combination of the theoretical response of a well in a closed boundary and the standard Arps decline curves. Fetkovich type-curve is derived assuming a constant-flowing pressure where this method only requires flow rate. The Arps plot was the counterpart of the Horner plot and constant pressure type curve was the equivalent of the PTA constant rate type-curves **(***Figure 4-2***).**

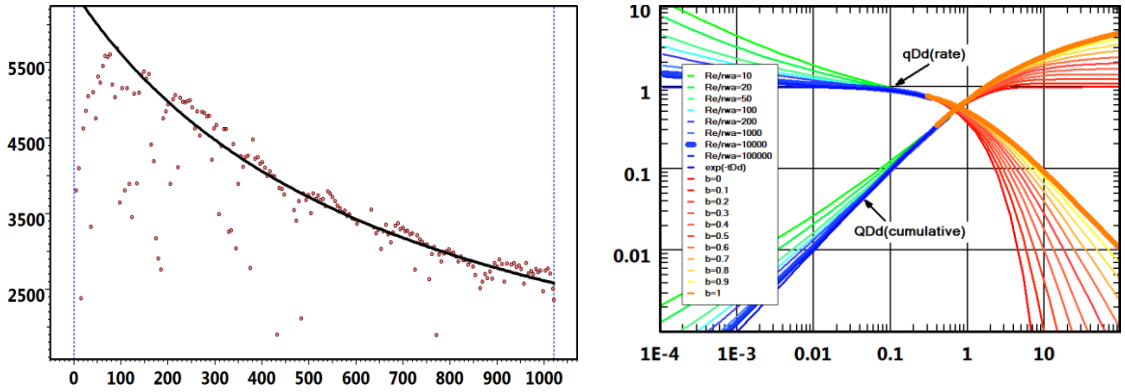

Figure 4-2 Arps plot (left) and Fetkovich type curve (right)

The main limitation for Fetkovich type-curve is the assumption of constant flowing pressure. Palacio and Blasingame [81] and Doublet and Blasingame [82] introduced the next breakthrough in RTA which was the analytical basis and integral plotting functions for variable-rate/variable pressure drop production data. The so-called Blasingame plot/type-curve *(Figure 4-3)* can be used for variable flowing pressure conditions. Rate-normalized pressure or productivity index (PI), PI integral and PI integral derivative are shown on log-log plot. In both cases, on the time axis, the logarithm of elapsed shut-in time was replaced by the logarithm of the material balance time, in order to align long-term Pseudo-Steady State (PSS) responses (*Table 4-3).*

Table 4-3 Blasingame method's equations

Material Balance Time	**Pressure-normalised rate**	**Normalised rate integral**	**Normalised rate integral derivative**
$t_c = \frac{Q}{q}$ (4-8)	$PI(t) = \frac{q(t)}{P_i - P_w(t)}$ (4-9)	$PI\ Int. = \frac{1}{t_e}\int_0^{t_e} PI(\tau)d\tau = \frac{1}{t_e}\int_0^{t_e} \frac{q(t)}{P_i - P_w(t)} d\tau$ (4-10)	$PIInt.Derivative = \frac{\partial(PI_{Int})}{\partial ln(t_e)}$ (4-11)

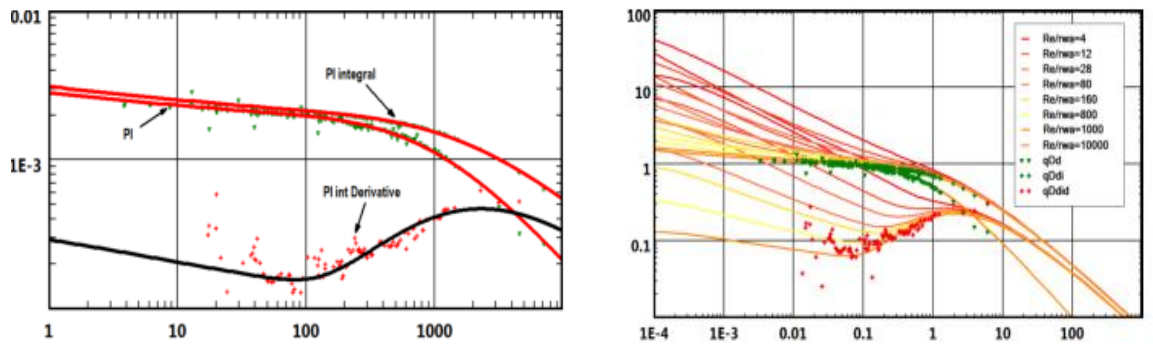

Figure 4-3 Blasingame log-log plot (left) and type-curve (right)

Blasingame introduced another big achievement in RTA, which is rate-normalised pressure. A review on the evolution of RTA, challenges and pitfalls is presented by Anderson [83]. *Table 4-4* lists the main findings in RTA context.

Table 4-4 Evolution of RTA methods

Year	Researcher	Method	PTA counterpart	Data to be used	Deliverables
1945	Arps	Decline curve analysis- Curve fitting	Horner	q(t), empirical , Boundary dominated	Production forecast , recoverable reserve
1980	Fetkovich	Type Curve	Type-curve	$q(t)$ (Transient and boundary dominated)	Permeability , skin, drainage area and shape
1993	Blasingame	Log-Log / Type curve	Derivative	$P_{wf}(t) and q(t)$	Permeability , skin, drainage area and shape

4.2.3 Temperature Transient Analysis (TTA)

Unlike mature RTA and PTA, TTA is a relatively new method in DDA area. This method has recently shown a great potential to characterise reservoir and near wellbore.

The rest of this chapter is allocated to the background of TTA, how non-isothermal simulation is initialised, used and verified in this thesis, to generate both pressure and temperature data, and finally the TTA workflow used in the following chapters.

4.2.3.1 TTA Background

Temperature variations in the reservoir are very small so that the often poor gauge resolution in the past was not able to detect small changes, besides they do not impact pressure much and therefore the reservoir was assumed isothermal. However, nowadays high-resolution gauges and fibre optic sensors can capture temperature changes as small as 0.002 deg [13]. This has been the main motivation for researcher to start studying temperature transient data and non-isothermal models. In addition, analysis of real field data [84, 85] has shown that while pressure shows a normal trend , temperature exhibits interesting heating and cooling behaviors (Figure 4-4). This observation was later confirmed by non-isothermal simulation results [86, 87]. Furthermore, sensitivity studies have proven the sensitivity of temperature features on petrophysical properties, such as permeability and porosity, as well as the near-wellbore zone (such as skin, skin-zone radius, skin-zone permeability)[87]. All these observations have motivated researcher to quantify temperature behaviors by developing mathematical equations and provide numerical and analytical solutions.

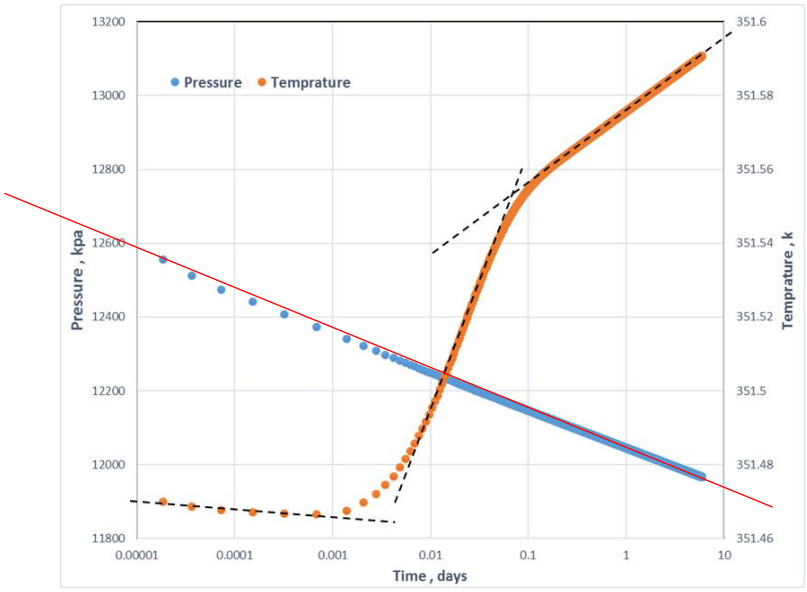

Figure 4-4 Temperature and Pressure data on a semi-log plot for a damaged formation. Synthetic model results

Regarding the analytical solution, Chekalyuk (1965) [88] was the first person, to the best of my knowledge, who developed a TTA analytical solution for constant-rate draw down test

using Boltzmann transformation. The next main attempt was by Ramazanov (2007) [87] who used method of characteristic to derive an analytical solution for slightly compressible liquid-producing vertical well. The main assumption from his method is that temperature stabilizes faster than pressure therefore he used a steady-state pressure solution to derive the transient temperature solution. TTA development was continued with the work of Muradov [89] who derived an analytical solution for liquid producing horizontal well for linear flow regime and by ignoring the heat conduction term within the reservoir, he used Fourier and Laplace transformation to derive analytical solutions. Recently Onur [90] developed analytical solution for both draw down and build-up periods by using Boltzmann transformation and Yilin Mao [88] used Laplace transformation for slightly compressible fluids. Finally, Dada [92] followed Ramazanov approach to develop an analytical solution for dry gas producing vertical well.

The application and value of TTA is also demonstrated using numerical modelling and solutions by App [85]. Duru and Horne [93, 94] also used a semi analytical-solution method known as operator splitting, for forward computation of transient, sand face temperatures, including the J-T and adiabatic-fluid-expansion effects. In a series of papers, Sui et al. [95, 96] proposed a non-isothermal model for multilayer commingled systems to predict bottom hole pressure and temperatures for slightly compressible fluids. They solved the temperature equation, including the effects of J-T, adiabatic-fluid expansion/compression, conduction, and convection, by use of a finite-difference technique. He later extended this work to single-phase gas reservoirs [94]. A synopsis of the key, previously discussed works on transient-temperature modeling and analysis is given in Table 4-5

Table 4-5 Evolution of TTA methods

Years	Author	Problem Solution	Analysis Method
1965	Chekalyuk	Analytical solution based on Boltzmann transformation for a line-sink well for single phase slightly compressible 1D radial flow, constant rate solution	None
1977 and 1984	Grag and Pritchett	Numerical solution for single phase or two phase geothermal reservoirs	Semi-straight line analysis for pressure data only
2007	Ramazanov et al	Decoupled analytical solution dependent on method of characteristics for single phase	None
2008	Sui et al	Analytical isothermal p-solution and numerical T-solution for commingled layered system, 1D radial flow	Non-linear regression

2010	Muradov et al	Analytical solution for Horizontal well for linear flow regime	Straight Line analysis
2010	Duru and Horne	Semi analytical solution using an operator-splitting method , 1D radial flow, variable-rate production history	Non-linear regression
2010	App et al	Numerical solution, sensitivity studies	Non-linear regression
2016	Onur et al	Analytical solution for build-up and draw down using Boltzmann transformation	Straight line
2013 ,2015	Palablyik et al	Numerical solution dependant on rigorous approach for liquid-dominated geothermal system	None
2017	Dada et al	Analytical solution for dry gas reservoir method of characteristics for single phase	Straight line
2017	Yilin Mao , Mehdi Zeidouni et al	Analytical solution for TTA and near wellbore damaged zone characteristics based on Laplace transformation	Straight line

4.2.4 TTA Governing Equations and Solutions

The governing mathematical model for TTA is derived based on the mass, momentum and thermal energy balance equations. Compared with diffusivity equation for PTA, TTA model is more complex and consists of conduction, convection, Joule-Thompson and adiabatic expansion terms. The conduction term is usually ignored, as the effect of that compared to the other terms is negligible in conventional production.

$$\frac{\partial T}{\partial t} + u_{co}(r,t)\frac{\partial T}{\partial r} = \varphi_t^* \frac{\partial P}{\partial t} + \varepsilon_{JTo} u_{co}(r,t)\frac{\partial P}{\partial r} \qquad (4\text{-}12)$$

Where ε_{JTo} is Joule-Thompson coefficient, φ_t^* is effective adiabatic-expansion coefficient, u_{co} is velocity of convective heat transfer.

As discussed previously this partial differential equation (PDE) can be solved by different methods, e.g. Laplace transformation, method characteristics, Boltzmann transformation etc. Full solution or asymptotic solutions for each period including early time due to expansion; as well as intermediate time, damaged zone, and late time (in virgin reservoir) due to JT can be derived. *Table 4-6* lists TTA analytical solutions for different flow regimes.

Table 4-6 TTA draw down analytical solutions for different periods (Onur et al [90])

Period	Equation
Full Solution	$T_{wf} = T_i + \frac{q_{sco}B_o\mu_o}{4\pi kh}\left[-\varepsilon_{JTo}\left[-Ei\left(\frac{r_w^2}{4\eta_o t}\right)+2S\right]+\left(\varphi_t^* - \varepsilon_{JTo}\right)Ei\left(-\frac{r_w^2}{4\eta_o t}-\frac{C_{pR}qB}{4\pi\eta_o h}\right)\right]$
Early time (Expansion)	$T_{wf} = T_i - m_{TeDD}\left[\log t + \log\left(\frac{\eta}{r_w^2}\right)+0.351378\right]$ (4-13)
Intermediate damage zone (JT effect)	$T_{sf} = T_i + m_{TLDDs}\left[\log t + \log\left(\frac{\eta_s}{r_w^2}\right)+0.351378+0.869S-\left(\frac{\varphi_{ts}}{\varepsilon_{JTso}}-1\right)\left[\log\left(\frac{C_{pRs}qB}{\eta_s h}\right)-0.8485\right]\right]$ (4-14)
Late time (JT effect)	$T_{wf} = T_i + m_{TLDD}\left[\log t + \log\left(\frac{\eta}{r_w^2}\right)+0.351378+0.869S-\left(\frac{\varphi_{t}}{\varepsilon_{JTo}}-1\right)\left[\log\left(\frac{C_{pR}qB}{\eta h}\right)-0.8485\right]\right]$ (4-15)

$m_{TeDD} = 0.183234\frac{qB\varphi_t}{kh/\mu}$ (4-16)	$m_{TLDDs} = 0.183234\frac{qB\varepsilon_{JTso}}{(k/\mu)_s h}$ (4-17)	$m_{TLDD} = 0.183234\frac{qB\varepsilon_{JTo}}{kh/\mu}$ (4-18)
$\varphi_t = \emptyset\frac{\rho_{C_p}}{\left(\rho_{C_p}\right)_t}\varphi_o$ (4-19)	$\left(\rho_{C_p}\right)_t = \emptyset\rho_o C_{po} + (1-\emptyset)\rho_s C_{ps}$ (4-20)	$\varphi_o = \left(\varepsilon_{JTo} + \frac{1}{\rho_o C_{po}}\right)$ (4-21)
$C_{pR} = \frac{\rho_{C_p}}{\left(\rho_{C_p}\right)_t}$ (4-22)	$\eta = \frac{k}{\emptyset c_T \mu}$ (4-23)	$\eta = \frac{k_s}{\emptyset c_T \mu}$ (4-24)

Where:

ε_{JT} is Joule-thompson coeffeicent, η_o hydraulic diffusivity constant for oil , φ_t^* effective adiabatic-expansion coefficient of the saturated-porous medium, C_{pR} is the ratio of the volumetric-heat capacity of oil to the volumetric-heat capacity of the fluid-saturated rock, φ_o adiabatic thermal expansion of oil, $\left(\rho_{C_p}\right)_t$ volumetric-heat capacity of fluid-saturated rock

4.3 Integrated DDA

As described PTA, RTA and TTA have their own limitations and advantages in terms of either measurement or analysis. Integration of all the data provides a great opportunity to fully characterise reservoir in temporal and spatial scales. A comparison between the methods is presented in *Table 4-7*;

In the rest of this chapter the TTA modelling and analysis workflow is described. This information is used in the following chapters to investigate the application of PTTA and TTA for various reservoir and well/completion scenarios.

	Temperature Transient Analysis (TTA)	**Pressure Transient Analysis (PTA)**	**Rate Transient Analysis (RTA)**
Data Quality	High Resolution / High Frequency	High Resolution / High Frequency	Low Resolution/Low Frequency
Test Design	Fully Controlled Experiment	Fully Controlled Experiment	Little controlled Test /Considerable Variance
	Snapshot / a Specific Event	Snapshot / a Specific Event	Surveillance/Monitoring Data
Period of Interest	Draw down	Build-up	Draw down
Main Flow Regime of Interest	Transient period (K & S of damaged zone)	Infinite Acting Radial Flow Kh& Skin	Pseudo-steady State (PSS) Drainage Area & Shape Factor
Diagnostic Capability	Low	High to very high	Average to low
Long Term Validity	Low (mainly used for short-term transient data)	Average to High	High to very high

Table 4-7 Comparison between TTA, PTA and RTA

4.4 TTA Modelling and Verification

Thermal studies require an accurate non-isothermal tool which can sufficiently capture different physics such as conduction, convection, Joule-Thomson and adiabatic expansion/compression. In order to generate sand face temperature and pressure , this thesis uses two CMG^{TM} simulator, i.e. non-isothermal STARS^{TM}[98] and Compositional GEM^{TM}[99], when thermal option is enabled.

Thermal model in both non-isothermal simulators is based on coupling energy balance and flow equation. The energy balance equation involves convection, conduction and heat losses to the surroundings. Regarding Joule-Thomson effect, it cannot be explicitly input to the STARS simulator. Therefore, this thermodynamic property is implicitly considered by activating Lee-Kesler equation of state (EOS) [100]. By doing so, enthalpy is treated as a function of both pressure and temperature. The basis of the Lee-Kesler method is to calculate ideal-gas enthalpy (H_{gi}^{ideal}) and enthalpy departure function (H_o^{depart}).

$$H_j = \sum_{i=1,nc} X_i \, H_{ji}^{ideal} + H_j^{depart} \qquad (4\text{-}25)$$

$$\Delta Hj^{depart} = \Delta H_j(s)\,(T_{pr}, P_{pr})_j + \omega_j \bullet \Delta H_j(r)\,(T_{pr}, P_{pr})_j \qquad (4\text{-}26)$$

Where ideal-gas enthalpy of each component is calculated from correlation coefficients and enthalpy departure function is estimated from pressure, temperature, component properties (Tc, Pc, acentric factor) and composition of the phases.

It should be noted that for some multiphase cases in the next chapter CMG-GEM^{TM}, compositional reservoir simulator, with activation of thermal option, is used. As far as thermal study is concerned the main difference between two simulators is that the latter one automatically takes into account the JT effect. In addition, in terms of PVT modelling, STARS use K-Value whereas GEM employs EOS. Regarding thermal conductivity, a fixed single value, unless otherwise stated, referred to effective thermal conductivity of saturated-porous media is considered. The effect of overburden and under burden heat loss is also ignored.

4.5 Verification of Numerical Results

The output of the numerical simulation is used as measured temperature and pressure for TTA studies in this thesis. Therefore, the validity of the numerical modelling results in this section

is checked against the available numerical and analytical solutions. Thermal models use a cylindrical reservoir with a single-phase line-sink well, the verification here is limited to single-phase as there is no available analytical solution for multi-phase TTA to compare with the numerical results, multi-phase TTA will be further discussed in chapter 5. Grid block pressure and temperature data represents sand face measurement used in the analysis. Two different cases are used for verification: dry gas and oil with connate-water saturated reservoir are modelled with only oil being mobile. This example is similar to the draw down field test case presented by App (2009)[85] and Onur (2016)[101]. The next case is a dry gas reservoir similar to the example provided by Dada (2016) [92].

As shown in *Figure 4-5* and *Figure 4-6*, the sand face pressure result of the non-isothermal simulator for line-source vertical well is verified with a commercial well test analysis software ,i.e. KAPPA^{TM}, and sand face temperature output is also confirmed with analytical solutions as well as a non-isothermal in-house simulator developed for gas in OpenFOAM® [92]. The figures confirm the acceptable compatibility between the output of non-isothermal simulator and available numerical and analytical models.

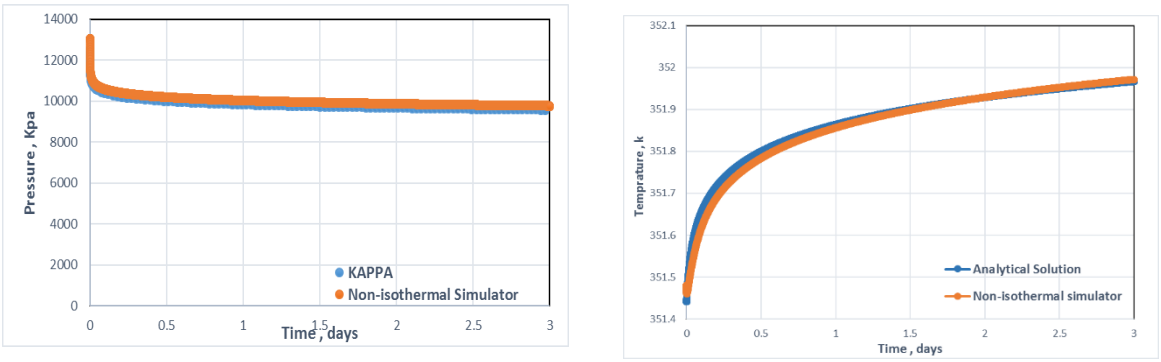

Figure 4-5 Verification of pressure (left) and temperature (right) model in Liquid producing wells

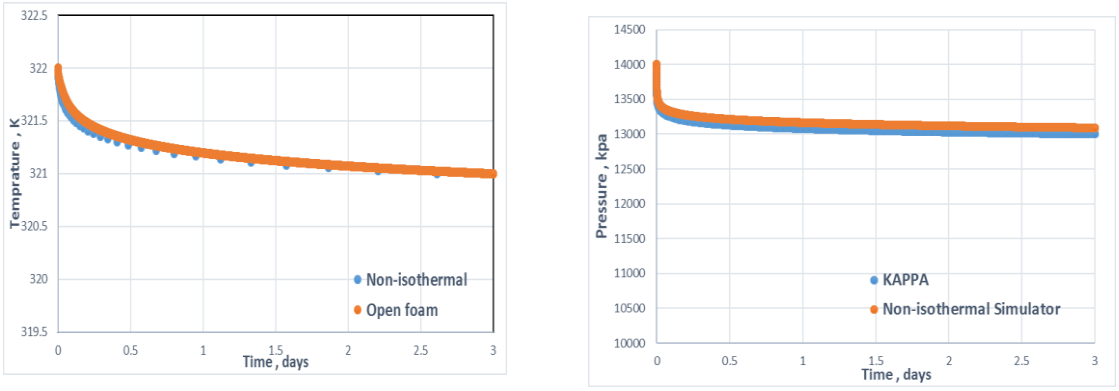

Figure 4-6 Verification of temperature (left) and pressure (right) model in gas producing well

4.6 TTA Workflow

The preferred TTA period in this thesis is draw down as most of the analytical solutions developed to date are applicable to it. The basis of the analysis is to use the liquid TTA analytical solution developed by Onur (2016) [90] and dry gas solution derived by Dada et al (2016) [92]. As TTA is still mostly in the straight-line analysis stage, the analysis is based on the slope of each TTA period on semi-log (or log-log) plot. In this thesis, the focus is on the slope of intermediate and late-time temperature periods, while the early-time expansion/compression straight-line is not used due to it often happening very fast to be well measured. TTA workflow used in the rest of this thesis will be shown later in *Figure 4-10* , the details of each step are elaborated below.

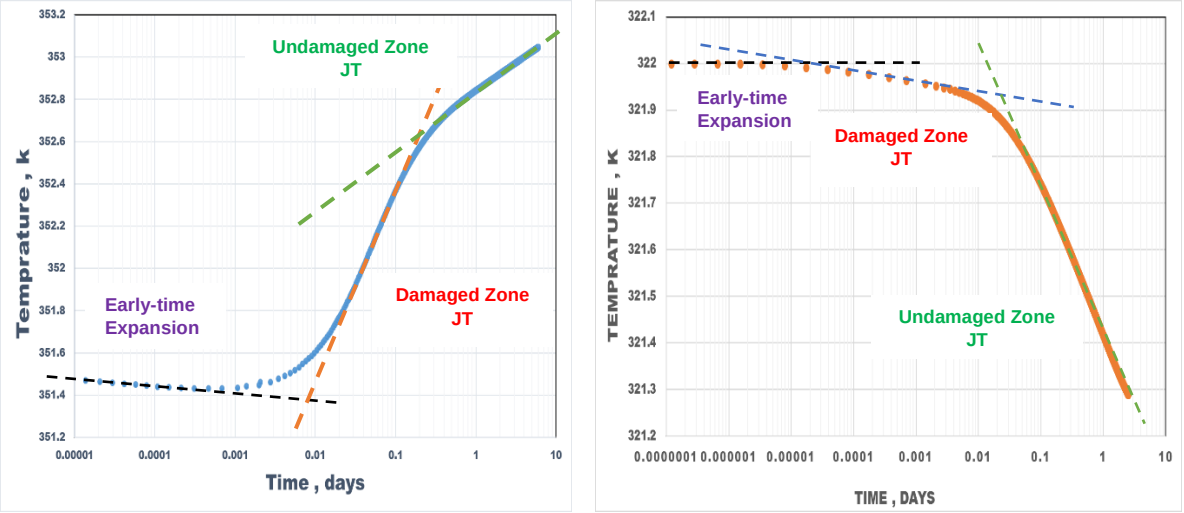

Figure 4-7 Temperature data for liquid (left) and gas (right) in damaged formation

1. Identify flow regimes on Temperature semi-log or log-log plot

In an infinite-acting, homogenous formation affected by near-wellbore formation damage, three straight line are expected; early-time expansion/compression, intermediate-time JT caused by damage zone and late-time JT representing undamaged formation (*Figure 4-7*). The trend of the temperature data in the two last periods depends on the sign of JT coefficient. For example, JT coefficient is negative for liquids, i.e. causing heating up, and normally positive for gases, i.e. cooling down, though the sign of the coefficient for gases depends on particular P-T conditions. It should be noted that these flow regimes can also be identified on temperature log-log plot however, unlike PTA, TTA derivative has not been shown a suitable tool for flow regime identification.

2. Determine the corresponding slope

The temperature slope is a function of both the reservoir (Kh) and thermal properties ($\varepsilon_{JTo}\ or\ \varphi_t$) , assuming q and other terms are known. This means that to estimate one unknown another parameter needs to be known/calculated from other sources. Table 4-8 summarises the slope of pressure and temperature for different periods and phases;

Table 4-8 slope equation for pressure and temperature (Liquid and gas)

Test Period	Slope Equation
Liquid Semi-log slop PTA	$m_p = 0.183234\frac{qB}{kh/\mu}$
Liquid Early-time semi-log slop TTA	$m_{TeDD} = 0.183234\frac{qB\varphi_t}{kh/\mu}$
Liquid Late-time semi-log slop TTA	$m_{TLDD} = 0.183234\frac{qB\varepsilon_{JTo}}{kh/\mu}$
Gas Late-time semi-log slop TTA	$m_{Tg} = \frac{B\Gamma T_i Q_{sc}}{2kh}[\eta^* - \varepsilon]$

3. Calculate thermodynamic properties (φ_t and ε_{JTo})

The Joule-Thomson coefficient (ε) and adiabatic coefficient (η) are two thermodynamic properties involved in TTA solutions. There are several approaches to directly or indirectly estimate them;

1. Special lab measurements
2. PVT simulation (e.g. PVTSim, PVTi, etc.))
3. Analytical equations or PVT EOS modelling
4. PVT black oil correlations
5. Indirectly from pressure and temperature measurements

As the direct measurement of these properties is not very common, the following describes how JT and adiabatic coefficient can be alternatively calculated from pressure and temperature measurement;

3.1. How to calculate Joule-Thomson coefficient

The only difference between the slope equation for the late-time temperature and pressure is Joule-Thomson coefficient. Therefore, the ratio of the late-time temperature slope to corresponding pressure one results in Joule-Thomson (JT) coefficient *(Figure 4-8*)

$$\frac{m_{TLDD}}{m_p} = \frac{0.183234\frac{qB\varepsilon_{JTo}}{kh/\mu}}{0.183234\frac{qB}{kh/\mu}} = \varepsilon_{JTo} \qquad 4\text{-}27$$

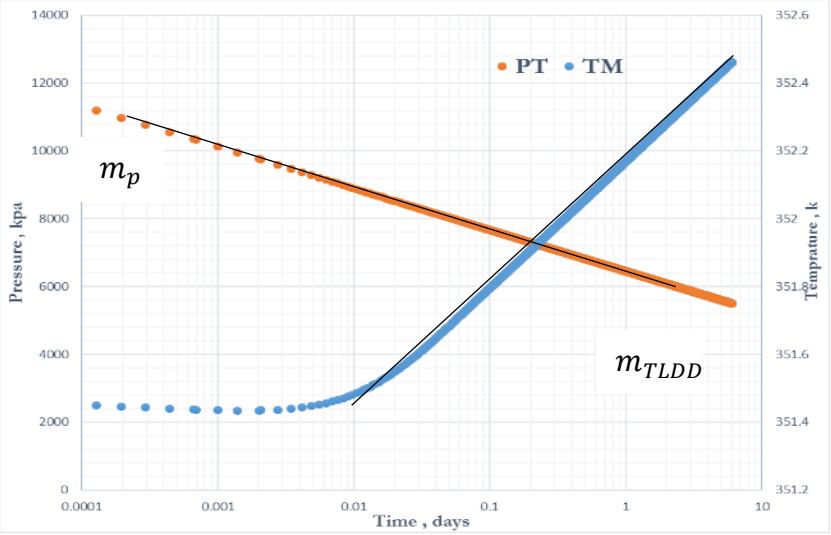

Figure 4-8 Pressure and temperature data on semi-log plot

3.2. How to calculate adiabatic coefficient

The average adiabatic coefficient can also be calculated from the maximal temperature decrease [87]. In the onset of production, sudden pressure drop occurs leading to adiabatic expansion and hence temperature cooling-down trend. The ratio of initial abrupt temperature to pressure changes gives the adiabatic expansion *(*Figure 4-9*).*

$$\eta = \frac{\Delta T}{\Delta P} \qquad 4\text{-}28$$

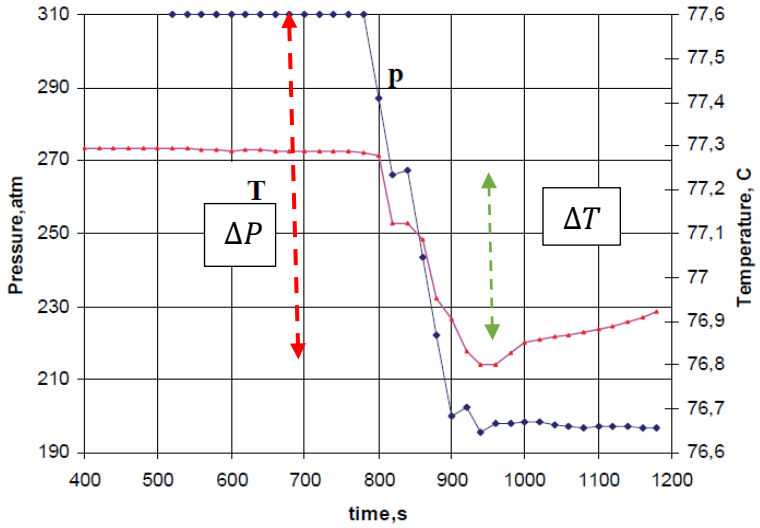

Figure 4-9 Pressure and temperature data in early-time expansion period [87]

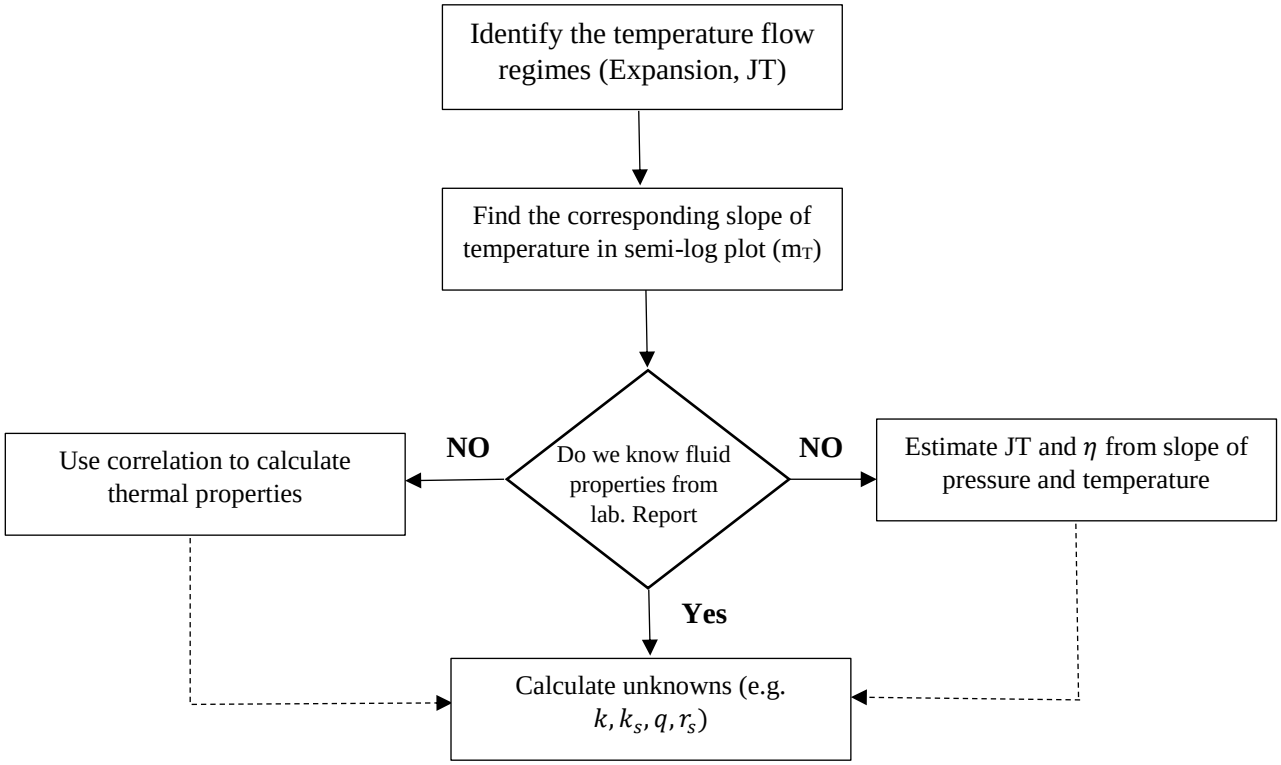

Figure 4-10 TTA workflow

4.7 Summary

This chapter introduced the concept of DDA and PTTA. This information provides a building block for the next three chapters, which are about PTTA. The history of PTA, RTA and TTA was first presented, and the methods then compared. The results of comparison revealed that, TTA is a better tool to characterise near wellbore, PTA is a proven method for reservoir characterisation and RTA is more suitable for boundary-dominated flow regimes. The limitations and advantages of each method creates an opportunity to integrate all the methods and thereby improve the accuracy of parameter estimation from near-wellbore to reservoir boundary.

The modelling approach and tools used for PTTA study in the next chapter was also described and verified. This was followed by presenting the TTA workflow for parameter estimation. Direct and indirect measurement/calculation of thermodynamic properties in TTA solutions was also demonstrated. The presented TTA workflow in the next chapters is followed to address different challenges and problems in PTTA.

Chapter 5 Pressure and Temperature Transient Analysis in Multiphase, Finite, Heterogeneous Reservoirs

5.1 Introduction

This chapter aims to extend the current knowledge of TTA to multi-phase, finite and heterogeneous formations. The underlying assumption for the available analytical TTA solutions is that there is a single-phase producing well in a homogenous, infinite-acting reservoir. In practice, it is highly likely to have a more complex case and consequently the application of the existing TTA solutions to be under question.

The case studies presented in this chapter are designed such that the violation of the various TTA assumptions is investigated. In the first scenario, the effect of multiphase flow on the validity of the TTA solutions is examined. Several multiphase cases are first modelled and analysed and then the required modifications are proposed.

The effect of different reservoir boundaries, e.g. closed and constant pressure ones, is also discussed and their corresponding signatures on temperature semi-log and log-log plot are identified. This is followed by addressing the impact of the reservoir heterogeneity, by studying two types of heterogeneity, on TTA results. The criteria and limitations for comparing TTA and PTA results is also further elaborated. Finally, the application of PTTA in limited entry wells using a synthetic case study is demonstrated.

5.2 PTTA in Multiphase Reservoir

The status of TTA research in producing wells is currently limited to single-phase reservoir. Single-phase oil [87-91] , dry gas [92] and water well [102, 103] solutions have been developed. However, there is no a study addressing the validity of the existing solutions in presence of other phases. By contrast, multi-phase PTA is a mature subject and many studies in this context have been carried out. This section starts with a brief introduction about the available multiphase PTA methods. This is followed by studying the effect of multiphase flow on TTA and PTTA where three different multiphase scenarios are modelled and analysed.

5.2.1 PTA Multiphase Methods

As described before, PTA has been the subject of many multiphase studies. The following summarises the three main methods in this context;

5.2.1.1 Perrine-Martine (P-M) Approach

This method was first introduced by Perrine[104]; modifying the single-phase PTA solutions by using the total mobility and the total multiphase compressibility. Martine[104] later provided a theoretical basis for this method. This method, called as Perrine and Martine (P-M), is practical, easy to implement and mainly used for two-phase liquid producing wells. *Table 5-1* summarises the terms modified in P-M method;

Table 5-1 Perrine - Martine Modifications

	Slope	Mobility	Flow rate
Single-phase	$m_o = \frac{162.6 q_o}{\lambda_o h}$	$\lambda_o = \frac{K_o}{\mu_o}$	q_o
Multi-phase	$m_l = \frac{162.6 q_t}{\lambda_t h}$	$\lambda_t = \frac{K_o}{\mu_o} + \frac{K_w}{\mu_w} + \frac{K_g}{\mu_g}$	$q_t = q_o B_o + \left(q_g - \frac{q_o R_s}{1000}\right) B_g + q_w B_w$

5.2.1.2 Pseudo-Pressure (P-P) Approach

For gas reservoirs, gas compressibility factor (z) and viscosity (μ_g) depend on pressure changes. Al-Hussainy et al. (1966) [105] formulated the pseudo pressure concept to deal with variations in these properties:

$$m(p) = 2\int_0^P \frac{P}{\mu_g z} dP \qquad 5\text{-}1$$

This allows the PTA liquid solution to be applied for gas. Raghavan [106]later found that the curves of P_{wf} vs $logt$ and $m(p)$ vs log t are very similar, at early time, and they form a straight line. This forms the theoretical basis of pseudo-pressure analysis.

5.2.1.3 Pressure-Squared (P-S) Approach

If it is assumed that the product of (μz) in Eqn. *5-1* is constant, then pseudo-pressure and the diffusivity equations can be simplified as follows;

$$m(p) = \frac{1}{\mu z}(P^2 - P_0^2) \qquad 5\text{-}2$$

$$\frac{1}{r}\frac{\partial}{\partial r}\left(r\frac{\partial P^2}{\partial r}\right) = \frac{\emptyset \mu C_t}{0.0002637k}\frac{\partial P^2}{\partial t} \qquad 5\text{-}3$$

The P-S approximation is valid only for low pressures (P < 2,000 psia) because μz is fairly constant at this pressure range. This is unlike the P-P transformation applicable for all pressure ranges. *Table 5-2* lists the three PTA multiphase methods, analysis plots and expected results;

Table 5-2 Comparison between PTA multiphase methods

	Plot	Result
P-M Method	P vs. time	Total mobility λ_t and skin
P-P Method	m(p) vs. time	Absolute/Effective permeability and skin
P-S Method	P^2 vs. time	Absolute/ Effective permeability and skin

The next section describes the three possible combinations of multiphase flow in the reservoir, shown in the *Table 5-3* and evaluates the effect of extra phase on the results of TTA and PTTA.

Table 5-3 Multi-phase case studies

	Oil	Water	Gas
Case-1	✓	✓	
Case-2		✓	✓
Case-3	✓		✓

5.2.2 Multiphase Case Studies

5.2.2.1 Case 1: Oil –Water System

Case one models an oil-water producing well in a single-zone, homogenous reservoir. The absolute reservoir permeability is 107 md and based on the relative permeability curve and the initial phase saturation, the total mobility of the fluids is calculated as 25 md/cp. This value is treated as an actual value to be compared with PTA and TTA results (It is assumed that during production the saturation changes are negligible). The oil and water flow rates of 270 and 153

m^3/day respectively result in a water cut of 36%. The relative permeability curves used in the simulation and the resulting oil and water flow rates are shown in *Figure 5-1* . This case was modelled in STARS.

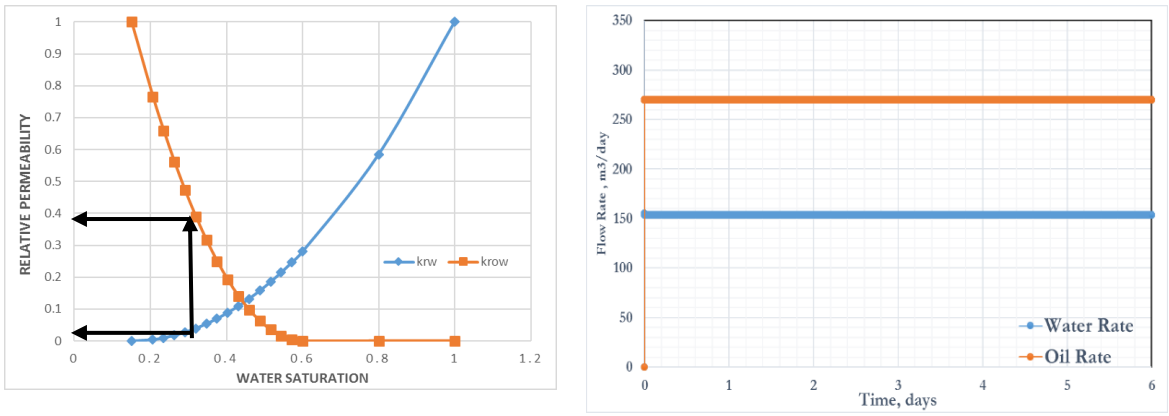

Figure 5-1 Relative permeability curve (left) and phase flow rates(right) for the oil-water case

- **PTA**

The pressure log-log and semi-log plot for this case is depicted in Figure 5-2. The log-log plot confirms that pressure describes the radial flow regime and the effect of boundaries have not yet been felt. The semi-log slope, the total liquid flow rate and the reservoir thickness are input into the P-M equation, *Table 5-1*, and the total mobility estimated. *Table 5-4* shows that the PTA result is in good agreement with the actual total mobility obtained using the relative permeability curves.

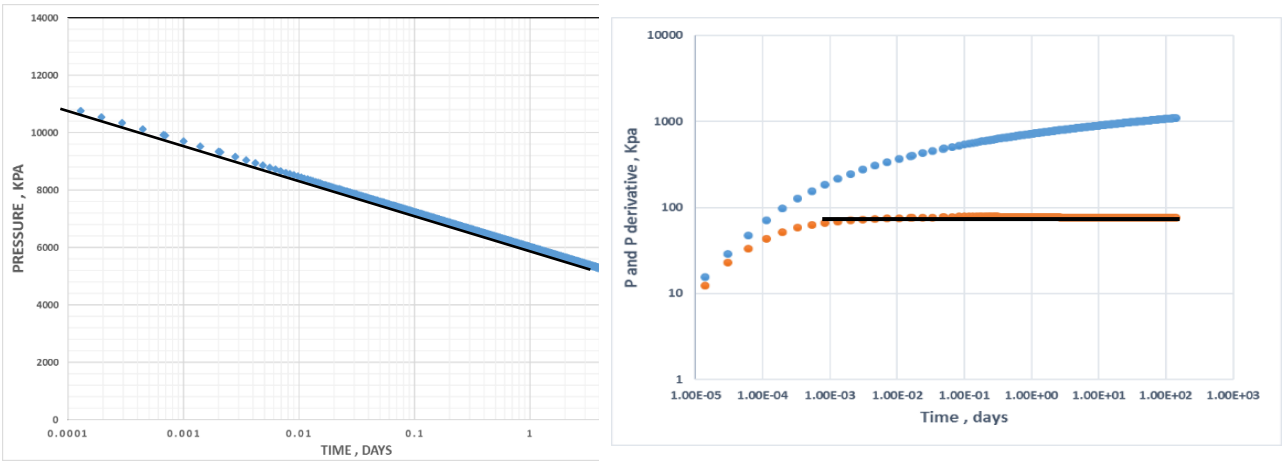

Figure 5-2 Semi-log (left) and log-log (right) pressure plot for oil-water case

Table 5-4 PTA result for oil-water case

Total flow rate (q_t) m^3/day	**Slope(m_p)** Pa/sec	**Thickness(h)** M	**Total Mobility(λ_t)** md/cp
423	177	30.48	**<u>24</u>**

- **TTA**

Figure 5-3 is the TTA semi-log and log-log plots. A damage is not present near wellbore and PTA has already confirmed an infinite-acting reservoir. The two straight-lines therefore represent the adiabatic expansion and Joule-Thomson effects respectively. The slope of the latter will be used for this analysis.

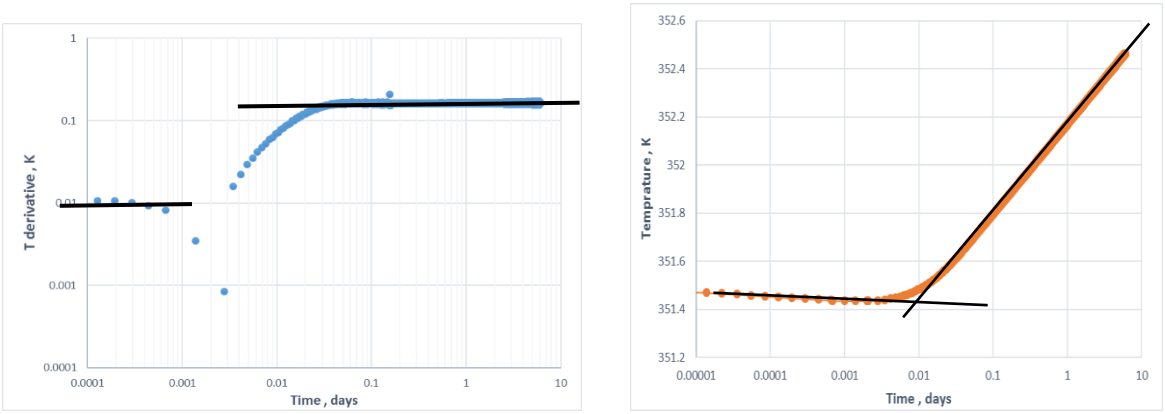

Figure 5-3 log-log(left) temperature plot for oil-water case and Semi-log(right)

Since there is not an analytical solution for TTA in oil-water producing well, I have modified single-phase liquid TTA solution in the following, similar concept as P-M multiphase method in PTA was used. An equivalent, single-phase liquid may then be assumed and the oil TTA solution (Eqn. 4-15) is modified as follows;

$$T_{wf} = T_i + m_{TLDD}\left[\log t + \log\left(\frac{\eta_t}{r_w^2}\right) + 0.351378 + 0.869S - \left(\frac{\varphi_t}{\varepsilon_{JTt}} - 1\right)\left[\log\left(\frac{C_{pRt}q_t}{\eta_t h}\right) - 0.8485\right]\right] \quad 5\text{-}4$$

Where;

$$m_{TLDD} = \frac{0.183234 q_t \varepsilon_T}{\lambda_t h} \quad 5\text{-}5$$

$$q_t = q_o B_o + q_w B_w \quad 5\text{-}6$$

The slope of TTA in the above formula is now a function of total flow rate, total mobility (λ_t) and total oil-water Joule-Thomson coefficient (ε_T). Total liquid flow rate can be measured from surface, but total JT coefficient needs to be estimated. Two methods to calculate the JT Coefficient in oil-water flowing system have been investigated:

- **Method 1**

This method modifies the definition of single phase JT to incorporate the effect of other phases as follows:

$$\varepsilon_T = \frac{1-\beta_t T_i}{(\rho C_p)_t} \qquad 5\text{-}7$$

Where;

$$\beta_t = S_o\beta_o + S_w\beta_w \qquad 5\text{-}8$$

$$(\rho C_p)_t = \emptyset(S_o\rho_o C_{po} + S_w\rho_w C_{pw}) + (1-\emptyset)\rho_s C_{ps} \qquad 5\text{-}9$$

This method requires detailed information on the thermal expansion coefficient, heat capacity and other parameters of both phases (*Table 5-5)*.

Table 5-5 Parameters used to calculate JT Coefficient in oil-water case

	Oil	**Water**
Phase saturation Dimensionless	0.7	0.3
Thermal Expansion Factor (β)(k^{-1})	0.00072	0.00045
Heat Capacity CP (J/kg.k)	2177	4168
Density ρ (kg/m3)	824	963

The calculation results are summarised in the table below;

Table 5-6 JT calculation method-1 results for the oil-water case

$\boldsymbol{\beta_t}$	0.000639	(k^{-1})
$\boldsymbol{(\rho C_p)_t}$	2520832	(J/m^3-k)
$\boldsymbol{\varepsilon_T}$	3.0765e-7	(k/pa)

- **Method 2**

Method 2 uses the slope of the late-time the radial flow regime slope for pressure and temperature to calculate the JT coefficient of oil-water mixture. The semi-log slope of pressure and temperature are 0.1635 and 527.4 respectively. The total JT coefficient calculated from the ratio of the slopes is:

$$\boldsymbol{\varepsilon_T} = \frac{m_{TTA}}{m_{PTA}} = \frac{0.1635}{527.4} = 3.1e-7k/pa$$

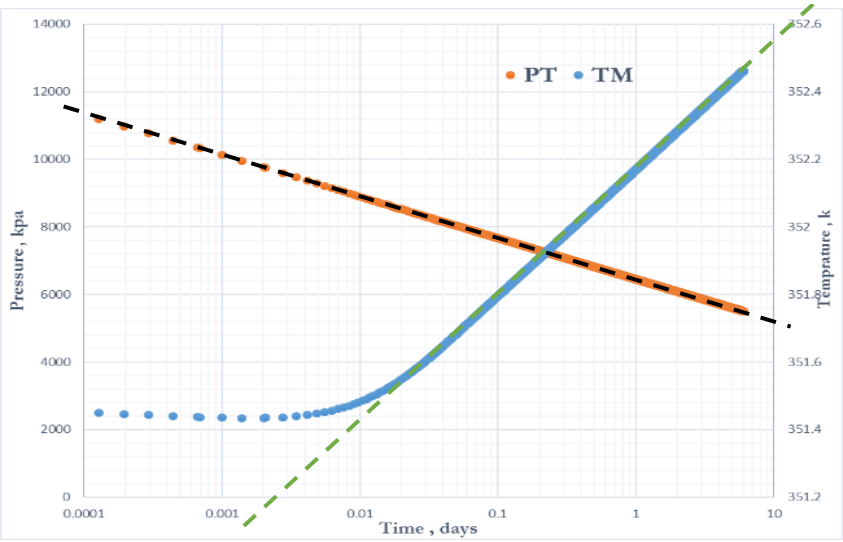

Figure 5-4 Semi-log pressure and temperature plot: JT calculation method-2: oil-water case

The JT coefficient calculated from method 1 and method 2 are consistent. The total mobility can now be estimated from *Eq. 5-5* as follows;

$$\lambda_t = \frac{0.183234 q_t \varepsilon_T}{mh} = 24.4 \text{ md/Cp}$$

This result is in close agreement with the previously calculated values from the relative permeability curve and that estimated by PTA. This shows that the proposed modifications in the thesis allow the application of TTA to be extended to oil-water system.

5.2.2.2 Case 2: Gas-Water System

The second multi-phase case is when both gas and water are mobile in the reservoir. The absolute permeability for this case is 10 md and effective permeability of gas and water is 2.7 mD and 2.8 mD respectively (similar to oil-water case, here it is assumed that saturations are fixed during production). *Figure 5-5* shows the production flow rate and the pressure and temperature data when the well produced gas and water. PTA and TTA results for this case are discussed below.

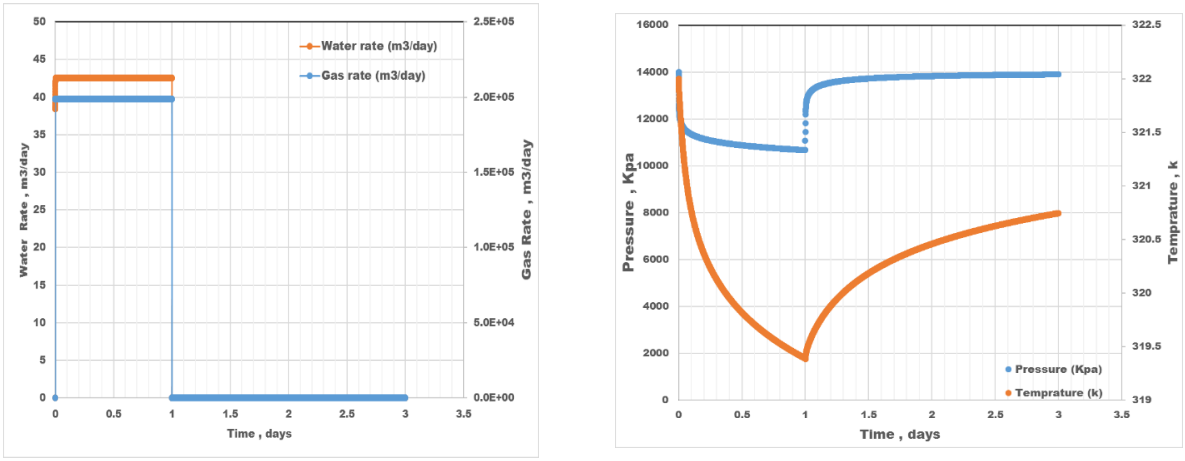

Figure 5-5 Gas and water production (left) and temperature and pressure (right)plots

- **PTA**

Figure 5-6 is the pseudo pressure calculated by *Eqn. 5-1* using build-up data. The effective permeability is estimated to be 2.64 md from the semi-log slope a value which is close to the value of the effective permeability of the gas.

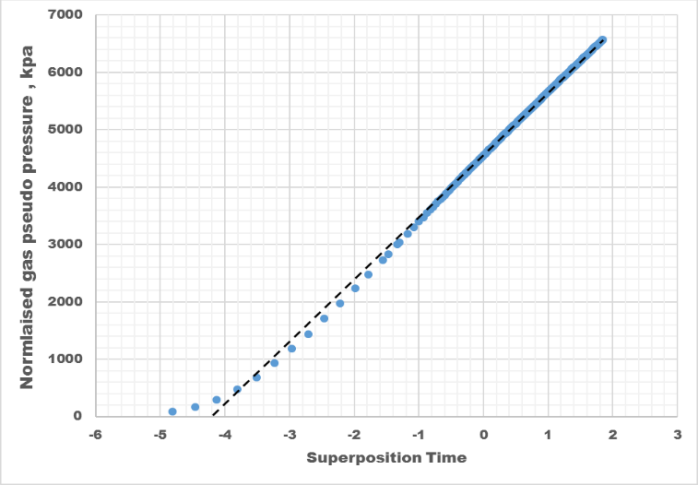

Figure 5-6 Pseudo-pressure versus time: Gas-water case

- **TTA**

The slope of gas TTA solution [89] requires more terms to be known, e.g. η^*, ε, B, than for the oil TTA solution.

$$T_{wb}(t) = T_i + m_{Tg} * \ln(t) - \frac{B\Gamma T_i Q_{sc}}{2kh}\left[\eta^{**} ln\left(\frac{\emptyset\mu c r_w^2}{4\lambda k}\right) + \varepsilon ln\left(\frac{200U_o\delta}{r_w^2(100+\delta)}\right) + \eta^*\gamma\right] \quad 5\text{-}10$$

Where;

$$m_{Tg} = \frac{B\Gamma T_i Q_{sc}}{2kh}[\eta^* - \varepsilon] \quad 5\text{-}11$$

$C_g = \frac{C_p\rho}{C_t}$	$\eta^* = \emptyset C_g \eta$
$C_t = \overline{\rho c_P} = \emptyset\rho C_p + (1-\emptyset)C_{pr}\rho_r$	$\eta = \frac{\beta_T T_i}{C_p\rho}$
$\varepsilon = \frac{1-\beta_T T_i}{C_p\rho}$	$m_{Tg} = \frac{B\Gamma T_i Q_{sc}}{2kh}[\eta^* - \varepsilon]$
$\eta^{**} = \eta^* e^{(-2\alpha U_o)}$	$\alpha = \frac{\varphi\mu c}{4\eta k}$

Where B is coefficient in pressure pseudo-pressure relationship, Γ is a constant in pressure solution, η^* formation averaged adiabatic coefficient, λ constant term, U_o velocity of convective heat transfer, δ deviation of analytical solution from logarithmic approximation, γ Euler-Mascheroni constant, ε Juole-thompson coefficient, C_g specific heat capacity of ags , C_t total formation volumetric heat capacity (Dada et al [89])

Two methods have been evaluated to determine the thermal properties involved in *Eqn. 5-11*.

- **Method 1**

The fluid properties are modified as follows to take into account the effect of multi-phase flow

The slope of pressure and pseudo pressure is also used to calculate the term B in *Eqn. 5-11* as 5.196e-13.

Gas-water Thermal Properties	
Joule-Thomson	$\varepsilon_{JT} = \frac{1 - (\beta_{gw})_T * T_i}{(C_p * \rho)_{gw}}$
Thermal Expansion Coefficient	$(\beta_{gw})_T = \beta_g * S_g + \beta_w * S_w$
Average formation heat capacity	$C_T = \emptyset(S_g \rho_g c_g + S_w \rho_w c_w) + (1 - \emptyset)\rho_r c_r$
Average fluid heat capacity	$(C_p * \rho)_{gw} = \emptyset(S_g \rho_g c_g + S_w \rho_w c_w)$
Formation averaged adiabatic coefficient	$\eta^* = \frac{\emptyset C_{gw} \beta_{gwT} T_i}{(C_p * \rho)_{gw}}$

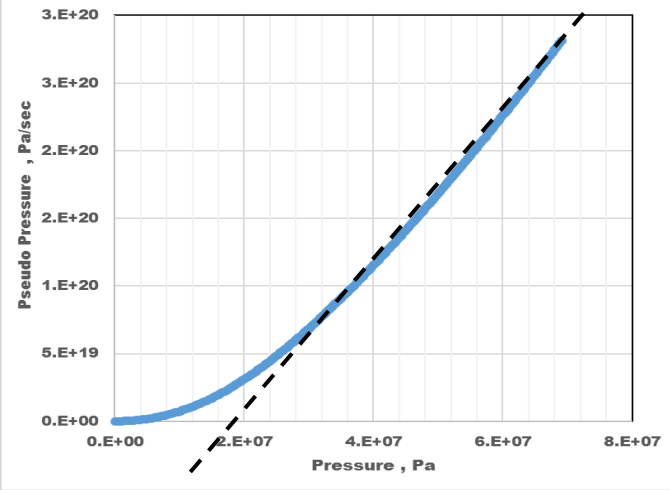

Figure 5-7 Pseudo pressure versus pressure plot to calculate B - Gas-Water case

Table 5-7 summarises the result of the calculation;

Parameters	Values	Unit
$\eta^* - \varepsilon$	3.26e-6	k/pa
ε	3.416e-6	k/pa
B	5.196e-13	Sec
$(\beta_{gw})_T$	0.0073	k^{-1}
$(C_p * \rho)_{gw}$	395829	$J/kg.m^3$
C_T	2350829	$J/kg.m^3$

Table 5-7 Result of the estimation: JT calculation method 1: Gas-water case

Having computed all the unknown parameters, the effective permeability of the gas is calculated from *Eqn. 5-11* as 3.67 md. This value is neither close to effective permeability of gas and nor to the absolute permeability.

As you can see the calculation process in this method for TTA gas-water system is cumbersome and tedious and the corresponding result is not even very accurate. These challenges cast doubt on practicability of this method for routine parameter estimation.

- **Method 2**

Pressure and temperature slope in SI unit for gas phase is defined as follows:

$$\frac{dP_{wf}}{d(lnt)} = m_p = \frac{B\Gamma T_i Q_{sc}}{2kh} \qquad 5\text{-}12$$

$$\frac{dT_{wf}}{d(lnt)} = m_{Tg} = \frac{B\Gamma T_i Q_{sc}}{2kh}[\eta^* - \varepsilon] \qquad 5\text{-}13$$

The term $[\eta^* - \varepsilon]$ can be calculated by dividing these two slopes (Eqn. 5-14) in a very simple manner followed by its insertion into Eqn. 5-11 to estimate the permeability. As a result, it is no longer necessary to go through the long, method 1 process of calculating all the thermodynamic terms from the corresponding equations.

$$\frac{m_{Tg}}{m_{pg}} = [\eta^* - \varepsilon] \qquad 5\text{-}14$$

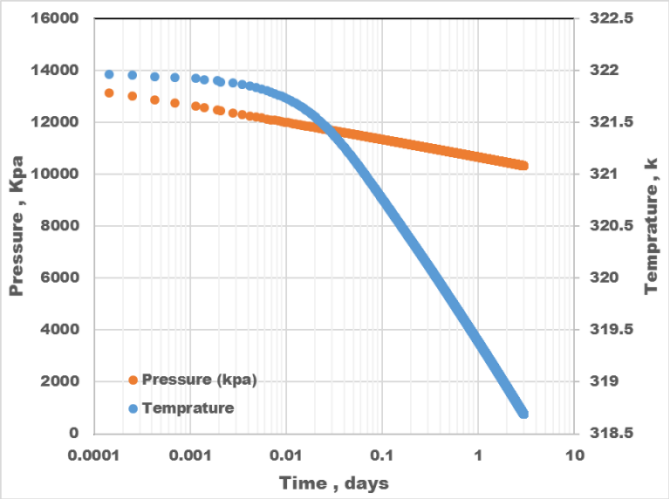

Figure 5-8 Pressure and temperature semi-log plot for gas-water case

Table 5-8 summarises the values of parameters calculated using method 2. The effective permeability of the gas calculated by this method is close to the actual value. This confirms that for a gas-water system, the method 2 not only provides a far simpler calculation procedure but also gives a more accurate result.

Parameters	m_T (k/sec)	m_P (Pa/sec)	$\eta^* - \varepsilon$ (k/pa)	K (md)
Value	0.646	309	2.087e-6	2.34

Table 5-8 Result of the estimation: JT calculation method 2: Gas-water case

5.2.2.3 Case 3: Oil-Gas System

The next case is for an under-saturated reservoir where the initial reservoir pressure is 1500 Psia and the bubble point is set at 1200 Psia. The model is designed so that after some time of production the bottom hole pressure drops below the bubble point resulting in a two-phase oil-gas system. The objective here is to investigate the effect of free gas on both pressure and temperature response.

The compositional module of CMG^{TM} software was used with the thermal option enabled and PVT behaviour modelled using WinProp^{TM} software was employed due to complexity of the PVT, i.e. phase changes. Different oil flow rate cases, between 90 to 150 m^3/day, were considered. Higher oil rate increases the pressure drop and reduce the time required for the free gas to appear in the reservoir.

- **PTA**

Figure 5-9 shows pressure trend for all the flow rate cases. Free gas appears in the reservoir once the pressure has dropped below the bubble point. A change in the total fluid mobility of the fluid occurs, as shown by the change in slope of the semi-log plot. According to *Figure 5-9*, from m_1 and m_2 absolute permeability and total mobility of the fluids in the reservoir can be estimated.

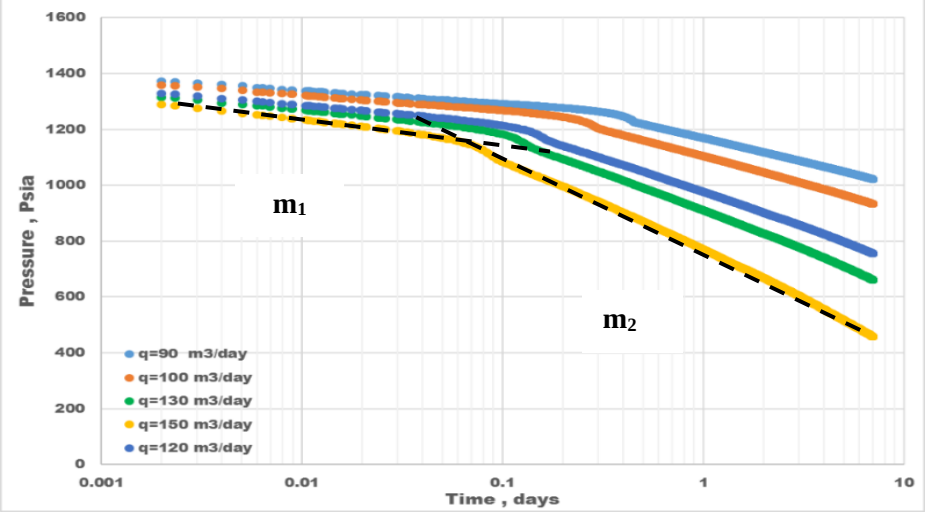

Figure 5-9 Pressure semi-log plot for gas-oil system

Figure 5-10 shows the in-situ gas-oil ratio for all the cases. It illustrates that gas production starts at different time and increases with different gradient depending on the oil flow rate in the reservoir.

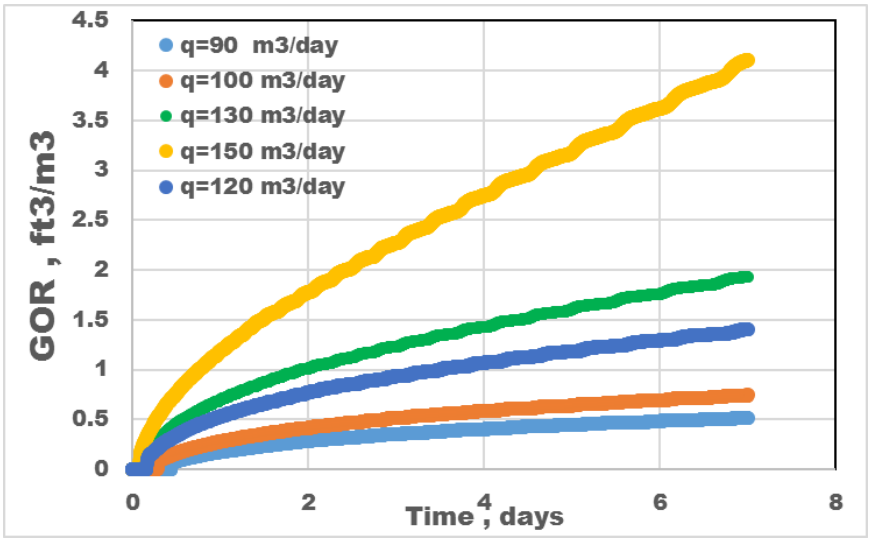

Figure 5-10 Gas-oil ratio for all the cases: gas-oil system

- **TTA**

Figure 5-11 indicates that transient temperature shows a more complex behaviour. Initially when oil is the only phase in the reservoir the temperature undergoes the normal trend for liquid starting with expansion followed by heating up due to JT effect. As soon as gas appears in the reservoir and the pressure changes, the temperature trend shows a change in slope. However, the most interesting phenomena takes place when the gas production in the reservoir increases, there is a critical point after which the JT cooling of gas becomes the dominating effect. This completely turns the temperature trend and results in the cooling-down trend on the temperature plot.

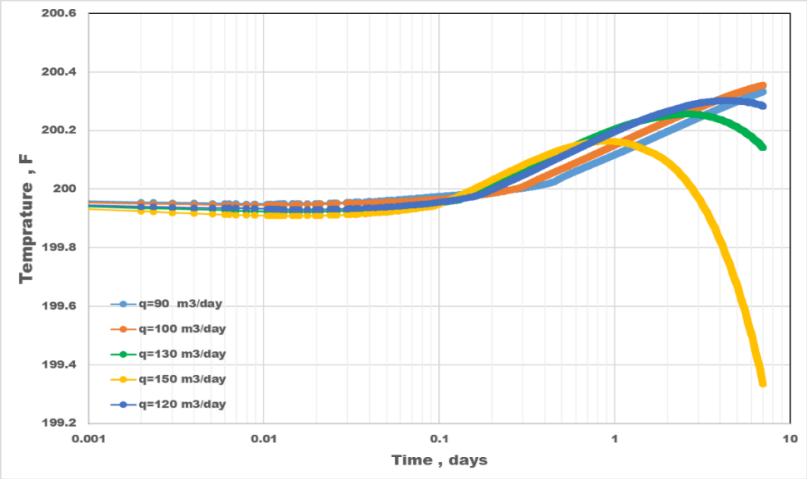

Figure 5-11Pressure semi-log plot for gas-oil system

Such dynamic changes of the trend make potential TTA in this type of reservoir very difficult given that this complexity will be further exacerbated by a variable gas flow rate, *Figure 5-10*, that also violates another assumption normally used in analytical derivations: constant flow rate .

5.3 PTTA in Bounded Reservoirs

PTA is a standard tool frequently used to reveal useful information about the reservoir boundaries, faults etc. Pressure data from a single well test in a high permeability reservoir or from multiple test data using deconvolution techniques can be used to characterise the reservoir boundaries. This contrasts with the current TTA solutions that were derived for an infinite-acting reservoir. This assumption was justified based on the fact, later will be shown in page 89, that the speed of the propagating temperature signal is much slower than that of the pressure wave. Observing the boundaries' effect on the temperature data is therefore impractical.

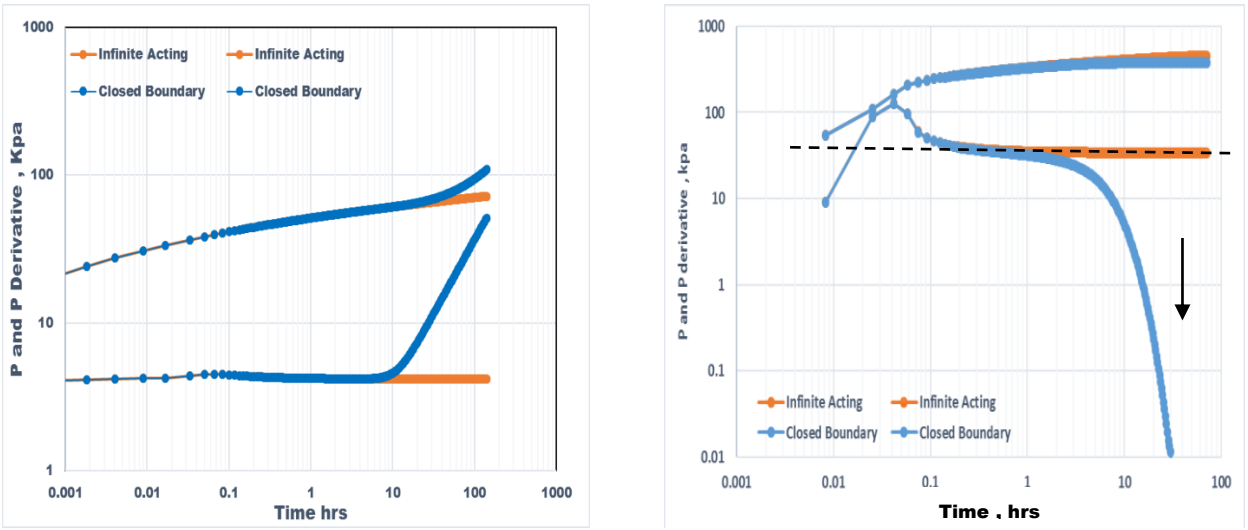

Figure 5-12 Effect of closed boundary on pressure draw down (left) and build-up (right) on a log-log plot

The thermal model predicts that temperature changes are a direct function of pressure variation, hence the effect of boundaries on pressure response might affect the temperature trend .In this section, the effect of a closed and a constant pressure boundary on both the pressure and the temperature response has been investigated.

5.3.1 Case 1: No-flow Boundary

The first case is single-phase oil producing well located in a reservoir with closed(no-flow) boundaries. The PTA and TTA result of this case were compared with the infinite acting reservoir response as follows:

- **PTA**

The well-proven tool to identify flow regimes in PTA is the log-log plot ,i.e. derivative plot. Each flow regime has a distinct signature. As shown in *Figure 5-12* , depending on the test, the features for closed boundary are different. For example for draw down the no-flow boundary feature is a unit slope line but for build-up is a roll-over curve.

- **TTA**

For this case study, the draw down test lasts for 6 days. The radius of investigation (ROI) after 6 days for pressure and temperature is calculated as follows;

$$r_{Pressure} = \sqrt{\frac{kt}{948\emptyset\mu c_t}} = \mathbf{425\ m} \qquad 5\text{-}15$$

$$r_{Temprature} = \sqrt{r_w^2 + c\frac{q}{\pi}t} = \mathbf{3.55\ m} \quad 5\text{-}16$$

Comparing the ROIs shows that pressure wave after 6 days already reached the lateral boundaries (located at 350 meter from the wellbore) while temperature response is still very close to the wellbore, making observation of the boundary effect on temperature data impossible.

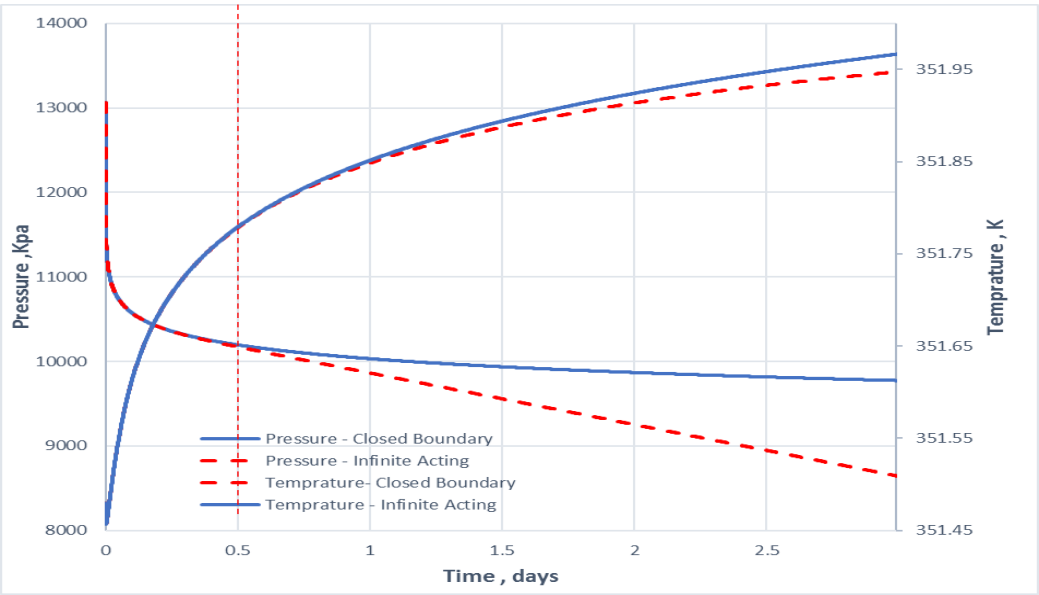

Figure 5-13 Cartesian Pressure and temperature plot: Comparing closed boundary with infinite acting cases

Figure 5-13 shows the temperature and pressure data for both infinite acting and closed boundary cases. As it can be seen, as soon as pressure wave reaches the boundary there is an extra pressure drop as the response deviates from radial flow regime and the reservoir changes from being infinite to one with a closed boundary. The temperature response at the sandface also deviates from infinite-acting line at exactly the same time as pressure response despite having a huge difference between their ROIs. This distorts the temperature semi-log slope and affects the parameter estimation.

Figure 5-14 depicts both the pressure and temperature data on a semi-log plot. The slope of the first temperature straight line is 1.5 times greater than the second one. If the first straight line, appearing at early time, was missed or misinterpreted as damaged zone, and the second slope was used for TTA calculation, the error in estimated parameter, e.g. permeability, would be around 150%.

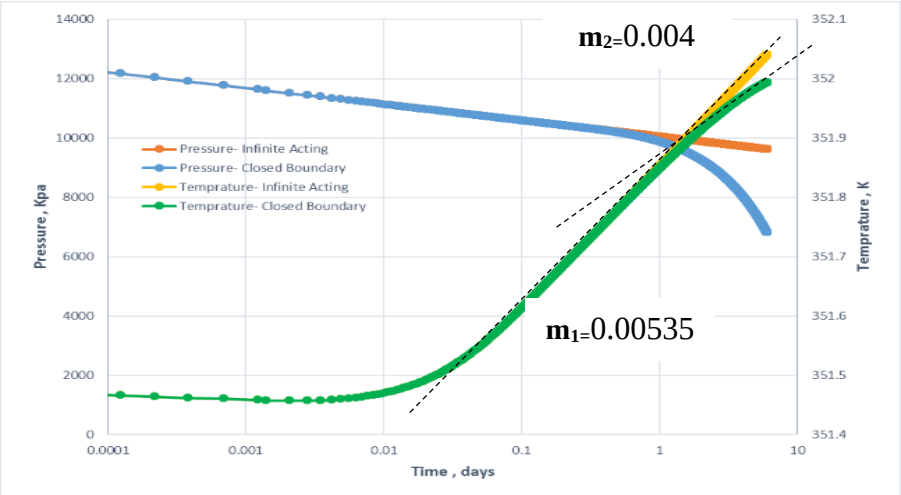

Figure 5-14 Semi-log pressure and temperature plot: Comparing closed boundary with infinite acting cases

Figure 5-15 also displays the temperature data on log-log plot. The signature of the boundary effect on the T derivative plot is its decline and deviation from the zero-slope line.

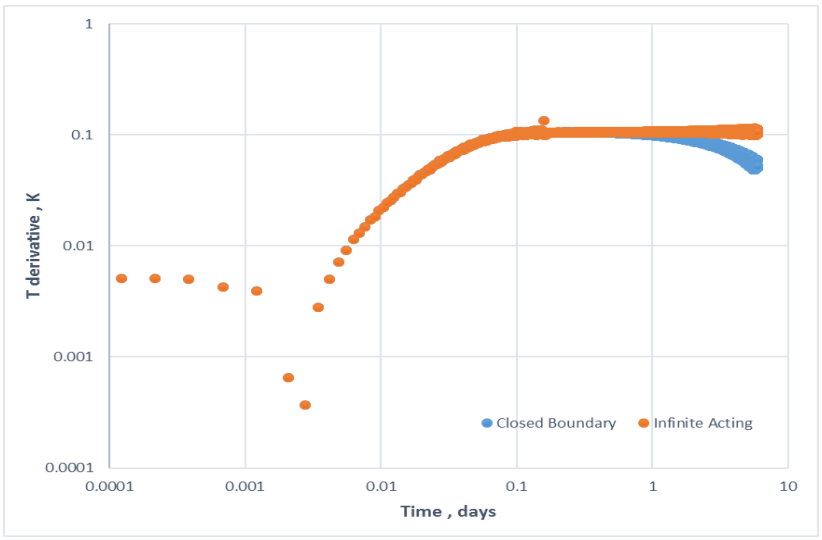

Figure 5-15 Temperature log-log plot: comparing a closed boundary and an infinite acting reservoir

5.3.2 Case 2: Constant-Pressure Boundary

The effect of constant pressure has also been investigated. A suitable aquifer was modelled to ensure a constant pressure.

- **PTA**

The signature for constant pressure boundary on the pressure log-log is a roll-over curve for both drawdown and build-up periods (*Figure 5-16* shows the log-log plot for draw down period)

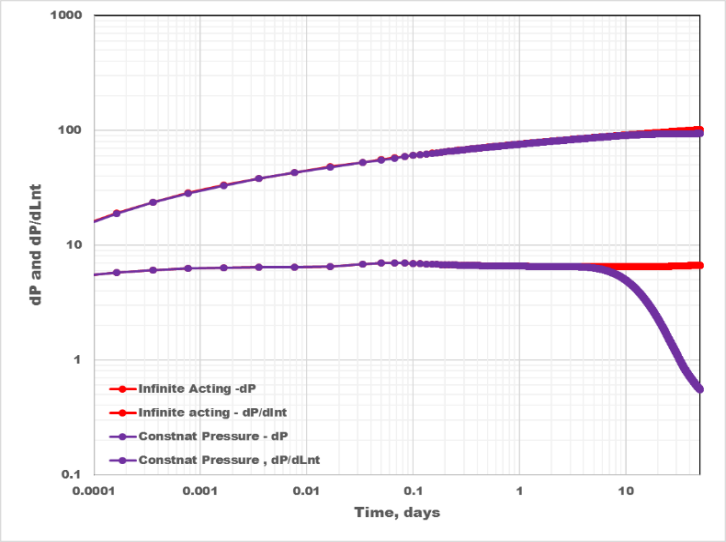

Figure 5-16 Pressure log-log plot: constant pressure boundary

- **TTA**

As for TTA, similar to closed boundary case, upon being affected by the pressure change due to the constant pressure boundary, the temperature slope starts to deviate from the radial flow regime. However, it should be noted that when there is a pressure support, the reservoir turns to steady-state condition and thereby pressure drop significantly reduces. As the main driving force for temperature is the pressure change, the effect of constant pressure might not be observed as clear as the closed boundary one. Figure 5-17 shows the semi-log for infinite and constant-pressure cases.

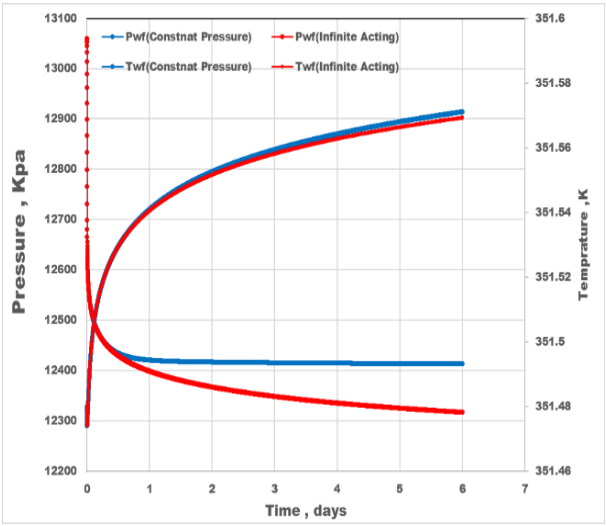

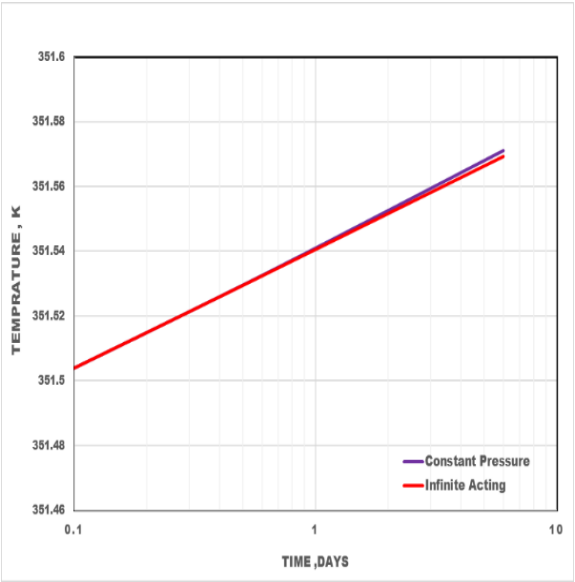

Figure 5-17 Pressure and temperature data for constant pressure and infinite acting reservoir

Another point that should be noted is that when there is limited pressure drop in the reservoir the heat conduction term starts to influence temperature changes. As explained before this term is normally ignored in analytical solutions. *Figure 5-18* shows how conduction affects the temperature slope in constant-pressure boundary cases. This alters the slope significantly and therefore affects the result of the analysis.

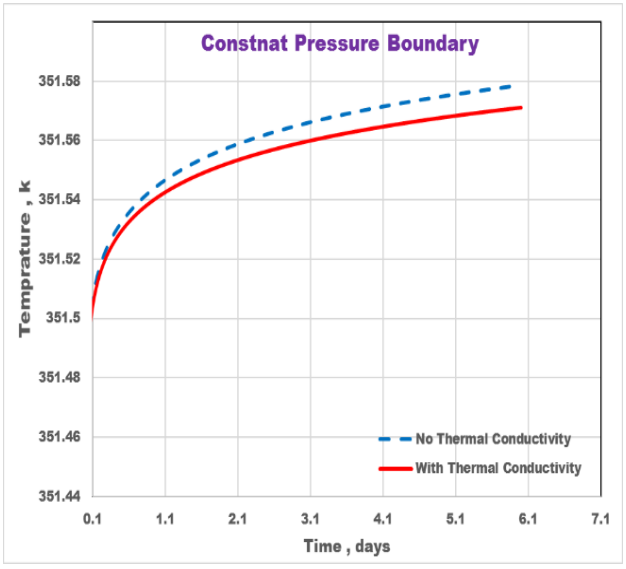

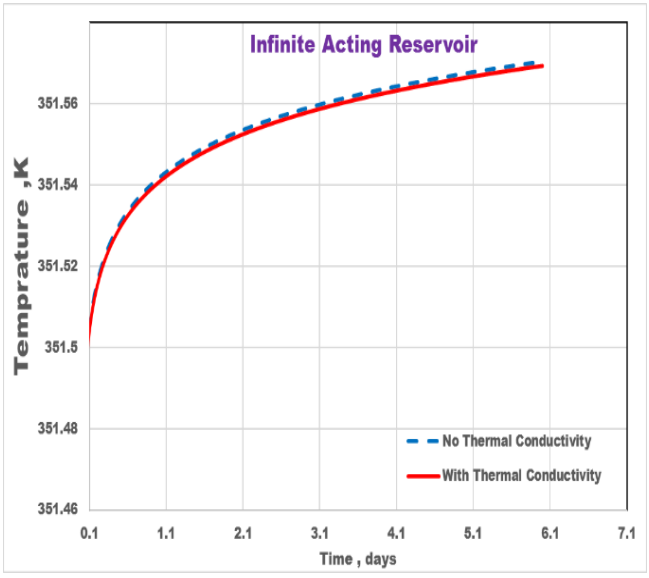

Figure 5-18 Effect of conduction - Constant pressure case

As shown in *Figure 5-19* , the effect of constant pressure boundary on temperature log-log plot is also deviation from zero slope line but might be harder to identify, depending on the magnitude of the heat conduction effect.

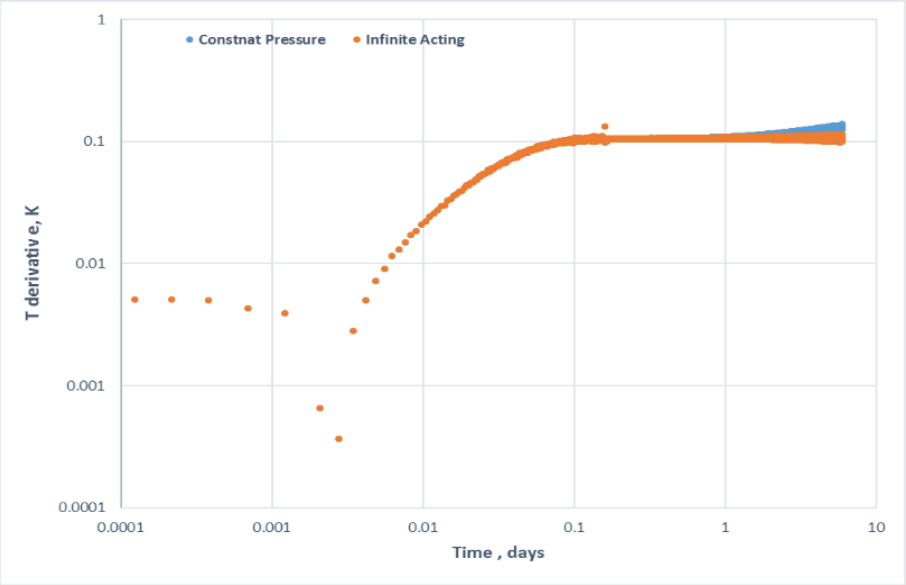

Figure 5-19 Temperature log-log plot: Constant Pressure case

In conclusion, care should be taken when using stand-alone TTA for parameter estimation. There is a high risk to misinterpret the effect of boundaries with damage zone, heterogeneity etc. The proposed workflow for PTTA in bounded reservoir is to first identify the flow regime using PTA, e.g. on the pressure build-up, derivative plot. Then the corresponding radial flow regime period can be selected on the temperature semi-log plot for parameter estimation.

5.4 PTTA in two types of Heterogeneous Reservoirs

The value of TTA in homogenous reservoirs, either using synthetic and real cases, has been demonstrated in the literature. However, in practice, no reservoir is perfectly homogenous and its permeability and all other rock properties, such as porosity varies between and within the zones *(Figure 5-20)*

Figure 5-20 Reservoir heterogeneity [107]

This section investigates the effect of reservoir heterogeneity on the results of TTA and PTTA results. Two types of reservoir heterogeneity are examined. First the permeability changes in the horizontal direction is considered, and then a composite reservoir with a different permeability in the damage zone is modelled.

5.4.1 Case.1: Reservoir with lateral changes of permeability

In this section four different realisation of permeability are considered with the mean of 107 md and the standard deviation from 10 to 40 md *(Figure 5-21).* In the following, the effect of this heterogeneity on PTA and TTA results is discussed.

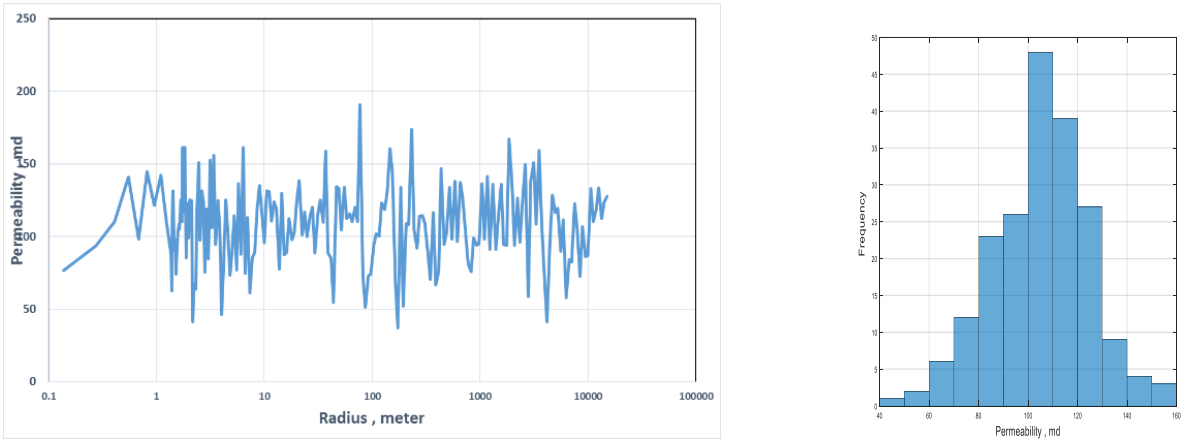

Figure 5-21 Permeability distribution {mean=107 md and STD =40 md}

- **PTA**

Figure 5-22 shows the pressure data in log-log and semi-log plots. Distinct features on the pressure derivative plot appear as the level of heterogeneity increases. The semi-log plot also shows that with single straight line fits the pressure data for all four levels of heterogeneity.

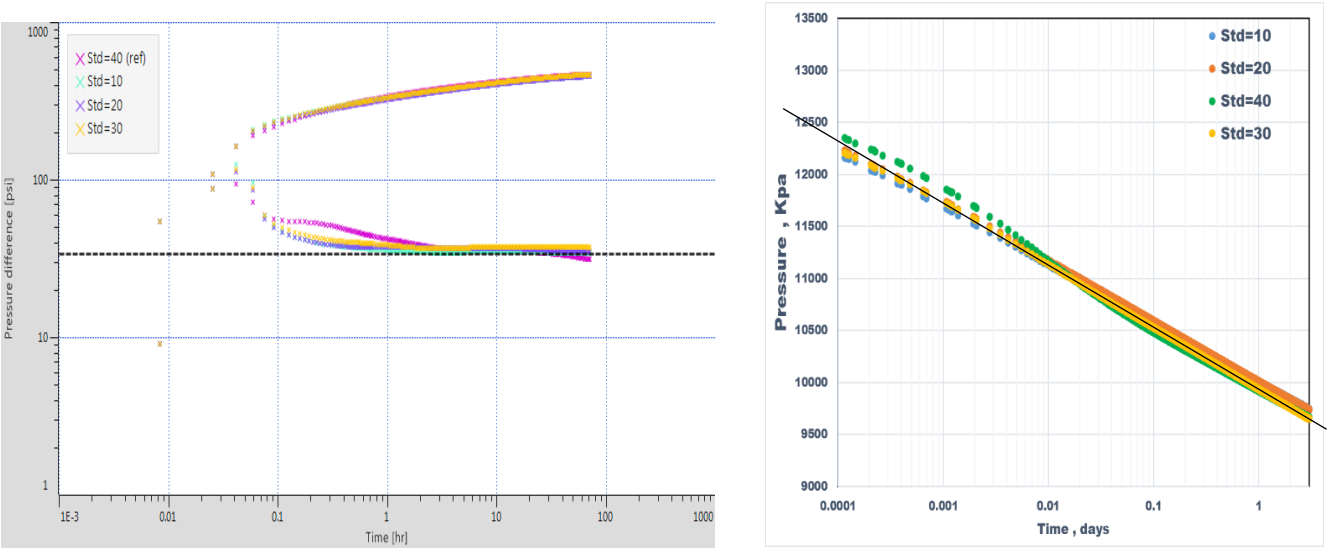

Figure 5-22 Pressure log-log (left) and semi-log (right) plots for all the heterogeneous cases

Table 5-9 lists the estimated permeability for all four realisations. The results deviates less than 10% from the arithmetic average permeability in the investigated area.

Table 5-9 Estimated permeability, from PTA, for all the cases

	STD=10	STD =20	STD=30	STD=40
Average Permeability (md)	105	98	97	100
Error %	2	8	9	7

- **TTA**

Temperature transient data for four levels of heterogeneity have also been analysed. Figure *5-23* shows the log-log and semi-log plot for all four TTA cases. As it can be seen even for the smallest standard deviation scenario, distinct features on both plots can be observed. This shows that the temperature reaction to even small permeability changes is distinguishable. The different levels of stabilisations on log-log plot is separated by a transition region.

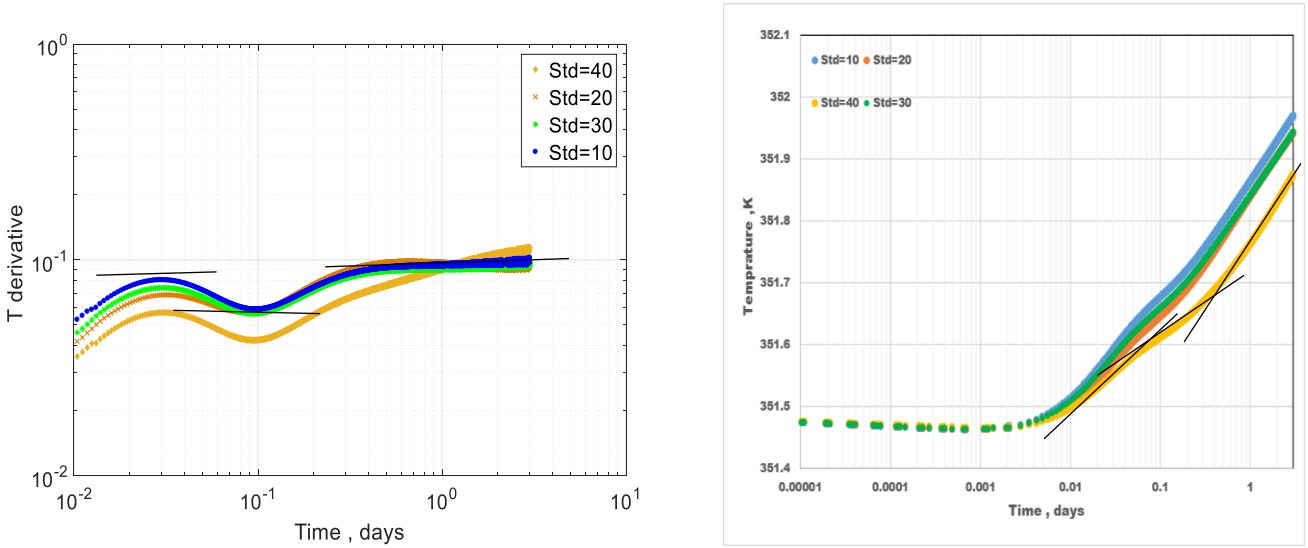

Figure 5-23 Temperature log-log (left) and semi-log (right) plots for heterogeneous cases

Permeability for all the straight lines on the semi-log plot is calculated and the average is reported in *Table 5-10*.According to the result, the TTA average permeability differs from PTA and actual result.

Table 5-10 TTA results: Heterogeneous cases

	STD=10	STD=20	STD=30	STD=40
Average Permeability (md)	131.5	142	141	160
Error %	23	32	32	50

- **PTTA**

The estimated permeability from PTA and TTA represents the average permeability in the investigated area. Due to the difference in the speeds of pressure and temperature waves, and different ROIs accordingly, the result of PTA and TTA in a heterogeneous reservoir might not be comparable. TTA result refers to local area near wellbore but PTA characterises farther inside reservoir. This leads to the conclusion that permeability calculated from TTA in heterogeneous reservoirs might be closer to the core, well log or RFT results rather than classical well test which go further into reservoir *(Figure 5-24).*

Another PTTA concern in heterogeneous reservoirs is that the second method for JT coefficient calculation, i.e. using PTA and TTA slopes, might no longer be applicable since it is difficult to the find the corresponding pressure and temperature slopes. Table 5-11 summarises the JT coefficient values calculated from the slope of pressure and temperature for all the realisations, the actual JT coefficient value is 4.45e-7 k/pa**.** As it can be seen, the error in the calculated JT coefficient increases as the reservoir becomes more heterogenous. Consequently, under such condition inaccurate estimation of permeability and flow rate will be obtained. Therefore, for heterogeneous reservoirs the method to calculate JT coefficient using its thermodynamic definition rather than rate of two slopes (method 2) is preferred.

Table 5-11 JT calculated from Method 2 in heterogeneous reservoir

	STD=10	STD=20	STD=30	STD=40
JT Coefficient, k/pa	3.945e-7	3.28e-7	3.79e-7	3.1e-7
Error,%	62	64	65	63.5

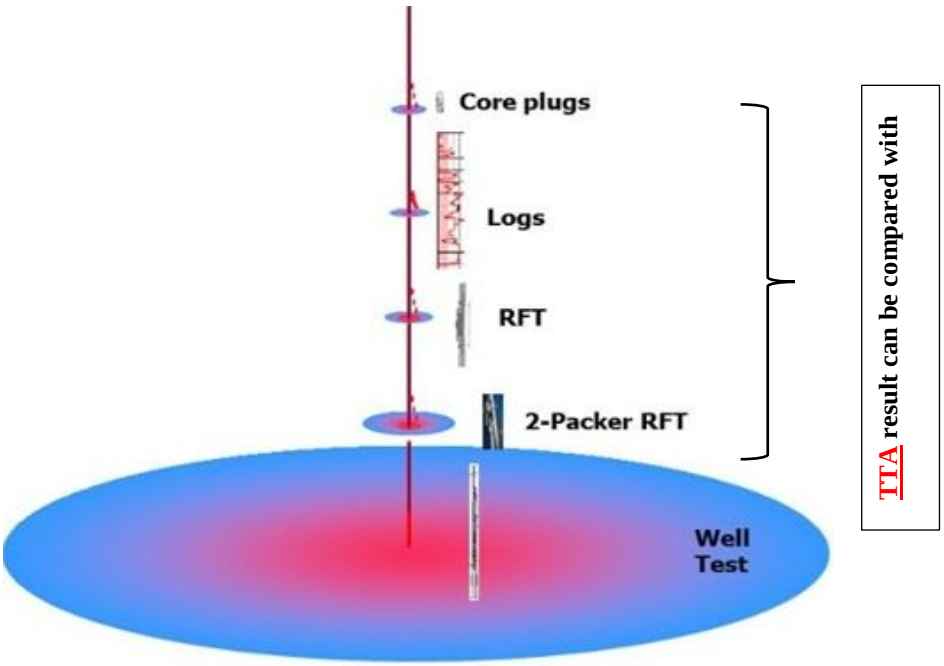

Figure 5-24 Radius of investigation for different analysis methods

5.4.2 Case 2: Reservoir with Formation Damage Region

Multi-composite system *(Figure 5-25)* is another type of heterogeneity where the reservoir is divided into several regions with different properties, e.g. permeability. Gas condensate reservoir with near-wellbore condensate bank, a homogenous formation with near-wellbore damage zone and a fractured reservoir with matrix and fracture permeabilities are examples of such reservoirs.

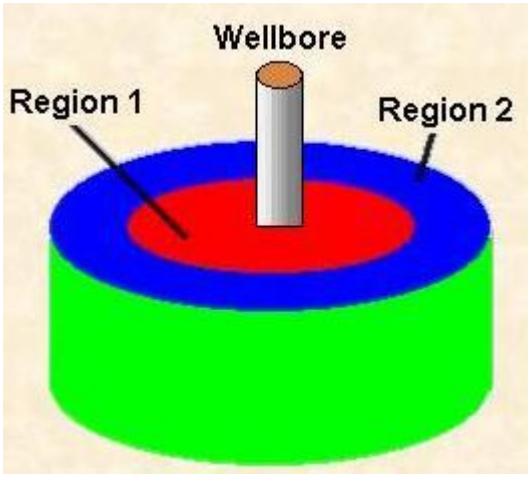

Figure 5-25 Multi composite reservoir[108]

This section presents the application of TTA and PTTA in a damaged formation. Characterisation of the altered zone has been reported as unique application of TTA. Temperature data in a damaged formation shows two distinct straight lines on a semi-log plot representing the damages and the virgin zones respectively. Some practical aspects of investigating the effect of the damage zone radius on the ability of temperature data to quantitatively analyse the formation damage is evaluated in this section.

The reservoir model in this section is a dual composite formation consisting of both damaged and undamaged zones. Four damage radii between 0.137 to 0.92 meter are considered. The damage permeability for all the cases is similar, 10 md, and the virgin permeability is 107 md. In the following the effect of damage radius on PTA, TTA and PTTA is discussed;

- **PTA**

Figure 5-26 shows the pressure log-log and semi-log plots for four different damage radii. According to Hawkins's formula, *Eq. 5-17*, increasing r_s would increase the skin and therefore creates extra pressure drop. A bigger separation between the level of stabilisations and pressure

plots on log-log plot is an indication of larger skin. PTA can provide information about skin factor, but does not provide details on its components (the damage permeability and its radius).

$$Skin = \left(\frac{k}{k_s} - 1\right) ln \frac{r_s}{r_w} \qquad 5\text{-}17$$

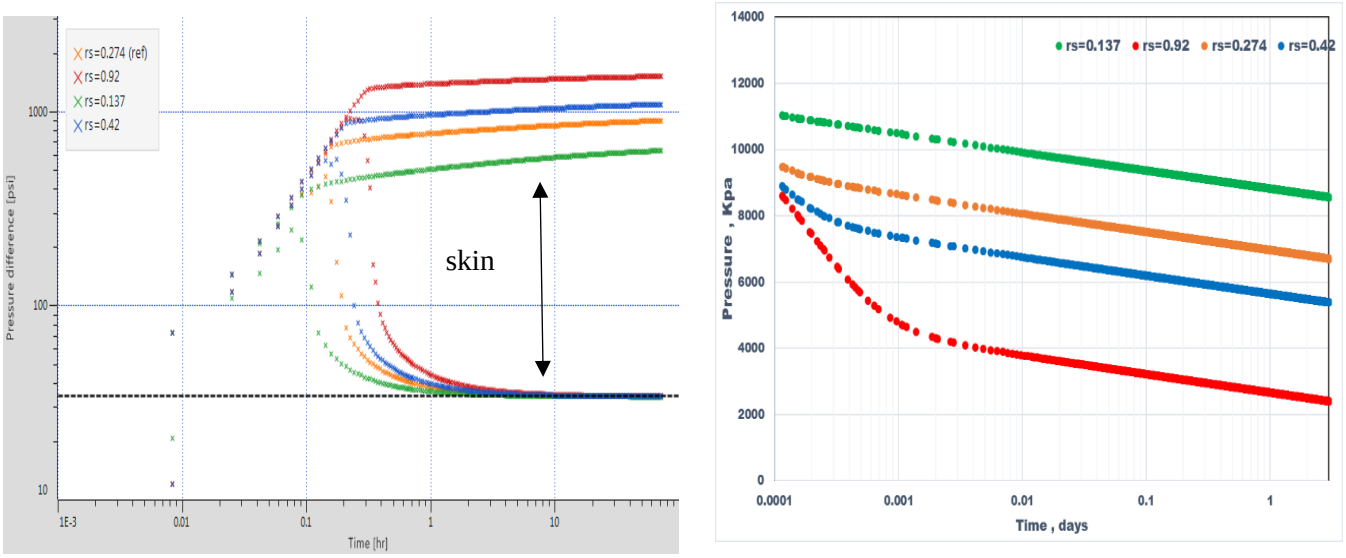

Figure 5-26 Pressure log-log (left) and semi-log (right) plots for different damage radii

- **TTA**

Regarding the temperature, the damage radius affects both the thermal expansion –dominated and the JT effect-dominated periods. The increased pressure drop caused by deeper damaged zone results in a larger cooling-down and heating-up effects. *(Figure 5-27).*

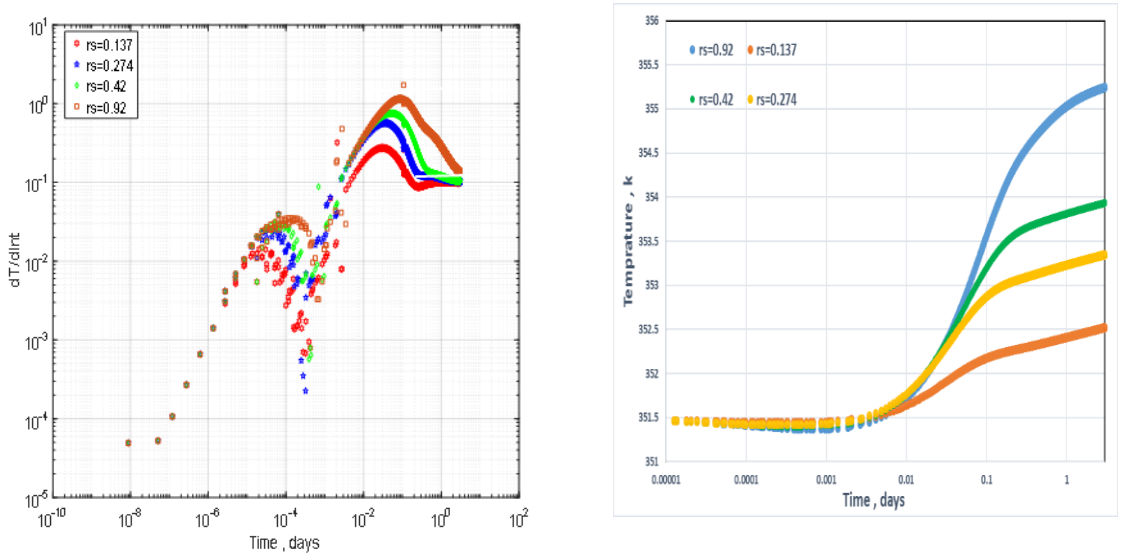

Figure 5-27 Temperature plot for different damage radius

Figure 5-27 also shows that the characteristic signature of a damaged formation on temperature log-log plot is the presence of two levels of stabilisations, which are inversely proportional to permeability. In contrast, on the PTA log-log plot, *Figure 5-26*, only one stabilisation can be observed and extra pressure due to skin can be seen as a bigger separation between the pressure and derivative plots.

Table 5-12 Damage zone and virgin reservoir permeability for different damage radius

Damage radius (m)	Damaged Region			Reservoir Region		
	m_1	k_s	Error %	m_2	k	Error %
r_s=0.137	0.6	42	320	0.2312	111	3.7
r_s=0.274	1.267	20.6	106	0.254	101.5	5.14
r_s=0.42	1.7	15	50	0.26	99	7.5
r_s=0.92	2.55	10.11	1.1	0.347	75	30

The semi-log slope of the temperature is used to characterise both damage zone and virgin reservoirs (*Table 5-12*)**.** According to the results, when the damage radius is less than 0.92 meter the estimated permeability is not accurate for the given test period, 3 days. In contrast, smaller damage zone results in a better estimation of virgin permeability.

According to the results, it can be concluded that TTA can effectively identifies the presence of a near-wellbore formation damage zone by a distinct semi-log straight line. The quantitative analysis of the damage zone improves as the depth of the damage zone become larger.

In addition, the corresponding damage and virgin-reservoir straight line is separated by a transition period. The TTA results obtained from the curve fitting are affected by this period when the test is not long enough. The suggested approach is to first confirm the existence of skin in the reservoir using PTA. This helps Engineers to be aware of the expected straight line for damage zone on temperature plot and reduces the risk of misinterpretation of this line as a clean reservoir response, when only one straight line appears on the temperature plot.

5.5 PTTA in Limited Entry Wells

TTA analytical solutions have been developed for vertical and horizontal wells, however, for both well geometries it is assumed that the well is perforated in the entire thickness of the

reservoir *(Figure 5-28)*. In the following, the application of TTA method in limited entry wells where it communicates with only a fraction of the producing thickness is investigated.

PTA in limited entry wells shows three flow regimes [106];

1. Radial flow over the open interval h_w .This yields the permeability-thickness product for the open interval $K_h h_w$ with infinitesimal skin of the well.
2. Spherical flow with the signature of negative half unit slope line on derivative plot. The spherical flow lasts until the upper and lower boundaries are reached. Analysis yields the permeability anisotropy$\frac{K_v}{K_h}$.
3. Radial flow over the entire reservoir thickness results in the second stabilisation on derivative plot. This yields the permeability-thickness product for the open interval $K_h h$ with total skin of the well.

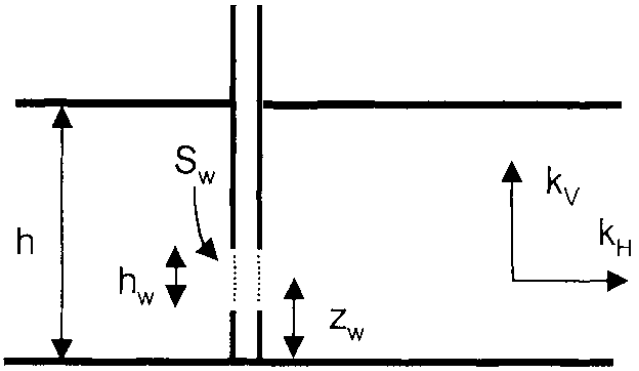

Figure 5-28 Limited entry well[109]

From the ratio of the first derivative and last derivative, the opening interval (h_w) can be estimated. However, in practice, partial penetration, responses rarely exhibit the three individual flow regimes as;

- The first radial flow is often missed due to occurring at a very early time or masked by wellbore storage. In this case $\frac{h_w}{h}$ and skin cannot be uniquely defined.
- The transition does not always follow a pure spherical flow behaviour.

In this section , a vertical well is modelled where it is completed in one fifth of the reservoir thickness (h=150 ; h_w=30). In the following the application of TTA, PTA and PTTA in limited entry well is discussed:

- **PTA**

Figure 5-29 illustrates the three flow regimes on pressure log-log plot. The first radial flow regime occurs within the first 6 minutes and may not be fully captured in practice. The ratio of the slope of the second radial flow regime to the first one and hence the fraction of the interval open to flow can be found as follows;

$$\frac{m_2}{m_1} = 0.2$$

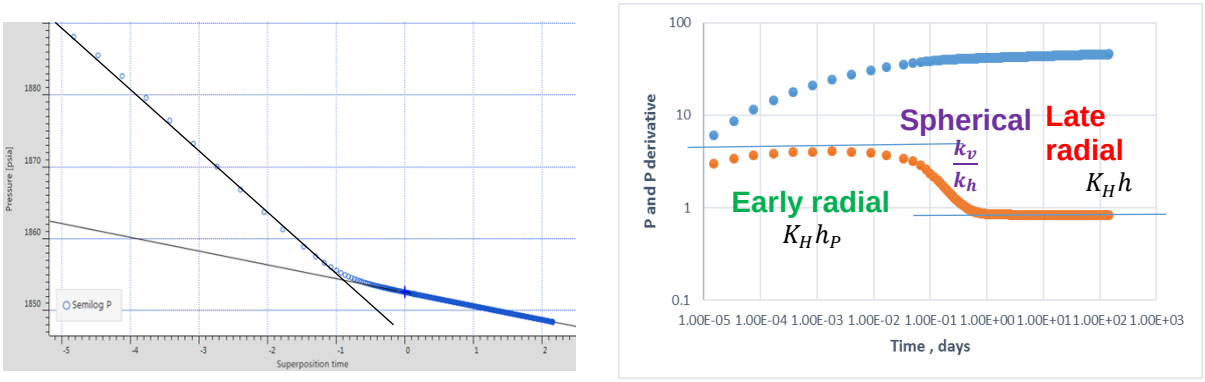

Figure 5-29 Semi-log (left) and log-log (right) plots for limited entry well

- **TTA**

As explained, missing the first radial flow regime using PTA is very likely. Lower speed of temperature propagation can be an opportunity here for TTA to be a complement for PTA in limited entry wells. Looking at TTA semi-log plot, *Figure 5-30*, there is only one straight-line level of stabilisation, lasting around 6 days, which represents the early radial flow regime.

By modifying the TTA radial equation, replacing h with h_w in *Eqn.5-18* , the product of $K_h h_w$ can be obtained. As the late radial flow regime in PTA gives $K_h h$, therefore from the ratio of late PTA radial flow regime and early TTA radial flow regime the opening interval can be estimated , provided the JT coefficient of the fluid is known or can be estimated.

$$m_T = -0.183234 \frac{q_{sco} B_o \mu_o \varepsilon_{JTo}}{k_o h_w} \qquad 5\text{-}18$$

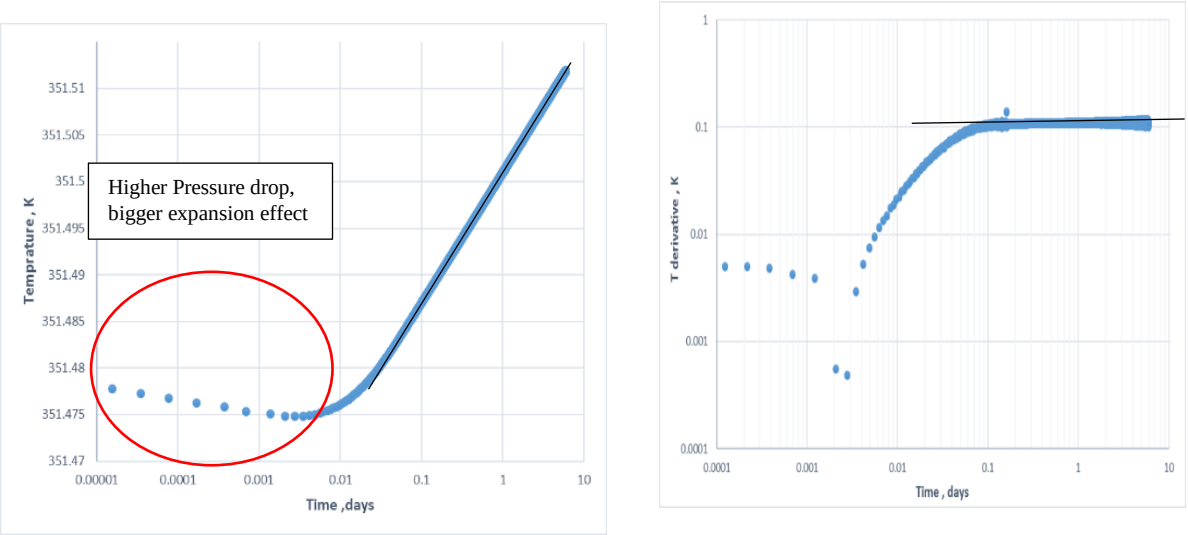

Figure 5-30 Temperature semi-log (left) and log-log (right) for limited entry well

$$\frac{m_P}{m_T} = \frac{h_w}{\varepsilon_{JTo} h} = \frac{47.22}{0.1093} = 0.2$$

The fractions of completed interval in the well calculated using PTTA and PTA are similar. This highlights the opportunity provided by integrating pressure and temperature data in limited entry wells.

5.6 Summary

This chapter has extended the current knowledge of TTA and PTTA to multiphase, bounded, heterogeneous and limited entry wells. The following summarises the main findings of chapter;

- **Multiphase Flow**

Two TTA methods for multi-phase oil-water and gas-oil was presented; one by modifying the current single-phase TTA solution to an equivalent single-phase model and another one with estimating multi-phase properties with integration of PTA and TTA slopes. For oil-water system both methods were shown to be very accurate to estimate the parameters. However, it was demonstrated that for gas-oil system, parameter estimation by the modified equation is cumbersome and not accurate enough too. In contrast, the integrated method by using PTA and TTA slopes for gas-water system was straightforward and more precise.

- **Bounded Reservoir**

The results of this chapter showed that when pressure change reaches the lateral boundary the temperature data is also affected even though the temperature change is still far from the boundary. The effect of temperature changes due to pressure changes is more pronounced for closed boundary case than constant pressure one.

- **Heterogeneous Formation**

The permeability estimated from the TTA and PTA represents the average permeability of the investigated area, but as speed of pressure and temperature propagation is different, therefore how far each signal has travelled would be different too, and as a result the output of TTA and PTA might not be similar and comparable. This difference affects the estimation of the JT coefficient from the slope of TTA and PTA as finding the corresponding slope might be difficult.

- **Limited Entry Well**

It was demonstrated that integrated PTA and TTA in limited entry wells helps to estimate open interval(thickness). This parameter normally can not be estimated by stand-alone PTA.

In summary, in complex flow situations the TTA should likely be treated together with the PTA and should not be regarded as an alternative. The result of these two methods can be comparable if certain conditions are satisfied.

Chapter 6 Flow Rate Allocation in Multi-Phase Multi-Zone I-Wells using PTTA

6.1 Introduction

Temporary and permanent, high-precision downhole pressure and temperature sensors are commonly installed in today's wells. There is a natural desire to use their measurements for zonal flow rate allocation where the in-well flowmeters or production logs are not easily or cheaply available. This chapter presents a new soft sensing method for multi-phase production allocation in multi-zone vertical wells using the modified version of recently developed TTA solutions.

The multi-phase TTA solution, presented in the previous chapter, together with the equivalent PTA solution are integrated in an algorithm to estimate zonal formation properties and consequently to allocate zonal water cuts and flow rates. This approach explores the potential of integrating transient pressure and temperature data into a continuous determination of zonal flow rate and water cut for various I-Well completion types.

The performance of virtual flow-metering algorithm proposed in this chapter is successfully tested with synthetic I-wells completed with various flow control devices in the presence of multi-phase flow. The inverse problem is formulated and employed to minimize the prediction-observation mismatch using Levenberg-Marquadt algorithm. It is shown that temperature data from a single drawdown and pressure data from the following build-up period can be sufficient to estimate layer parameters in a multi-layer reservoir. In addition, the robustness of the presented algorithm under various measurement uncertainties such as faulty gauges, noise and gauge bias/drift is also investigated.

6.2 Flow Rate Measurement and Allocation Background

Downhole reservoir surveillance hardware that could directly measure zonal flow rates and phase cuts is either under development or brings an increased risk in the complexity and cost of their installation. Hence these monitoring devices are not normally installed and instead, the process of sequentially closing of the zonal ICVs for zonal build-ups with measurement of the total well production has become the basis of the standard practice for zonal allocation. However, this type of well test only results in the flow rate value measured at a particular time.

The procedure also results in losing production and may also be difficult when restarting a closed well or zone. Costly production logging may be an alternative providing an inflow rate and/or a phase-cut profile. However, this measurement is also made at a specific time without the possibility of continuously delivering the current phase-cut and production rate.

The alternative is to use the indirect measurements of temperature, pressure and total well rate to calculate multi-phase, multi-zonal flow rates. The soft-sensing or virtual flow metering methods have been used in many reservoir monitoring and reservoir simulation model updating case studies [110, 111]; gas-lifted wells [112], underbalanced drilling [113], conventional and multi-lateral wells[114], gas cone allocation in multi-zone reservoirs [115]and well-testing optimisation and automation[116].

The in-well virtual flow-metering type soft-sensing methods have been divided into passive and active applications *(Figure 6-1)*;

- **Passive soft sensing:** This method needs information from different measurement sources to estimate reservoir parameters and zonal flow rate. The application of passive soft-sensing method has been studied by man researchers For example, Muradov et al [23]developed an automatic zonal flow rate allocation algorithm for I-wells using real-time downhole (P/T) measurements. They tested three well-known numerical optimisation algorithms (steepest descent, Gauss –Newton algorithm (GNA) and LM algorithm) and EKF together with a comprehensive physical model to describe pressure and temperature changes across the IWC. Muradov and Davies (2011a) also showed the application of DTS data for zonal flow rate and pressure allocation in advanced wells. Several classical distributed temperature interpretation methods were used together with an extension of the temperature tangent analysis technique for multi-phase flow rate profiling in I-wells.
- **Active soft sensing:** Malakooti et al [46] recently improved passive soft-sensing by using data from the routine cycling of ICVs in an I-Well. The active soft-sensing algorithm employs a second optimisation step to design the next multi-rate test once the zonal properties have been estimated. In the first step the zonal properties such as reservoir pressure, productivity index, water-cut, gas-liquid ratio is calculated by minimising the total mismatch between the measured data and the values predicted by the multi-phase flow model. A generalised reduced gradient (GRG) nonlinear optimisation method is used. The optimal ICV settings for the next multi-rate test is then found with a gradient

free optimisation method, the Deformed Configuration techniques. This step identifies the next flow rate that has a higher mismatch in order to better explore the search space.

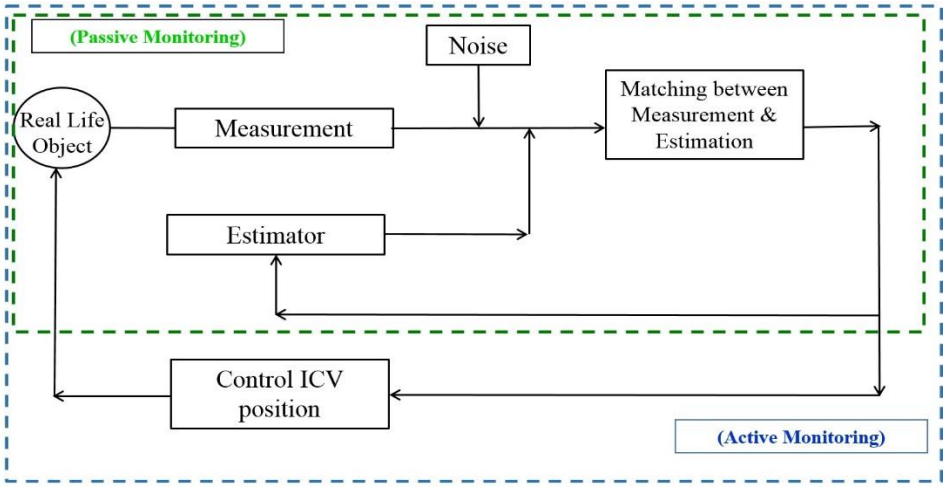

Figure 6-1 Passive and active soft-sensing workflow [46]

One limitation of published soft-sensing methods is that they rely on a shut-in period to measure a pressure build-up in multiple zones and/or to obtain a stabilised reservoir pressure. The newly developed soft-sensing method described in this chapter can be fitted into passive category. The algorithm integrates pressure and temperature transient data for multi-phase multi-zone flow rate allocation. Parameter estimation is improved by use of draw down (production) data in the minimisation process.

The following section describes some of the practical aspects of data measurement. Both forward and inverse modelling approaches have been evaluated. Finally, the application of the soft-sensing method for reservoir characterisation, flow rate allocation and completion monitoring based on various case studies will be illustrated.

6.2.1 Measurement Sources and Practical Consideration

In theory, soft-sensing methods can use any type of measurement, For example, Malakooti [43]used stabilised and transient pressure data, pressure drop across ICVs, steady-state temperature downstream of ICVs and total flow rate. However, there are some practical limitations that have to be considered when using data from real wells. Some practical considerations for selecting measurement sources in soft-sensing algorithms will now be discussed;

- **Transient and steady state pressure:** Annulus and tubing pressure and temperature data from PDGs are often the main source of information for real-time flow rate soft sensing in intelligent wells. Permanent gauges can record pressure transients from both planned well tests and another operational shut-ins. The preferred period for PTA is zonal build-up test as the flow rate is completely stopped and thus constant. Higher quality data can thus be expected. By contrast, the draw down data can be subject to higher noise level. *Figure 6-2* compares the pressure draw down and build-up data from a well test in a North Sea oil well.

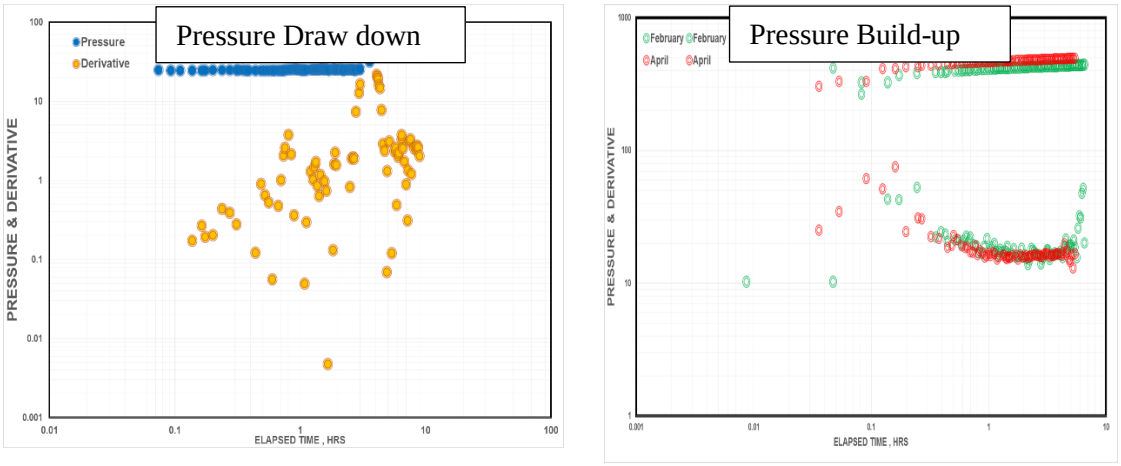

Figure 6-2 Pressure draw down (left) and build-up (right) data measured in a deviated well in North Sea

- **Pressure drops across ICVs:** In theory by using pressure downstream and upstream of ICVs, zonal flow rate can be calculated from Bernoulli equation, Eq. 6-1.

$$\Delta P_{ICV} = \frac{8 C_u \rho_{mix} q_{ICV}^2}{\pi^2 C_v^2 d_v^4} \qquad 6\text{-}1$$

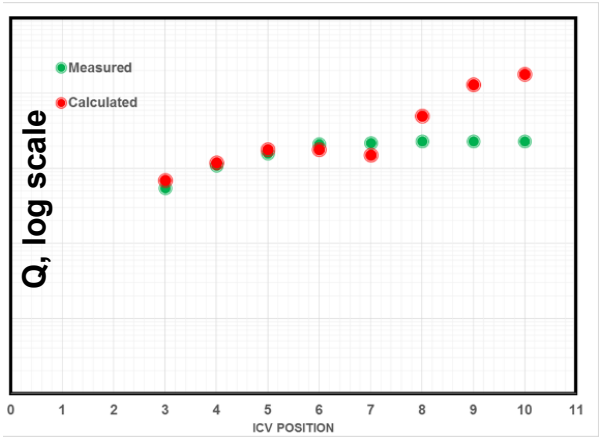

ICV Position	Pressure drop across ICV (Psia)
3	257
4	180
5	110
6	40
7	8
8	8
9	8
10	6

Figure 6-3 Flow rate allocation using pressure drop across ICVs

Figure 6-3 compares the flow rate calculated using ICV pressure drop and actual values for a deviated well in North Sea during ICV cycling process. As it can be seen after position 7, the pressure drop across gauge is not high enough and the correspondingly calculated flow rate is incorrect. This means that at the higher ICV positions, the differential pressure resolution and gauge placement will influence the flow rate estimation accuracy. Therefore, the practical application of Bernoulli after position 7 for this I-well installation is inappropriate.

- **Steady-state and transient temperature**: as discussed previously, the to-date most used period for interpreting transient temperature is the draw down period with several solutions available for this period. During build-up period the heat conduction also becomes important affecting the complexity of analytical solutions.

Other potential measurement sources include total (well) phase rates measured either at the surface or downhole. This study combines the interpretation of measurements of transient build-up pressure and draw down temperature; stabilised pressure in the annulus; and total flow rate into an algorithm for parameter estimation and flow rate allocation.

6.3 Modelling and the Algorithm

6.3.1 Methodology: New Soft-Sensing Method

This chapter describes the forward and inverse methods that have been developed to determine the zonal flow rate and estimate the reservoir properties in multi-layer I-Wells. The measured data for the algorithm, i.e. temperature and pressure, was generated for various scenarios using the previously described non-isothermal simulator. The inverse model was also formulated to determine the reservoir and thermal properties such as permeability, skin, Joule-Thompson coefficient as well as zonal flow rate by applying non-linear regression. The following analytical solutions are employed to calculate the predicted temperature and pressure data: single-phase transient build-up pressure (Eq. 4-5), the transient draw down temperature (Eq. 4-15), multi-phase oil-water, Perrine-Martin Equation for PTA (table 5-1), the developed TTA (Eq. 5-4) and also productivity index (Eq. 6-10). It should be noted that the multi-phase cases in this chapter are limited to oil-water system since the results of the previous chapter showed that the modification proposed for oil-gas system was not very accurate). The discrepancy between measured and calculated values is then minimised using an appropriate optimisation algorithm.

- **The Inverse Model**

A deterministic optimization algorithm, Levenberg-Marquadt (LMA), is programmed to iteratively update the unknown parameters until the objective function is sufficiently minimized. L-M a gradient-based method which it's restricted procedure allows to define the upper and lower bound in the algorithm to limit the search space. This algorithm is implemented in many well test analysis software such as KAPPA as it is a quite efficient method for over-determined problems, i.e. the number of model parameters to be estimated is much smaller than the number of observed/measured data to be history matched. Two forms of the LMA equation are shown below -an objective function is constructed to describe the discrepancy between measured and simulated temperature and pressure data.

$$f(x) = \frac{1}{2}\|d - g(x)\|_2^2 = \frac{1}{2}(d - g(x))^T C_n^{-1}(d - g(x)) \qquad (6\text{-}2\ a)$$

$$f(x) = \frac{1}{2} I_p \sum_{i=1}^{N_p} \left\{ w_{p,t} \left[\frac{p_{obs,t} - p_{cal}(x, t_t^p)}{\sigma_p^2} \right] \right\}^2 + \frac{1}{2} I_T \sum_{j=1}^{N_T} \left\{ w_{T,t} \left[\frac{T_{obs,t} - T_{cal}(x, t_t^p)}{\sigma_T^2} \right] \right\}^2 \quad (6\text{-}2\ b)$$

Where d = measured P&T data obtained synthetically from non-isothermal simulator,

$$d = \left[p_{i1,} \dots\dots\dots, p_{iN}, T_{i1,} \dots\dots\dots, T_{iN} \right]^T \qquad 6\text{-}3$$

g(x) = calculated analytical temperature and pressure,

$$g(x) = \left[p_{i1,} \dots\dots\dots, p_{iN}, T_{i1,} \dots\dots\dots, T_{iN} \right]^T \qquad 6\text{-}4$$

$x = \left[q_i, k_i, S_i, \phi_i, \varepsilon_{JT}, \dots\dots \right]^T$, in which x is the parameter-of-interest, comprising k (permeability), q (rate) and S (skin) or ϕ (porosity) or ε_{JT} (Joule-Thompson coefficient) for each zone. In equation 6-2 b; Ip and I_T terms are indicators which can only be either a "1" or a "0". They are employed for matching either pressure, temperature or both. $w_{p,t}$ and $w_{T,t}$ are the weights for pressure and temperature data, respectively which can be 0 or a positive number. σ_p and σ_T represent the standard deviations of the errors associated with the pressure data and the temperature data.

- **Modelling and Data Selection Procedure**

A non-isothermal simulator is employed to produce the transient sand face temperature and the pressure acquired from downhole gauges during well testing. The result of numerical simulator has a reasonable compatibility with analytical solution however, the remaining mismatch can

be attributed to the assumptions used to derive analytical solution, numerical error etc. (*Fig. 4-5 and Fig. 4-6)*

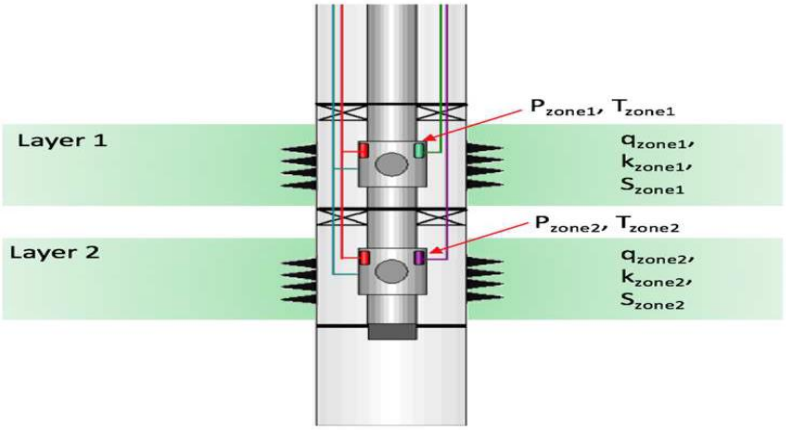

Figure 6-4 two-layer I-well completion

A vertical intelligent completion producing from two zones in commingled flow is considered as the base case. The two layers are isolated from each other by shales and a packer in the annulus of the completion. Each zone is equipped with PDGs, measuring pressure and temperature in tubing and annulus, and different flow control devices, e.g. ICVs and AICDs (*Figure 6-4).* The synthetic 6-days well test comprised of 4 days' constant drawdown followed by 2-days build-up (Figure 6-5*)***.** The simulated transient pressure and temperature response for both layers were extracted and then compared against predicted value.

A pre-processing step prior to history matching is to reduce the number of measured pressure and temperature data points while ensuring that the new data set is still representative of all the data. In this study, a series of data point with logarithmic time spacing were selected for analysis (*Figure 6-6*).

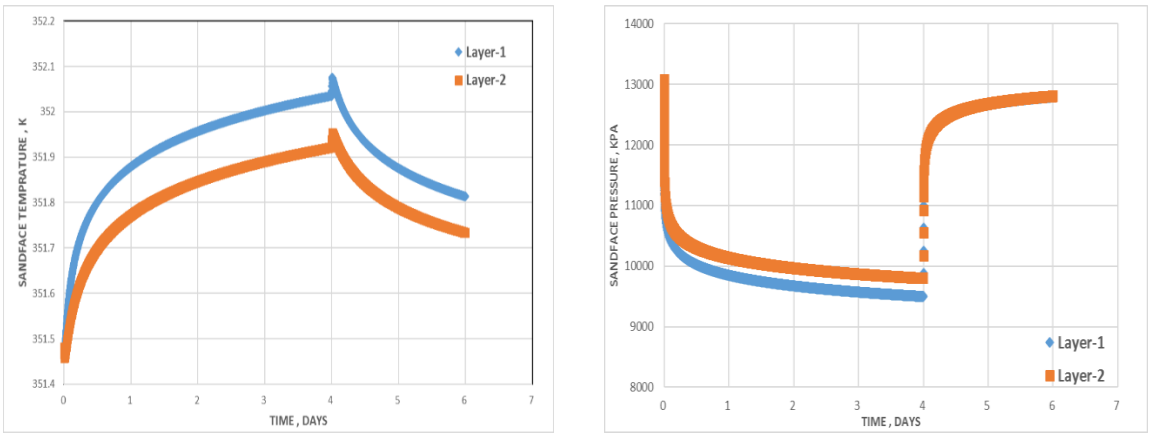

Figure 6-5 Example of Pressure (right) and Temperature (left) responses for a two-zone reservoir

Other key pre-processing steps can be required when analysing real data such as denoising and outlier removal. Early-radial flow regime for pressure build-up test and late-time JT period in draw down temperature are selected for history matching described in Figure 6-7 summarises the soft-sensing workflow used in this chapter; the following sections

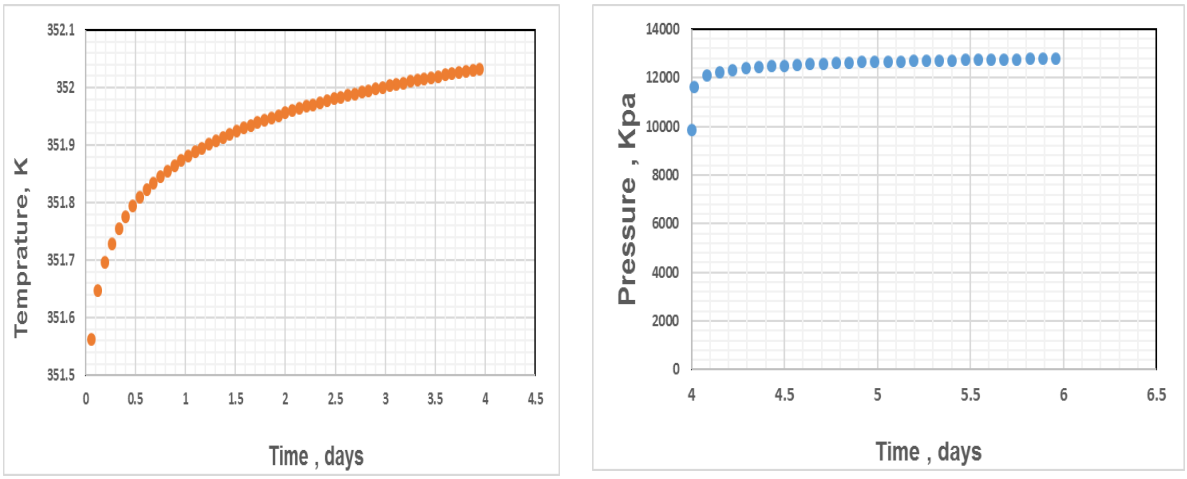

Figure 6-6 Example of Reduced number of data point used for minimisation process

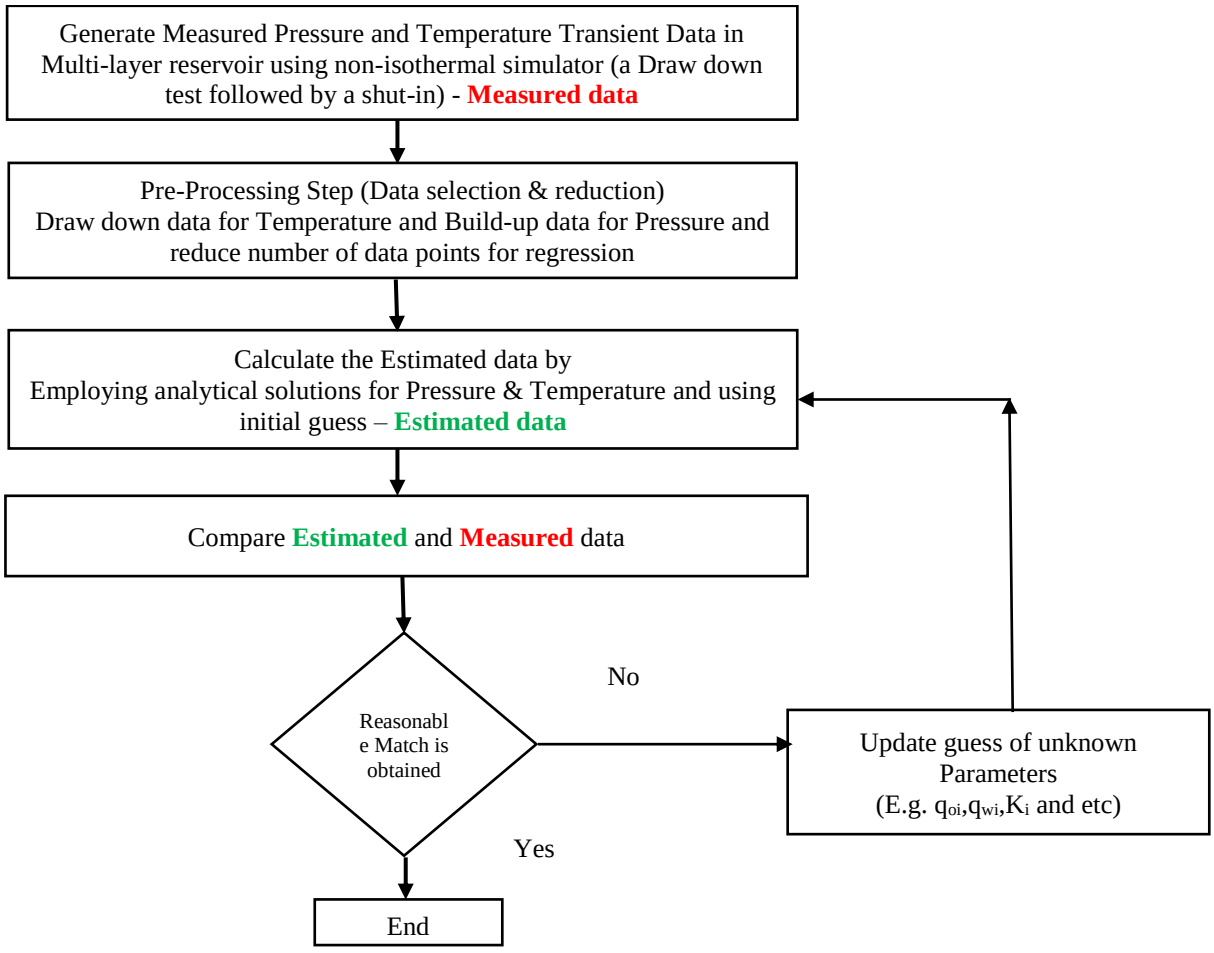

Figure 6-7 Soft-sensing workflow for the inverse model

6.4 Synthetic Case Studies

In the following sections, the application of the soft-sensing method for different objectives including reservoir characterisation, flow rate allocation and completion monitoring are presented.

6.4.1 Case 1: Single-Phase Oil-Production from a Multi-Layer Reservoir

The completion produces from two zones with different permeability and flow rates, but the rest of formation, thermal and produced fluid properties are similar. The ICVs in this vertical well are in the fully open position (no extra pressure drop being imposed by the valve restriction). Both pressure and temperature gauges are providing reliable measurements. The drawdown period is sufficiently long that the temperature profile reaches the late JT period.
The objective of this analysis is to determine the zonal oil flow rate and permeability using the workflow in Figure 6-7. As it can be seen in *Table 6-1*, the regression analysis shows convergence and zonal flow rate and permeability is estimated very well despite having the initial guesses being far from the true values. Figure 6-8 and Figure 6-9 compare the measured pressure and temperature data with the predicted calculation(with initial guess and after regression).

	True Value		**Initial Guess**		**Regression Results**		**Relative Error**	
	K (md)	Q(m^3/d)	K (md)	Q(m^3/d)	K (md)	Q(m^3/d)	$\frac{\Delta k}{k}$ (%)	$\frac{\Delta q}{q}$ (%)
Layer-1	100	180	400	400	102	184	2	2.5
Layer-2	150	270	400	400	152	272	1.4	1

Table 6-1 Regression results for case 1: Single-phase oil producing well with both gauges functioning

It should be noted that the workflow could be extended to more than two layers and with different unknown parameters. However, increasing the number of unknown parameters increases the risk of not converging to a unique solution during history matching process.

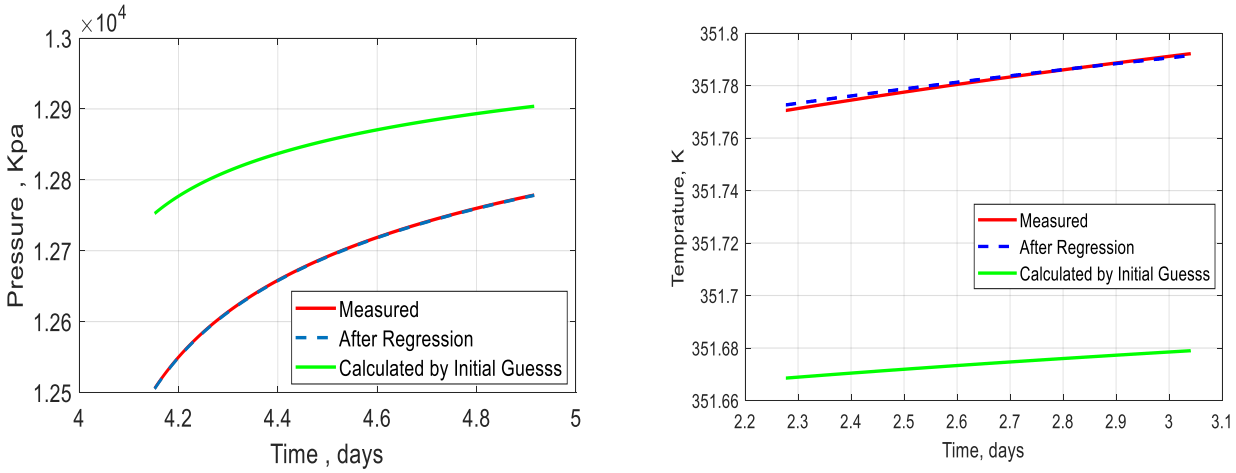

*Figure 6-8 Pressure and Temperature plot for **Layer-1** after and before regression*

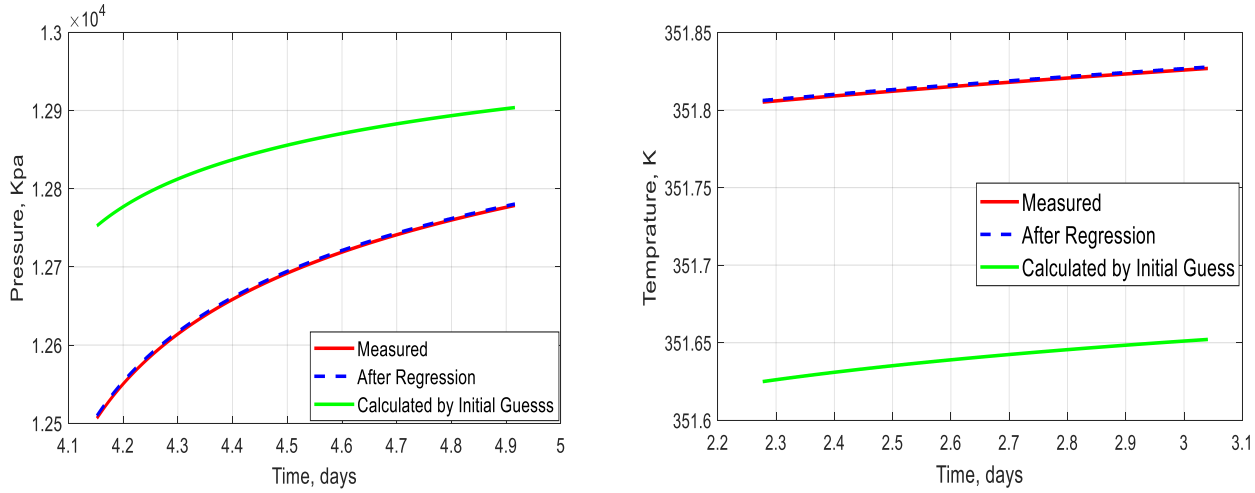

*Figure 6-9 Pressure and Temperature plot for **Layer-2** after and before regression*

6.4.2 Case 2: Effect of Missing Measurements due to Faulty Gauges

Faulty gauges are not uncommon. In the worst case scenario, a gauge can stop recording data and may not be repairable and replaceable. Loss of a gauge reduces the ability to monitor the well and zone performance. The following example illustrates such a scenario. It is similar to the previous case but only one gauge is available while the second one is faulty. The true values and initial guesses used to initialise the optimisation problem are similar to the ones in the previous case. *Table 6-2 and Table 6-3* show the results when only the temperature or only the pressure gauges are available respectively. These tables show that the workflow does not converge to actual values unless both P and T gauges are available. Different initial guesses

were also tested. It was found that the use of a close initial guess could not compensate for the lack of the second complementary gauge measurement.

It should be noted that the combination of an ideal data set with negligible measurement error and a sufficiently representative model might allow the estimation of parameters with a single measured parameter. However, in reality, it is not always possible to have a good data set or model. This example highlights the importance of pressure and temperature data integration when analysing multi-zone reservoirs.

Table 6-2 Case 2 results: only Temperature Gauge is in service

	True Value		**Initial Guess**		**Regression Results**		**Relative Error**	
	K (md)	Q (m^3/d)	K (md)	Q (m^3/d)	K (md)	Q (m^3/d)	$\frac{\Delta k}{k}$ (%)	$\frac{\Delta q}{q}$ (%)
Layer-1	100	180	150-400	300- 400	47	98	53	46
Layer-2	150	270	75- 400	150- 400	76	158	49	42

Table 6-3 Case 2 results: only Pressure Gauge is in service

	True Value		**Initial Guess**		**Regression Results**		**Relative Error**	
	K (md)	Q (m^3/d)	K (md)	Q (m^3/d)	K (md)	Q (m^3/d)	$\frac{\Delta k}{k}$ (%)	$\frac{\Delta q}{q}$ (%)
Layer-1	100	180	150-400	300- 400	293	528	193	194
Layer-2	150	270	75- 400	150- 400	295	532	96	97

6.4.3 Case 3: Flow Rate Allocation and Reservoir Characterisation with Formation Damage

The objective of the next case study is to simultaneously estimate the flow rate and characterise the virgin and damaged zone permeability. A two-layer reservoir with a damage zone is modelled in *Figure 6-10* .The unknown parameters have now increased to four (zonal flow rate, skin, and damage and undamaged permeability) for each zone.

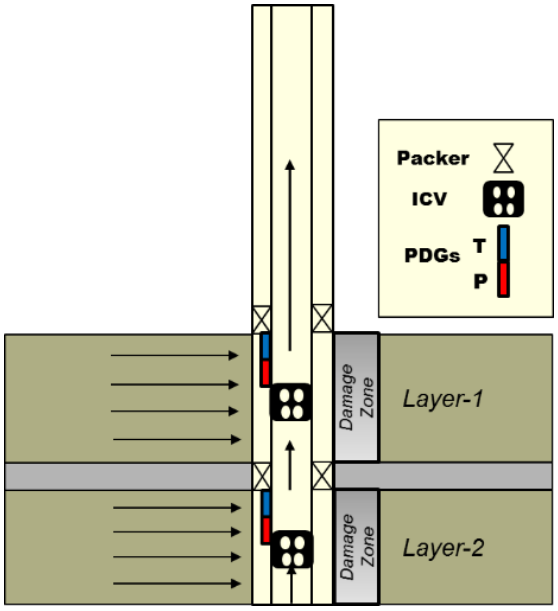

Figure 6-10 Two-zone reservoir with formation damage schematic: case 3

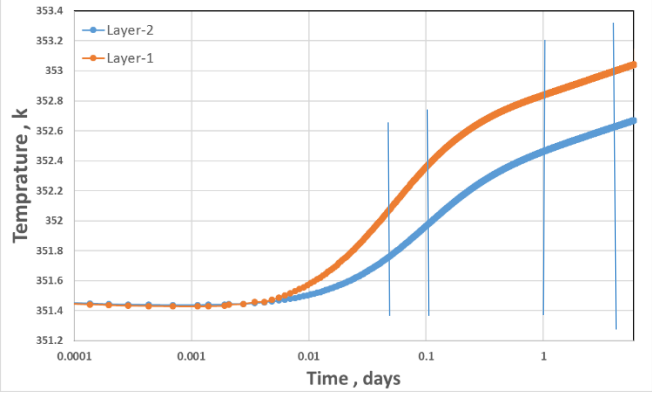

Figure 6-11 Layer draw down temperature data; case 3: with damaged zone

Figure 6-11 shows the measured draw down temperature data for this example. The TTA analytical solution for damaged reservoir, *Eqn. 4-14*, was added to the forward models in the algorithms to predict the observations. Each zone uses one equation for pressure and two equations for temperature to calculate the unknown parameters.

Table 6-4 shows the result of the regression analysis. The accuracy of estimated parameters is still acceptable. However, increasing the number of unknown parameters affects the precision of the results. Furthermore, the layers' damage zones are relatively shallow. The small damage radius, as described in the previous chapter, will affect the match and quality of the solutions for this inverse problem.

Table 6-4 Case 3 result: flow rate allocation and damaged formation characterisation

	True Value				**Regression Results**				**Relative Error**			
	Q (m^3/ day)	K (md)	k_s (md)	Skin	Q (m^3/ day)	K (md)	k_s (md)	skin	$\frac{\Delta Q}{Q}$ (%	$\frac{\Delta k}{k}$ (%	$\frac{\Delta k_s}{k_s}$ (%	$\frac{\Delta Skin}{Skin}$ (%
Layer-1	270	100	20	4.9	290	107	21	3.9	7.5	7	5	20
Layer-2	130	50	10	3.6	155	60	13.2	2.91	19	20	31	19.2

The Hawkins formula and the estimated values of parameters, i.e. k, k_s and skin allows the damage radius to be determined.

$$S = \left(\frac{k}{k_s} - 1\right) \ln \frac{r_s}{r_w} \quad \rightarrow \quad r_s = r_w exp^{\left(\frac{S}{\left(\frac{k}{k_s} - 1\right)}\right)} \qquad 6\text{-}5$$

Table 6-5 case 3: Damage radius estimation

	Damage Radius (m)	
	Actual Value	Estimated Values
Layer-1	0.34	0.386
Layer-2	0.24	0.39

The results indicate the value of integrating pressure and temperature data to obtain information on the zonal flow rate and layer properties for multi-zone formations. This information cannot be achieved using stand-alone TTA or PTA.

6.4.4 Case 4: Multiphase Oil-Water Producing Well in Multi-Layer Reservoir

- **Theory and Workflow**

The knowledge of zonal phase flow rate and water cut is essential for reservoir management. Well control strategy is often optimised based on the total flow rate and the level of water

production from each layer. The success of proactive [3] and reactive optimisation[117] significantly increases when real-time monitoring of zones is practised. Manipulating ICVs across zones or adjusting the surface choke are two main real-time means to react to water breakthrough.

The previously described algorithm will now be modified to determine zonal phase flow rate and water cut. The modified TTA solution for oil-water system, *Eqn.5-4*, is combined with P-M multi-phase PTA solution in the algorithm to predict the estimated data.

Estimation of the phases' flow rate requires extra information. In addition to the objective function presented above to estimate the general zonal parameters, the zonal water (q_{w_i}) and oil (q_{o_i})flow rate can be estimated by minimising the mismatch between total (well) oil (Q_o) and water flow rate (Q_w), defined as follows;

$$Mismatch_1 = \left(Q_{o,measured} - Q_{o,calculated}\right)^2 \qquad 6\text{-}6$$

$$Mismatch_2 = \left(Q_{w,measured} - Q_{w,calculated}\right)^2 \qquad 6\text{-}7$$

Where;

$$Q_o = \sum_{i=1}^{n} q_{o_i} \qquad 6\text{-}8$$

$$Q_w = \sum_{i=1}^{n} q_{w_i} \qquad 6\text{-}9$$

The predicted water and oil flow rate are calculated by combining the inflow performance relationship (IPR) and water cut formula. IPR relates the zonal oil flow rate to the draw down (difference between average reservoir pressure and stabilised annulus pressure). A linear IPR model (Eqn 6-10) and the standard zonal water cut expression (Eqn 6-11) are defined as follows ,

$$q_{o_i} = PI_{o_i}(P_{ave_i} - P_{an_i}) \qquad 6\text{-}10$$

$$WC_i = \frac{q_{w_i}}{q_{w_i} + q_{o_i}} \qquad 6\text{-}11$$

The algorithm for phase flow rate and water cut determination includes two steps *(Figure 6-12)*;

- In the first step, pressure and temperature measurement is used to estimate unknown reservoir and thermal properties and total liquid flow rate of each zone.

- In the second step; the estimated parameters in step 1 along with the stabilised zonal pressure and total oil and water flow rate are used to determine the zonal water cut and the phase flow rate .

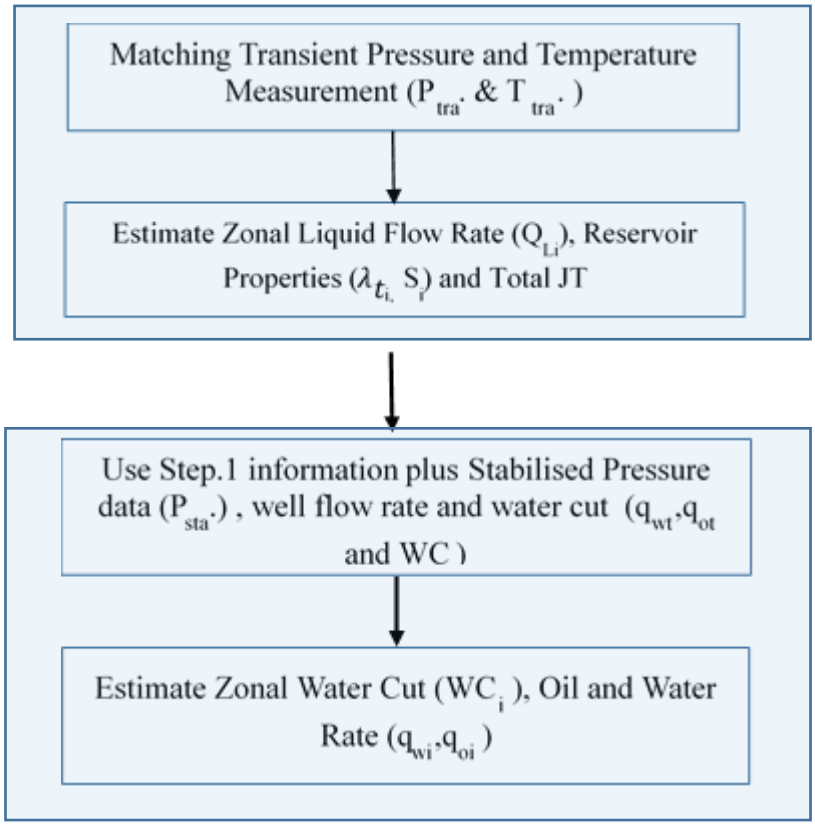

Figure 6-12 Workflow for Multiphase Soft-Sensing

- **Case 4: Multi-Phase Soft-Sensing**

The application of the multi-phase soft-sensing workflow is tested in case 4. The synthetic model consists of two zones where both oil and water are mobile in the reservoir and are produced at sandface. The water cut of the layers is 20% and 44% respectively.

A sufficiently large aquifer was added to the reservoir model to ensure the pressure could stabilise and the steady-state productivity index and phase flow rate measured and calculated. The “roll-over” on pressure log-log plots, *Figure 6-13,* confirms that steady-state has been reached for both layers.

Table 6-6 shows the first-step results where the reservoir, thermal properties and total liquid flow rate are calculated. These values are used in the next step to estimate the water cut. *Table 6-7* lists the reservoir parameters and the zonal water cut accurately estimated by the Fig 6-12 workflow.

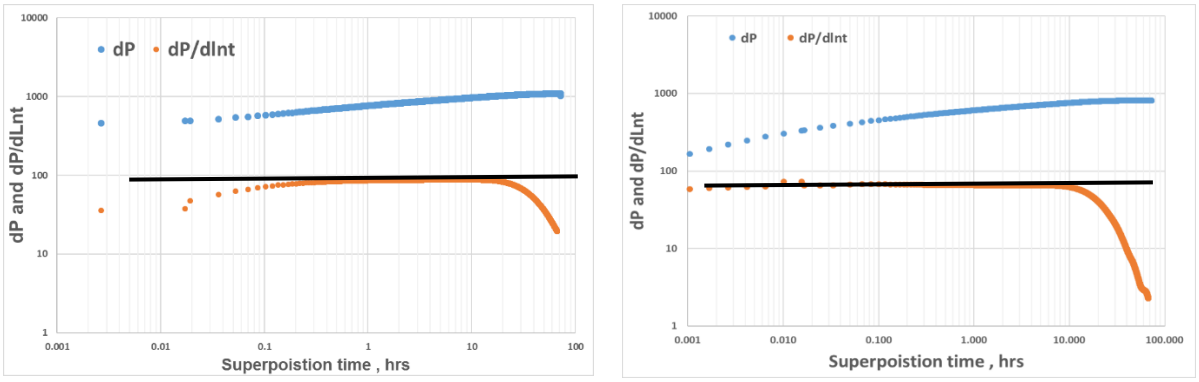

Figure 6-13 Case 4: multiphase oil-water: Pressure build-up log-log plot for zone-1 (left) and zone-2(right)

Table 6-6 Case 4- Step 1: Estimated Reservoir Parameters

	True Value			Regression Results			Initial guess			Relative Error		
	$\boldsymbol{\lambda_t}$ (md)	$\boldsymbol{Q_t}$ (m^3/d)	JT ´10^{-7} (K/Pa)	$\boldsymbol{\lambda_t}$ (md)	$\boldsymbol{Q_t}$ (m^3/d)	JT ´10^{-7} (K/Pa)	$\boldsymbol{\lambda_t}$ (md)	$\boldsymbol{Q_t}$ (m^3/d)	JT ´10^{-7} (K/Pa)	$\frac{\Delta\boldsymbol{\lambda_t}}{\boldsymbol{\lambda_t}}$ (%)	$\frac{\Delta\boldsymbol{q}}{\boldsymbol{q}}$ (%)	$\frac{\Delta\boldsymbol{\varepsilon_{JT}}}{\boldsymbol{\varepsilon_{JT}}}$ (%)
Layer-1	2.36	338	-3.58	2.4	344.7	-3.36	5	500	-5	1.6	2	6.5
Layer-2	1.21	234	-2.88	1.16	225	-2.82	5	500	-5	4	4	2

Table 6-7 Case 4 -Step 2 : Estimated zonal water cut

	Actual Values	Regression Results	Relative Error
	Water-cut, fraction	Water-cut, fraction	$\frac{\Delta\boldsymbol{WC}}{\boldsymbol{WC}}$ (%)
Layer-1	0.2	0.192	4
Layer-2	0.44	0.456	3.6

6.4.5 Case 5: Novel Workflow for AFCD Monitoring and Modelling

- **Theory and Workflow**

One of the main challenges in autonomous flow control devices (AFCDs) modeling and monitoring is the uncertainty in the device's performance during multiphase flow. Single-phase flow performance curves for some AFCD types can be calculated using Eqn. 2-1. Multiphase flow, however, requires experiments to tune the model that is later used to predict the performance of the AFCD-completed well throughout its production lifetime. This information is normally costly and not easily available. Therefore, the question is how these devices perform when water/gas production increases and how significantly this affects the oil recovery and completion performance prediction.

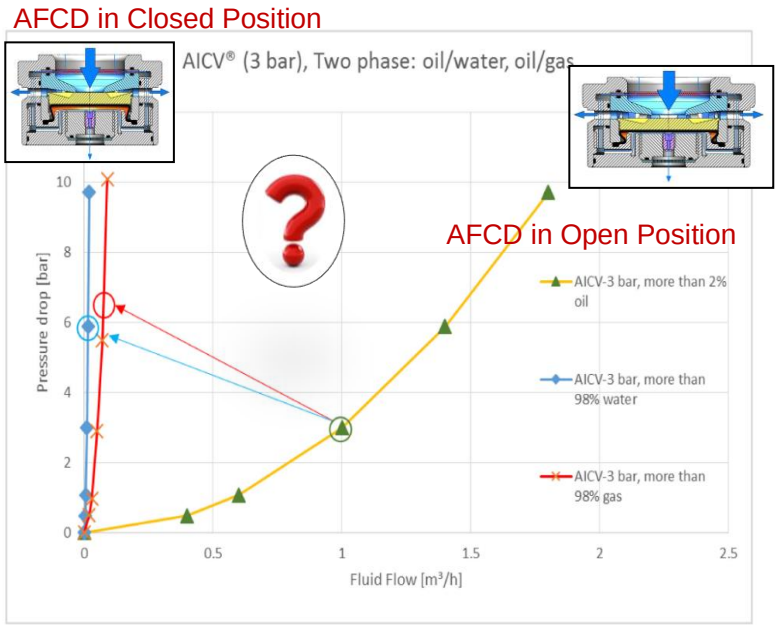

Figure 6-14 AFCD single phase performance plot [59]

In this section, the proposed workflow is modified to predict the performance of AFCDs in multi-phase flow conditions. The details of the proposed workflow are presented in *Figure 6-15* . According to the workflow, estimation of the zonal properties, JT and zonal liquid flow rate is followed by determining zonal water cut while pressure drop across the valve is measured. This workflow can be repeated to monitor the performance of AFCDs when the water cut in the well/zone is changing.

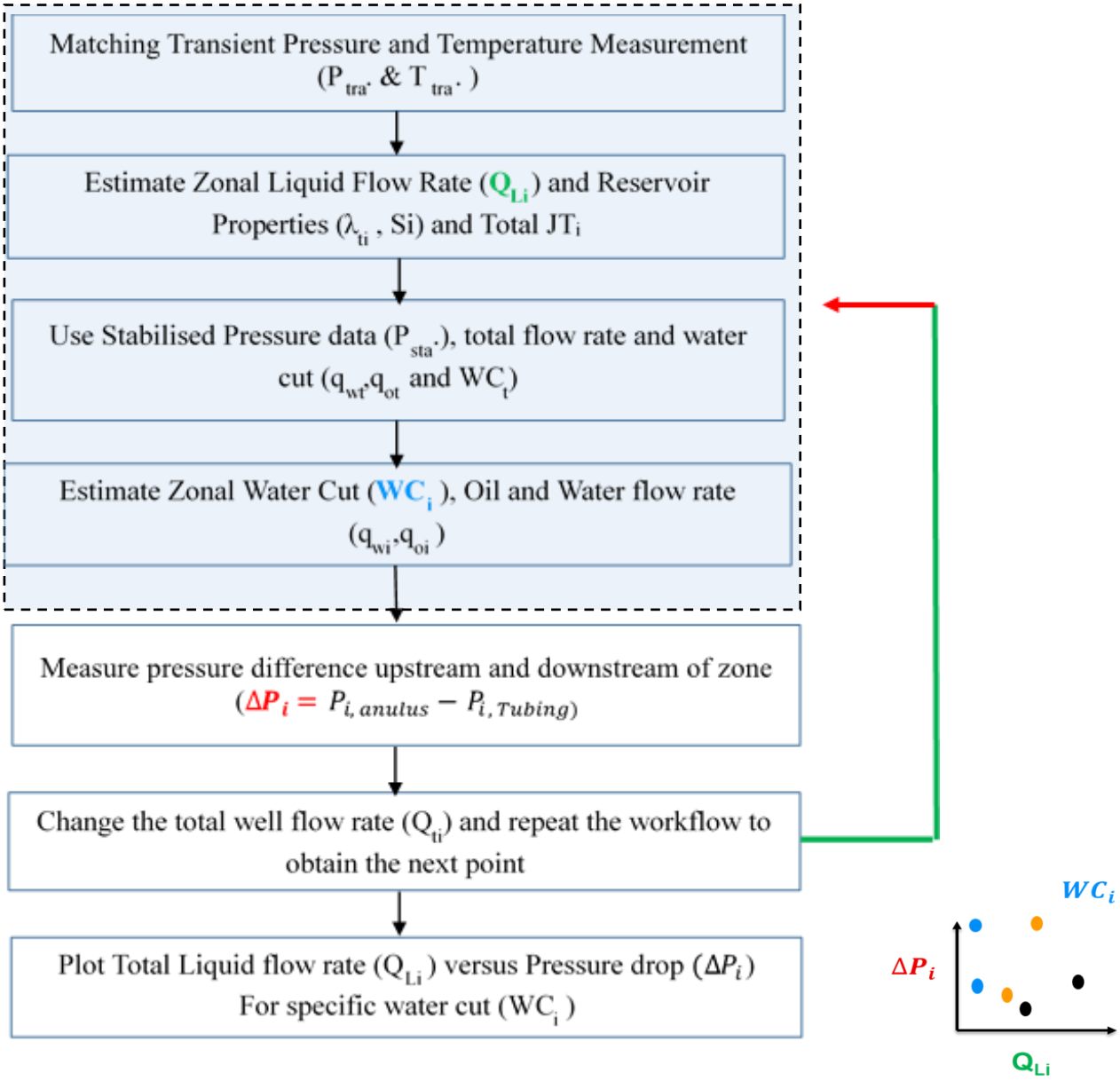

Figure 6-15 AFCD modelling and monitoring workflow

- **Case 5: Application of Multiphase Soft-Sensing in AFCD well**

A two-zone I-well completed with multiple AFCDs initially produces 100% oil. Water sometime later breaks through and the AFCD opening area adjusts according to the current zone water cut. For simplicity, an 'up-scaled AFCD' is modelled for each zone hosting 12 actual AFCDs. Note that the 'up-scaled AFCD' flow performance is not necessarily representative of the actual AFCD's one.

Figure 6-15 workflow is followed for two different occasions in well's life: the 100% oil production and the two-phase oil-water production case. In each case a two-rate test is taken. The algorithm first estimates the reservoir properties (Table 6-8) and the water cut (Table 6-9). The process is then repeated for the second flow rate. *Figure 6-16* shows the AFCD performance curve at two flow rates for the water cut of zone-1 and 2 generated using the Figure 6-15 workflow.*Figure 6-17* also compares the results of the calculation with the flow performance curve used as an input for the simulation. The results confirm good agreement between the calculated and input data. By increasing the number of flow rate changes in multi-rate test, more data point can be obtained by the workflow; which improves the accuracy of fitted equation(curve). By fitting an exponential function to the multiphase flow curve, the unknown parameters in the selected AFCD equation. Eqn 2-3, for multiphase flow condition (assuming this equation is valid) can be determined and subsequently the tuned solution can be obtained (more information can be found in Eltaher 2017 [58]).

Table 6-8 Case 5: Estimated parameters for AFCD modelling and monitoring study

	True Value			Regression Results			Initial guess			Relative Error		
	$\boldsymbol{\lambda_t}$ (md)	$\boldsymbol{Q_t}$ (m3/d)	JT ´10-7 (K/Pa)	$\boldsymbol{\lambda_t}$ (md)	$\boldsymbol{Q_t}$ (m3/d)	JT ´10-7 (K/Pa)	$\boldsymbol{\lambda_t}$ (md)	$\boldsymbol{Q_t}$ (m3/d)	JT ´10-7 (K/Pa)	$\frac{\Delta\boldsymbol{\lambda_t}}{\boldsymbol{\lambda_t}}$ (%)	$\frac{\Delta\boldsymbol{q}}{\boldsymbol{q}}$ (%)	$\frac{\Delta\boldsymbol{\varepsilon_{JT}}}{\boldsymbol{\varepsilon_{JT}}}$ (%)
Layer-1	2.36	350	-3.58	2.397	356	-3.36	5	500	-5	1.56	1.7	6
Layer-2	1.21	170	-2.88	1.191	167	-2.79	5	500	-5	1.57	1.7	3

Table 6-9 Case 5: Estimated water cut for AFCD modelling and monitoring study

	Water-cut, fraction (Actual Values)	Initial Guess (Water-cut, fraction)	Regression Results (Water-cut, fraction)	Relative Error ($\frac{\Delta\boldsymbol{WC}}{\boldsymbol{WC}}$ (%))
Layer-1	0.2	0.5	0.2026	1.3
Layer-2	0.44	0.5	0.4437	1

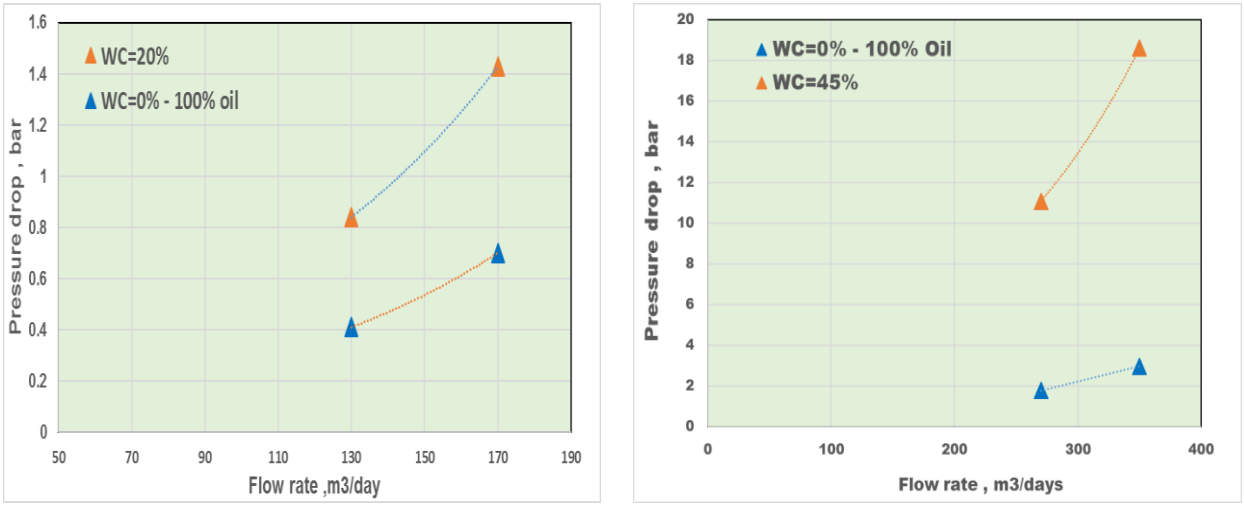

Figure 6-16 Case 5: AFCD performance curve for zone 1 (left) and zone 2 (right)

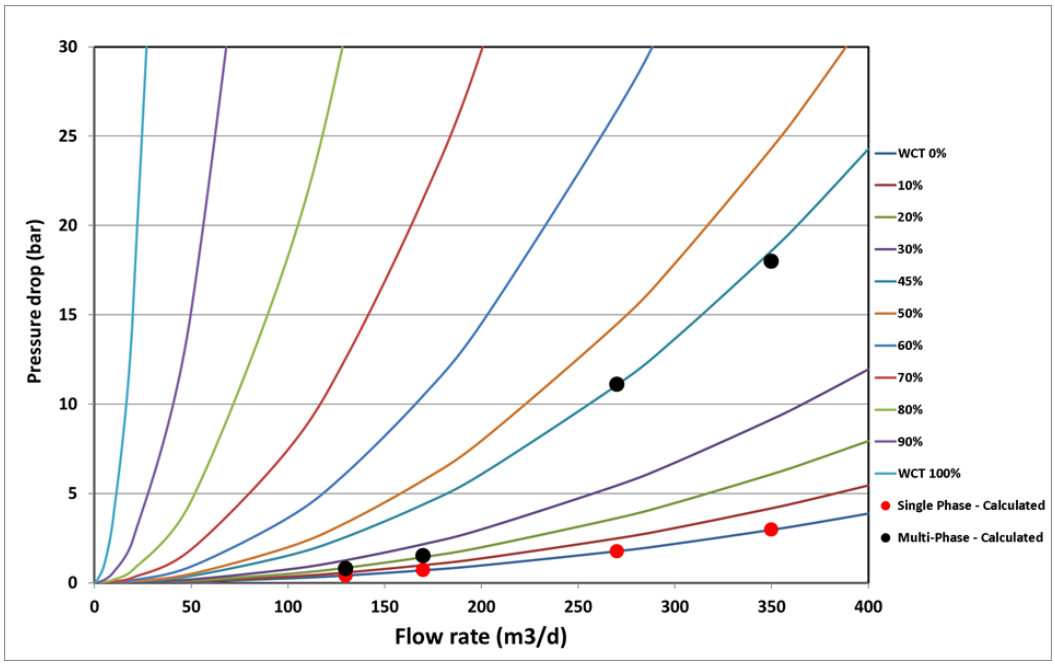

Figure 6-17 Comparison between calculated AFCD performance data(markers) and the input data used in the simulation (dash lines)

6.5 Measurement Uncertainty

Data measurement and analysis are always subject to uncertainties[46]. The common types of uncertainties include;

- **Measurement Uncertainty**

Noise, gauge drift and bias are some common types of uncertainties that affect the quality of data and hence the accuracy of the analysis.

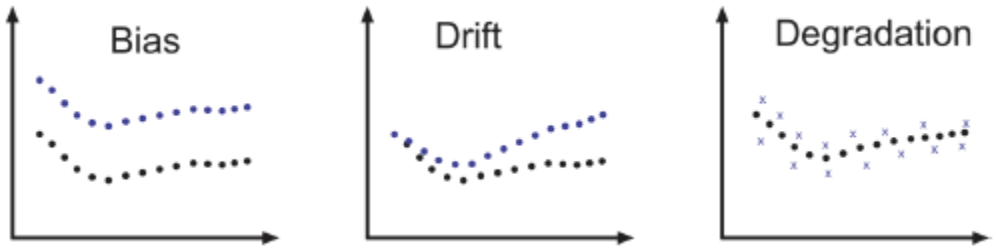

Figure 6-18 Measurement uncertainties [46]

- **Model Uncertainty**

Model uncertainty is also present when analyzing e.g. real data sets. It is mainly due to the assumptions used in analytical solutions and optimization algorithms.

The effect of two common types of measurement uncertainty: noise and bias have been investigated. The effect of model uncertainty in this section has been removed through generating measured data by the analytical solutions. This provides ideal data with a perfect match with the result of the analytical models.

- **Effect of Noisy Measurement**

Different level of random noise has been introduced into ideal measured data calculated by Eqns. 4-2 and 4-15. *Figure 6-19* illustrates temperature and pressure data with the noise added between 0.5 to 5% of their measured changes. The noisy pressure and temperature data is then used to estimate unknown parameters, e.g. permeability *(k)* and flow rate *(q)*. The results for three different scenarios are compared where either or both of the pressure and temperature data are noisy.

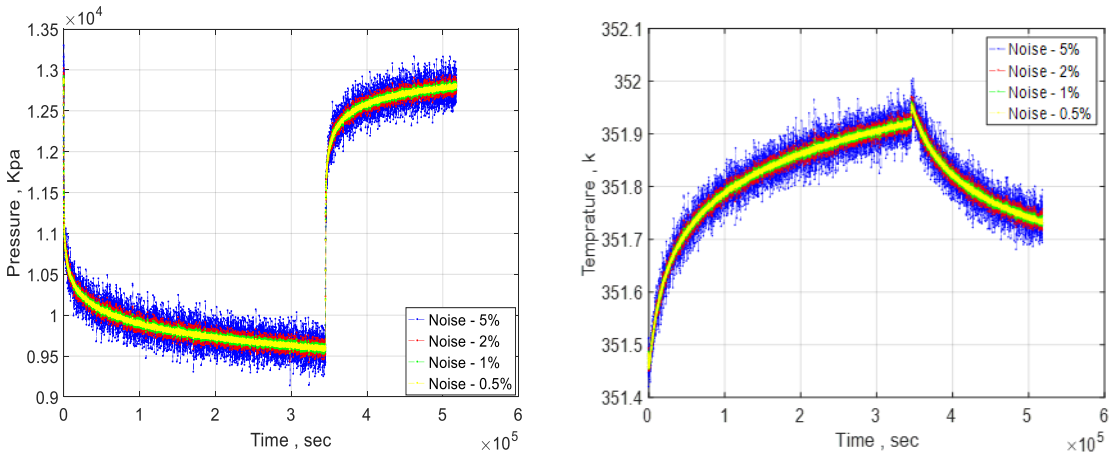

Figure 6-19 Noisy pressure (left) and temperature (right)

Table 6-10 reports the estimated parameters when either noisy pressure or temperature is used for analysis. The results indicate that an increasing noise level reduces the accuracy of estimated permeability and flow rate from regression.

Table 6-10 Estimated reservoir parameters derived from noisy data

Noise (percent)	Noisy Temperature data		Noisy Pressure data		Actual	
	Q(m^3/day)	K(md)	Q(m^3/day)	K(md)	Q(m^3/day)	K(md)
0.5%	128.5	49	125.5	48	130	50
1%	127	48	122	47		
2%	124	47	113	43		
5%	116	43	92	34		

Figure 6-20 compares the error in the estimated permeability based on stand-alone pressure and temperature and together data with 5% random noise. This figure shows that integrating pressure and temperature data with random noise reduces the error compared to the use of stand-alone pressure or temperature data. The value of PTTA in a noisy measurement environment is therefore confirmed for this given case study.

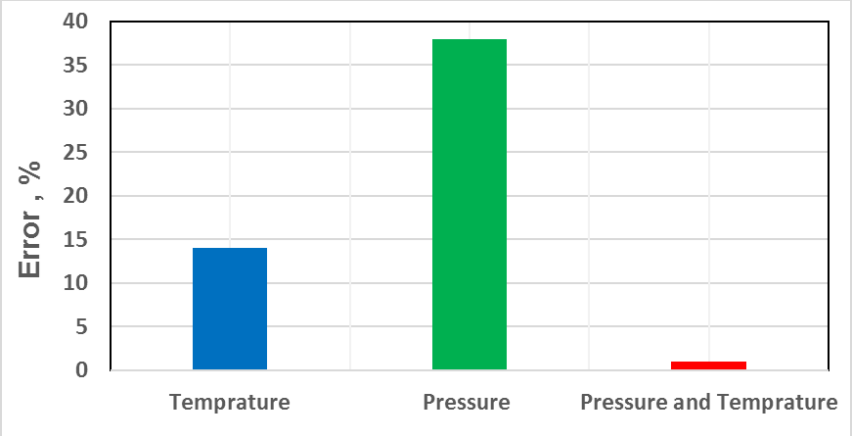

Figure 6-20 Comparing estimated permeability for 5% noise in either and both measurements

- **Effect of Gauge Bias and Drift Error**

Another common error in data measurement is gauge bias or drift. This error remains constant and does not alter when the value of the measured data changes. The algorithm has been tested for bias errors ranging from 35 KPa to 200 KPa (*Figure 6-21*).

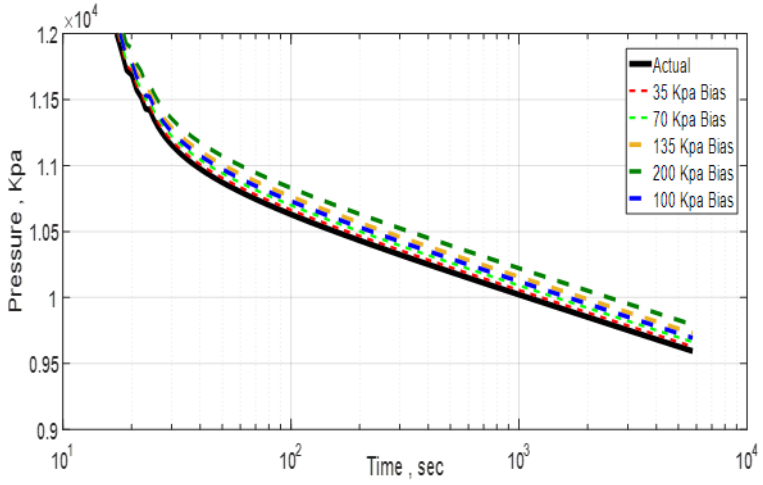

Figure 6-21 Pressure gauge bias

The unknown parameters to be estimated are layer flow rate and permeability. From the regression results the following conclusion are drawn;

- <u>Measurement of either T or P:</u>

When either pressure or temperature data from a biased gauge are used, the algorithm has not converged, and the unknown parameters cannot be estimated.

- Dual Measurement T and P:

When both pressure and temperature are measured, and bias exist only in one of the gauges, the unknown parameters can be estimated. However, as shown in *Figure 6-22*, the higher bias increases the error in parameter estimation.

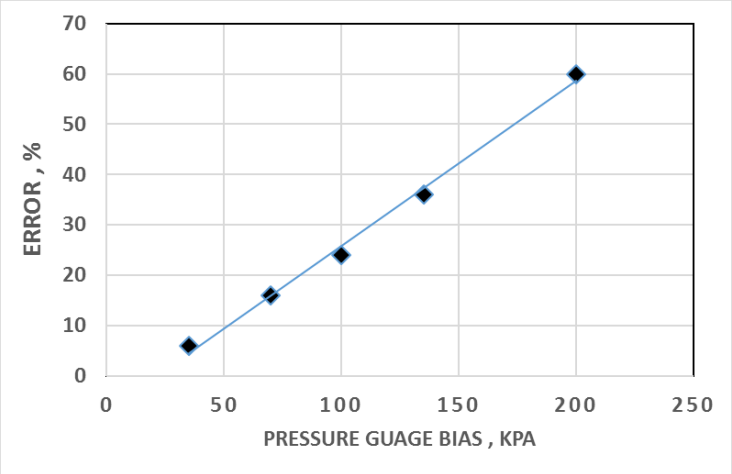

Figure 6-22 Effect of Pressure gauge bias on permeability estimation

Another advantage of the presented soft-sensing method is that gauge bias can be treated as another unknown in the algorithm. Therefore, this parameter can be estimated during the error minimization process.

$$P_{Calculated} = P_{Model} + Bias\ Error \qquad 6\text{-}12$$

In this example, for all the cases, including bias error into algorithm as the third unknown resulted in perfect estimation for permeability, flow rate and bias error itself.

6.6 Summary

This chapter presented a new soft-sensing method by integrating TTA and PTA in a regression algorithm. The method can potentially be used for wide range of applications such as flow rate allocation, reservoir characterisation and completion monitoring. It was shown that the new algorithm reduces dependency on shut-in periods by taking advantage of widely available production data. For example, a production period followed by a shut-in can be sufficient for the analysis. The integration also provides information about damage zone such as permeability and radius (assuming the Hawkins model applies).

The single-phase version of the algorithm was successfully employed to determine layers' permeability, skin and flow rate. It was later shown that zonal phase flow rate and water cut can also be estimated by following the proposed multi-phase algorithm and only by integration of pressure and temperature measurements. The algorithm was also further modified to calculate the multiphase flow performance curves for AFCD modelling and monitoring. This method was introduced as an alternative approach for expensive and hardly available experimental data.

The effects of measurement uncertainties such as noise and bias/drift on the robustness of the algorithm were also investigated. It was shown that in the given example the integrated PTTA is more robust than the use of standalone pressure or temperature analysis.

Chapter 7 Variable Flow Rate Solutions for TTA and PTA

7.1 Introduction

This chapter addresses the effect of variable flow rate on both TTA and PTA. Theoretical models and analytical solutions normally assume an instantaneous, constant rate production change response. In reality this assumption is not met in many situations, since maintaining a well at a constant (sandface) flow rate is difficult, unless it is shut in at the sandface.

The pressure and temperature change caused by the flow rate variation distorts the pressure and temperature response and reduces the validity of analysis if the 'ideal, step-like rate change or unitary response' solutions are applied directly. This chapter discusses different methods to address this problem. Normalisation methods including rate-normalised and pressure-normalised temperature are first presented and their success at reconstructing the underlying, unitary response is subsequently analysed.

A data-driven deconvolution algorithm is also developed, verified and tested as an alternative solution to this problem. Finally, the results of normalisation and deconvolution algorithm on the synthetic cases and a real data set from an I-well are compared and discussed.

7.2 Variable Rate in PTTA

TTA and PTA major analytical solutions are developed under idealistic assumption of constant rate production. However, in reality, the absence of downhole shut-in valve results in wellbore storing in the remaining inflow (or discharging the outflow) for some time before the flow rate becomes constant. This variable flow rate during the draw down or buildup period also distorts the pressure and temperature signal during the early time period. This affects PTA since the early time measurement, being affected by wellbore storage, results in masking the pure (i.e. unitary) reservoir response, hindering reservoir characterisation from the early time data.

TTA is also vulnerable to rate changes. Pure TTA solution also prefers production-period data where ramp-up or smooth flow rate changes jeopardises the analysis. The problem in TTA is made worse since the temperature changes being measured compared to the gauge resolution are often smaller than that for pressure. Therefore, the reconstruction (e.g. by the traditionally used in PTA the deconvolution method) of the pure temperature response from the actual measurement can be more complicated and less reliable.

The variable rate problem in the published PTA and TTA literature has been addressed using the following solutions;

- Forward modelling: Superposition and, generally, convolution
- An interpretation approach: Normalisation
- Unitary response reconstruction: Deconvolution

TTA however is new and still has less to offer in the area of studies in data reconstruction and analysis. This chapter proposes some solutions to TTA's variable rate problem. The description of variable rate test used for the analysis is followed by discussing multiple methods to restore the unitary temperature and pressure signal caused by rate changes. The results of the methods are later compared using synthetic and real-field data sets.

7.3 Multi-Rate Test: Modelling and Test Design

Figure 7-1 shows a multi-rate test flow rate (at sandface) in a synthetic model single-phase oil producing vertical well. A series of four step-wise rate changes are followed by a period of constant production, the well is then shut in for a pressure build-up period.

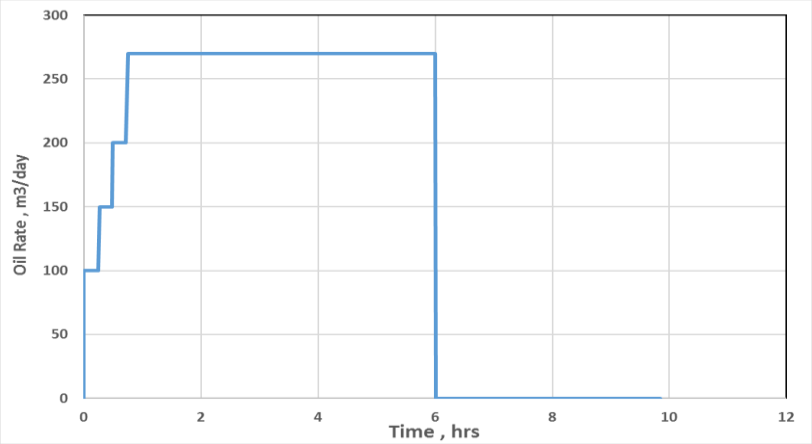

Figure 7-1 Multi-rate flow test flor rate (at sand face) in an oil production well

Figure 7-2 also indicates how the early-time pressure and temperature signal behaves with the flow rate changes. In the following sections different methods including superposition, normalisation and deconvolution are presented to restore the unitary, early-time response from the data in *Figure 7-2* . The result of each method will be compared against a single-rate response where the well produces with a constant rate for the entire 10 hrs. The corresponding pressure and temperature response of the single-rate test are then extracted and used as a reference for comparison.

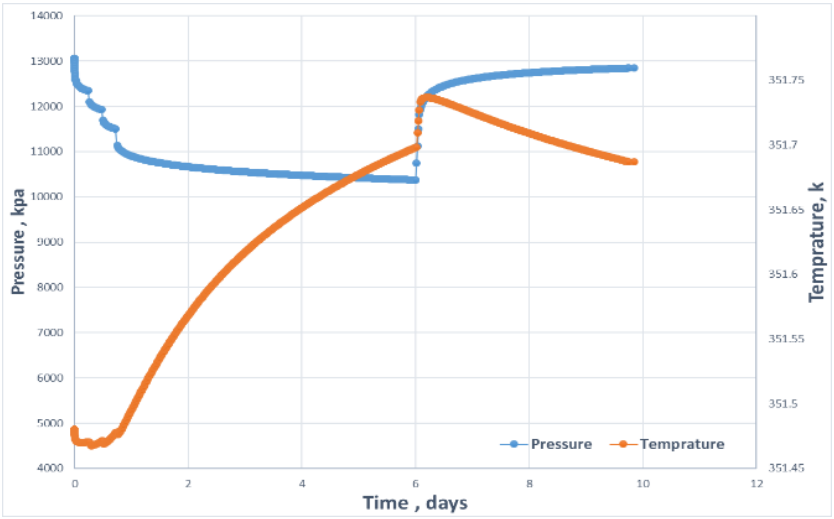

Figure 7-2 Pressure and temperature data corresponding to the Figure 7-1 multi-rate test

7.4 Superposition and Convolution

The underlying idea of convolution, known as Duhamel's principle, in PTA is to superimpose the unit constant-rate change pressure solution (i.e. unitary response) by the means of integrating it and using the continuous rate profile (q) to produce the variable rate wellbore pressure-drop function (ΔP). Therefore, the convolution integral is defined as follows:

$$\Delta P(t) = \int_0^t q(\tau) g(t-\tau) d\tau \qquad 7\text{-}1$$

Where g (unitary response) is a time derivative of constant-unit-rate pressure change ($g = \frac{d\Delta P_{wf}}{dt}$).

Muradov et al (2011)[118] indicated that the liquid temperature PDE is mostly linear in conventional production and therefore it is valid to use this superposition/convolution form (Eqn. 7-1) in a multi-rate test in our study as well. They showed, *Figure 7-3* , that the second draw down temperature response is the sum of a continuation of the first rate initiated temperature change plus the temperature change generated by the incremental rate at the appropriate elapsed time:

$$T_{wb}\left(t > t_{q\ change}\right) = T_{wb}(q_1, t) + T_{wb}\left(q_2 - q_1, t - t_{q\ change}\right) \qquad 7\text{-}2$$

Therefore, similar to PTA, the TTA convolution integral can be defined as;

$$\Delta T_{wf}(t) = \int_0^t q(\tau) g(t-\tau) d\tau \qquad 7\text{-}3$$

Where g(unitary response) is the unit-large constant-rate change temperature solution ($g = \frac{d\Delta T_{wf}}{dt}$).

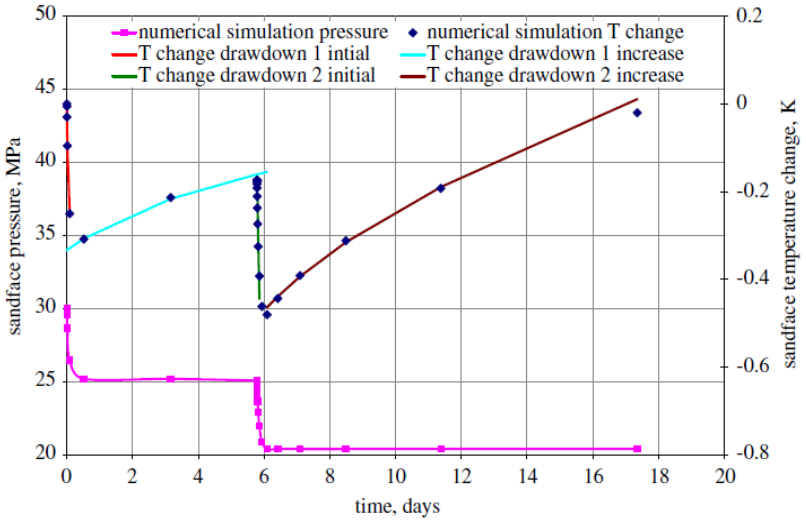

Figure 7-3 Multi-rate temperature response [118]

In the following two solutions for variable rate problem used in PTA (and proposed for TTA) will be presented;

7.5 Normalisation

The initial objective of rate normalisation in PTA was to remove/correct for the effect of a variable flow rate from the pressure data. Rate normalisation can be defined as an approximation of convolution integral as follows;

$$\Delta P(t) = \int_0^t q(\tau) g(t-\tau) d\tau \qquad 7\text{-}4$$

$$\Delta P_{wf}(t) \approx q(t) g(t) \qquad 7\text{-}5$$

$$g(t) \approx \frac{\Delta P_{wf}(t)}{q(t)} = \frac{P_i - P_{wf}(t)}{q(t)} \qquad 7\text{-}6$$

Rate normalization can remove the effects of wellbore storage provided the sand face flow rate data is available. It is thus a practical tool for analysing a pressure drop response affected by e.g. wellbore storage. Fetkovich and Vienot [119] confirmed the applicability of rate normalization in variable rate gas and multiphase flow cases. Thompson[120] proposed the criteria in which it is appropriate to use the rate normalization method, for example he mentioned when pressure data is strongly affected by boundaries or for build-up period normalisation cannot be used. Later Raghavan [121] identified some other important situations where rate normalization should not be used — e.g. when phase segregation or periodic /fluctuating rates have occurred.

Despite these limitations, Normalisation still is a practical approach as substantial information can be obtained with a minimum of effort. The application of different normalisation methods in PTA and TTA is discussed in the following sections,

7.5.1 Rate-Normalised Pressure (RNP)

Figure 7-4 shows the pressure response due to either the equivalent single-rate change or the variable rate change described in *Figure 7-2*.The two signals initially deviate from each after but converge at the late time. As a result of this the variable test PTA is not directly applicable.

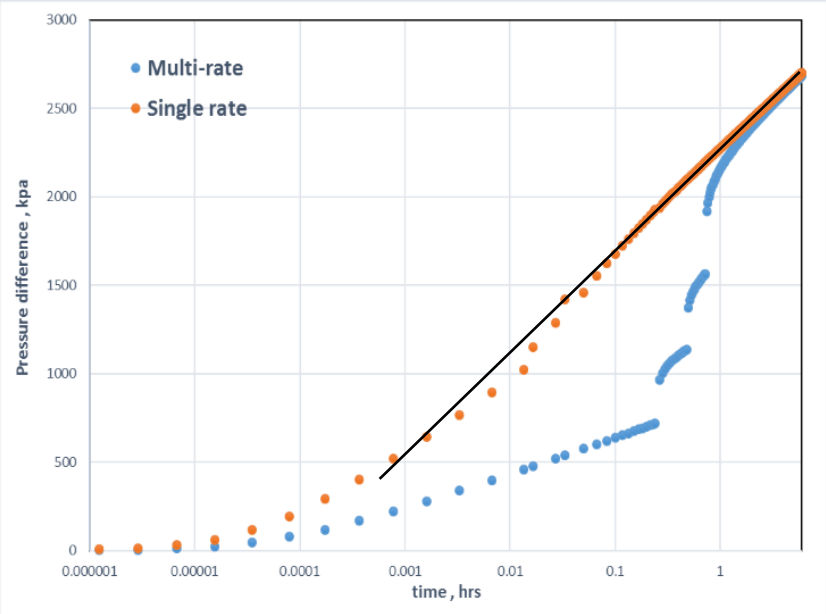

Figure 7-4 single-rate versus multi-rate semi-log pressure response

Figure 7-5 compares the rate-normalised pressure and the equivalent single rate solutions. The normalised data reconstructs the unitary signal and successfully reproduces the single rate response. However, there are still some differences, which might affect PTA interpretation and analysis.

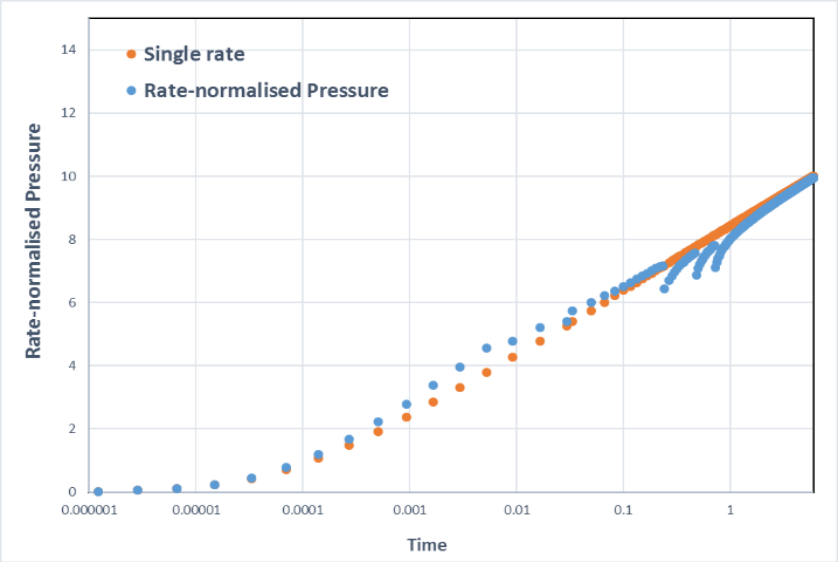

Figure 7-5 Rate-normalised pressure versus single-rate solution for the Figure 7-1 multi-rate test

7.5.2 Normalisation for TTA

The main difference between PTA and TTA normalisation is that temperature changes can be attributed to both flow rate and pressure changes (flow rate changes create pressure draw down/build-up leading to temperature variation, *Eqn 4-12*). *Figure 7-6* shows how temperature data, in cartesian and semi-log, is affected by variation of flow rate. The slope of both the early-time expansion and the late-time JT periods are different from the single-rate change response curve so that TTA directly using this data will result in incorrect estimations.

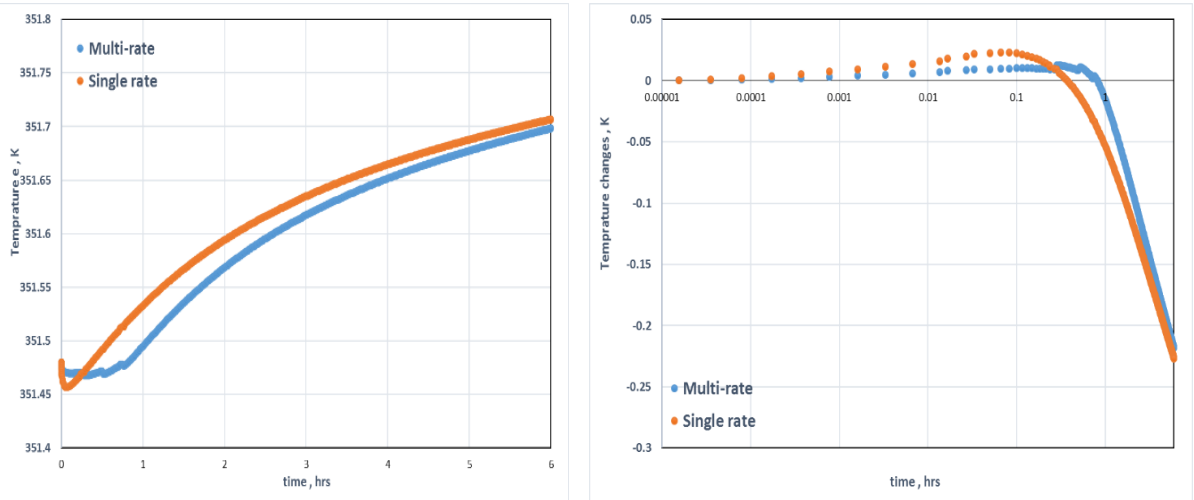

Figure 7-6 temperature (left) and temperature changes (right) for single and multi-rate cases

7.5.2.1 Rate-Normalised Temperature (RNT)

The convolution integral and the corresponding rate-normalised temperature equations can be defined as follows when the temperature change is due to a variable flow rate,

$$\Delta T_{wf}(t) = \int_0^t q(\tau) g(t-\tau) d\tau \qquad 7\text{-}7$$

$$\Delta T_{wf}(t) \approx q(t) g(t) \qquad 7\text{-}8$$

$$g(t) \approx \frac{\Delta T_{wf}(t)}{q(t)} = \frac{T_i - T_{wf}(t)}{q(t)} \qquad 7\text{-}9$$

Figure 7-7 shows the result of the rate-normalised temperature. It successfully restores the early-time data during the first-rate change period (mainly the first drawdown in the series, not affected by superposition, scaled purely by the rate change), but the improvement for the other rate changes is not observed. So, this method was not very successful in this example.

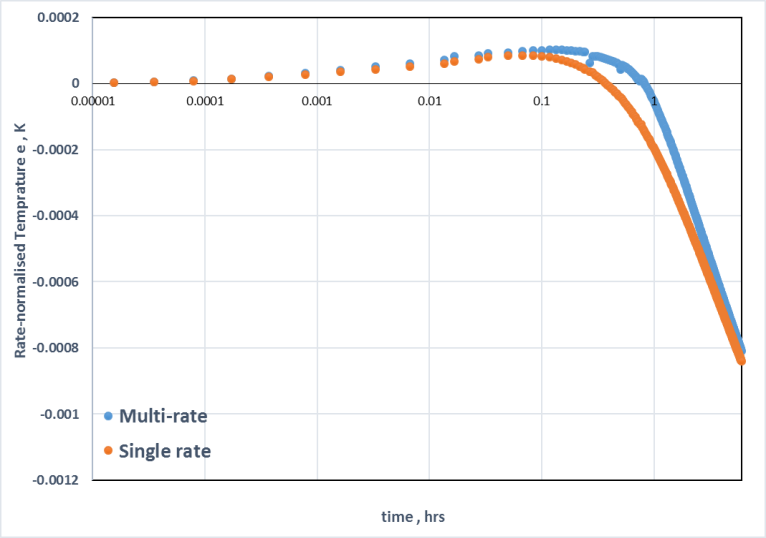

Figure 7-7 Rate-normalised temperature versus equivalent single-phase solution

7.5.2.2 Pressure-Normalised Temperature (PNT)

The main limitation for the "rate-normalised temperature" method is that flow rate data is required to normalise temperature data (let alone the RNT may not work as shown above). However, continuous measurement of zonal flow rate is not normally available and where it is available the frequency of the rate and the temperature measurements may not be identical.

According to thermal model, *Eqn. 4-12*, temperature variation can be related to pressure changes. Therefore, this creates an opportunity to substitute rate data with pressure data , where

the continuous pressure measurement are available, in the convolution integral. The modification in temperature convolution integral and the corresponding pressure-normalised temperature formula is presented below,

$$\Delta T_{wf}(t) = \int_0^t \Delta P_{wf}(\tau) g(t-\tau) d\tau \qquad 7\text{-}10$$

$$\Delta T_{wf}(t) \approx \Delta P_{wf}(t) g(t) \qquad 7\text{-}11$$

$$g(t) \approx \frac{\Delta T_{wf}(t)}{\Delta P_{wf}(t)} = \frac{T_i - T_{wf}(t)}{\Delta P_{wf}(t)} \qquad 7\text{-}12$$

Figure 7-8 depicts the pressure-normalised temperature solution. As can be seen, the result of this method is very similar to that of the rate-normalised temperature, with the similar conclusion: PNT does not seem to be applicable.

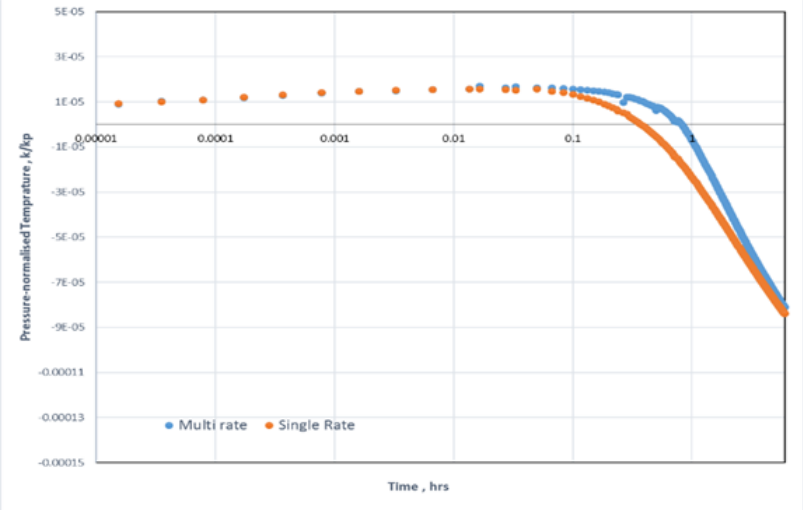

Figure 7-8 pressure-normalised temperature versus single-rate temperature solution

7.6 Deconvolution

Normalisation is a practical approach but fails under several circumstances. The robust, mathematical solution of the variable rate case is deconvolution, a method that does not have the limitations of normalisation since it solves the convolution integral explicitly (provided it can be solved for a given model and data quality). Deconvolution for PTA is a well-developed method with multiple algorithms available for its solution. Deconvolution methods are best categorized based on the approach used to solve the convolution integral. The two main approaches are Laplace and time domain solutions. *Table 7-1* and *Table 7-2* list the evolution

of both methods in the PTA literature;

Researcher	Deconvolution Solution in Time Domain
Coats *et al.*[122]	Time Domain Deconvolution (Linear Programming)
Hutchinson and Sikora[123]	Time Domain Deconvolution (Direct Solution)
Katz*et al*.[124]	Time Domain Deconvolution (Direct Solution)
Jargon and van Poolen[125]	Time Domain Deconvolution (Direct Solution)
Bostic and Agarwal[126]	Time Domain Deconvolution (Direct Solution)
Kuchuk *et al*.	Time Domain Deconvolution (Least Squares Solution)
Baygun *et al*.[127]	Time Domain Deconvolution (Least Squares Solution)
von Schroeter *et al*.[128]	Time Domain Deconvolution (Total Least Squares Solution/Regularization)
Levitan*et al[129]*	Time Domain Deconvolution (Total Least Squares Solution/Regularization)
Ilk *et al[130]*	Combination of Laplace domain and time domain solution

Table 7-1 Evolution of time domain deconvolution methods

Table 7-2 Evolution of Laplace domain deconvolution methods

Researcher	Deconvolution in Spectral Domain
Roumboutsos and Stewart[131]	Laplace Domain Deconvolution
Bourgeois and Horne[132]	Laplace Domain Deconvolution
Onur and Reynolds[133]	Laplace Domain Deconvolution
Mendes *et al*.[134]	Laplace Domain Deconvolution
Cheng *et al*.[135]	Fourier Domain Deconvolution
Ilk *et al*[130]	Combination of Laplace domain and time domain solution
. Ahmadi *et al*.[136]	Laplace Domain Deconvolution

7.6.1 Deconvolution Algorithm for Variable Rate PTA and TTA

This section develops a data-driven deconvolution algorithm for variable rate TTA and PTA based on Laplace domain methods. The convolution theorem of integral transform analysis states that the convolution product is equal to the product of the transforms. For example, the Laplace solution of the PTA convolution is as follows;

$$\bar{g} = \frac{\overline{\Delta P}}{\bar{q} * s} \qquad 7\text{-}13$$

The deconvolution operation becomes a simple division in the Laplace domain, once the input functions have been transformed into it. This method requires an accurate approximation function for the tabulated pressure and flow rate data as well as a robust numerical Laplace inversion to deal with any discontinuities occurring in flow rate. Figure 7-9 illustrates the

general workflow for Laplace domain deconvolution algorithm. The details of each step are elaborated in the next sections.

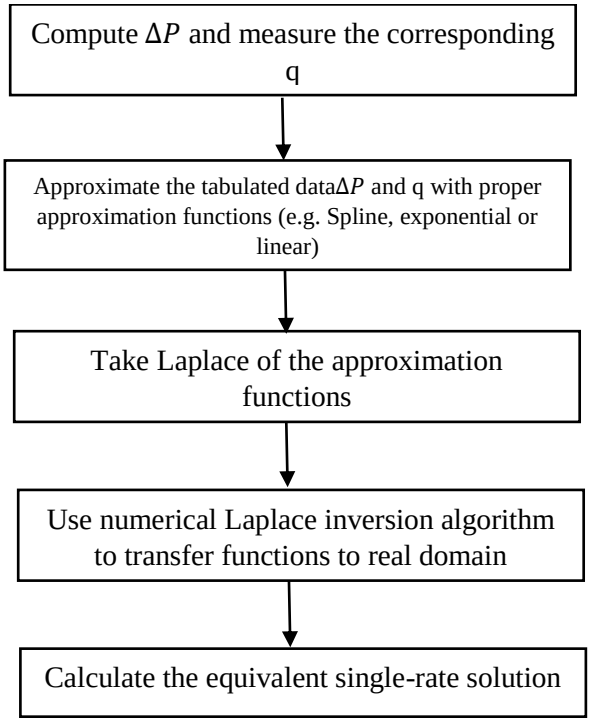

Figure 7-9 The Deconvolution workflow in the Laplace domain

7.6.2 The Approximation Function

The first step in developing deconvolution in Laplace domain is to approximate measured parameters such as wellbore pressure changes (ΔP), flow rate (q) and temperature changes (ΔT) with an appropriate approximation functions. Numerous approximation functions , from linear interpolation, exponential function, stepwise and piece wise functions[131, 133], B-spline[130] and cubic spline[134, 137], have been introduced in the literature. The main selection criteria for a good approximation function are;

1. Does it represent the tabulated data with acceptable accuracy?
2. Does it provide a smooth trend for the tabulated data?
3. Can the Laplace form of approximation function be achieved?

The measured parameters in PTA are usually the wellbore pressure, p_{wf}(or pressure change,ΔP) and flow rate, q, which are measured over a finite time interval as a set of discrete of points $t_1<t_2< \ldots <t_N$. The measured pressure or rate data represent a sample of an underlying function

f(*t*) [where, *f*(*t*) represents either pressure or rate or temperature] [133]. The Laplace transform of the sampled data is then given by ;

$$\bar{f} = \int_0^{t_1} e^{-st} f(t)dt + \int_{t_1}^{t_N} e^{-st} f(t)dt + \int_{t_N}^{\infty} e^{-st} f(t)dt$$
$$= I_1 + I_2 + I_3 \qquad 7\text{-}14$$

Where I_1, I_2, and I_3 represents the first, second, and third integrals in Eqn. 7-14. The application of Eqn.7-14 needs the knowledge of how the function behave over the interval of (0, t_1) and (t_N,∞). An extrapolation procedure should therefore be employed for these time intervals to accurately transform the sampled data to the semi-infinite Laplace domain[130]. This study concentrates on the second integral of *Eqn. 7-14*. The data was sampled as *f*1, *f*2, . . . , *fN* at discrete times *t*1, *t*2, . . . , *tN* from an underlying function *f*(*t*) Hence the second integral in Eq. 7-14 can be written as :

$$I_2 = \int_{t_1}^{t_N} e^{-st} f(t)dt = \sum_{i=1}^{N-1} \int_{t_i}^{t_{i+1}} e^{-st} f(t)dt \qquad 7\text{-}15$$

There are many ways to approximate a set of measured data. One of the simplest and most widely used method is to employ linear interpolation for each successive pair of recorded data points, i.e.

$$f(t) = f_i + d_i(t - t_i) \qquad \text{For} \qquad t_i \le t \le t_{i+1} \qquad 7\text{-}16$$

Where d_i represents the slope between two adjacent points;

$$d_i = (f_{i+1} - f_i)/(t_{i+1} - t_i) \qquad 7\text{-}17$$

The Laplace solution for this approximation function is;

$$I_2 = \sum_{i=1}^{N-1} \left[\frac{f_i e^{-st_i}}{s} + \frac{d_i\left(e^{-st_i} - e^{-t_{i+1}}\right)}{s^2} - \frac{f_{i+1} e^{-st_{i+1}}}{s} \right] \qquad 7\text{-}18$$

Another alternative piecewise linear approximation is step-wise approximation. This is especially useful for flow rate changes, where the slope of the chords is zero Eqn 7-18 can now be simplified as ;

$$I_2 = \sum_{i=1}^{N-1} \left[\frac{f_i e^{-st_i}}{s} - \frac{f_{i+1} e^{-st_{i+1}}}{s} \right] \qquad 7\text{-}19$$

This chapter approximates pressure and temperature changes as a piecewise function (Eqn 7-18) and the flow rate is represented with a step-wise function (Eqn 7-19).

7.6.3 Numerical Laplace Inversion

The next step in developing a Laplace-domain deconvolution is to transfer the solution from the spectral domain to the real-time domain. Numerical Laplace inversion algorithm is employed if an analytical solution for this transformation cannot be obtained. The common transformation method is the Stehfest[137] numerical algorithm.

One main problem with the Laplace transformation is that it is only possible when the function is continuous. This approach fails for step-wise flow rate changes and the inversion becomes instable. Two new numerical Laplace inversion algorithms have been recently introduced ; Gaver-Wynn-Rho (GWR)[138] and Den Iseger [139] that are claimed to be robust in the case of discontinuities.

For comparing the results of these three numerical Laplace invasion algorithms for our application, computer program codes were developed (Stehfest and Den Iseger in Matlab and GWR in Mathematica) The flow rate was also first approximated using a step-wise function and then transferred back to the time domain using the numerical inversion methods.

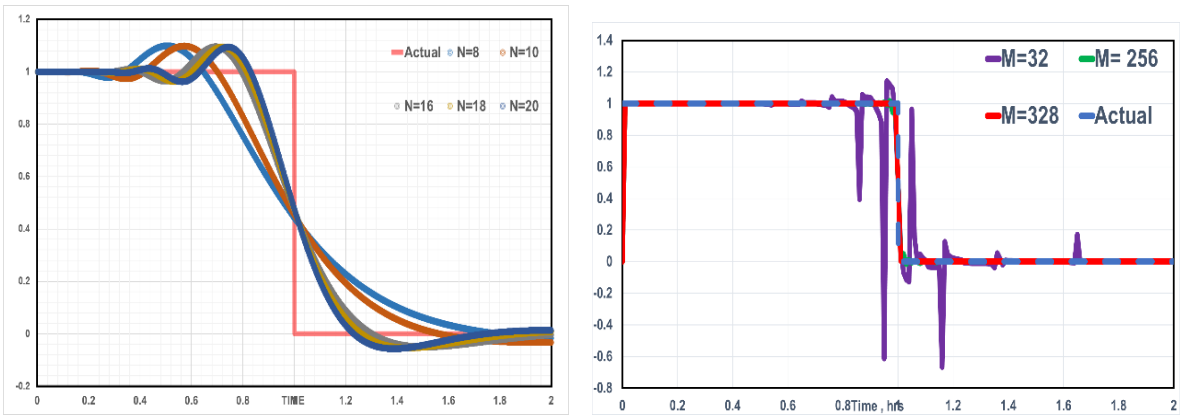

Figure 7-10 Stehfest (left) and GWR (right) numerical Laplace inversion methods for a step-wise function

Figure 7-10 shows that the Stehfest algorithm cannot detect the sharp changes on flow rate even when the tuning parameter, N, was increased. GWR achieves a better performance with an increase on the tuning parameter, M, improving the match. However, this also increases the run time affecting the practicality of this method. By contrast, *Figure 7-11* shows that Den

Iseger method provides a perfect match to the actual response. Therefore, Den Iseger algorithm is selected to be used for the TTA deconvolution method in this study.

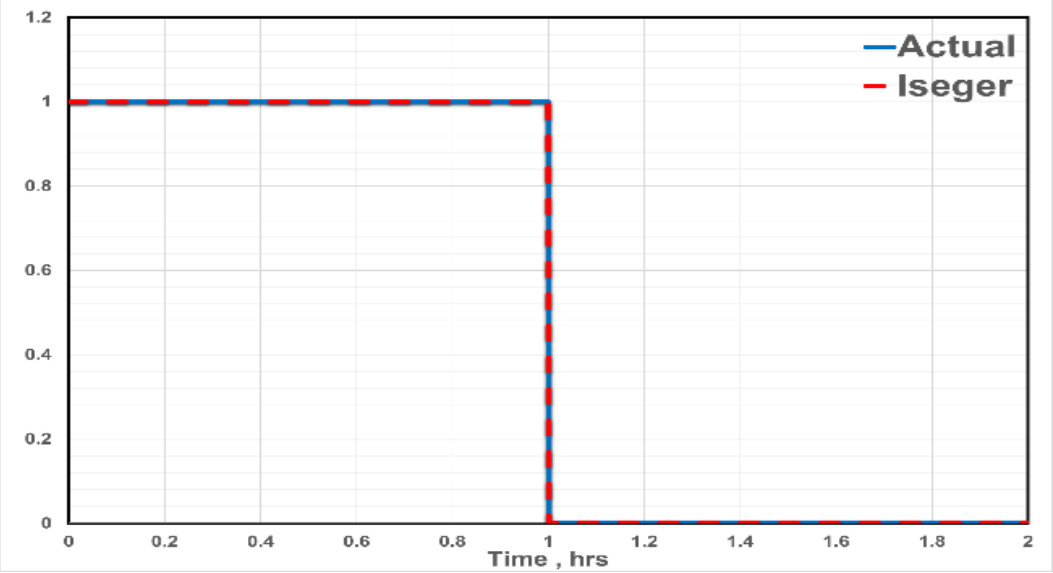

Figure 7-11 Den Iseger numerical invasion algorithm for step-wise function

7.6.4 Verification of the Deconvolution Algorithm's Robustness

The next step is to verify the result of the deconvolution algorithm, now that a suitable approximation function and robust numerical inversion algorithm has been selected. A draw down test followed by build-up period is modelled and the result of the pressure-rate deconvolution is compared with the equivalent single-rate solution.

The steps in the *Figure 7-9* algorithm was followed by approximating the flow rate with step-wise function and the pressure changes by a piecewise linear function.

Figure 7-12 verifies that developed deconvolution workflow perfectly matches the equivalent single-rate solution. It will now be used to reconstruct the temprature and pressure signals for the *Figure 7-1* multi-rate flow test.

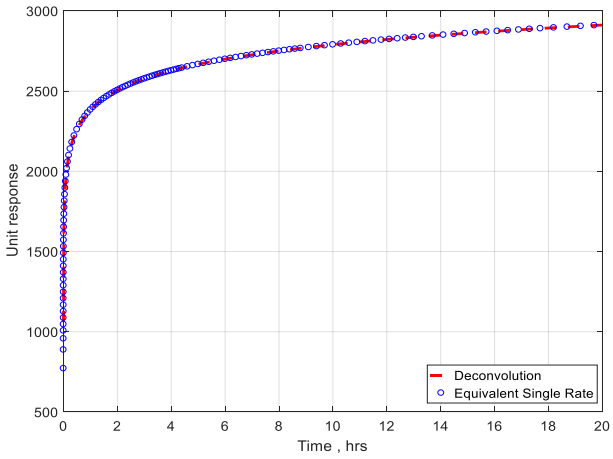

Figure 7-12 Comparison between deconvolution result and actual single-rate solution

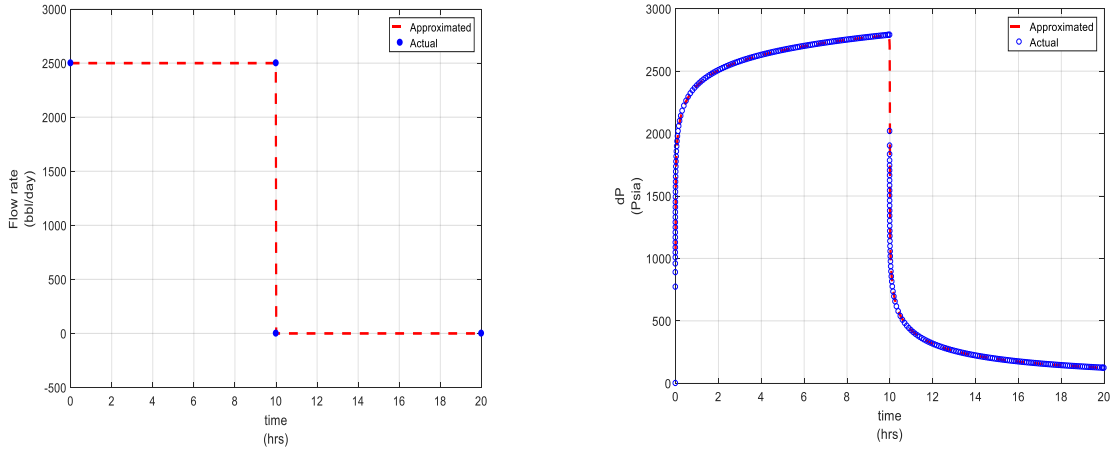

Figure 7-13 Approximated flow rate (left) and pressure changes (right)

7.6.5 Rate-Pressure Deconvolution (RPD)

Figure 7-14 compares the result of normalisation, deconvolution and single-rate solutions, for the *Figure 7-1* multi-rate flow test, where the changes in pressure is attributed to flow rate. The results confirm that deconvolution(PRD) provides an exact solution for the problem while normalisation only delivers an approximation. Furthermore, there is a perfect agreement between the PRD's semi-log slope and the actual solution. Having an accurate slope is essential for PTA since the analysis workflow is based on the semi-log and log-log slope.

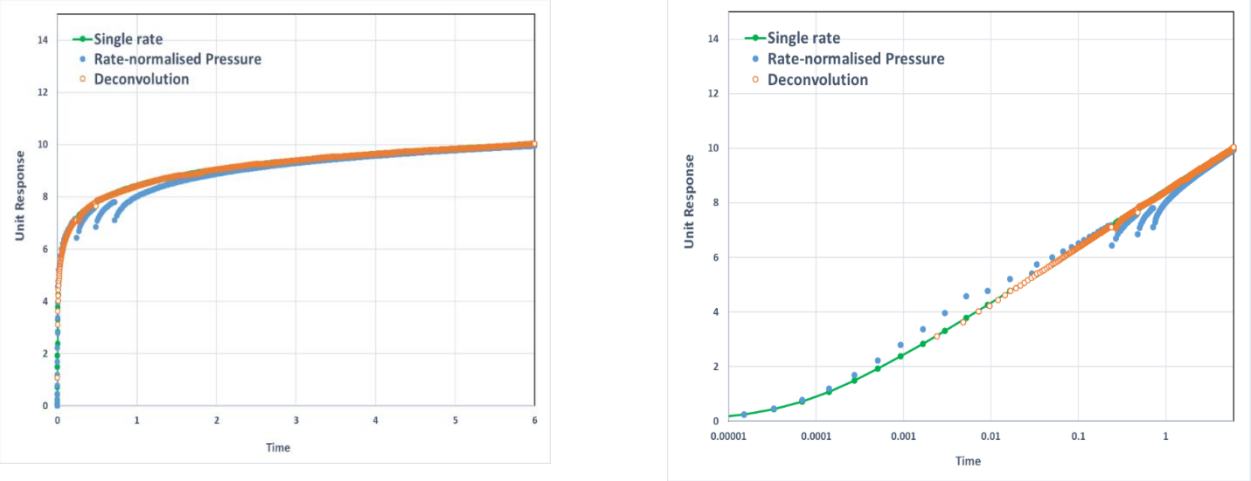

Figure 7-14 Comparison between RPD deconvolution, normalisation and single-rate solution: semi-log (right) and Cartesian plot (left)

7.6.6 Rate-Temperature Deconvolution (RTD)

The flow rate and temperature data are approximated with step-wise and piece wise functions respectively for RTD in a similar manner to that employed for RPD.

Figure 7-15 compares the results for normalisation and deconvolution. Both methods efficiently restore the early-time response (i.e. the first-rate change, for the reason explained earlier), while deconvolution reconstructs the later variable-rate response better than normalisation. None of the methods could provide an exact solution though. A good match of the temperature derivatives at the late time is however promising.

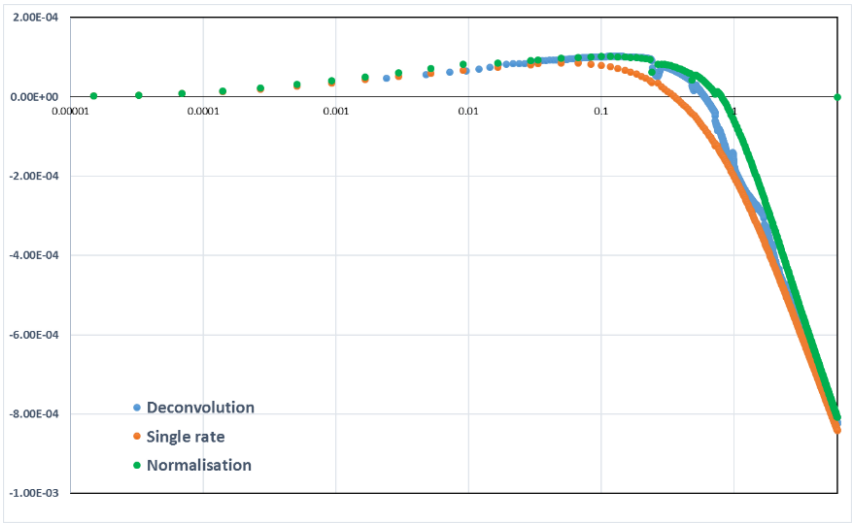

Figure 7-15 Comparison between RTD deconvolution, normalisation and single-rate solution

7.6.7 Pressure-Temperature Deconvolution (PTD)

The pressure and temperature changes shown in *Figure 7-1* is a multi-rate test can be approximated using piecewise linear function for PTD as there are no discontinuities in the data.

Figure 7-16 shows the comparison between the results of the three methods. It again confirms the better performance of deconvolution when compared with normalisation for the variable rate solution. Similar for RTD, the fact that the temperature derivatives are well reconstructed for both the early-time and late-time periods allows using the TTA solutions, rendering these methods promising.

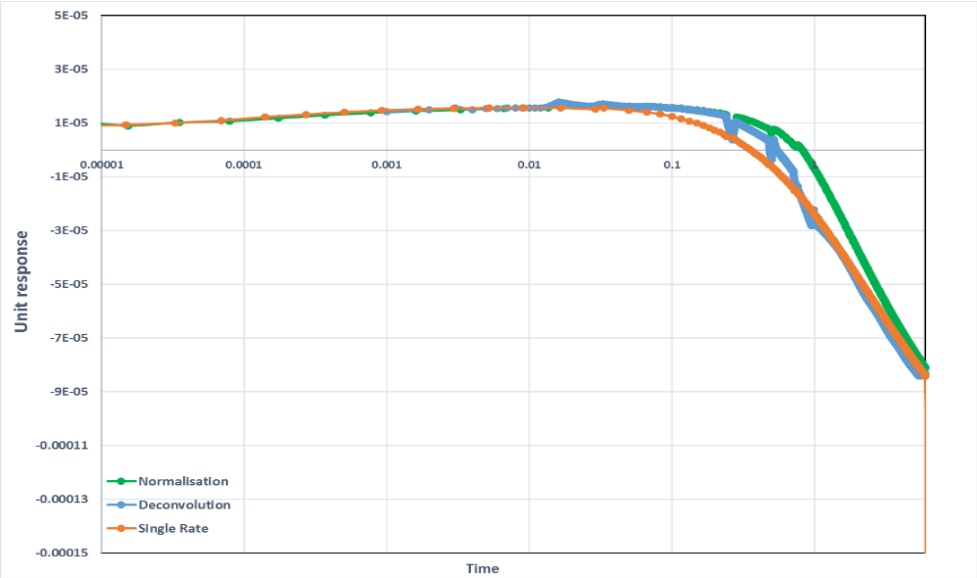

Figure 7-16 Comparison between PTD deconvolution, normalisation and single-rate solution

7.6.8 Draw down and Build-up Deconvolution

This section investigates the application of TTA deconvolution for analysis of a well test consisting of a drawdown followed by a build-up. *Figure 7-17* shows the flow rate and corresponding pressure and temperature data.

Flow rate, pressure and temperature changes were approximated with an appropriate function as described previously. *Figure 7-18* shows the RTD and TPD analysis of this test. Deconvolution solution has not succeeded in matching the equivalent single rate solution for both cases in the build-up period.

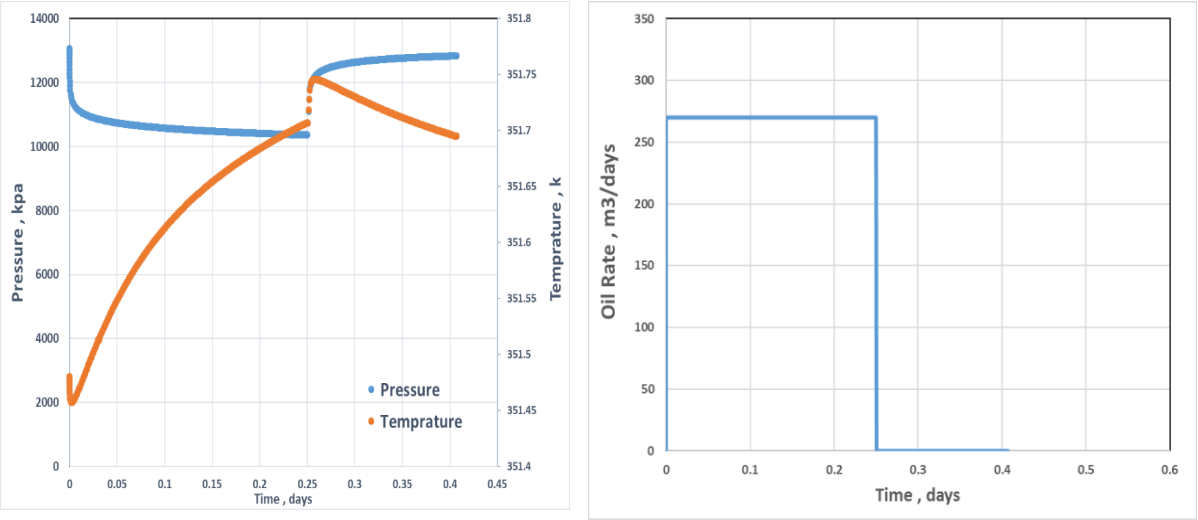

Figure 7-17 flow rate (right) and pressure and temperature data (left)

The main reason for this can be due to the fact that thermal heat conduction cannot be overlooked in build-up period in the TTA equation, so essentially, unlike PTA, the physics describing the temperature build-up and drawdown can differ. So, the use of the same unitary response function for both these periods in deconvolution may be incorrect. Temperature changes cannot therefore be solely attributed to the pressure disturbance or effect of previous production, therefore, superposition of the production with no flow build-up periods in TTA may not be correct.

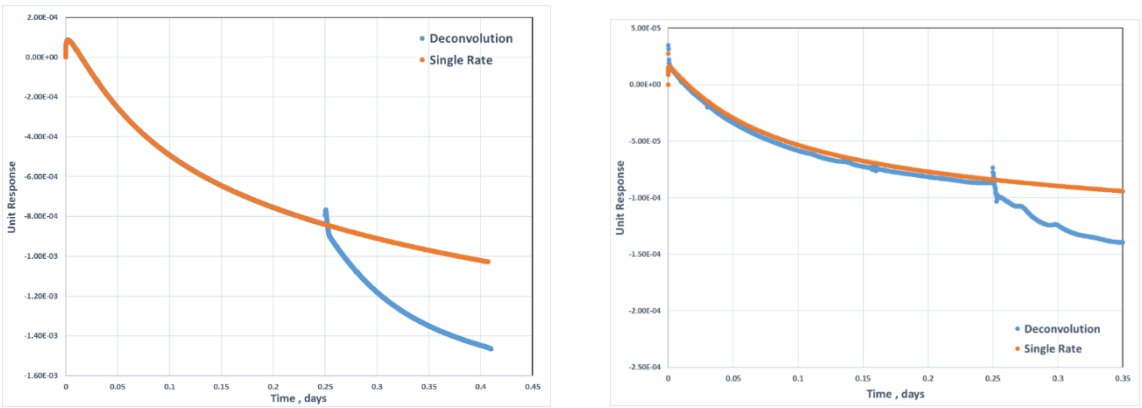

Figure 7-18 rate-temperature (left) and pressure-temperature (right) deconvolution

7.7 Real Data Application

In this section, the application of the presented variable rate solutions is further discussed using a real data. The data set is for a slanted I-Well completed in three zones. Each zone is equipped with an ICV and PDGs. The full description of the field and well completion will be presented in the next chapter.

ICV cycling is a recommended, routine practice for I-Wells to test the hydraulic control system and minimise problems coming from minor amounts of scale being deposited. Data gathered during this operation can be useful for reservoir characterisation. ICV, in this well, has 11 positions (0-10 inclusive), the first two positions have zero or nearly flow rate area (closed). Movement of ICV positions leads to flow rate changes which is similar to multi-rate test. The resulting response affects pressure and temperature measurements.

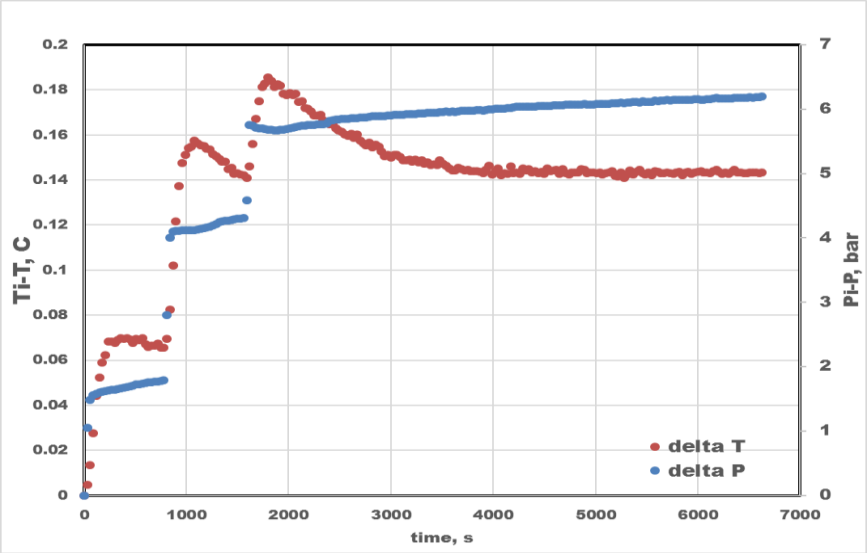

Figure 7-19 Pressure and temperature data during ICV cycling

Figure 7-19 shows the upstream pressure and temperature data collected during cycling of the Zone 2 ICV. According to the figure, although ICV moves from position 6 to 10, pressure and temperature only differentiates between positions 6 to 8 and no observable changes can be seen after position 8. As discussed in the previous chapter, this is due to the fact that the opening area of the valve for position 9 and 10 is already big enough and do not impose a notable restriction.

The pressure and temperature response caused by variable flow rate in this case will be analysed using normalisation and deconvolution methods to extract the equivalent single-rate change T response. The combination of data available defines the next step. The flow rate for each ICV position is not measured accurately since there is only one multi-phase flow meter measuring the well's total downhole flow rate. Pressure drop across ICV, as discussed in chapter 6, does not provide an accurate estimation of zone flow rate for all the positions in question. Therefore, a combination of pressure and temperature data was selected for further analysis. Pressure-normalised temperature, *Eqn.7-12*, and pressure-temperature deconvolution were employed. *Figure 7-20* shows the approximated pressure and temperature changes with a piecewise linear function for deconvolution solution

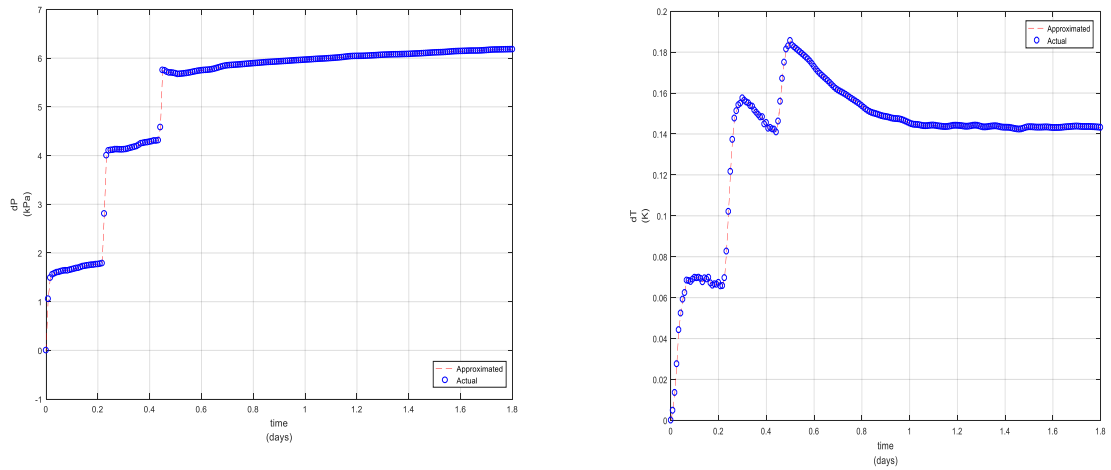

Figure 7-20 Approximated pressure and temperature

The result of the normalisation and deconvolution methods for this data set is illustrated in *Figure 7-21* .As it can be seen, the normalisation result is discontinuous while deconvolution provides a continuous trend and slope.

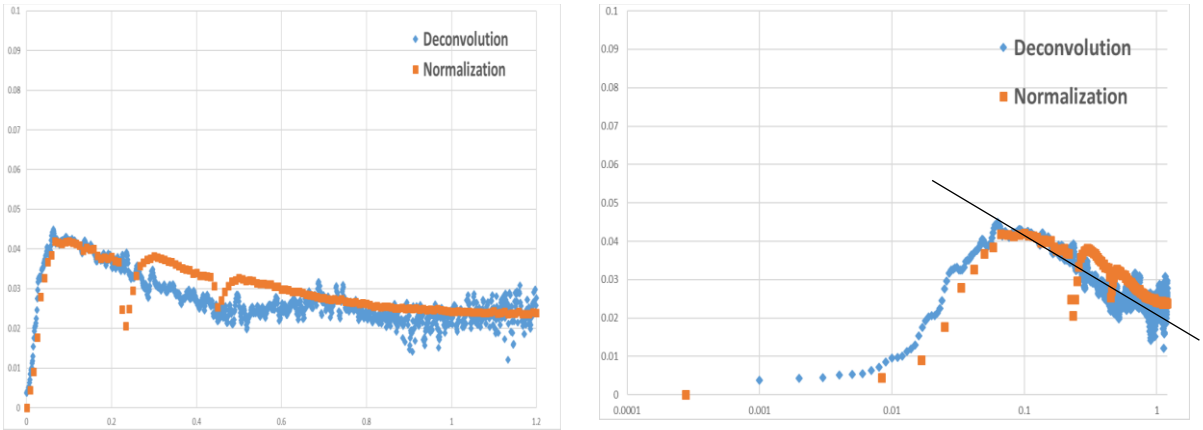

Figure 7-21 Deconvolution and normalisation results on semi-log and Cartesian plot

Figure 7-22 compares the actual single-rate response with the result of these deconvolution and normalisation. The actual response, called as Series3, is taken from the real measurement when the ICV in the adjacent zone, zone-1, is shut-in. As it can be seen there is an inconsistency between the results; however, based on the synthetic cases we may expect that deconvolution could match the actual response to some extent *(Figure 7-18).*

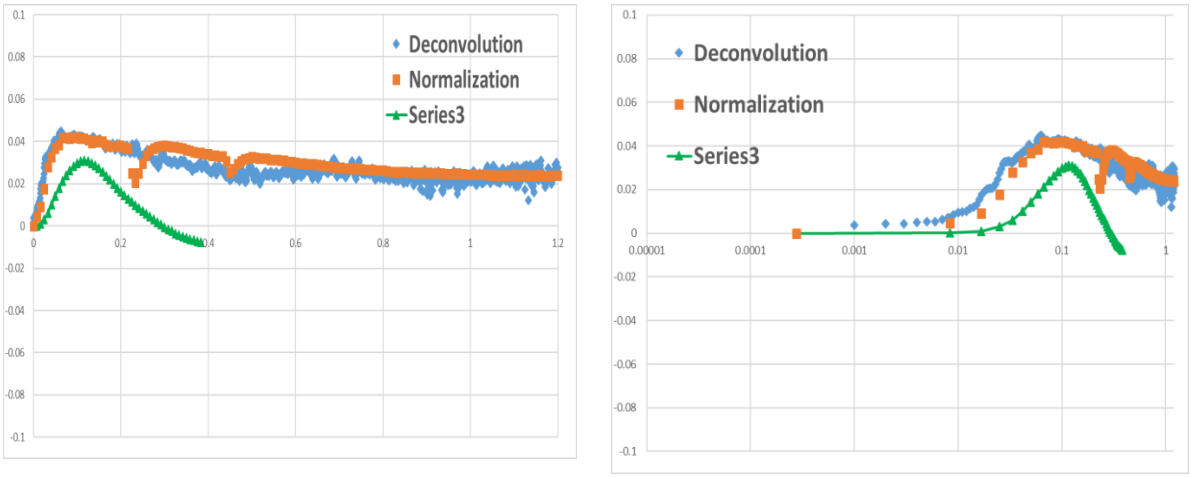

Figure 7-22 Comparing the result with actual response

Two possible reasons which lead to this inconsistency are as follows,

1. Both temperature and pressure data are collected upstream of ICV but downstream of ICD in this I-well. Non-linear pressure drop caused by ICD restriction may, therefore, distort the measured data and affect the results of deconvolution/normalisation accordingly (The effect of ICD pressure drop on PTA will be discussed in the next chapter.)
2. In multi-zone wells the measured zonal pressure drop can not only be due to production from the zone itself but also production from adjacent zones too *(Figure 7-23).* As a result, the problem is no longer linear and therefore both normalisation and deconvolution method are affected (in this case the zone upstream of Zone 2 was not produced)

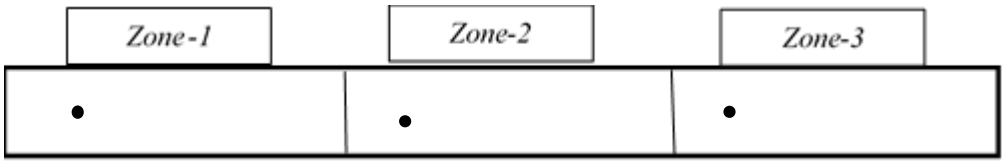

$$P_i - P_{wf(zone-2)} = \Delta P_1 + \Delta P_2 + \Delta P_3$$

Figure 7-23 Zonal pressure drop annuls of in multi-zone wells

As a result, this data set might not be an ideal measurement to apply the proposed methods for variable flow rate test TTA.

7.8 Summary

In this chapter, the variable rate problem in both PTA and TTA was addressed. Different methods such as normalisation and deconvolution were used to reconstruct the unit response for an equivalent single-rate change solution. It was shown that rate-normalised temperature and pressure-normalised temperature was not very successful in restoring the temperature signal. A data-driven deconvolution method was also developed and verified. It was demonstrated that deconvolution results in exact solution for variable rate in PTA and provide better result for TTA. However, it was not able to match the transition regime between the fluid expansion – dominated and JT effect-dominated periods of the T response.

The attempt to apply the methods to the real data set was not successful, with the possible reasons including the non-ideality of the dataset affected by the sandface flow control completion.

Chapter 8 Pressure Transient Analysis in Advanced Wells Completed with Flow Control Devices

8.1 Introduction

This chapter aims to investigate the impact of non-linear pressure drop created by flow control devices on conventional pressure transient analysis. FCDs modify the inflow profile of a multi-zone well completion. Their imposition of an extra pressure drop at the sand face has proven to be particularly effective at delaying the breakthrough of (unwanted) water or gas in wells with long completion lengths. It is widely accepted that a FCD completion improves the field's economics; but the question of whether and how a FCD completion affects the accuracy of the standard PTA workflows has not been addressed.

An integrated, dynamically coupled, wellbore and reservoir model is employed to define the criteria within which the FCD pressure drop can be treated as an additional skin. This model will be used to supply the completion performance data for studying when the FCD's nonlinear nature distorts the pressure signal and affects the analysis. A general workflow for the analysis of PTA data measured in liquid producing wells completed with FCDs that produces realistic values of the formation damage skin has been developed. The workflow has also been adapted for routine monitoring of wells completed with FCDs.

The value of this study is illustrated by its application to two data sets from the North Sea's Golden Eagle field. These data sets provide an ideal test that validates the analysis due to well completions design with multiple levels of inflow control together with "state-of-the-art", downhole sensors.

8.2 Background and Problem Description

As described previously I-wells are equipped with in-well high precision sensors and gauges and different FCDs. It is important to note that the monitoring and control capabilities of an I-well should be considered as a system. For instance, ICVs control production or injection but also support high quality reservoir monitoring by acting as a downhole shut-in valve to test each zone separately on build-up. This reduces the wellbore storage and phase redistribution effect, increasing the quality of the measured, zonal pressure build-up data and its subsequent PTA. High resolution pressure and temperature gauge's up- and down-stream of an ICV can also often be used to estimate zonal flow rates and water cuts[46].

A FCD's flow performance has the potential to improve the completion's inflow profile by sacrificing the well's productivity [140], but its presence may also alter the classical PTA response by imposing an extra, non-linear pressure drop, which is normally a function of fluid properties and the square of the flow rate, see e.g. *Eqn. 8-1* for a nozzle-type ICD**.** *Eqn. 8-1's* non-linearity might lead to the different-from-sandface reservoir pressure response measured in the annulus and tubing, making conventional interpretation methods inaccurate.

$$\Delta P_{ICD} = \frac{C_u \rho_{mix} q^2}{2 C_v^2 A_c^2} \qquad (8\text{-}1)$$

Where ρ_{mix} is the mixture density, A_c is the ICD opening area, C_v is the discharge coefficient, q is the flow rate and $C_u$is a conversion constant.

This chapter studies the effect of such non-linear pressure drop, e.g. due to ICDs, on the pressure transient analysis. For simplicity it is assumed that only the ICD-completion is responsible for the "non-Darcy" pressure drop. The following questions will be addressed in the next sections;

- How do ICDs affect pressure measurement in the annulus and tubing?
- Do ICDs affect the skin and permeability estimates from Pressure Transient Analysis (PTA)?
- Is the conventional PTA workflow sufficient for ICD completed wells?
- If not, can corrections be proposed to the current PTA workflow to incorporate the ICD effect?

Finally, the developed workflow is applied to well test data from a real North Sea well.

8.3 Methodology: Dynamic, Integrated Wellbore-Reservoir Modelling

Before analysing the real well data, the effect of an ICD completion on PTA is analysed with the integrated, transient, dynamic, coupled wellbore-reservoir model described in *chapter 3*. This simulation model provides insight on how to approach the real data in the context of this problem. As shown in *Figure 8-1*, the wellbore model consists of a three zone, horizontal intelligent well with both nozzle type ICDs and ICVs for production control and monitoring. The flow path in this completion is designed such that the reservoir fluid first goes to the annulus through ICDs and then ICVs are used to connect the annulus to the tubing. For simplicity, the ICD completion is modelled as one equivalent, 'up-scaled ICD' per zone that has the cumulative diameter equal to the total number of ICDs installed in each compartment.

The 'ICD strength' relates the flow rate across an ICD and its pressure drop ('stronger' ICDs are more restrictive). The ICDs may have a uniform strength (i.e. each zone is exposed to the same ICD strength) or a variable strength distribution along the wellbore. They will both be compared with a non-restrictive completion equivalent to either an open hole or a stand-alone-screen (SAS) completion). The reservoir simulation model was built with 30*30*11 grid blocks and local grid refinement (LGR) near the wellbore to ensure proper representation of the pressure changes (*Figure 8-1*). For simplicity, the well is placed in the middle of a homogenous reservoir with no flow boundaries and five connections per zone linking the reservoir to the wellbore. Both fixed flow rate and tubing head pressure are used for production control. The well test schedule requires the zones to be tested sequentially by closing the ICVs across each zone.

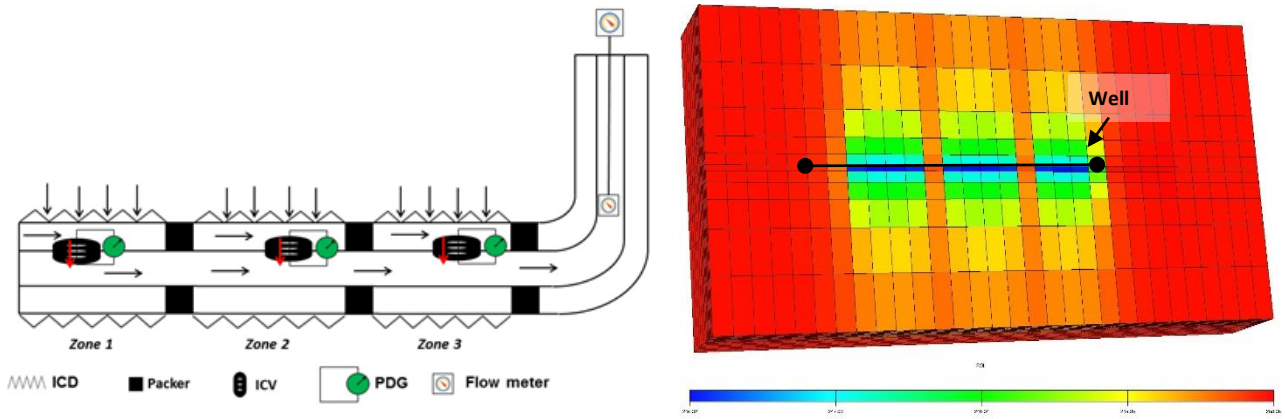

Figure 8-1 The Wellbore Completion (left) and the reservoir model (right)

8.4 The Effect of an ICD completion on PTA

As this chapter mainly focuses on PTA in horizontal wells, before talking about the impact of FCDs, a brief introduction on the expected flow regimes and corresponding equations for this particular well geometry is first presented. This is followed by investigating the impact of ICD completion on PTA for various production scenarios.

Figure 8-2 illustrates five distinct flow regimes that are expected to be identified from the derivative plot ($P' = \frac{dP_{wf}}{dlnt}$) during conventional PTA of a horizontal well. Each flow regime provides specific information about the reservoir and/or the completion. For example, the damage skin (S_d) and the product of the permeability in x and z direction ($K_x.K_z$) can be estimated from the early radial flow regime using equations in *Table 8-1*.

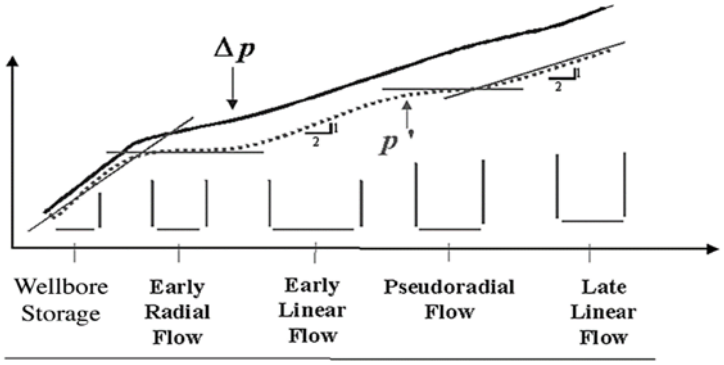

Figure 8-2 Possible flow regimes for horizontal wells on log-log plot [141]

$$P_i - P_{wf} = \frac{162.6q\mu B}{\sqrt{k_r k_v} L_w}\left[\log_{10}\left(\frac{\sqrt{k_r k_v}}{\emptyset \mu C_t r_w^2}\right) - 3.227 + 0.868 S_d\right] \quad (8\text{-}2)$$

$$\sqrt{k_r k_v} = \frac{162.6q\mu B}{mL_w} \quad (8\text{-}3)$$

$$S_d = 1.151\left[\frac{\Delta P_{ihr}}{m} - \log_{10}\left(\frac{\sqrt{k_r k_v}}{\emptyset \mu C_t r_w^2}\right) + 3.227\right] \quad (8\text{-}4)$$

Table 8-1 Early-radial flow regime equations in horizontal wells[138]

8.4.1 Impact of ICD Completion on PTA of Wells Producing at a Constant Rate

The first case examines the effect of ICD on pressure data for a well producing at a constant-rate. *Figure 8-3* illustrates the influence of the pressure drop imposed by ICDs of different effective diameters (or strength) per zone for the same production rate. The resulting pressure trend for both the draw down and build-up period at the well's toe section as measured both upstream and downstream of the ICD is shown in *Figure 8-3*. The presence of the ICDs is only observed in the drawdown period, i.e. the pressure build-up data measured upstream of the ICDs overlays the downstream measured data during this zero-flow rate period. Note that wellbore storage is absent since the downhole shut-in is modelled. This assumption 1) focuses the analysis on the impact of the ICD analysis, and 2) models a situation close the real well case discussed later.

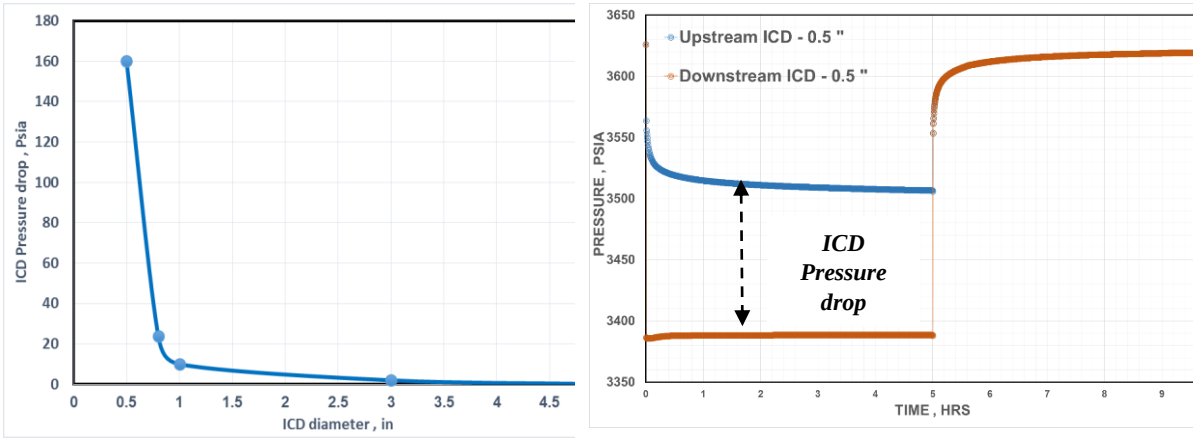

Figure 8-3 Pressure Drop across an ICD vs. effective Diameter Drawdown (left) and Build-Up Pressure Profiles for a ½ in. ICD completion (right)

Figure 8-4 shows the log-log PTA plot for the toe zone of a well completed with either a Standalone Screen (SAS) or an (upscaled) ICD of ½ in. or 1.0 in. diameter. PTA is limited to the early radial flow regime in x-z plane and the evaluation of the ($k_x.k_z$) parameter. Straight-line analysis estimated the *Table 8-2* values of permeability and skin using of *Eqn.8-3 and 8-4* derived for conventional PTA (the actual horizontal and vertical permeability and skin factor are 50, 5 md and zero respectively). The smaller diameter ICD dramatically increased the estimated skin value while retaining the same permeability product for all the three cases (*Figure 8-4*). This skin represents both the damage zone and ICD pressure losses and therefore can no longer be used to estimate quality of the damage zone alone. On the other hand, the derivative plots (inversely proportional to permeability) are identical.

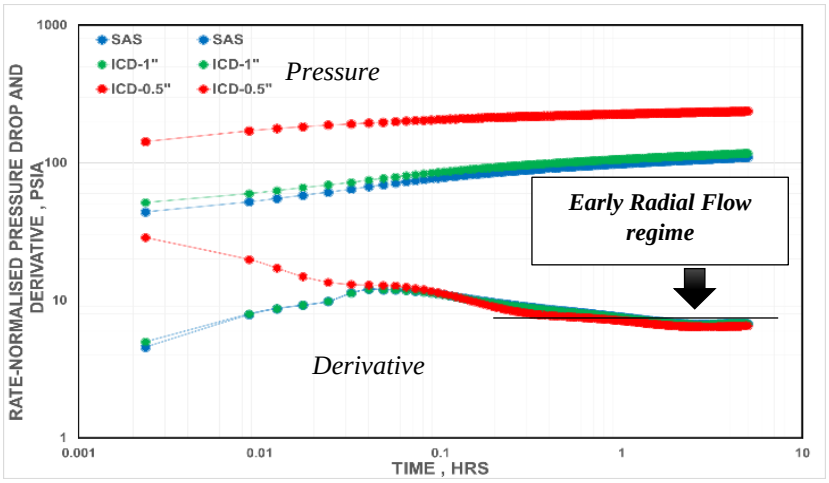

Figure 8-4 Log-log PTA plot for the Draw-Down Period (Constant rate)

Table 8-2 Parameters estimated

Completion	Semi-log slope (psi/day)	$(k_x k_z)^{½}$ (md)	Total Skin
SAS	18.5	12.6	0.31
1.0 in ICD	18.5	12.8	1.0
½ in ICD	18.7	13.0	10.5

Figure 8-5 shows the zonal flow rates and the ICD pressure drops to be almost constant after a short transition time. (This figure also shows that installing an ICD increases the flow rate of toe zone. This results in more uniform inflow along the completion, achieving the major objective of the ICD completion).

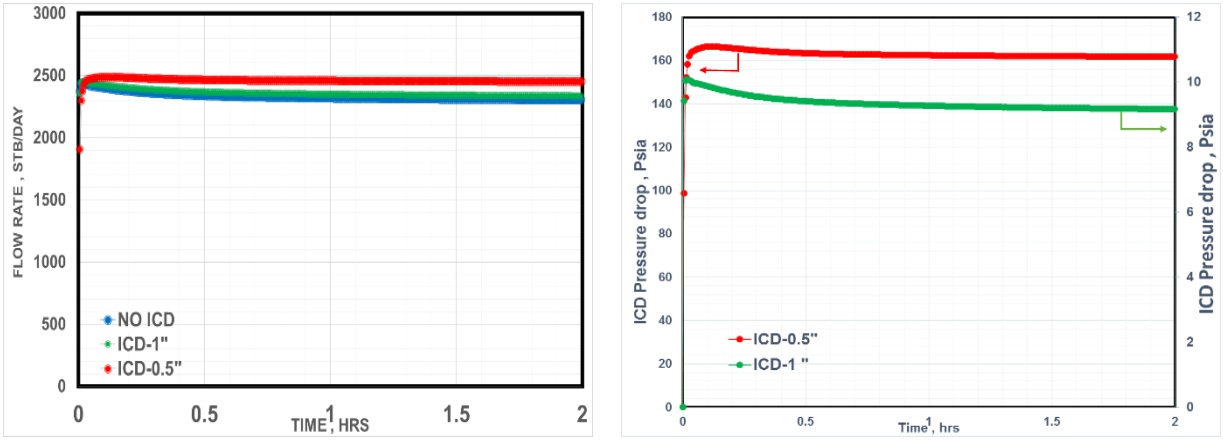

Figure 8-5 Zonal Flow Rate vs. Time (constant rate) and ICD Pressure Drop vs. Time (constant rate)

Figure 8-6 summarizes the PTA of the pressure build-up period. The pressure plots are distinct with the derivative curves being nearly identical. Our simulation assumed perfect downhole shut-in, hence the flow rate is a time independent parameter (i.e. sand face flow rate stops or starts nearly instantaneously subject to the inter-zone interference), even though the plots for all three completions start at different pressure value due to their differing ICD pressure drops.

It should be noted here that repeating the above study for the Heel and Centre zones of the horizontal well gave the same results as the Toe zone.

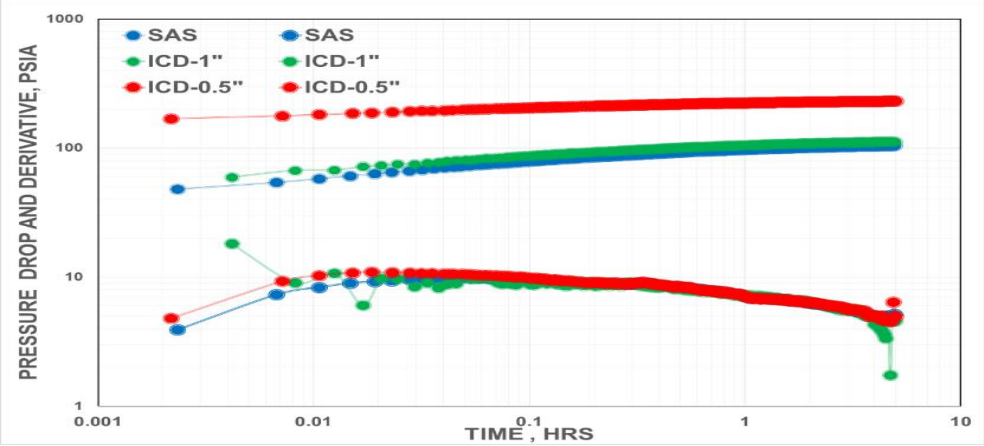

Figure 8-6 Log-log PTA plot of the Build-Up Pressure vs. Time (constant rate)

8.4.2 PTA for Wells with ICDs producing at a Constant Well Head Pressure

The well is controlled, for the second case, with a constant wellhead pressure. The flow rate is now a time dependent parameter and the pressures drop across the ICD is both time and rate dependent (*Figure 8-7*).

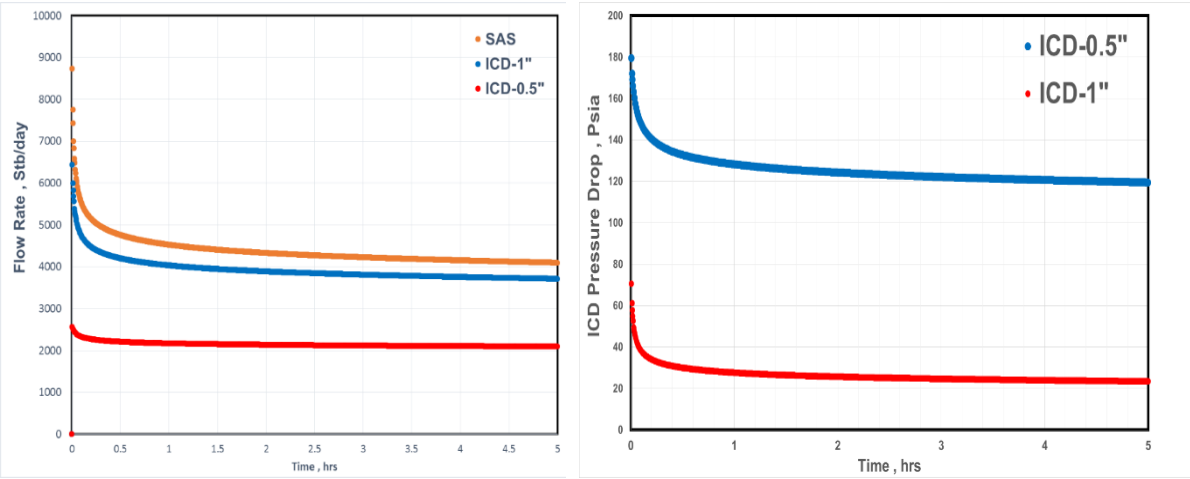

Figure 8-7 Zonal Flow Rate vs. Time (left) and ICD Pressure Drop vs. Time (right)

Figure 8-8 shows log-log plot for pressure build-up and draw down data. The rate-normalized pressure and the pressure derivatives are all different; hence, the estimated permeability and skin factor for the ICD completions will be incorrect (*Table 8-3*). By contrast, the pressure build-up derivative plots **(***Figure 8-8)* are not affected by ICD pressure drop (since the flow rate, and the pressure loss across the ICDs, eventually disappears), though the pressure change curves are also distinct, resulting in an overestimated skin.

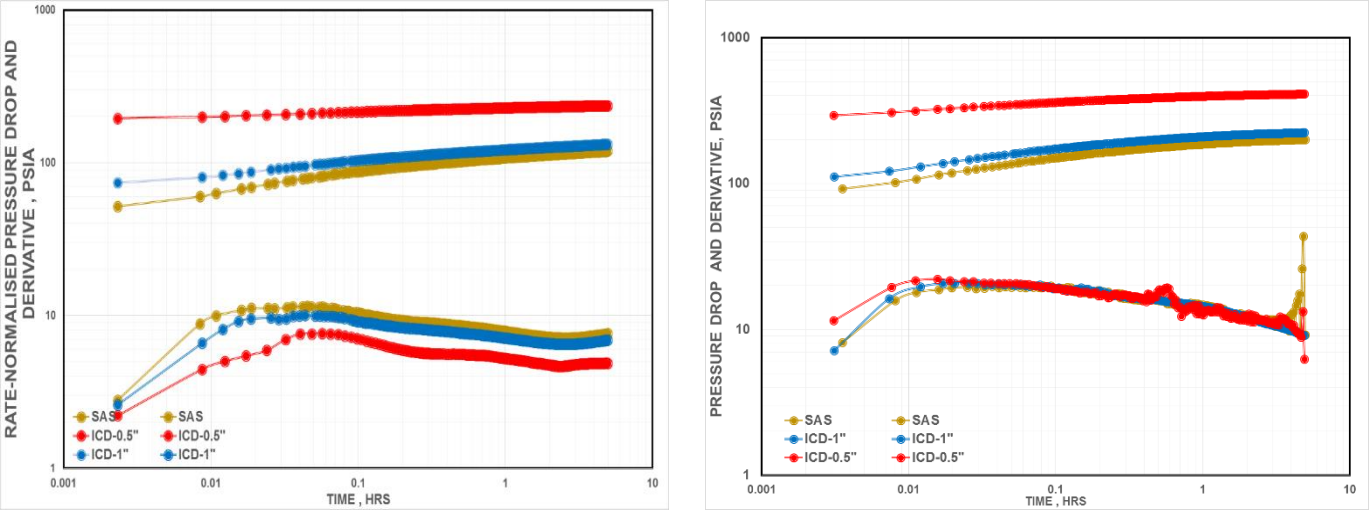

Figure 8-8 Log-log PTA plot of Draw down Pressure plot (left) and Log-log PTA plot of Build-Up Pressure (right)

Table 8-3 Results for Draw-Down PTA

ICD Size	Slope (psia/day)	$(k_x k_z)^{1/2}$ (md)	$(k_x k_z)^{1/2}$ Error	Total Skin
SAS	32	13	-	0.5
1 in	26	14	+ 9 %	2.5
0.5 in	11	20	+ 53 %	18

8.4.3 Effect of ICD Pressure Drop in Multi-Zone Measurement

The pressure is measured in the heel section of tubing for this case. The measured pressure is now affected by the FCDs installed across all the three zones. The results for a uniform and variable ICD strength along the wellbore for a constant well production rate are shown in *Figure 8-9*. For a uniform ICD strength distributed along the wellbore, the effect of ICDs is still mainly on the pressure plot; but variable ICD strength along the wellbore complicates the problem so that both pressure and pressure derivative plots are distorted. The conventional interpretation methods for both uniform and variable ICD strength cases are similarly affected for variable flow rate production with a constant tubing head pressure, if analysing pressure measured at the heel, although the results are not shown here.

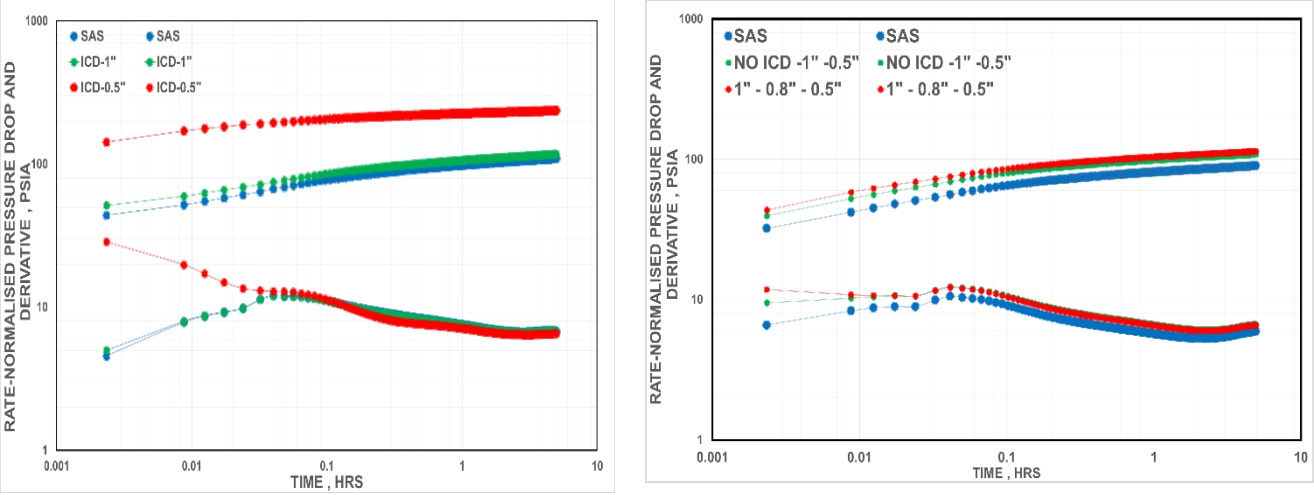

Figure 8-9 Uniform ICD along the wellbore and Variable ICD along the wellbore

8.4.4 Discussion

The above result indicates that in this case the pressure drop across the ICDs can be treated as being relatively time-independent additive when the variation in flow rate is insignificant; such as during the build-up periods when the flow rate is essentially zero. This extra pressure drop only affects the estimated skin value. It is thus necessary to develop a workflow to decompose the elements of the total skin and separate the contribution of a formation damage and an ICD skin completion from each other, e.g. as follows:

$$\Delta P_{ICD}(x,t) = \frac{C_u \rho_{mix} q_{ICD}^2(x,t)}{2C_v^2 A_c^2} \quad if \quad \frac{\partial q}{\partial t} \cong 0 \quad \Delta P_{ICD}(x) = \frac{C_u \rho_{mix} q_{ICD}^2(x)}{2C_v^2 A_c^2} \qquad 8\text{-}5$$

$$\Delta P_{wellbore}(x) = \Delta P_{reservoir}(x) + \Delta P_{ICD}(x) + \cdots \qquad 8\text{-}6$$

The above studies also indicated that both the pressure and the pressure derivative curves will be affected when there is a significant change in the zonal flow rate, e.g. during the PTA's drawdown period. In addition, a variable diameter ICD completion affects the applicability of conventional PTA when pressure data measured downstream of the ICDs (i.e. not at the sand face) is analyzed.

Solutions have been developed to incorporate the ICD term into the current PTA workflow for two scenarios when either zonal pressure or pressure at the heel section of a multi-zone well has been recorded.

8.5 PTA for a Single-zone FCD Completion

It has been shown that in the case modelled, the zonal pressure can be used for PTA analysis of a FCD completed well during zonal shut-in with the effect of FCDs only affecting the total skin values. The total skin estimated by PTA is the difference between the performance of an actual well and an ideal well (with zero skin) that obeys all the assumptions made by Darcy's Law [142]. Two approaches have been used to decompose the total skin for PTA :

- **First Method:** The total skin (S_t) is defined as a combination of all the individual skin terms *(Eqn. 8-7),* such as the skin due to perforation, well deviation, etc. This method requires all types of skin values to be calculated using a correlation, variety of empirical equation for different types of skin can be found in *Bourdet 2002* [109].

$$S_t = S_d + S_{pp} + S_p + S_\theta + S_f + S_{cz} \qquad (8\text{-}7)$$

  Where S_d is the skin due to formation damage, S_{pp} is completion pseudo skin due to partial penetration, S_p is the skin due to perforation, S_{cz} is the skin due to rock compaction, S_θ is the geometrical skin due to well inclination and S_f is the skin due to hydraulic fracture

- **Second Method**: This method has been made available in some commercial PTA software, *e.g. Saphir* , where all the components of the total skin, apart from the Formation Damage skin, are included as a single term called geometrical skin *(Eqn. 8-8).* The geometrical skin is determined by the difference between the model skin and the model skin for a fully penetrating vertical well with no formation damage. Therefore, several skin terms add up automatically and damage skin, which is the most important form of skin for Production Engineers, can be calculated.

$$S_t = S_d + S_{geometrical} \qquad (8\text{-}8)$$

8.5.1 ICD Skin in Vertical Wells

Hawkins [143] described the effect of extra pressure drop caused by the presence of a formation damage skin as:

$$\Delta P_d = \frac{141.2qB\mu}{kh} S_d \qquad (8\text{-}9)$$

and

$$S_d = \left(\frac{k}{k_s} - 1\right) \ln \frac{r_d}{r_w} \qquad (8\text{-}10)$$

Where k_s and r_d are permeability and radius of the damage zone, k is the original permeability and r_w wellbore radius. S_d is incorporated into the line-source PTA solution through the boundary condition:

$$P_{wD}(t_D) = P_D(1, t_D) + S_d \qquad (8\text{-}11)$$

The pressure drop due to the ICDs can also be added in the same manner, providing the variation in flow rate is small. As decribed before , for a nozzle/orifice type ICD pressure drop is definied ,

$$\Delta P_{ICD} = \frac{C_u \rho q^2}{2C_v^2 A_c^2} \qquad (8\text{-}12)$$

The rate q here is the production rate before the zonal shut-in, and the area is the equivalent (a.k.a. 'upscaled)' area of the ICDs installed across the zone tested. Note that this approach requires knowing the ICD-completion parameters (e.g. how many devices/screens are open to flow/clean) at the time of test.

The dimensionless ICD skin for a vertical well can be defined as follows;

$$S_{ICD} = \frac{kh}{141.2q\mu\beta} \Delta P_{ICD} = \frac{kh}{141.2\mu\beta} * \frac{C_u \rho_{mix} q}{2C_v^2 A_c^2} \qquad (8\text{-}13)$$

Moreover, PTA in a vertical ICD completed well will be modified as;

$$P_{wf} = P_i + 70.6 \frac{qB\mu}{kh} \left[ln \left(\frac{1688 \emptyset \mu c_t r_w^2}{kt} \right) - 2S_t \right] \qquad (8\text{-}14)$$

Where:

$$S_t = S_d + S_{ICD} \qquad (8\text{-}15)$$

8.5.2 ICD Skin in Horizontal Wells

The corresponding expression for the skin due to a horizontal, open hole completion is more complicated than that for a vertical well. The damage skin for a horizontal well must be calculated from the early radial flow period since the linear flow regime includes both the damage and convergence terms. The extra pressure drop due to damage adjacent to the well bore for early radial flow is calculated as:

$$\Delta P_d = \frac{141.2qB\mu}{\sqrt{K_x K_z}L_w} S_d \qquad (8\text{-}16)$$

The skin due to ICD is then defined as:

$$S_{ICD} = \frac{\sqrt{K_h K_v}L_w}{141.2qB\mu}\Delta P_{ICD} = \frac{\sqrt{K_h K_v}L_w}{141.2B\mu} * \frac{C_u \rho_{mix} q}{2C_v^2 A_c^2} \qquad (8\text{-}17)$$

and the total skin and pressure drop for early radial flow regime is defined as follows;

$$P_i - P_{wf} = \frac{162.6q\mu B}{\sqrt{k_r k_v}L_w}\left[\log_{10}\left(\frac{\sqrt{k_r k_v}}{\emptyset\mu C_t r_w^2}\right) - 3.227 + 0.868S_t\right] \qquad (8\text{-}18)$$

Where S_T is defined by Eqn. 8-15 or by the normalized version as follows ;

$$S_T = \frac{h}{h_w}\sqrt{\frac{k_r}{k_v}}\left(S_{damage}\right) + S_{ICD} \qquad (8\text{-}19)$$

8.5.3 Workflow to Decompose the Total Skin for ICD Completed Wells

Figure 8-10 summarizes the workflow to decompose the total skin for ICD completed wells based on the above formula. Option 2 is recommended if commercial well test software is available while option 1 being preferred when the reservoir, well and completion models are not very complex and reliable correlations for the value of the different component of the skin are available.

In this study, the second option will be employed to decompose the total skin of two well data sets from the Golden Eagle field.

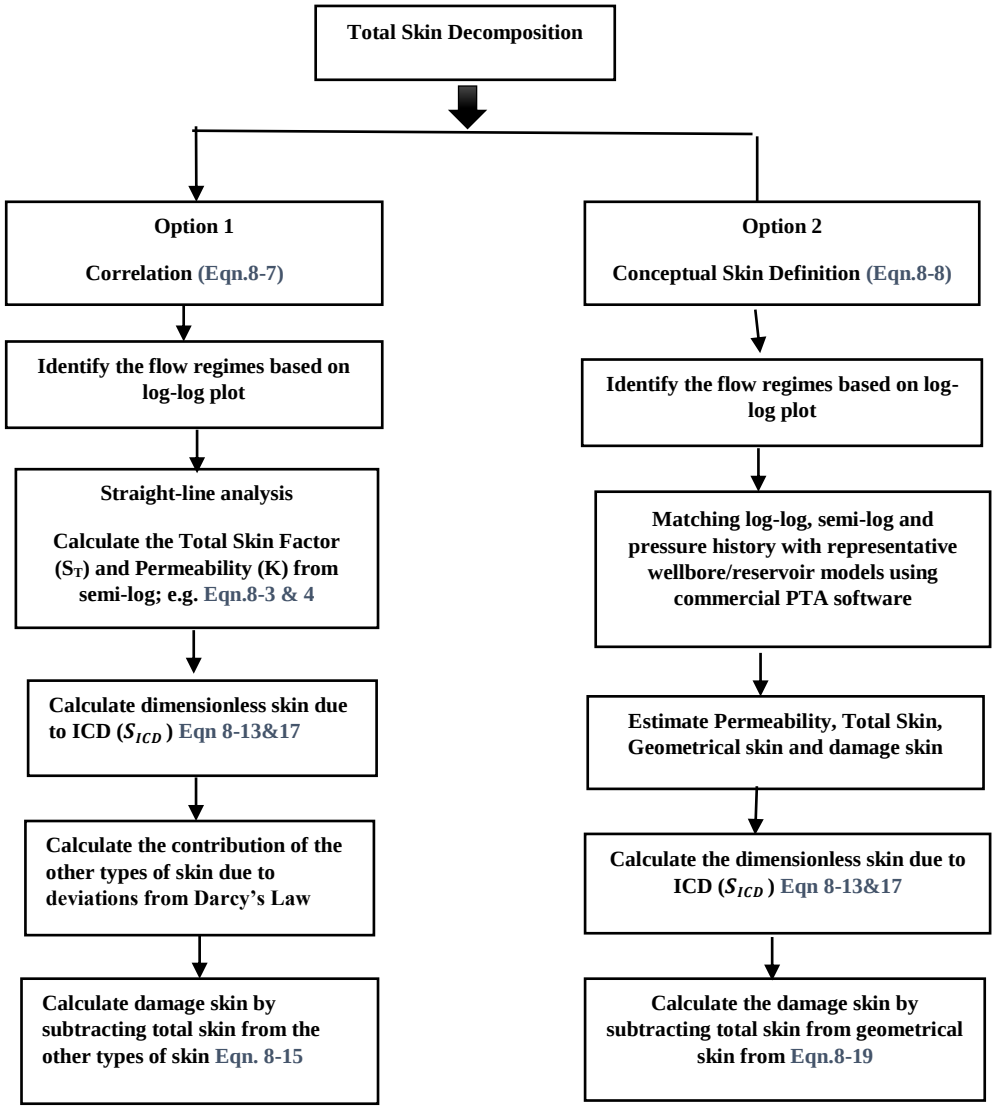

Figure 8-10 Workflow to decompose the Total Skin for ICD completed wells

8.6 PTA in Multi-zone FCD Completion

This section investigates the effect of a FCD on a single-point pressure measurement in the tubing. It is assumed that horizontal well consists of a number of segments or zones, each of which is completed with a FCD. A PDG measures the pressure data at the heel section of the well downstream of all the devices. Therefore, the measured pressure is the system response included all the ICDs.

The 3D diffusivity equation governs the flow into a multi-segment horizontal well , illustrated in *Figure 8-11* ,as follows [144];

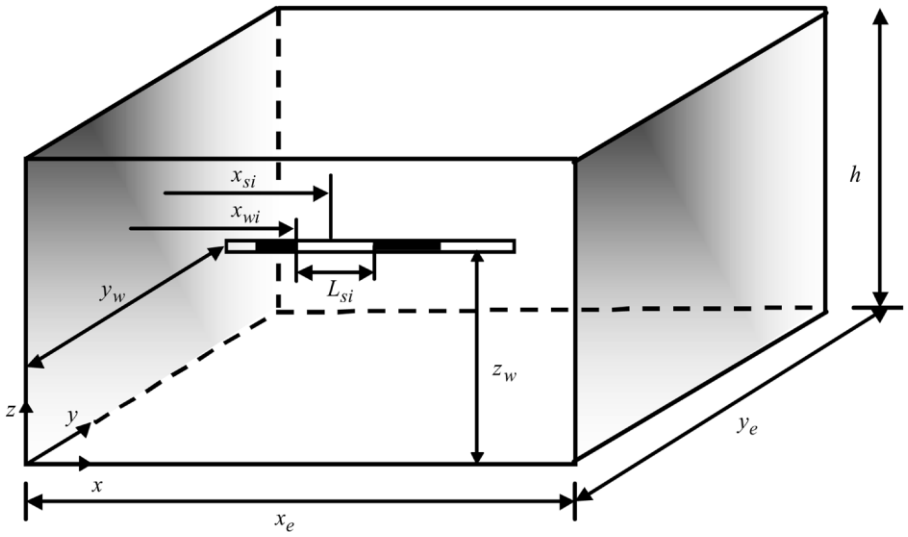

Figure 8-11 Multi-segment selectively completed horizontal well model[144]

$$\frac{\partial^2 P_D}{\partial x_D^2} + \frac{\partial^2 P_D}{\partial y_D^2} + \frac{\partial^2 P_D}{\partial z_D^2} + S_D = \frac{\partial P_D}{\partial t_D} \qquad (8\text{-}20)$$

Where S_D is the source (a.k.a. Green's or impulse response) function .This complex problem was solved using the Laplace and Fourier transformation by *Yildiz 2004 [144]*. *Eqn 8-21 and 8-22* includes the effect of skin in each segment (the full derivation of the equation is presented in appendix 1)

$$\tilde{P}_{jD}(s) = \sum_{i=1}^{n_{seg}} A_{ji}(s)\, \tilde{q}_{iD}(s) + \tilde{q}_{jD}(s) S_{pthj} \qquad (8\text{-}21)$$

Where;

$$S_{pthj} = \frac{k}{\sqrt{k_x k_z}} \frac{h}{L_{sj}} S_{ptvj} \qquad (8\text{-}22)$$

This equation implies that the pressure drop in each segment/zone j is due to the flow in all the segments indicated by i. This multi-segment well solution can be modified for ICD completed wells, if we assume the ICD pressure drop is an additive to the reservoir pressure drop, as follows;

$$\tilde{P}_{jD}(s) = \sum_{i=1}^{n_{seg}} A_{ji}(s)\, \tilde{q}_{iD}(s) + \tilde{q}_{jD}(s) S_{pthj} + q_{jD}^2(s) S_{ICDj} \qquad (8\text{-}23)$$

Where the dimensionless ICD skin can be defined as follows;

$$S_{ICDj} = \frac{C_u \rho_{mix}}{2C_v^2} * \frac{kh}{141.2\mu_o B_o} * \frac{q_t}{L_H^2 A_j^2} \qquad (8\text{-}24)$$

The *Eqn.8-23* provides a solution in Laplace domain for multi-segment FCD completed wells. However, many problems affect the practicality of this solution. The first one is that this equation is non-linear and must be solved iteratively (e.g. by the Newton method) a time-consuming and tedious process. Convergence issues due to multiple summations, e.g. *Eqn B-8* in appendix B, is another problem. The wellbore effect should also be included in this solution to give the pressure at the heel section of the tubing (as mentioned previously, for this case it is assumed that only one PDG is in place in the tubing, downstream of all the zones which might be the case for many FCD completion). For example, the following wellbore pressure drop equation needs to be coupled to the reservoir pressured drop to calculate P_{wD}. More details about such a coupling can be found in Tang et al 2005 [142].

$$P_{wD} - P_{jD} = \frac{N_{Ret} f_t}{8} \frac{\pi x_{jD}}{C'_{hd}} - \frac{\pi}{16 C'_{hd}} \left[\sum_{i=1}^{j-1} \left(x_{jD} - \frac{2i-1}{2M} \right) \frac{1}{M} D_{fi} q_{hiD} + \frac{D_{fi} q_{hiD}}{8M^2} \right] \qquad (8\text{-}25)$$

Where, C'_{hd} is the horizontal well conductivity, N_{Ret} is Reynolds number , f_t friction factor , D_{fi} is a term which is the function of both Reynolds number an friction factor .[145]

Moreover, the solution also needs to be returned to time domain using a numerical Laplace inversion algorithm such as Stehfest. In addition to all the challenges mentioned above, the major concern for the results of such a problem is non-uniqueness of the solution as the non-linear problem needs to be solved iteratively using initial guess. Due to the highlighted issues, it was decided to limit this study to single-zone FCD solution, given that this approach is consistent with the real data set that will be analysed later in the following chapter.

8.7 Application to the Golden Eagle Field

8.7.1 Golden Eagle Field Description

The Golden Eagle Area Development (GEAD), located in the UKCS approximately 100 km North East of Aberdeen, comprises the Golden Eagle, Peregrine and Solitaire fields **(***Figure 8-12***).** The three fields are produced via a combination of platform and subsea wells from three drill centres: a wellhead platform adjacent to the central processing platform (Golden Eagle wells), a Southern manifold subsea drill centre (Peregrine wells) and a Northern manifold

subsea drill centre (Golden Eagle and Solitaire wells). Production commenced in October 2014 and water injection began shortly thereafter.

All three fields contain a light, under-saturated black oil within two geological formations: the Lower Cretaceous Punt sandstone and the Upper Jurassic Burns sandstone. In Golden Eagle the two formations were, and possibly still are, in communication in at least one area of the field such that the two formations contain the same oil and share a common virgin pressure gradient. Peregrine also contains oil in both the Punt and Burns sands, but these are different from each other and also from the oil in Golden Eagle. Solitaire contains oil in the Burns sand only and this is similar to Golden Eagle.

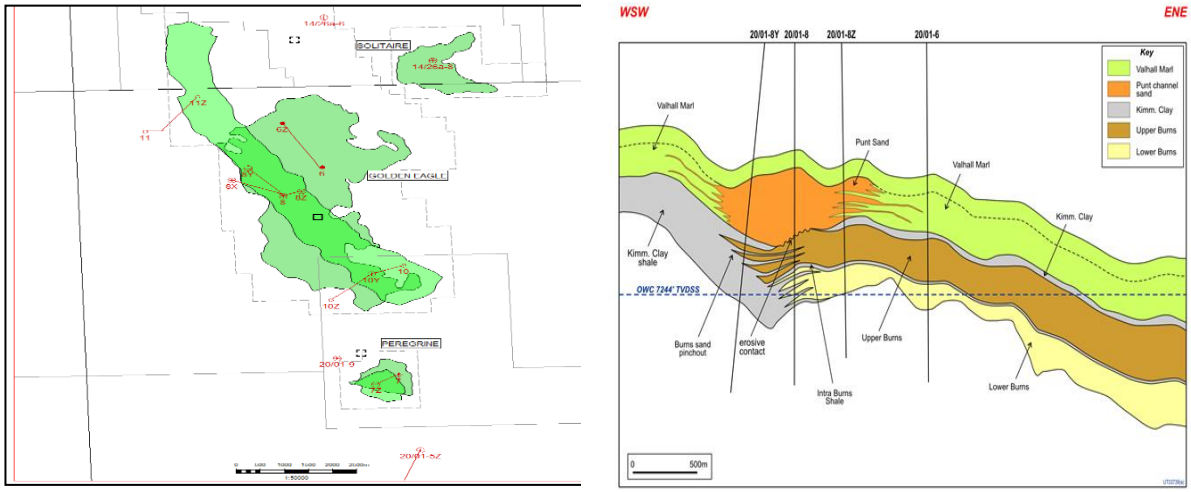

Figure 8-12 Golden Eagle Area Development Map and Cross Section through Central Golden Eagle Field

The recovery mechanism in the Burns formation is by peripheral water flood. Water injectors supplementing the natural aquifer influx from regionally extensive sands. In general, water injectors are located down-dip, just below the free water level, to allow the oil to be swept towards the producers. The development strategy for the Punt is also via water flood, but use a pattern flood along the length of the Punt channel. This is because the Punt sands are fully oil bearing across most of the Golden Eagle accumulation with sand pinch out to the east and west. The structure only dips below the free water level in the extreme north and southeast of the field. Punt producers are located towards the Punt sand highs, with injectors generally in the structural lows. Producers and injectors alternate along the axis of the Punt fairway with a higher density of producers towards the crest of the structure near the 20/1-8 appraisal well, where the greatest thickness of net pay is encountered **(***Figure 8-12***).**

8.7.2 Well Completion Design

The majority of the 14 production and 5 water injection wells are completed using intelligent well technology (IWT) with up to three separate zones in each well. Mechanical packers providing zonal isolation allowing each zone to be flowed independently via a hydraulically actuated ICV or comingled in any combination. A pre-development geomechanics study determined that downhole sand control was required in all wells and subsequent laboratory testing supported the use of stand-alone screens (SAS) as the preferred sand control method. It is well documented in the industry that SAS completions have a mixed experience in terms of performance and reliability. Many of the SAS reliability concerns have been attributed to the screen to open-hole annulus remaining unpacked. A flowing fluid will always take the path of least resistance, allowing the sand laden fluid to travel along the entire screened length until it enters the tubing at the uppermost screen. In many cases this results in erosion of the filtration media and ultimately in a loss in sand control. Given the variability in the formation, strength expected in the GEAD wells this was seen as a major concern.

For GEAD it is believed that ICDs have the potential to increase the operating envelope of SAS in the GEAD producers when combined with strategically placed, open hole (OH) swellable packers. The aim is to minimize tubing to annular flow and controlling the flux rate per screened section, thus reducing the risk of erosional damage to the screen. The benefits of ICDs have been widely reported in terms of water/gas production management in horizontal wells, but less commonly for sand screen erosion control. ICDs were not installed in the water injection wells.

Figure 8-13 is a schematic diagram of a three zone, production well. The pressure and temperature sensors are located immediately above the ICV for each zone. The uppermost gauge mandrel immediately below the production packer is a combined flowmeter and pressure/temperature sensor. A three optical-fiber cable bundle is clamped to the inner production string. It covers the three reservoir intervals; the Upper Punt, Lower Punt and Burns in this case. Distributed temperature sensing is provided by one of the fibers for inferring the water injection profile during shut-in warm backs. Unfortunately, the resolution has proved to be insufficient for production inflow profiling.

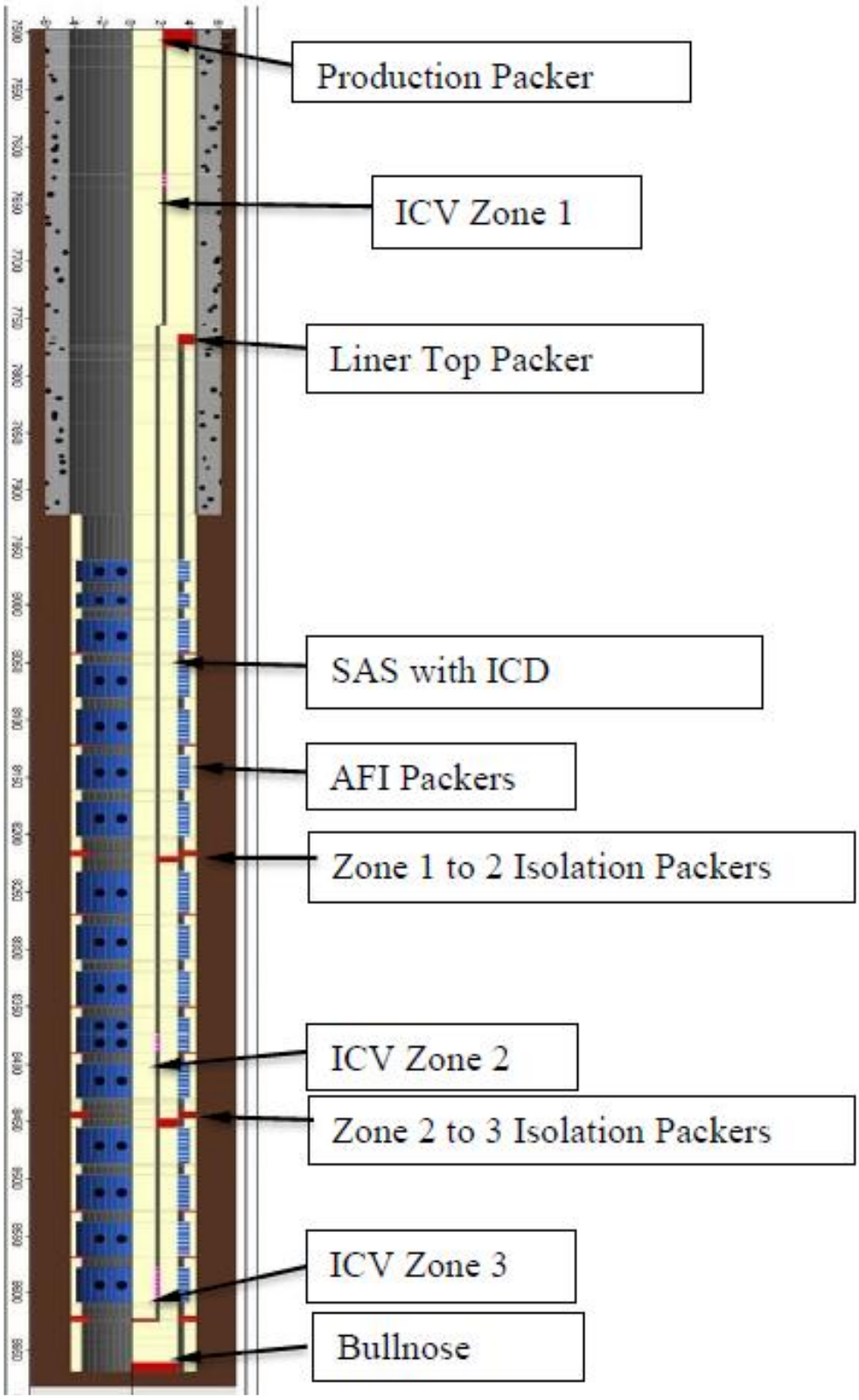

Figure 8-13 Golden Eagle 3 Zone Sand face Completion Schematic

8.7.3 PTA in I-wells Completed with ICDs and ICVs

In the following pressure data from two I-wells with similar completions, as shown in *Figure 8-13*, will be used for the analysis .The main concern for Reservoir/Production Engineer of this field is to know how ICD affects the PTA analysis and whether formation damage is present and mitigation strategies ,e.g. stimulation and etc.

8.7.3.1 Intelligent Well A (Zone 1)

Well A is a three zone, production well with a deviation of 60º. The flow rate and annulus pressure for the upper zone, Zone 1, is shown in *Figure 8-14*. There are three main pressure build-ups. PBU1, the longest, was conducted immediately after the initial well clean up. The total rate is measured by a multiphase flow meter with the zonal rate being allocated by PDGs that directly measure the pressure in the annulus and tubing.

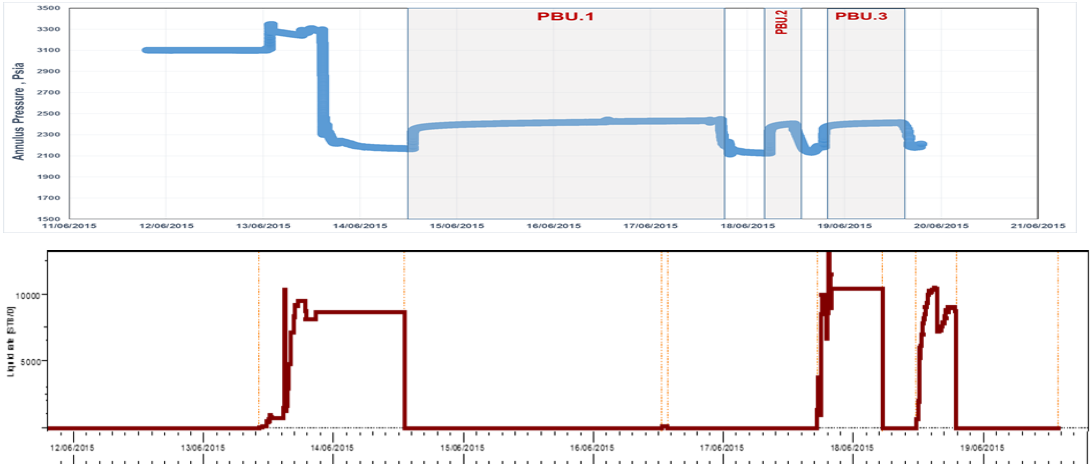

Figure 8-14 Zone 1 Pressure and Flow Rate History

Pressure data from all the three build-up period is used for analysis. As shown in *Figure 8-15*, three pressure build-up periods are overlaid in the log-log plot meaning that the pressure and derivative plots are almost identical; hence there are no significant changes in either the reservoir or near wellbore throughout the study period.

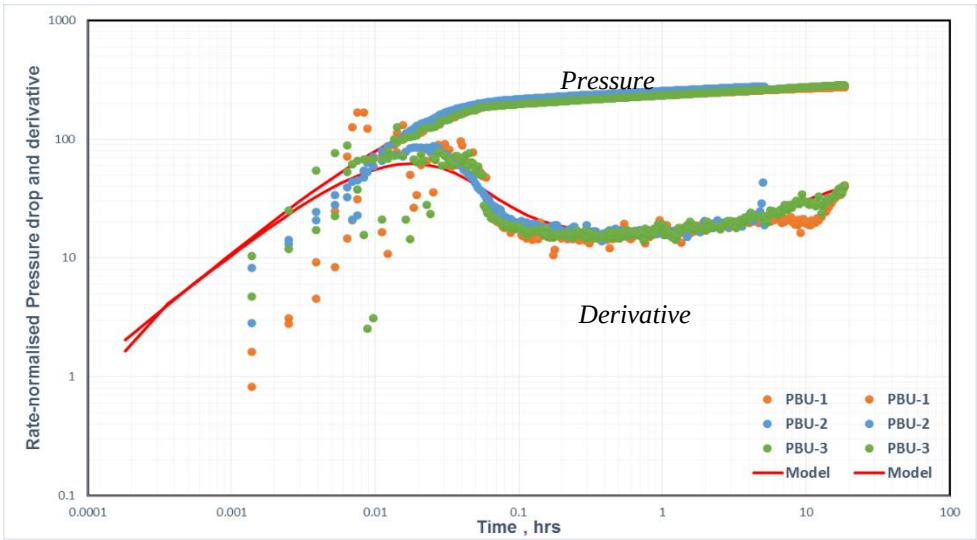

Figure 8-15 Log-log PTA plot for well A, Zone-1, PBU data

Commercial software was used to estimate the permeability and skin, the value of which is compared with the calculated skin for a vertical, fully penetrating open hole model *(Eqn.8-6).* The best match to all PBU data was obtained with a 60°, deviated well in a homogenous reservoir model **(***Figure 8-15***).** As reported in *Table 8-5* the geometrical skin of this deviated well is negative, while the total skin is positive**.** The difference between these two values is the sum of the ICD and the formation damage skins.

Table 8-4 Zone 1 Properties

Parameters	Values
Density (lb/ft^3)	48
Zonal Flow Rate (STB/day)	8700
Nozzle Area (in^2)	2.6
Number of Nozzles	30
Discharge Coefficient	0.84
Oil viscosity (CP)	1.2

In order to find the contribution of damage and ICD skin separately, the second approach in the proposed workflow **(***Figure 8-10***)** was followed. The estimating permeability and total skin is combined with the information about nozzle area, zonal flow rate, discharge coefficient and fluid density **(***Table 8-4***)** to calculate the dimensionless skin due to ICD ,using the *Eqn.8-13* , as **0.31**. Finally, by subtracting the ICD skin from the "*Damage+ICD*" skin the pure Formation

damage skin is extracted as **1.5**. Small ICD pressure drop and thus ICD skin is consistent with our priori knowledge that the ICDs in this well are not employed to impose significant extra pressure drop but to prevent the open hole annulus velocity exceeding 1ft/s. The results of the analysis are listed in *Table 8-5* showing that we have identified the presence of formation damage skin of **1.5**.

Table 8-5 Skin Estimation for Well A, Zone 1, PBU data

Permeability, md	**1,080**	Total Skin	**0.89**
Geometrical Skin	**-0.95**	Pressure drop across ICD, psi	**7**
Anisotropy Skin	**-0.0325**	ICD Skin	**0.31**
(Formation Damage + ICD) Skin	**1.84**	Formation Damage Skin	**1.53**

8.7.3.2 Intelligent Well B (Zone-3)

The second data set is provided by well B, a three zone IW of similar completion design to well A. *Figure 8-16* presents the PTA of zone 3 for two PBU periods in February and April, which were conducted after a production period with two different flow rate. There is small observable change in skin between the two PBUs but the quality of data is not as good as that for Zone 1 in well A and the duration of the PBUs is relatively short. This will affect the interpretation results and hence reduce the level of confidence in the results.

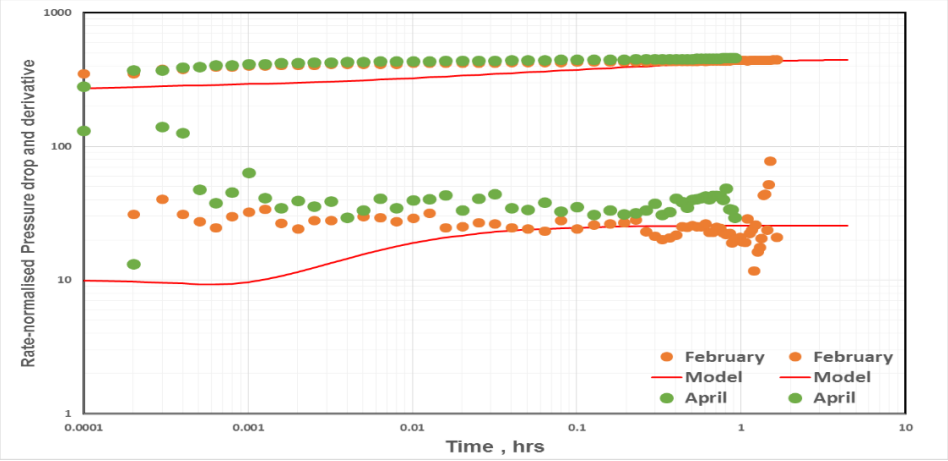

Figure 8-16 Log-Log PTA plot for Well B, Zone 3, and PBU data

Nevertheless, the proposed workflow was followed for the longer and better quality data set in February resulting in ICD skin of **0.1**, and therefore based on *Eqn.8-12* the Formation damage skin of **0.34** (*Table 8-6*).

Table 8-6 Skin Estimation for Well B, Zone 3, and PBU data

Permeability, md	200	Total Skin	1.2
Geometrical Skin	0.767	Pressure drop across ICD, psi	0.628
Anisotropy Skin	-0.01	ICD Skin	0.1
(Formation Damage + ICD) Skin	0.434	Formation Damage Skin	0.34

8.8 Recommendations for ICD Performance Monitoring

A common production surveillance concern is identifying plugging and erosion of ICD restrictions or screens, as well as changes in the formation damage over time. A quick check on the ICD status is to overlay the historical PBUs' pressure derivative plots. It is important to note that as the flow rate might be different before each pressure build-up, only rate-normalized pressure plots should be compared. The level of stabilization, which represents the permeability, should remain constant, while the separation between the level of the stabilization and pressure plots, indicative of the total skin, may change over time. Inconsistency in pressure plots can be due to ICD plugging/ erosion. For example, *Figure 8-17* shows three idealized cases where the effect of ICD plugging and erosion is compared. In this figure, it is assumed that there are 30 nozzles per ICD joint, similar to the presented real field data. Increasing the pressure draw down, shifting pressure plot upward, or decreasing, shifting down ward, is the result of ICD plugging and erosion respectively.

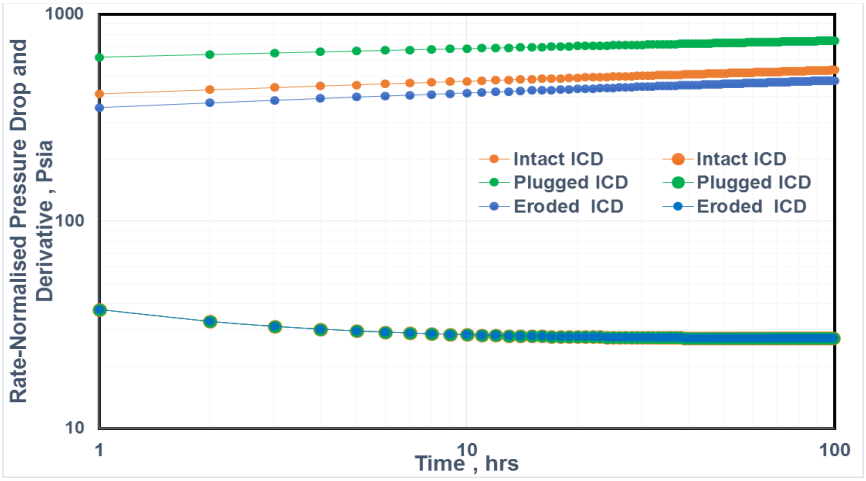

Figure 8-17 Log-log Pressure and Derivative Plots for ICD Performance Monitoring

8.9 Summary

The effect of inflow control devices on pressure transient analysis and the correction required to use a conventional PTA workflow in advanced well completions shut-in test has been analyzed. The results of this work help to distinguish between the damage skin and the extra pressure drop due to ICDs. In summary:

- The non-linear pressure drop in ICDs is a rate and time dependent parameter. When the zonal flow rate variation is significant, both pressure and derivative plots in the drawdown period can be affected. This results in the incorrect estimation of permeability and skin from PTA.
- Variable ICD diameter distribution along the completion affects the pressure measured downstream of the ICD completion, making the standard PTA methods inaccurate.
- The pressure drop across the ICDs becomes time independent when flow rate change is insignificant or is zero, i.e. during pressure build-up periods. Conventional PTA method are now applicable. However, the additive ICD pressure drop (prior to shut-in) contributing to the estimated skin needs to be estimated and accounted for.
- A workflow to decompose the total skin estimated in an ICD completed well has been developed. The formation damage skin and ICDs can be separately determined, given the ICD completion performance at the time of test is certainly known. The application of the workflow on two real intelligent well data sets was demonstrated where the level of formation damage in each zone was identified.
- The derivative overlay can be used as an effective way to monitor the condition of ICDs. Inconsistency in pressure plots can be indicative of ICD plugging/erosion.

It should be noted that in the previous chapters (4 to 7) it was assumed that pressure and temperature data was measured in the sandface and therefore was not affected by FCDs' restriction.

Conclusions & Future Work

9.1 Conclusions

This thesis provided solutions for some important subjects in I-Wells context by developing new modeling and monitoring approaches. The relatively new TTA was further investigated in this thesis by integrating TTA with PTA and applied for reservoir characterization, flow rate allocation and completion monitoring. The following describes the main questions addressed and answered by this thesis;

1. What is the role of different types of FCDs in the well clean-up process? How do, in particular, autonomous FCDs, with their sensitive reaction to drilling and completion fluids, perform during the cleanup? How to improve clean-up in I-Wells completed with FCDs?
2. How can the current TTA knowledge be extended to the multi-phase, bounded and heterogeneous reservoir? How to integrate TTA and PTA methods and for which applications can PTTA potentially be used? Can PTTA be used for flow rate allocation in multi-phase multi-zone reservoirs? Can TTA be utilised for the variable rate problem when the temperature signal is affected by the flow rate variation?
3. What is the impact of non-linear FCD pressure drop on conventional PTA? How to incorporate this impact into the current PTA workflow?

The main findings of each chapter are described below;

- **Chapter 3: Dynamic Wellbore and Near-Wellbore Clean-up in Wells with a Flow Control Completion**

1. An integrated dynamic wellbore-reservoir modeling approach was prepared. The proposed modeling approach fully captures the required physics and also model the entire process from filtrate invasion to flow back period.
2. Non-uniform inflow from different parts of long horizontal wells, due to HTE and reservoir heterogeneity, reduce the clean-up efficiency in some compartments such as the toe.
3. The ICD-completion enhances the flow contribution from the low permeability and the toe zones. This increases their drawdown and consequently helps achieve the lift-off

pressure for better clean-up.

4. The effect of ICD completion, however, is a trade-off between the inflow profile equalization in one hand and reducing the reservoir drawdown for some zones on the other hand. The impact of this important aspect of ICD design workflow is discussed.
5. AFCD completion performance in the clean-up process is affected by the drilling and completion fluid composition, the pattern of filtrate invasion and the well trajectory.
6. Deeper invasion of water-based filtrate at the heel of a horizontal well in a homogenous reservoir results in the heel's AFCDs maintaining their restrictive behaviour for a longer period compared to the toe's AFCDs. This increase both the flow contribution from the toe and its rate of clean-up. As a result, the risk of not exceeding the lift-off pressure at the heel and not cleaning it up properly increases. This is the opposite to what is normally observed in other well completion types.
7. It is shown that SCOVs can improve the clean-up efficiency of an AFCD completion, especially in the heel and lower parts of the well. However, if their operation strategy is inappropriate the risk of the heel-to-toe effect due to uneven clean-up profile may increase.
8. Viscosified brine can potentially accelerate AFCD completion clean up (subject to its impact on the overall flow performance), however, its impact will be limited to early time if a large volume of drilling fluid filtrate has invaded into the reservoir.

- **Chapter 4: PTTA in I-wells: Background, Modelling, and Workflow**

1. The value of integrated PTTA and DDA was discussed in this chapter. It is explained that mature PTA and RTA are proven tools for analysing the middle-time and late-time regimes leading to reservoir and boundary characterization respectively. However, TTA is a promising tool for near-wellbore description. As pressure, temperature and flow rate are normally measured in I-wells, integrating all the measured data provides an opportunity to fully characterise reservoir from near wellbore to boundary.
2. A workflow for TTA was presented where different steps such as identifying flow regimes, finding the corresponding slopes and determining the thermodynamic properties such as the JT and thermal adiabatic expansion coefficients was followed by estimating the unknown parameters. This workflow was applied in the later chapters in multiple applications.

- **Chapter 5: PTTA in I-wells: Case Studies: PTTA in Multiphase, Bounded and Heterogeneous Reservoirs**

1. The current TTA methods are all developed under the assumption of single-phase flow in an infinite acting and homogenous reservoir. However, these simplifying assumptions are very restrictive, making the current TTA methods inapplicable in many practical cases.
2. Three different multiphase cases including oil-water, gas-water, and oil-gas were used to investigate the application of TTA method in the presence of a second flowing phase. The current TTA methods were further extended to incorporate the effect of water when oil and gas are the main producing phases.
3. The results indicated that TTA for solution gas derive reservoirs is more complex. The temperature slope changes when the pressure drops below bubble point and gas appears in the reservoir. The initial JT effect still follows the normal heating-up trend. In addition, the increase in the free gas fraction results in the temperature featuring a turn to cooling-down trend.
4. The speed of the temperature wave's propagation is much slower than for the equivalent pressure wave. It is unlikely that the reservoir boundaries effect on the temperature signal can be observed. However, the results indicated that as soon as pressure reaches the lateral boundaries, the temperature slope varies accordingly (regardless of how far temperature wave has traveled into the reservoir).
5. Stand-alone TTA should be used cautiously in bounded reservoirs. The semi-log straight line due to boundary effects can be easily misinterpreted as a radial flow regime or damaged zone. It is suggested to identify the flow regimes by PTA first and then select the corresponding radial flow regime on temperature data for the analysis.
6. The permeability estimated from TTA and PTA represents the average permeability in the investigated area. The speed of the pressure and temperature wave implies that the analysis of TTA and PTA in heterogeneous formations may investigate different volumes, which results in different results. This dissimilarity can affect the estimation of JT coefficient from the slope of TTA and PTA and so finding the corresponding slope (i.e. for the same volume of investigation) is important.
7. Synthetic data was used to investigate the application of PTTA in limited entry wells. It was shown that open interval can be estimated as a result of this integration. Such

results cannot be determined from stand-alone PTA due to missed/masked early-time flow regime.

- **Chapter 6: PTTA in I-wells: Flow Rate Allocation in Multi-Phase Multi-zone I-Wells using PTTA**

1. Direct measurement of zonal flow rate in multi-layer reservoir is not a common practice in the industry. However, the widely available pressure and temperature data can be used for flow rate allocation.
2. A new soft-sensing method, based on integrated TTA and PTA, was developed. The application of the method to a wide range of application such as flow rate allocation, reservoir characterization, and completion monitoring was demonstrated.
3. The new algorithm reduces the need to shut-in the well production by taking advantage of the changes in the well's production rate that always occur during well operation (e.g. only a draw down period followed by a build-up is sufficent to estimate the unknow paramters in multi-layer formations). This integrated analysis can also determine the presence and depth of a near wellbore zone of reduced permeability (formation damage).
4. The modified version of the algorithm for the multi-phase reservoir showed that the combination of transient and steady-state measurement can be used to estimate the zonal water cut and phase flow rate.
5. The multiphase version of the algorithm was further adapted to calculate the multiphase flow performance curves for AFCD modeling and monitoring, subject to the assumptions and caveats listed in the chapter, and measurement availability. This method might be an alternative to the requirement for experimental AFCD flow performance data.
6. The effect of measurement uncertainties on the robustness of the algorithm was also presented. It was shown how the results of the algorithm are affected by random noise, biased/drift error, and missing measurements.

- **Chapter 7: PTTA in I-wells: Variable Flow Rate Solutions for TTA and PTA**

1. Variable flow rates affect the early-time pressure and temperature signal such that they cannot be directly used in conventional PTA or TTA. This problem is addressed in this

chapter for both PTA and TTA. Normalization and deconvolution methods are explored for reconstruction of the response of an equivalent single-rate solution, for the given test model.

2. The Rate-Normalized Temperature (RNT) and Pressure-Normalized Temperature (PNT) methods were presented. The application of these methods to reconstruct the single-rate response was not successful.
3. A data-driven deconvolution method was also explored and tested. It was demonstrated that deconvolution provides an exact solution for the variable rate in PTA and a good result for TTA.

- ***Chapter 8 :*** **Pressure Transient Analysis in Advanced Wells Completed with Flow Control Devices**

1. The non-linear pressure drop in ICDs is a rate-dependent parameter. It is shown that both pressure and derivative plots in the drawdown period will be affected when zonal flow rate variation is present. This results in an incorrect estimation of permeability and skin.
2. Variable ICD diameter distribution along the completion affects the pressure measured downstream of the ICD completion which can make standard PTA methods inaccurate.
3. During pressure build-up periods at zonal shut-in, when the sandface flow rate change is zero the pressure drop across ICDs becomes also zero and the conventional PTA method is applicable. However, the additive ICD pressure drop (prior to the test) does contribute to the estimated skin and needs to be decomposed.
4. Based on the proposed workflow the total skin in an ICDs-completed well can be decomposed and the contribution of formation damage skin and ICDs can be determined. The application of the workflow to two real intelligent well data sets was demonstrated while the level of formation damage in each zone was sufficiently identified.
5. It was shown that the pressure derivative overlay can be used as an effective way to monitor the condition of ICDs. Inconsistency in subsequent pressure plots could be indicative of ICD plugging or erosion.

9.2 Suggestions for Future Work

The results of this thesis can be further extended by the following studies;

- **Clean-up in Advanced Wells with FCDs *(Chapter 3)***
  1. The sensitivity of AFCDs to completion and drilling fluids makes well clean-up a challenging process in such completion. This thesis recommended SCOVs to improve the well clean-up process. However, this fully open device increases the risk of the HTE leading to irregular clean-up along the completion. The well clean-up can be further improved by developing a specific closing strategy for each zonal SCOV. This strategy will advise on the order that the SCOVs should be closed and when.
  2. Well clean-up includes different events such as external mud cake removal and permeability restoration or reduction of high saturation of filtrate in the near-wellbore zone due to completion and drilling fluids etc. Therefore, it is recommended to develop comprehensive clean-up monitoring guidelines to demonstrate how to use pressure, temperature and flow rate data measured during this process. It should be noted that some challenges such as variable flow rate, the effect of cooling from filtrate mud and etc. could be included in the guideline. Knowledge of these events will help Production Engineers in the decision-making process for well management
- **Integrated PTTA *(Chapters 4 to 7)***
  1. A novel TTA model can be developed to quantify the added value of PTTA in solution gas drive reservoirs. This model requires handling the dynamic changes of temperature when the gas fraction increases and as a result, the Joule-Thompson trend changes and the phase change –induced effects kick in.
  2. The thesis examined how different reservoir boundaries affect the temperature data. A mathematical model for TTA in bounded reservoirs would further increase the application of this promising method.
- **PTA in FCD completed wells *(Chapter 8)***
  1. This thesis offered a solution for a single-zone test to take into account the effect of a non-linear FCD pressure drop. It is recommended to extend this work to multi-zone reservoirs with FCDs of variable strength.

2. The modified PTA was tested in FCD completed well for liquid production well. It is recommended to continue this research to include gas with the non-linear flow performance elements which are expected to further complicate the problem.
3. Temperature data is often measured downstream of FCDs in I-wells. It is suggested to investigate the effect of FCD restriction on temperature response.

References

1. Tor Ellis , A.E., Inflow Control Devices—Raising Profiles, in OilField Review Winter. 2009, Schlumberger.
2. Al-Khelaiwi, F.T.M., A Comprehensive Approach to the Design of Advanced Well Completions, in Institute of Petroleum Engineering. 2013, Heriot-Watt University.
3. Haghighat Sefat, M., et al., Reservoir uncertainty tolerant, proactive control of intelligent wells. Computational Geosciences, 2016. **20**(3): p. 655-676.
4. Augustine, J.R., An Investigation of the Economic Benefit of Inflow Control Devices on Horizontal Well Completions Using a Reservoir-Wellbore Coupled Model. 2002, Society of Petroleum Engineers.
5. Mathiesen, V., B. Werswick, and H. Aakre, The Next Generation Inflow Control, the Next Step to Increase Oil Recovery on the Norwegian Continental Shelf. 2014, Society of Petroleum Engineers.
6. Halvorsen, M., G. Elseth, and O.M. Naevdal, Increased oil production at Troll by autonomous inflow control with RCP valves. 2012, Society of Petroleum Engineers.
7. Mathiesen, V., et al., Autonomous Valve, A Game Changer Of Inflow Control In Horizontal Wells. 2011, Society of Petroleum Engineers.
8. Eltaher, M.K.E., Modelling and Applications of Autonomous Flow Control Devices, in Institute of Petroleum Engineering. 2017, Heriot-Watt University.
9. Fripp, Michael., et al., The Theory of a Fluidic Diode Autonomous Inflow Control Device, is SPE Middle East Intelligent Enegy Conference and Exhibition, SPE 167415,2013, Society of Petroleum Engineers: Manama,Bahrain.
10. Zhao, L., et al., Fluidic Diode Autonomous ICD Range 2A Single-Phase Testing, in SPE Oilfield Water Management Conference and Exhibition. 2014, Society of Petroleum Engineers: Kuwait City, Kuwait.
11. Aakre, H., et al., Smart Well With Autonomous Inflow Control Valve Technology. 2013, Society of Petroleum Engineers.
12. Elverhøy, Anita B., Aakre, Haavard, Mathiesen, Vidar., Autonomous Inflow Control for Reduced Water Cut and/or Gas Oil Ratio ,190016-MS SPE Conference Paper - 2018
13. Da Silva, M.F., K.M. Muradov, and D.R. Davies, Review, Analysis and Comparison of Intelligent Well Monitoring Systems. 2012, Society of Petroleum Engineers.

14. Horne, R.N., Listening to the Reservoir—Interpreting Data From Permanent Downhole Gauges. 2007.
15. Chorneyko, D.M., Real-Time Reservoir Surveillance Utilizing Permanent Downhole Pressures - An Operator's Experience. 2006, Society of Petroleum Engineers.
16. Nestlerode, W.A., The Use Of Pressure Data From Permanently Installed Bottom Hole Pressure Gauges. 1963, Society of Petroleum Engineers.
17. Da Silva, M.F., K.M. Muradov, and D.R. Davies, Review, Analysis and Comparison of Intelligent Well Monitoring Systems. 2012, Society of Petroleum Engineers.
18. Koelman, J.V.V., J.L. Lopez, and H. Potters, Optical Fibers: The Neurons For Future Intelligent Wells. Society of Petroleum Engineers.
19. Tabatabaei, M. and D. Zhu, Fracture Stimulation Diagnostics in Horizontal Wells Using DTS Data. 2011, Society of Petroleum Engineers.
20. Sierra, J.R., et al., DTS Monitoring of Hydraulic Fracturing: Experiences and Lessons Learned. 2008, Society of Petroleum Engineers.
21. Huckabee, P.T., Optic Fiber Distributed Temperature for Fracture Stimulation Diagnostics and Well Performance Evaluation. 2009, Society of Petroleum Engineers.
22. Kabir, C.S., et al., Real-Time Estimation of Total Flow Rate and Flow Profiling in DTS-Instrumented Wells. 2008, International Petroleum Technology Conference.
23. Muradov, K.M. and D.R. Davies, Zonal Rate Allocation in Intelligent Wells. 2009, Society of Petroleum Engineers.
24. Almutairi, F.H. and D.R. Davies, Detection of Scale Deposition Using Distributed Temperature Sensing. 2008, Society of Petroleum Engineers.
25. Wilson, A., Distributed-Temperature-Sensing Method Detects Wax and Optimizes Treatment. 2013.
26. Mishra, A., S.H. Al Gabani, and A. Jumaa Al Hosany, Pipeline Leakage Detection Using Fiber Optics Distributed Temperature Sensing DTS. 2017, Society of Petroleum Engineers.
27. Oftedal, A., et al., Interwell Communication as a Means to Detect a Thief Zone Using DTS in a Danish Offshore Well. 2013, Offshore Technology Conference.
28. Xu, B. and F. Forouzanfar, Reservoir Rock and Fluid Characterization Using Distributed Temperature Sensing DTS Systems Data. 2017, Society of Petroleum Engineers.
29. Tabatabaei, M. and D. Zhu, Fracture-Stimulation Diagnostics in Horizontal Wells Through Use of Distributed-Temperature-Sensing Technology. 2012.
30. Koelman, J.V.V., J.L. Lopez, and H. Potters, Optical Fibers: The Neurons For Future Intelligent Wells. 2012, Society of Petroleum Engineers.

31. Molenaar, M.M., et al., First Downhole Application of Distributed Acoustic Sensing (DAS) for Hydraulic Fracturing Monitoring and Diagnostics. 2011, Society of Petroleum Engineers.
32. In 't Panhuis, P., et al., Flow Monitoring and Production Profiling using DAS. 2014, Society of Petroleum Engineers.
33. Hull, J.W., L. Gosselin, and K. Borzel, Well-Integrity Monitoring and Analysis Using Distributed Fiber-Optic Acoustic Sensors. 2010, Society of Petroleum Engineers.
34. Farshbaf Zinati, F., J.-D. Jansen, and S.M. Luthi, Estimating the Specific Productivity Index in Horizontal Wells From Distributed-Pressure Measurements Using an Adjoint-Based Minimization Algorithm. 2012.
35. Yoshioka, K., et al., A New Inversion Method to Interpret Flow Profiles From Distributed Temperature and Pressure Measurements in Horizontal Wells. 2009.
36. Cannon, R.T. and F. Aminzadeh, Distributed Acoustic Sensing: State of the Art, in SPE Digital Energy Conference. 2013, Society of Petroleum Engineers: The Woodlands, Texas, USA.
37. Civan , F., Reservoir Formation Damage (Third Edition), in Reservoir Formation Damage (Third Edition). 2016, Gulf Professional Publishing: Boston. p. 1-6.
38. Ding, Y., et al., Modelling of Both Near-Wellbore Damage and Natural Cleanup of Horizontal Wells Drilled With a Water-Based Mud. 2002, Society of Petroleum Engineers.
39. Al-khelaiwi, F.T., et al., Advanced Well Flow Control Technologies can Improve Well Clean-up. 2009, Society of Petroleum Engineers.
40. Olowoleru, D.K., et al., Efficient Intelligent Well Cleanup using Downhole Monitoring. 2009, Society of Petroleum Engineers.
41. Kerem, M., M. Proot, and P. Oudeman, Analyzing Underperformance of Tortuous Horizontal Wells: Validation With Field Data. 2008.
42. Gottumukkala, V., et al., Best Cleanup Practices for an Offshore Sandstone Reservoir With ICD Completions in Horizontal Wells. 2009, Society of Petroleum Engineers.
43. Jamiolahmady, M., et al., A Thorough Investigation of Clean-up Efficiency of Hydraulic Fractured Wells Using Statistical Approaches, in SPE Annual Technical Conference and Exhibition. 2014, Society of Petroleum Engineers: Amsterdam, The Netherlands.
44. da Silva, D.V.A. and J.D. Jansen, A Review of Coupled Dynamic Well-Reservoir Simulation∗1This research was carried out within the context of the ISAPP Knowledge Centre. ISAPP (Integrated Systems Approach to Petroleum Production) is a joint project of

TNO, Delft University of Technology, ENI, Statoil and Petrobras. IFAC-PapersOnLine, 2015. **48**(6): p. 236-241.

45. Al-Khelaiwi, F.T., et al., Advanced Wells: A Comprehensive Approach to the Selection between Passive and Active Inflow Control Completions. 2008, International Petroleum Technology Conference.
46. Malakooti, R., et al., Flow Control Optimisation to Maximise the Accuracy of Multi-phase Flow Rate Allocation. 2015, Society of Petroleum Engineers.
47. Hu, B., et al., Integrated Wellbore-Reservoir Dynamic Simulation. 2007, Society of Petroleum Engineers.
48. Nikjoo, E., et al., Pressure Transient Analysis in Advanced Wells Completed with Flow Control Devices. 2017, Society of Petroleum Engineers.
49. Sagen, J., et al., A Coupled Dynamic Reservoir and Pipeline Model – Development and Initial Experience. 2007, BHR Group.
50. Hu, B., et al., Use of Wellbore-Reservoir Coupled Dynamic Simulation to Evaluate the Cycling Capability of Liquid-Loaded Gas Wells. 2010, Society of Petroleum Engineers.
51. Bendiksen, K.H., et al., The Dynamic Two-Fluid Model OLGA: Theory and Application. 1991.
52. Sagen, J., et al., A Dynamic Model for Simulation of Integrated Reservoir, Well and Pipeline System. 2011, Society of Petroleum Engineers.
53. Hu, B., Z.G. Xu, and E.H. Uv, Modelling and Simulation of the Co-Flow of Reservoir Fluids and Drilling/Completion Mud in the Ultra-Long Multilateral Horizontal Wellbores. 2009, BHR Group.
54. Wu, Z., R.N. Vaidya, and P.V. Suryanarayana, Simulation of Dynamic Filtrate Loss During the Drilling of a Horizontal Well with High-Permeability Contrasts and Its Impact on Well Performance. 2009.
55. Tran, M.H., Y. Abousleiman, and V.X. Nguyen, The Effects of Filter-Cake Buildup and Time-Dependent Properties on the Stability of Inclined Wellbores. 2010, Society of Petroleum Engineers.
56. Zain, Z.M., A. Suri, and M.M. Sharma, Mechanisms of Mud Cake Removal During Flowback. 2000, Society of Petroleum Engineers.
57. Krogh, E., S. Mjaaland, and E. Sletfjerding, Dynamic Flow Simulation of a Well Clean-up Operation at the Asgard Field. 2009, Society of Petroleum Engineers.
58. Eltaher, E.K., et al., Autonomous Inflow Control Valves - their Modelling and "Added Value". 2014, Society of Petroleum Engineers.

59. Aakre, H., et al., Autonomous Inflow Control Valve for Heavy and Extra-Heavy Oil. 2014, Society of Petroleum Engineers.
60. Nugraha, I., et al., Optimizing Reservoir Performance through Utilization of Autonomous Inflow Control Valve – Lessons Learnt from the World's First Installation. 2016, Society of Petroleum Engineers.
61. Miller, C.C., A.B. Dyes, and C.A. Hutchinson, Jr., The Estimation of Permeability and Reservoir Pressure From Bottom Hole Pressure Build-Up Characteristics. 1950.
62. Horner, D.R., Pressure Build-up in Wells, in 3rd World Petroleum Congress, 28 May-6 June, The Hague, the Netherlands 1951, World Petroleum Congress.
63. Ramey, H.J., Jr., Non-Darcy Flow and Wellbore Storage Effects in Pressure Build-Up and Drawdown of Gas Wells. SPE Journal 1965.
64. Ramey, H.J., Jr., Short-Time Well Test Data Interpretation in the Presence of Skin Effect and Wellbore Storage. SPE Journal 1970.
65. Agarwal, R.G., R. Al-Hussainy, and H.J. Ramey, Jr., An Investigation of Wellbore Storage and Skin Effect in Unsteady Liquid Flow: I. Analytical Treatment. SPEJ, 1970.
66. Gringarten, A.C. and H.J. Ramey, Jr., Unsteady-State Pressure Distributions Created by a Well With a Single Horizontal Fracture, Partial Penetration, or Restricted Entry. SPE Journal 1974.
67. D.Bourdet , T.M.W., A new set of type curves simplifies well test analysis World Oil 1983a(196): p. 19-106.
68. Bourdet, D., Pressure Behavior of Layered Reservoirs With Crossflow, in SPE California Regional Meeting, 27-29 March, Bakersfield, California 1985, Society of Petroleum Engineers. p. SPE- 13628-MS.
69. Kuchuk, F.J. and P.A. Kirwan, New Skin and Wellbore Storage Type Curves for Partially Penetrated Wells. SPE Journal 1987.
70. Daviau, F., et al., Pressure Analysis for Horizontal Wells. SPE Journal 1988.
71. Clark, D.G. and T.D. Van Golf-Racht, Pressure-Derivative Approach to Transient Test Analysis: A High-Permeability North Sea Reservoir Example (includes associated papers 15270 and 15320). SPE Journal 1985.
72. von Schroeter, T., F. Hollaender, and A.C. Gringarten, Deconvolution of Well Test Data as a Nonlinear Total Least Squares Problem. 2001, Society of Petroleum Engineers.
73. Ramey, H.J., Jr., Practical Use of Modern Well Test Analysis. 1976, Society of Petroleum Engineers.

74. Ramey, H.J., Jr., Advances in Practical Well-Test Analysis (includes associated paper 26134). SPE Journal 1992.
75. Gringarten, A.C., From Straight Lines to Deconvolution: The Evolution of the State of the Art in Well Test Analysis. SPE Journal Paper, 2008.
76. Gringarten, A.C., Computer-Aided Well Test Analysis. 1986, Society of Petroleum Engineers.
77. Gringarten, A.C., et al., Use of Downhole Permanent Pressure Gauge Data to Diagnose Production Problems in a North Sea Horizontal Well. 2003, Society of Petroleum Engineers.
78. Ehlig-Economides, C.A., et al., A Modern Approach to Reservoir Testing (includes associated papers 22220 and 22327). 1990.
79. Arps, J.J., Analysis of Decline Curves. SPE Journal 1945.
80. Fetkovich, M.J., Decline Curve Analysis Using Type Curves. SPE Journal, 1980.
81. Palacio, J.C. and T.A. Blasingame, Decline-Curve Analysis With Type Curves - Analysis of Gas Well Production Data. 1993, Society of Petroleum Engineers.
82. Doublet, L.E., et al., Decline Curve Analysis Using Type Curves--Analysis of Oil Well Production Data Using Material Balance Time: Application to Field Cases. 1994, Society of Petroleum Engineers.
83. Mattar, L., J.A. Rushing, and D.M. Anderson, Production Data Analysis - Challenges, Pitfalls, Diagnostics. 2006, Society of Petroleum Engineers.
84. Bahrami, H. and J. Siavoshi, A New Method In Well Test Interpretation Using Temperature Transient Analysis For Gas Wells. 2007, International Petroleum Technology Conference.
85. App, J.F., Field Cases: Nonisothermal Behavior Due to Joule-Thomson and Transient Fluid Expansion/Compression Effects. 2009, Society of Petroleum Engineers.
86. Duru, O.O. and R.N. Horne, Combined Temperature and Pressure Data Interpretation: Applications to Characterization of Near-Wellbore Reservoir Structures. 2011, Society of Petroleum Engineers.
87. Ramazanov, A., et al., Thermal Modeling for Characterization of Near Wellbore Zone and Zonal Allocation. 2007, Society of Petroleum Engineers.
88. Chekalyuk , E.B., Thermodynamics of Oil Formation in in Russian .Nedra , Moscow. 1965.
89. Muradov, K.M. and D.R. Davies, Novel Analytical Methods of Temperature Interpretation in Horizontal Wells. SPE Journal, 2011.
90. Onur, M. and M. Çinar, Temperature Transient Analysis of Slightly Compressible, Single-Phase Reservoirs. 2016, Society of Petroleum Engineers.

91. Mao, Y. and M. Zeidouni, Analytical Solutions for Temperature Transient Analysis and Near Wellbore Damaged Zone Characterization. 2017, Society of Petroleum Engineers.
92. Dada, A.O., K.M. Muradov, and D.R. Davies, Novel Solutions and Interpretation Methods for Transient, Sandface Temperature in Vertical, Dry Gas Producing Wells. 2016, Society of Petroleum Engineers.
93. Duru, O.O. and R.N. Horne, Modeling Reservoir Temperature Transients and Reservoir-Parameter Estimation Constrained to the Model. 2010.
94. Duru, O.O. and R.N. Horne, Joint Inversion of Temperature and Pressure Measurements for Estimation of Permeability and Porosity Fields. 2010, Society of Petroleum Engineers.
95. Sui, W., et al., Model for Transient Temperature and Pressure Behavior in Commingled Vertical Wells. 2008, Society of Petroleum Engineers.
96. Sui, W., et al., Determining Multilayer Formation Properties from Transient Temperature and Pressure Measurements. 2008, Society of Petroleum Engineers.
97. Sui, W., et al., Determining Multilayer Formation Properties from Transient Temperature and Pressure Measurements in Comingled Gas Wells. 2010, Society of Petroleum Engineers.
98. CMG-STARS, Advanced Process and Thermal Simulator C.C.M.G.L. Alberta Editor. v2015.10.5715.22942.
99. CMG, G., Compositional and Unconventional Oil and Gas Simulator. 2015, Computer Modelling Group Ltd: algary, Alberta, Canada.
100. Lee, B.L. and M. G.Kesler, A generalized thermodynamic correlation based on three-parameter corresponding states. AIChE Journal, 1975. **21**(3): p. 510-527.
101. Onur, M. and M. Cinar, Analysis of Sandface-Temperature-Transient Data for Slightly Compressible, Single-Phase Reservoirs. SPE Journal, 2017.
102. Onur, M., et al., Transient temperature behavior and analysis of single-phase liquid-water geothermal reservoirs during drawdown and buildup tests: Part II. Interpretation and analysis methodology with applications. Journal of Petroleum Science and Engineering, 2016. **146**(Supplement C): p. 657-669.
103. Palabiyik, Y., et al., Transient temperature behavior and analysis of single-phase liquid-water geothermal reservoirs during drawdown and buildup tests: Part I. Theory, new analytical and approximate solutions. Journal of Petroleum Science and Engineering, 2016. **146**(Supplement C): p. 637-656.

104. Martin, J.C., Simplified Equations of Flow in Gas Drive Reservoirs and the Theoretical Foundation of Multiphase Pressure Buildup Analyses. 1959, Society of Petroleum Engineers.
105. Al-Hussainy, R., H.J. Ramey, Jr., and P.B. Crawford, The Flow of Real Gases Through Porous Media. 1966.
106. Raghavan, R., Well Test Analysis: Wells Producing by Solution Gas Drive. 1976, Society of Petroleum Engineers.
107. Corbett, P., H. Hamdi, and A. Kazemi, Basic Concepts in Well Testing for Reservoir Description. 2011: The Ball Room, Station Hotel, Guild Street, Aberdeen.
108. Fekete. Reference Manual 2014.
109. Bourdet, D., Well Test Analysis : the use of advanced interpretation models. 2002: Elsevier.
110. Naevdal, G., et al., Reservoir Monitoring and Continuous Model Updating Using Ensemble Kalman Filter. 2005.
111. Geir, Æ., T. Mannseth, and E.H. Vefring, Near-Well Reservoir Monitoring Through Ensemble Kalman Filter. 2002, Society of Petroleum Engineers.
112. Bloemen, H., et al., Soft Sensing for Gas-Lift Wells. 2006.
113. Lorentzen, R.J., et al., Underbalanced Drilling: Real Time Data Interpretation and Decision Support. 2001, Society of Petroleum Engineers.
114. Leskens, M., J.P.M. Smeulers, and A. Gryzlov, Downhole Multiphase Metering In Wells By Means Of Soft-sensing. 2008, Society of Petroleum Engineers.
115. Gryzlov, A., R.F. Mudde, and W. Schiferli, Inverse Modelling of the Inflow Distribution for the Liquid/Gas Flow in Horizontal Pipelines. 2009, BHR Group.
116. Cramer, R., S.V.J. Jakeman, and L. Berendschot, Well Test Optimization and Automation. 2006, Society of Petroleum Engineers.
117. Grebenkin, I., K. Muradov, and D. Davies, A stochastic approach for evaluating where On/Off zonal production control is efficient. Journal of Petroleum Science and Engineering, 2015. **132**(Supplement C): p. 28-38.
118. Muradov, K. and D. Davies, Temperature transient analysis in horizontal wells: Application workflow, problems and advantages. Journal of Petroleum Science and Engineering, 2012. **92–93**: p. 11-23.
119. Fetkovich, M.J. and M.E. Vienot, Rate Normalization of Buildup Pressure By Using Afterflow Data. 1984.

120. Thompson , L., Analysis of Variable Rate Pressure Data Using Duhamel's Principle. 1985, University of Tulsa: Tulsa.
121. Raghavan , R., Well Test Analysis. 1993, New Jersey: Prentice-Hall.
122. Coats, K.H., et al., Determination of Aquifer Influence Functions From Field Data. 1964.
123. Hutchinson, T.S. and V.J. Sikora, A Generalized Water-Drive Analysis. 1959, Society of Petroleum Engineers.
124. Katz, D.L., M.R. Tek, and S.C. Jones, A Generalized Model For Predicting The Performance Of Gas Reservoirs Subject To Water Drive. 1962, Society of Petroleum Engineers.
125. Jargon, J.R. and H.K. Van Poollen, Unit Response Function From Varying-Rate Data. 1965.
126. Bostic, J.N., R.G. Agarwal, and R.D. Carter, Combined Analysis of Postfracturing Performance and Pressure Buildup Data for Evaluating an MHF Gas Well. 1980.
127. Baygü, B., F.J. Kuchuk, and O. Arikan, Deconvolution Under Normalized Autocorrelation Constraints. 1997.
128. von Schroeter, T., F. Hollaender, and A.C. Gringarten, Deconvolution of Well-Test Data as a Nonlinear Total Least-Squares Problem. 2004.
129. Levitan, M.M., Practical Application of Pressure-Rate Deconvolution to Analysis of Real Well Tests. 2005.
130. Ilk, D., P.P. Valko, and T.A. Blasingame, Deconvolution of Variable-Rate Reservoir Performance Data Using B-Splines. 2006.
131. Roumboutsos, A. and G. Stewart, A Direct Deconvolution or Convolution Algorithm for Well Test Analysis. 1988, Society of Petroleum Engineers.
132. Bourgeois, M. and R.N. Horne, Well Test Model Recognition Using LaPlace Space Type Curves. 1993.
133. Onur, M. and A.C. Reynolds, Well Testing Applications of Numerical Laplace Transformation of Sampled-Data. 1998.
134. Mendes, L.C.C., M. Tygel, and A.C.F. Correa, A Deconvolution Algorithm for Analysis of Variable-Rate Well Test Pressure Data. 1989, Society of Petroleum Engineers.
135. Cheng, Y., W.J. Lee, and D.A. McVay, A Deconvolution Technique Using Fast-Fourier Transforms. 2003, Society of Petroleum Engineers.
136. Ahmadi, M., et al., Improving Well-Performance-Data Analysis in Laplace Space by Using Cubic Splines and Boundary Mirroring. 2012, Society of Petroleum Engineers.

137. Stehfest, H., "Algorithm 368: Numerical Inversion of Laplace Transforms,". Comm. Assoc.Computing Machinery, 1970(13, 47).
138. Abate, J. and P.P. Valkó, Multi-precision Laplace transform inversion. International Journal for Numerical Methods in Engineering, 2004. **60**(5): p. 979-993.
139. Iseger, P.d., Numerical Transform Inversion Using Gaussian Quadrature. Probability in the Engineering and Informational Sciences, 2006. **20**: p. 1-44.
140. Birchenko, V.M., et al., Application of inflow control devices to heterogeneous reservoirs. Journal of Petroleum Science and Engineering, 2011. **78**(2): p. 534-541.
141. John Lee , J.R., John Spivey, Pressure Transeint Testing. 2003. **9**.
142. Kappa, Kappa DDA Book. 2016.
143. Hawkins, M.F., Jr., A Note on the Skin Effect. 1956. **SPE-732-G**.
144. Yildiz, T., Inflow Performance Relationship for Perforated Horizontal Wells. 2004.
145. Tang, Y., et al., Effects of Formation Damage and High- Velocity Flow on the Productivity of Perforated Horizontal Wells. 2005.

Appendix A

- **Wellbore Model in OLGA**

As described in the section 3.4.1. the wellbore models throughout this thesis were built by OLGA software. The models require initial and boundary conditions to be defined. For clean-up studies a pressure node was used as surface boundary condition, where a controller also employed to adjust choke size and thereby get the target flow rate. The inflow from the reservoir also was explicitly modelled by distributing the near-wellbore simulator as a source along the wellbore. As for the initial conditions pressure and temperature for different pipes was specified and heat transfer option was also enabled.

Also, as discussed in section 3.6, FCDs were modelled by a valve which has either fixed, for ICD case, or variable flow area AICD. Regarding the latter the device was connected to a transmitter and controller. The transmitter reads the section/zone' WCT/hold-up and controller are used to change the opening area based the defined tables in section 3.6.2.

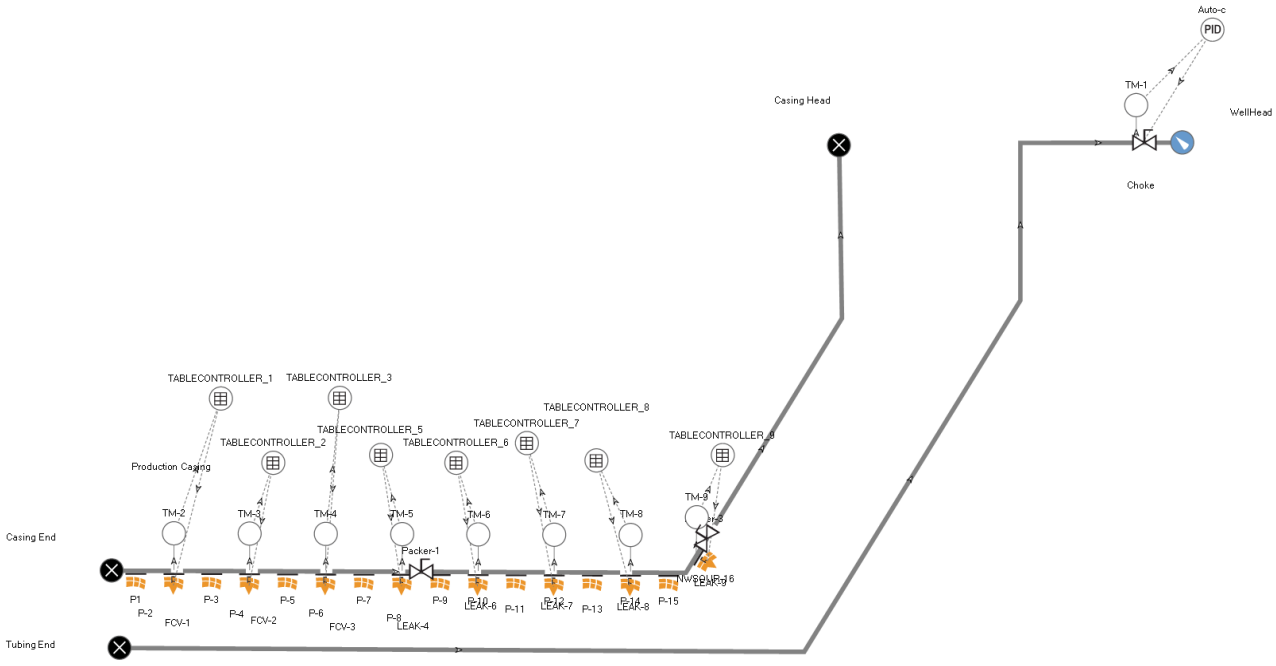

Figure A-1 - The well model completed with AICDs built by OLGA software

Appendix B

The governing equation for multi-segment well is as follows;

$$\frac{\partial^2 P_D}{\partial x_D^2} + \frac{\partial^2 P_D}{\partial y_D^2} + \frac{\partial^2 P_D}{\partial z_D^2} + S_D = \frac{\partial P_D}{\partial t_D} \qquad \text{(B-1)}$$

Where $S_D$source is (green) function and described as follows,

$$S_D = G_D \sum_{i=1}^{n_{seg}} \frac{q_{iD}}{L_{siD}} [H(x_D - \lambda_i^-) - H(x_D - \lambda_i^+)] \qquad \text{(B-2)}$$

$$G_D = 2\pi h_D k_D \delta(z_D - z_{wD}) \delta(y_D - y_{wD}) \qquad \text{(B-3)}$$

The following solution is derived by *Yildiz 2004* [141] ;

$$\tilde{P}_{jD}(s) = \sum_{i=1}^{n_{seg}} A_{ji}(s)\, \tilde{q}_{iD}(s) + \tilde{q}_{jD}(s) S_{pthj} \qquad \text{(B-4)}$$

Where;

$$S_{pthj} = \frac{k}{\sqrt{k_x k_z}} \frac{h}{L_{sj}} S_{ptvj} \qquad \text{(B-5)}$$

$$A_{ji}(s) = F_{1ji}(s) + F_{2ji}(s) \qquad \text{(B-6)}$$

$$F_{1ji}(s) = \frac{K_D h_D}{x_{eD}} \sum_{n=1}^{4} \sum_{k=0}^{\infty} \sum_{l=-\infty}^{\infty} \Psi_{0nkl} \qquad \text{(B-7)}$$

$$F_{2ji}(s) = \frac{2K_D h_D x_{eD}}{\pi^2 L_{hiD} L_{hjD}} \sum_{n=1}^{4} \sum_{k=0}^{\infty} \sum_{l=-\infty}^{\infty} \sum_{m=1}^{\infty} \Omega_{mnkl} \frac{R_{xmi} R_{xmj}}{m^2} \qquad \text{(B-8)}$$

$$\Psi_{0nkl} = K_0\left(\sqrt{s}\beta_1\right) + K_0\left(\sqrt{s}\beta_2\right) \qquad \text{(B-9)}$$

$$\Omega_{mnkl} = K_0\left(\sqrt{\xi_m}\beta_1\right) + K_0\left(\sqrt{\xi_m}\beta_2\right) \qquad \text{(B-10)}$$

$$\beta_1^2 = (2ly_{eD})^2 + z_{kn}^2 \qquad \text{(B-11)}$$

$$\beta_2^2 = (2y_{wD} - 2ly_{eD})^2 + z_{kn}^2 \qquad \text{(B-12)}$$

$$z_{k1} = 2h_D k + r_{weD} \qquad \text{(B-13)}$$

$$z_{k2} = 2h_D(k+1) - r_{weD} \qquad \text{(B-14)}$$

$$z_{k3} = 2h_D k + (2z_{wD} + r_{weD}) \qquad \text{(B-15)}$$

$$z_{k4} = 2h_D(k+1) - (2z_{wD} + r_{weD}) \qquad \text{(B-16)}$$

$$\xi_m = \sqrt{s + (m\pi/x_{eD})^2} \qquad \text{(B-17)}$$

$$R_{xmi} = sin(m\pi\lambda_i^+/x_{eD}) - sin(m\pi\lambda_i^-/x_{eD}) \qquad \text{(B-18)}$$

And dimensionless parameters also defined as;

$$x_D = x\sqrt{k/k_x}/\mathrm{L} \qquad \text{(B-19)}$$

$$y_D = y\sqrt{k/k_y}/\mathrm{L} \qquad \text{(B-20)}$$

$$z_D = z\sqrt{k/k_z}/\mathrm{L} \qquad \text{(B-21)}$$

$$h_D = h\sqrt{k/k_z}/\mathrm{L} \qquad \text{(B-22)}$$

$$k_D = \sqrt{k/k_z k_x} \qquad \text{(B-23)}$$

$$L_{hD} = L_h\sqrt{k/k_x}/L \qquad \text{(B-24)}$$

$$\lambda_i^- = x_{siD} - L_{siD}/2 \qquad \text{(B-25)}$$

$$\lambda_i^+ = x_{siD} + L_{siD}/2 \qquad \text{(B-26)}$$

$$L_{tD} = \sum_{i=1}^{nseg} L_{iD} \qquad \text{(B-27)}$$

$$r_{weD} = \frac{r_w}{2L}\left[\left(k_x/k_y\right)^{0.25} + \left(k_y/k_z\right)^{0.25}\right] \qquad \text{(B-28)}$$